ANL-6646
Biology and Medicine
(TID-4500, 19th Ed.)
AEC Research and
Development Report

ARGONNE NATIONAL LABORATORY
9700 South Cass Avenue
Argonne, Illinois

RADIOLOGICAL PHYSICS DIVISION
SEMIANNUAL REPORT

January through June 1962

J. E. Rose, Division Director
L. D. Marinelli, Associate Division Director

February 1963

Preceding Report:

ANL-6474 - July through December 1961

Operated by The University of Chicago
under
Contract W-31-109-eng-38
with the
U. S. Atomic Energy Commission

DISCLAIMER

TABLE OF CONTENTS

Page

Theory of alkaline earth metabolism. The power function makes possible a simple but comprehensive model of skeletal systems
John H. Marshall 5

Decay-time apparatus
O. J. Steingraber and I. B. Berlman. 30

Nanosecond fluorescence decay-time measurements
I. B. Berlman 32

A study of the α/β ratio in liquid organic scintillation solutions
I. B. Berlman 33

A measurement of the photoluminescent quantum yield of liquid scintillators. A preliminary report
W. R. Anderson and I. B. Berlman. 34

Dissociative attachment of subexcitation electrons in liquid water, and the origin of radiolytic "molecular" hydrogen
Robert L. Platzman 42

Cosmic-ray neutron background research. Hexafluorobenzene scintillator
Jacob Kastner and B. G. Oltman 43

Studies of low-activity phototube materials
H. A. May and P. E. Hess 44

Neutron production in massive shields and effect upon the low-energy gamma-ray background
H. A. May. 50

Observation of background in a large water shield
H. A. May. 66

Effect of silver halide content on the film dosimetry of a Sr^{90}-Y^{90} applicator
Amrik S. Chhabra. 68

Appendix: Energy absorption of 40-keV photons by a single grain of AgBr surrounded on all sides by gelatine and other material of low Z 76

TABLE OF CONTENTS

Page

Effect of long decay chains on the counting statistics in the analysis of radium-224 and radon-222
H. F. Lucas, Jr. and D. A. Woodward. 78

RaD (Pb^{210}) in the human skeleton. Estimates of the exponent of the retention function, the skeletal content and the dose rate in people with high radium content
Richard B. Holtzman. 92

Natural airborne radioactivity RaD (Pb^{210}) and RaF (Po^{210}) in the human body and environment
Richard B. Holtzman. 94

The translocation of radium daughters to the skeletons of Thorotrast patients
L. D. Marinelli and H. F. Lucas, Jr. 95

Geological occurrence of natural radium-226 in ground water of Illinois
Grover H. Emrich and Henry F. Lucas, Jr.. 102

Correlation of the Ra^{228} and Ra^{226} content of man with that of the food and water of his environment
H. F. Lucas, Jr., D. E. Wallace, A. F. Stehney and F. H. Ilcewicz 103

A cytogenetic study of some radium dial-painters and their progeny
Neil Wald, Charles E. Miller, Wayne H. Borges and Jip Kim 104

Patterns of radium retention in mice as related to man
Asher J. Finkel and Charles E. Miller 105

The late effects of radium deposition in humans
Robert J. Hasterlik, Asher J. Finkel and Charles E. Miller . 106

Recovery from radiation-induced cleavage delay in gametes of Arbacia punctulata
Patricia McClement Failla. 107

Periodic events in bone
D. J. Simmons 110

TABLE OF CONTENTS

Page

The retention of Ba^{133} in beagles
R. E. Rowland 113

Radium in human teeth: A quantitative autoradiographic study
R. E. Rowland 116

Local distribution and retention of radium in man
R. E. Rowland 129

High-resolution autoradiographic and microradiographic studies of bone and teeth from human radium cases
R. E. Rowland 139

Skeletal retention of the alkaline earth radioisotopes and bone dosimetry
R. E. Rowland 140

The effects of atmospheric stability and horizontal shear on the accumulation and diffusion of radon
John E. Pearson and Harry Moses. 151

Publications 169

Papers accepted for publication 172

Papers submitted for publication. 173

THEORY OF ALKALINE EARTH METABOLISM

The Power Function Makes Possible a Simple but Comprehensive Model of Skeletal Systems

John H. Marshall

Abstract

A simple way has been found to incorporate the power function, so useful in describing the retention of radioactive bone-seekers,[1] into a metabolic model which agrees surprisingly well with data for the behavior of radioisotopes of calcium, strontium, barium, and radium in dog and in man. The power function is a mathematical expression in which the independent variable (time) is raised to a constant power (usually not an integer). Although it has been considered merely an empirical device for approximating data, the power function may have a deeper significance in the evolution of complex systems. The behavior of the model can be completely determined by a set of three parameters. One such set is the excretion rate, the accretion rate, and the one-day retention of a radioisotope. The model can approximate the activity per gram of calcium both in the blood and in the body as a whole from minutes to years following either an intravenous injection or continuous feeding. The mathematics are applicable not only to adult but also to growing skeletal systems. Simple expressions relate the metabolic parameters defined by Bauer, Carlsson, and Lindquist[2] to the parameters of the power function as modified by Tyler[3] and to the turnover rate derived by Kulp and Schulert[4] from their data on Sr^{90} in man due to fallout. Thus, two divergent groups of measurements of the average turnover time of the adult human skeleton, 5-6 years [Bauer et al.[2] and Heaney and Whedon[5]] and 30-40 years [Kulp and Schulert[4] and Bryant and Loutit[6]] can be reconciled by a single model. Under certain conditions, one can predict the time required for a radioisotope to reach equilibrium within the body, the time after which retention must follow an exponential rather than a power function. Though, of course, its predictions are sometimes only rough approximations to biological data, the model strikes a useful compromise between accuracy and simplicity, thus providing a convenient means for interrelating existing experiments and suggesting new ones.

Introduction

Alkaline earth metabolism is dominated by the metabolism of bone,[7] which acts like a complex banking system for calcium and calcium-like elements. Most deposits of calcium within bone occur in submicroscopic crystals of the calcium phosphate mineral, hydroxyapatite. These crystals are only 25-75 Angstroms in diameter, so that most calcium atoms are

within a few lattice sites from the surface of a crystal. (Whether the larger alkaline earth ions are deposited within a crystal or are forced to its surface during crystallization is not known.) These tiny crystals are embedded in an organic matrix perforated by canalicules which interconnect a system of bone cells and lead to the nearest blood-carrying capillary. There are so many capillaries throughout the skeleton that one can seldom find a bone crystal more than 100 to 200 microns from the blood supply. Thus, in a real sense, the blood is the central exchange of the calcium banking system.

Calcium can be deposited from the blood wherever bone cells lay down calcifiable matrix. Calcium deposits can be withdrawn from the bone and returned to the blood whenever other bone cells remove or resorb the matrix together with the crystals it contains. These processes of bone formation and resorption occur not only during skeletal growth but also at lower rates in scattered sites throughout adult life. Smaller amounts of calcium can be deposited and withdrawn by processes which leave bone intact. These include transfers of calcium to and from extracellular fluid, crystal surfaces, and the crystals themselves. Finally, tissues other than bone contribute to calcium transfer within the body-blood system. All of these processes, working together, yield a wide distribution of holding times for calcium or for the other alkaline earth atoms: an atom which leaves the blood (and is not excreted) may return to the blood in minutes, days, or years. As in the banking analogy, one may classify all deposits (fluid and crystal) according to their holding times. Thus, the body contains very short term deposits, very long term deposits, and possibly all gradations in between.

The problem is to approximate this complex metabolic system by a mathematical model. Several useful models have been based upon compartmental analysis [Maletskos,[8] Bauer and Ray,[9] and Aubert and Milhaud[10]]. But one can make considerable progress toward a solution without postulating discrete compartments. In what follows, the attempt is made to derive results from as few postulates as possible and to explain them in physiological language. Figure 1 shows which postulates lead to each result. Comparisons between theory and experiment are shown in Figures 3-7, and 13. Meanings of symbols are summarized under Terminology in the next to last section of the paper. Figure 15 gives experimental values and theoretical predictions for the parameters which undoubtedly will need revision as data and understanding accumulate.

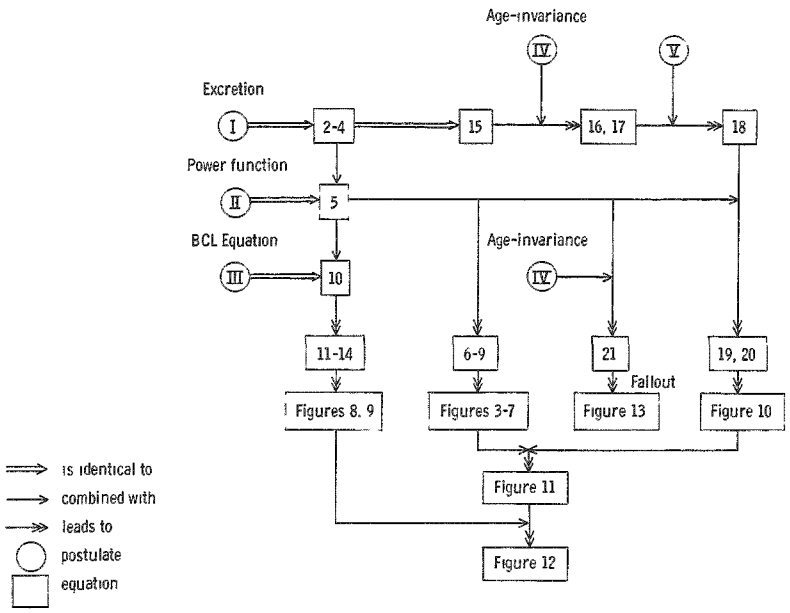

Figure 1

Logical flow diagram for this paper. Equation 21 appears in an appendix to this paper now in preparation for a subsequent report.

The Excretion Postulate

The first postulate provides the key to the rest of the analysis by relating the activity of an alkaline-earth radioisotope in the blood to the rate of change of its total activity in the body. This postulate is as follows:

> (I) The number of radioactive atoms excreted from the body per unit time is proportional to the number in the serum at that time.

This is reasonable provided there is no significant change in the physiological parameters which govern the excretion of ordinary atoms. Alkaline-earth atoms are carried to the possible excretory outlets by the blood. The part of the blood that serves as primary carrier is the serum, the cell-free fluid of the blood. The number of radioactive atoms involved is always so small that a homeostatic or feedback effect upon them is unlikely to disturb a simple proportionality. Of course, radiation damage could distort excretion, but in most data this does not appear to be a serious restriction upon the excretion postulate. This postulate is deceptively similar to one which yields only exponential solutions, but note that the word "body" appears only once, so that any function of time is a possible solution. Radioactive decay is not treated in this paper. Instead, activities are assumed either to be long-lived or to have been corrected

for decay. The nature of the constant of proportionality and the question of time-delay between excretion from the serum and excretion from the body can best be discussed by means of a diagram.

Consider the possible transfers of calcium to and from the serum and the digestive tract as shown in Figure 2. (Ignore the boundary marked "body" for the moment.) The calcium taken in by mouth may either be absorbed into the serum or excreted directly in the feces. Calcium which transfers out of the serum may return at some later time because of a multitude of bodily processes, as indicated by the closed loops. Calcium which transfers from the serum to the digestive tract may either be reabsorbed into the serum or excreted in the feces. The latter fraction is called the endogenous fecal calcium, and its rate of transfer is represented by k_f (grams of calcium per day); the former fraction, the reabsorbed digestive juice calcium, is not directly observable in a radioisotope experiment on the body as a whole, and the question as to its magnitude can be bypassed by means of a topological artifice. Instead of considering the body to be bounded by the skin or by the epithelium (which would exclude the digestive tract entirely), let us take as the system for analysis the body as outlined in Figure 2. The loop representing the reabsorbed digestive juice is now within the body and can be considered in the same manner as all the other calcium loops within the body. There is a second advantage in analyzing the body of Figure 2 rather than the real body. One can regard an atom of calcium, or of one of the alkaline-earth radioisotopes, as being excreted the moment it leaves the serum on its way to an excretory outlet. Thus, the theory may be kept simple, while the complications of excretory delay are handled as possible experimental corrections to data before comparison with theory.

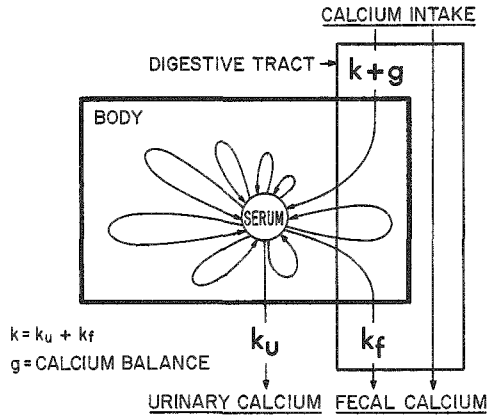

Figure 2

Metabolic diagram

Consider the transfers of calcium from the point of view of the body of Figure 2. There are the many processes which remove calcium from the serum and return it after widely differing intervals (as suggested by the lengths of the looping arrows). Of course, most of these calcium transfers involve bone, but at this point in the analysis, it is unnecessary to specify them more closely. In particular, one need not assume that the rates of transfer into and out of the serum are equal - they will not be equal if the bodily rates of absorption and excretion are not equal. The rate of excretion of calcium from the body is the endogenous excretion rate k, which is the sum of the urinary part k_u and the fecal part k_f. The

rate of absorption of calcium into the body must therefore be k + g, where g is the usual "calcium balance" or growth rate (grams of calcium per day).

Now suppose that the calcium taken in by mouth is accompanied by an alkaline-earth radioisotope. Although this radioactivity will be absorbed into the serum at a rate that is generally not related in a simple way to the rate for calcium, one can express it simply as follows:

$$\dot{q} = \mu(k+g)\ F \tag{1}$$

where $\dot{q}$ is the rate of introduction of activity into the serum (microcuries per day), μ is an empirical absorption factor for the radioelement relative to calcium for a given physiological state (including diet), and F is the specific activity of the food in microcuries per gram of calcium. Similarly one can write:

$$\dot{x} = \eta\ k\ S \tag{2}$$

where $\dot{x}$ is the rate of excretion of activity from the serum (microcuries per day), η is an empirical excretion factor for the radioelement relative to calcium for a given physiological state, and S is the specific activity of the serum in microcuries per gram of calcium. As the calcium excretion rate k has a urinary and a fecal part, the excretion factor η is also separable into a urinary factor η_u and a fecal factor η_f which, from Expression (2), can be seen to combine as follows:

$$\eta k = \eta_u k_u + \eta_f k_f \quad . \tag{3}$$

Keeping in mind the body of Figure 2, one finds that Expression (2) is identical to the excretion postulate (I), and that ηk (considered as a single parameter, not two independent parameters) is the desired constant of proportionality.

The excretion postulate, Expression (2), may now be rewritten in an equivalent differential form that lends itself to further analysis:

$$q\ dR/dt = -\eta\ k\ S \tag{4}$$

where q is a quantity of radioactivity (microcuries) which is introduced into the serum at time t = 0, and R is the fractional retention of this activity in the body as a function of time. From this point, the analysis moves in two directions (Figure 1), one pursuing the consequences of Expression (4) without assuming the mathematical form of R or S, the other assuming that they are represented by power functions.

The Power Function Model

The second postulate provides the basis for a metabolic model by relating the activity of an alkaline-earth radioisotope in the body to a particular decreasing function of time. This postulate is as follows:

> (II) When a radioisotope has been introduced into the serum at time zero, its subsequent retention in the body follows the form of a modified power function until equilibrium has been attained.

This postulate is difficult to justify a priori on physiological grounds and, in some cases, it is known to be only a rough approximation to reality. However, the success of the power function as a description of data suggests that the mathematical consequences of this postulate are worth pursuing.

A power function is an expression in which the independent variable is raised to a constant power. Here it has the form t^{-b}, where t is the time and b is a positive fraction between zero and one. When such an expression is plotted versus time on log-log graph paper, the result is a straight line. As a description of radioisotope data, this function fails at very short times after injection because it increases without limit as t approaches zero, but with a simple modification[3] - the addition of a small constant time ϵ resulting in the form $(t+\epsilon)^{-b}$ - this difficulty is corrected. Originally a mathematical artifice, the constant ϵ turns out in the next section to have a direct relation to internal metabolism.

In mathematical form the second postulate is written:

$$R = \epsilon^b (t+\epsilon)^{-b} \qquad \begin{matrix} 1 > b > 0 \\ t \leqq t_y \end{matrix} \qquad (5)$$

where ϵ^b has been chosen as the coefficient in order that the bodily retention R of the radioisotope be unity at time zero. If R, as given by Equation (5), is plotted versus time, t, on log-log paper, a straight line results only for times much greater than ϵ, which, when data are fitted, is found to have values between 0.01 and 10 days (Figure 15). The coefficient ϵ^b corresponds to the extrapolated retention at one day and is identical to the coefficient a in the usual power function expression $R = at^{-b}$. Analysis of the time limit t_y, at which equilibrium is attained, will be deferred until a later section, but t_y turns out to be long enough not to interfere with the intervening analysis.

The two postulates (I and II) can now be combined and compared to data. Forming the time derivative of R from Expression (5) and

substituting it into Equation (4) yields an expression for the serum specific activity, S, as a function of time after a single introduction of activity q into the serum:

$$S = q\, b\, \epsilon^{b}\, (t+\epsilon)^{-b-1}/\eta k \quad . \tag{6}$$

A companion expression for the body is the following:

$$B = q\, \epsilon^{b}\, (t+\epsilon)^{-b}/c \tag{7}$$

where B is the average specific activity of the body in microcuries per gram of calcium. Expression (7) was obtained by multiplying R from Expression (5) by the activity, q, and dividing by body calcium, c, (grams). Expressions (6) and (7) are fitted to data in Figures 3-7. The values of the three parameters, b, ϵ, and ηk, were determined graphically in order to obtain a reasonably good fit for both B and S over the whole range of time.

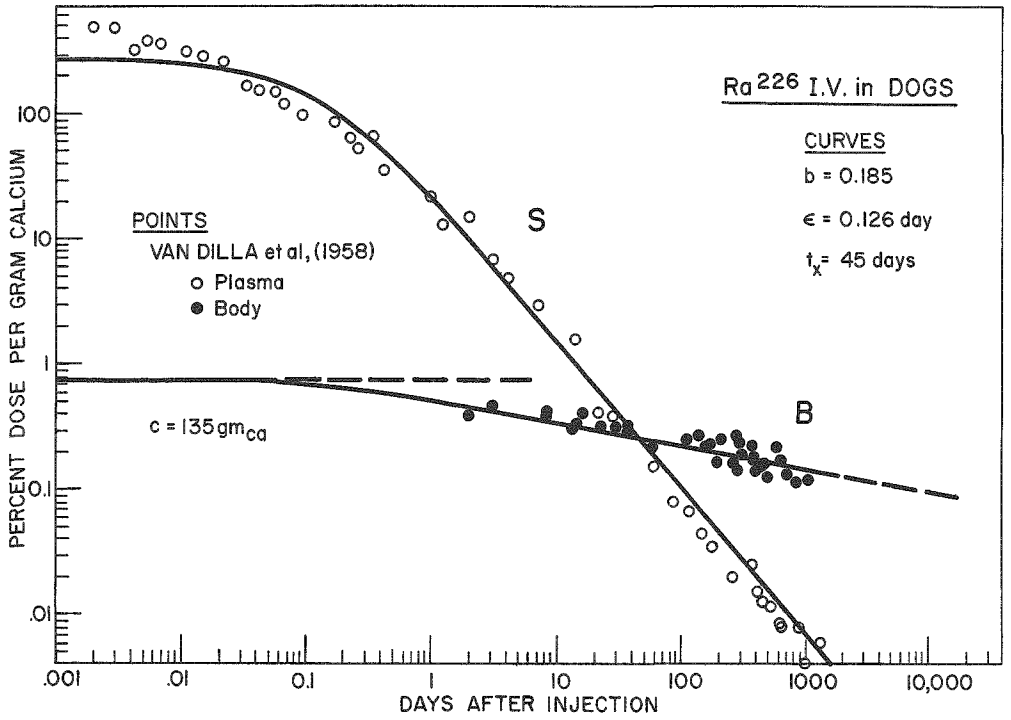

Figure 3

Data for the retention of Ra^{226} in the body and in the plasma of several groups of beagles that were about 1.3 years of age at the time of the intravenous injection. The points were taken from Van Dilla et al.[11] and replotted using 135 g as body calcium and 1.00×10^{-4} g calcium/g plasma. The curves S and B are given by Expressions (6) and (7) using a value of b a little smaller than those reported by Van Dilla.

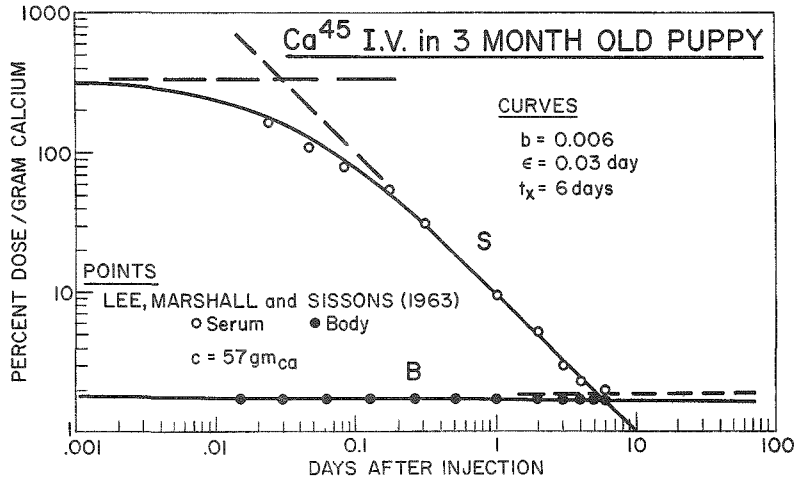

Figure 4

Data for an intravenous injection of Ca^{45} in a rapidly-growing 3-month-old puppy from Lee et al.[12] Note the short crossover time and the very small value of ϵ required by the serum data. Given a small ϵ, one needs a small value of b to fit B and S.

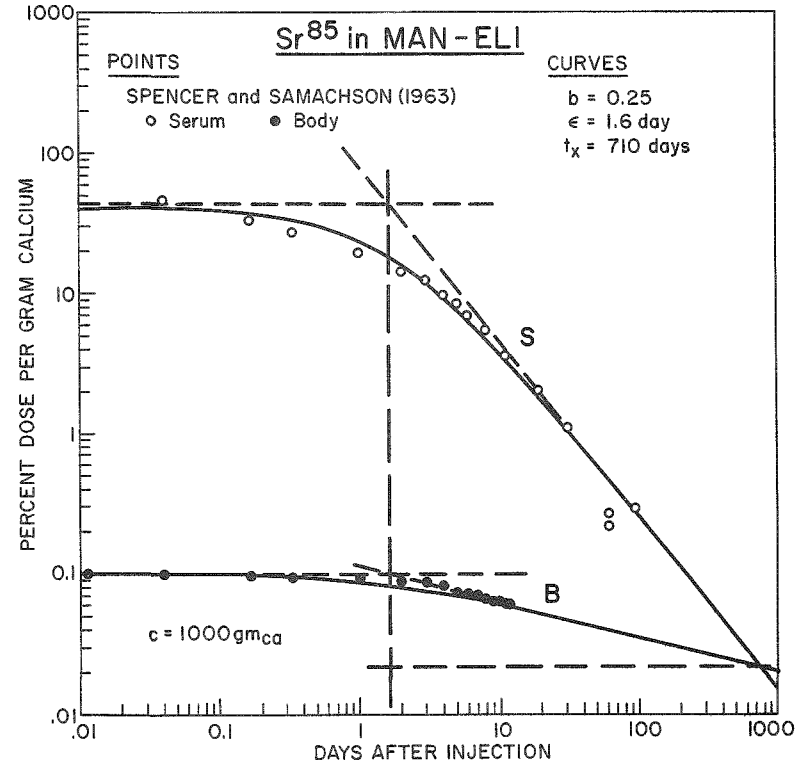

Figure 5

Data for an intravenous injection of Sr^{85} in man [Spencer and Samachson[13] Patient code ELI]. Urinary calcium was low (about 56 mg/day) so that ηk was low and t_x high, though probably actual crossover time would have been a few hundred days rather than the extreme 710 day extrapolation shown.

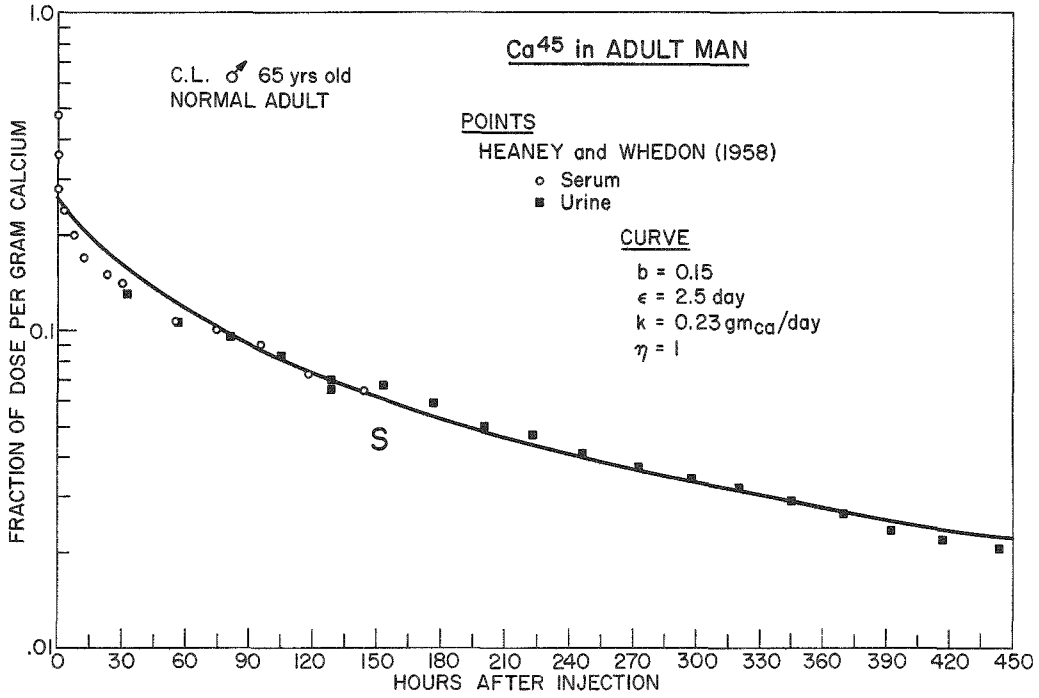

Figure 6

Data for Ca^{45} in the serum following an intravenous injection in a normal man [Heaney and Whedon[5]]. Since urine is derived directly from serum, it is safe to assume their Ca^{45} specific activities are equal at long times after injection. S is taken from Expression (6) and shows how the power function expression looks on semilog paper.

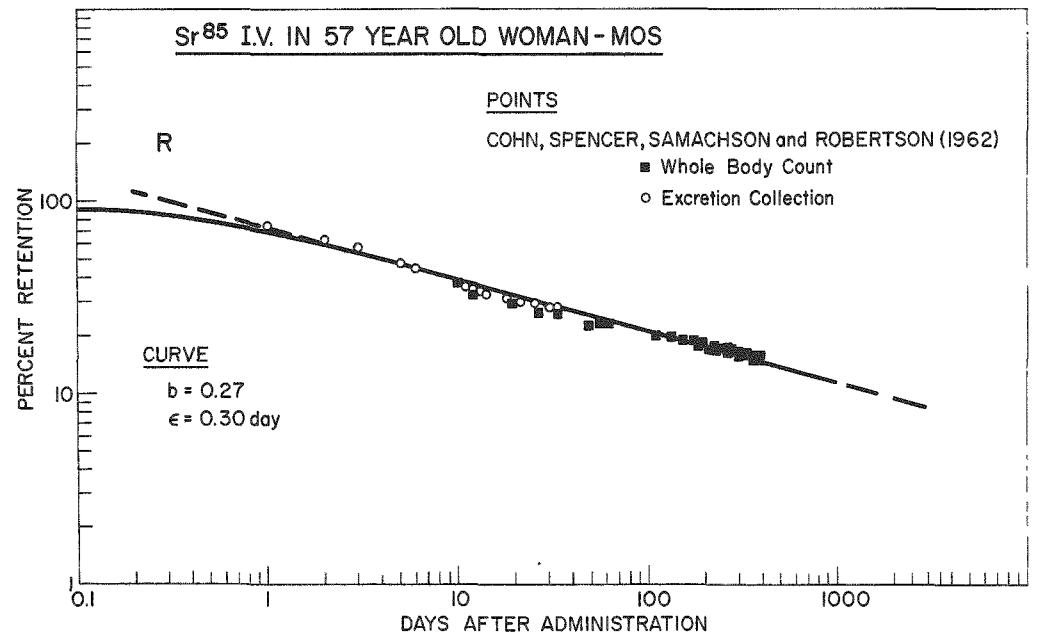

Figure 7

Data for the retention of Sr^{85} in a 57-year-old woman [Cohn et al.[14] Patient code MOS]. The whole-body counter data between 33 and 397 days was fitted by the expression $0.52\ t^{-0.2}$. The present model requires a different fit, as shown. Perhaps an exponential plus a power function would be more accurate, but the additional complexity does not yet seem justified.

Crossover time. Probably the most striking aspect of both the data and the model is shown in Figure 3. After a single intravenous injection, the serum specific activity S crosses and falls below the body specific activity B. In these data there appears to be no tendency for S and B to depart from the power function relations for three years after injection, despite the fact that S was equal to B at about 45 days. Evidently, one must not confuse equality with equilibrium. The fact that the ratio B/S keeps increasing with time indicates that radioisotope equilibrium has not yet been attained. The time at which S crosses B, the crossover time t_x, is given by a simple expression:

$$t_x = b\, c/\eta k \tag{8}$$

which is obtained by setting S from Expression (6) equal to B from Expression (7) and solving for t. [Because t_x is at least a hundred times larger than ϵ (Figure 15), the latter can be completely neglected in Expression (8).]

The ratio B/S is also given by a simple expression over a wide range of times:

$$B/S = t/t_x \qquad \epsilon \ll t \leq t_y \quad . \tag{9}$$

Crossover time appears to be a useful concept. Although it is difficult to measure exactly, knowledge of even its order of magnitude, which varies under different metabolic conditions (Figures 3-5), is valuable for the understanding of experimental data. For example, wherever new bone is formed within the skeleton, it appears to have approximately the same specific activity as the serum at the time of its formation.[15-18] Therefore, bone which forms at a time t_x after a single intravenous injection of an alkaline-earth radioisotope may be expected to have the same specific activity as the body as a whole, and bone which forms earlier or later than this time should have a specific activity which is proportionately higher or lower, respectively, than that of the body. Thus, Expression (9) is useful in the interpretation of autoradiographs and in the evaluation of distributions of radiation dose within the skeleton.

Relation to Internal Metabolism

In the previous section, power-function expressions were developed which represent the behavior of a radioisotope in the serum and in the body following an intravenous injection. Here these expressions will be subjected to the mathematical method of analysis developed by Bauer, Carlsson, and Lindquist.[19] First, consider the method itself.

The Bauer-Carlsson-Lindquist Equation. The basic assumption of the BCL method can be rephrased as the third postulate:

> (III) At any time following its introduction into the serum, the activity of a radioisotope in the body (or in part of the body) can be separated conceptually into two fractions, the first changing in proportion to the serum specific activity, S, the second changing in proportion to the time integral of S.

In mathematical form, this postulate is the BCL equation:

$$q\,R = E\,S + A\int_0^t S\,dt \qquad (10)$$

where E is a quantity (grams of calcium), and A is a rate of transfer (grams of calcium per day). Time zero refers to the time at which activity q was introduced into the serum. Here, the fractional retention R is any function of time.

An approach to the physiological meaning of A and E can be made by examining Expression (10). Whatever radioactivity has equilibrated with S, and hence is changing in proportion to S, will be part of the first or equilibrated fraction ES. Thus, E itself is directly related to the amount of body calcium which is capable of equilibrating with serum calcium within a given time (at least when a radioisotope of calcium has been used as the tracer). Whatever radioactivity has transferred from the serum to sites in the body, from which sites it has not yet returned to the serum, will be part of the second or uptake fraction $A\int_0^t S\,dt$. Thus, A itself is directly related to the rate of uptake of calcium from the serum to deposits whose holding times for calcium are greater than a given time.

The skeletal system has such a wide distribution of holding times for calcium that if one chooses a longer time of reference, more calcium will be capable of equilibrating with serum calcium. Therefore, E may be expected to increase with time when Expression (10) is applied to experimental data. This time-dependence has given rise to some doubt as to the physiological meaning of E. However, an experimental dependence of E upon the time of its measurement, relative to the time of injection with a radioisotope of calcium, is simply a reflection of the complexity of the body, a system which includes short-term liquid deposits, long-term solid deposits, and a multitude of deposits whose terms are intermediate.

Thus, the meaning of E can be generalized: E is not just a single parameter, having a single value in an invariant system, but a parameter distribution, representing a whole spectrum of values for a given system. If one measures E a few minutes after injection, one obtains a measure

of the amount of calcium in the extremely short term deposits of the part of the extracellular fluid near the vascular system. If one measures E years after injection, its value may approach that of total-body calcium because then it includes the calcium content of all deposits whose holding times, or turnover times, or terms for calcium are describable in years. So the usual measurement of E at a time of about 5 days after injection, which may be designated E_5, is a measure of the calcium content of all those deposits which have terms of less than five days (whether the term is limited by resorption or by exchange). And similarly, A_5 is a measure of the rate of uptake from the serum of calcium destined for deposits which have terms of more than 5 days. These measures are not exact because deposits whose terms are comparable to the time of measurement will straddle the two conceptual fractions. However, it seems unlikely that the third postulate will be replaced by another postulate of comparable simplicity because two fractions, separated by a time of measurement, have a natural symmetry. [Existing analytical methods such as that of Heaney and Whedon[5] are here considered as variants from the same two-fraction postulate.]

So far, the most useful aspect of the parameter distributions A and E is the experimental fact that A_5 shows a rather close correspondence to the rate of accretion of calcium accompanying the formation and mineralization of new bone.[2, 12, 17] Thus, published values of A_5 have been referred to as accretion rate (Bauer) or bone formation rate (Heaney). When A is measured between 3 and 7 days after injection, it may be designated A_5. The method of solution of the BCL equation for A and E at a single time t, is not given here,* but it is practically equivalent to the two-time method ordinarily used if time t is taken to be the mean of the two times. Values of A_5 are now available for a variety of experimental animals and for different metabolic conditions in man, so A_5, which in most contexts can be called the accretion rate, is a useful parameter for the characterization of the metabolic state of a skeletal system.

The power function model. Now if one substitutes R from Expression (5) and S from Expression (6) into Expression (10) and solves for A and E, remarkably concise expressions result:

$$A = \eta k\, R/(b + 1 - R) \tag{11}$$

$$E = \eta k\, (t + \epsilon)/(b + 1 - R) \tag{12}$$

in which A and E are time-dependent because R represents the power function expression for retention. As the time increases, A slowly decreases because R decreases; physiologically this results from the return of radioactivity to the serum from progressively more and more deposits

*To appear in a subsequent report.

as the time becomes comparable to, and then exceeds, their terms. These deposits are meant to include both those in a liquid state and those in a solid state. They are distributed both macroscopically and microscopically - macroscopically in different regions of bone or soft tissue, and microscopically in different locations from the blood vessels through intervening fluid to the bone crystals. On the other hand, E increases with time until at long times, when long-term deposits are included, it becomes comparable to the total weight of calcium in the body. Expression (11), plotted in Figures 8 and 9, provides the link between the metabolic parameter distribution A and the parameters of the power function model.

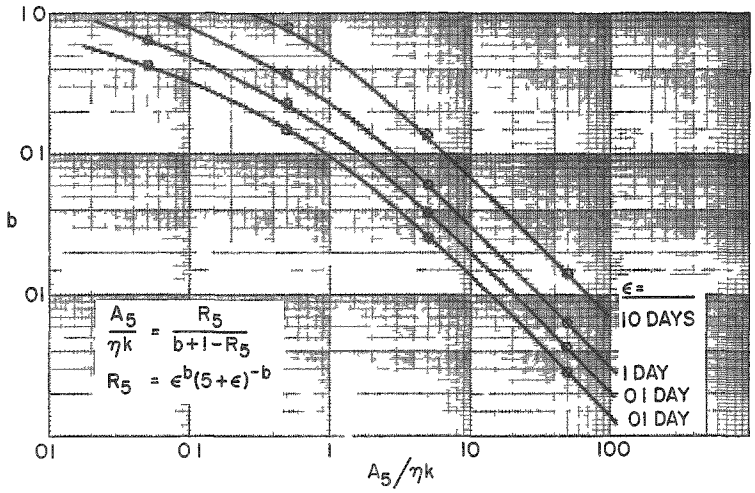

Figure 8

The relation between the power function parameters b and and the metabolic parameters A_5 (accretion rate) and k (excretion rate) The family of curves is calculated from Expression (11) for t = 5 days.

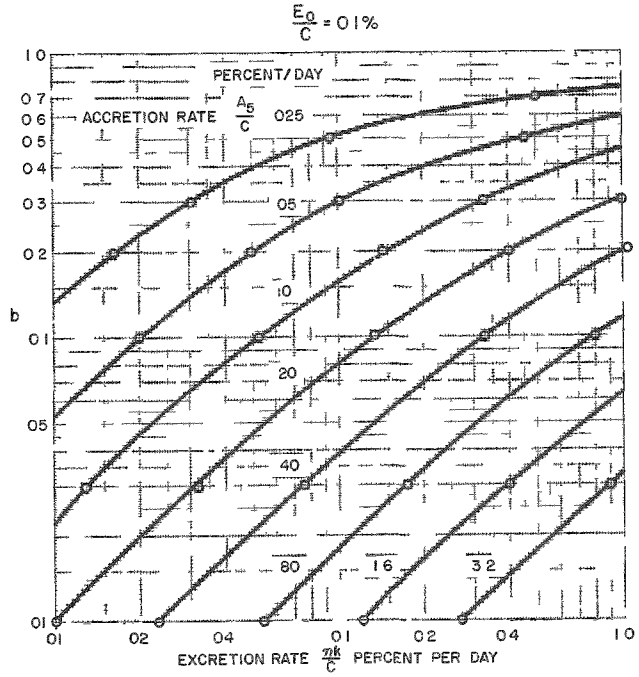

Figure 9

Relation between b, A_5, and ηk for constant initial pool E_0 calculated from Expression (11). This plot provides an estimate of the sensitivity of the power function parameters to changes in accretion or excretion rate prior to injection. Here E_0/c = 0.1%.

The values of A and E for time zero reveal the physiological significance of the parameter ϵ. The apparent weight of calcium with which a radioisotope has equilibrated immediately following injection is

$$E_0 = \eta k \epsilon / b \tag{13}$$

and the apparent rate at which calcium is leaving this initial pool is

$$A_0 = \eta k / b \quad . \tag{14}$$

Therefore ϵ, which is identical to E_0/A_0, is the turnover time of the initial pool as simulated by the power-function model.

Thus, the Bauer-Carlsson-Lindquist equation and the power-function model are mutually elucidating, and not only at short times after injection. There is something unphysiological about the power-function Expression (12) for E; as time t increases, E continues to increase without limit, and this is a physiological impossibility. The radioisotope might be a tracer for calcium, and the rates of transfer of calcium within the body might be constant, so that the parameter distributions A and E would be invariant. It turns out that the trouble stems from the fact that the time integral of R, as given by the power function model, has no upper limit at long times. But the way to correct this discrepancy between the mathematical model and what is physiologically reasonable, without introducing any more adjustable parameters, is to go back to the beginning of the analysis and pursue a consequence of the excretion postulate that is completely independent of both the power-function and the BCL equation.

Equilibration Time

If one integrates Expression (4) from the time of injection until the time t, one obtains the excretion postulate in an equivalent and perhaps more familiar form:

$$\int_0^t S \, dt = q(1 - R)/\eta k \quad . \tag{15}$$

This merely states that the time integral of the serum specific activity times the excretion rate, ηk, is equal to the activity which has been excreted up to any time, t, following an intravenous injection.

A similar expression results from integration of Expression (4) if one asks the mathematically similar question as to how S would behave as a function of time after the start of a series of closely-spaced intravenous injections:

$$S = \dot{q} \, (1 - R)/\eta k \tag{16}$$

where $\dot{q}$ is the rate of introduction of activity into the serum, and R is any function of time which describes the retention of activity following a single intravenous injection. The companion expression for the average specific activity of the body follows from integration of the expression $Bc = qR$,

$$B = \dot{q} \int_0^t R \, dt/c \quad . \tag{17}$$

Expressions (16) and (17) can be used with Expression (1) to obtain S and B for continuous radioisotope intake in food or water.

In performing the integrations which result in Expressions (16) and (17), a fourth postulate has been implicitly introduced, which can be made explicit as follows:

> (IV) The function R, which describes the retention of a radioisotope following a single intravenous injection in a particular instance, is not dependent upon the age of the body at the time of injection.

This postulate of age-invariance is a powerful tool because it permits integration of the function R, but it must not be used indiscriminately. It seems to hold for considerable periods during the growth of an animal, provided the rate of growth does not change too much. It also seems to hold for adult animals. It should not be expected to hold through adolescence. Note in Figure 1 that postulate (IV) is not needed in many applications and can be tested independently for adult man using fallout data.

A fifth and last postulate completes the set that seems to be required for a comprehensive model:

> (V) If a skeletal system were subject to a continuous introduction of radioactivity into the serum at a constant rate for an endless time, the body specific activity B would eventually become equal to the serum specific activity S.

Subject to this postulate, which has numerous physiological implications concerning discrimination between radioelements and the availability of aging bone, one can set S from Expression (16) equal to B from Expression (17) and let time t increase without limit with the result that

$$\int_0^\infty R \, dt = c/\eta k \quad . \tag{18}$$

This beautiful and powerful result was found by Brues and Tyler,[20] who generalized from the approach of compartmental analysis. It means that,

whenever the postulates (I) (IV) and (V) are true, there is a definite mean time of retention for the atoms of a radioisotope within the body, a time which does not depend on the particular form of R but is given solely by the ratio of the weight, c, of calcium in the body to the excretion rate ηk. It means that the area under a curve of R versus time is a physiologically characteristic time $(c/\eta k)$.

An exponential termination for the power function model. Expression (18) provides a limit for the physiological applicability of the power function. From the behavior of E in Expression (12), it is clear that this limit is related to the time required for the equilibration of all the calcium in the body. A system in which a tracer has equilibrated acts as a single compartment with respect to that tracer. If one assumes that the radioisotope equilibrates within the body at a time t_y after a single intravenous injection, then subsequent to that time and subject to postulate (IV), both B and S must be exponential functions of time. The exponential expression for the retention R, which fits smoothly both in value and in slope with the power function expression for R at a time t_y, is the following:

$$R = \left(\epsilon^b t_y^{-b} e^b\right) e^{-bt/t_y} \qquad t \geq t_y \qquad (19)$$

where t_y is the equilibration time for the body as a whole, and R has been determined by requiring that both its value and its time derivative be equal to those of Expression (5) at time t_y. Now, if both Expressions (5) and (19) are substituted for R in Expression (18), the time t_y can be found in terms of the parameters of the power function model:

$$t_y/t_x = (1-b)^{1/(1-b)} (t_x/\epsilon)^{b/(1-b)} \qquad (20)$$

This remarkable expression is plotted in Figure 10. It means that under certain conditions (postulates IV and V), the power function model is able to predict its own limit of applicability. The transition from power function to exponential function would actually occur gradually rather than at a single time, but the latter seems to be the most reasonable behavior that can be simulated by a three-parameter model.

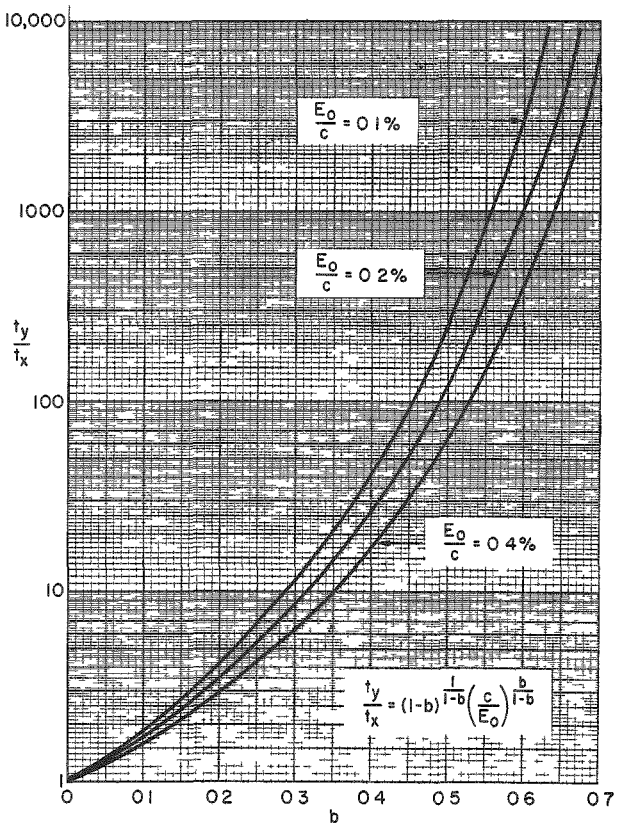

Figure 10

Relation between equilibration time and crossover time calculated from Expression (20). Note that $E_0/c = \epsilon/t_x$.

In fact, Expressions (19) and (20) appear to be well-behaved even for the very small values of b that are characteristic of rapidly-growing puppies: as b approaches zero, t_y approaches t_x, t_x itself becomes very short (a few days), and the retention function for the complete model [Expressions (5) and (19)] approaches $R = e^{-(\eta kt/c)}$. This is just the behavior one would expect for a rapidly-growing animal. Bone enlarges not by expansion but by apposition at some microscopic surfaces and resorption at others. (If two markers were fixed anywhere in one bone at any age, and no cartilage intervened, then the distance between those markers would remain the same for the life of the bone.) In other words, rapid growth requires rapid remodelling of existing bone, so that the body of a rapidly-growing animal, not long after injection of a tracer, should act as a single compartment.

Thus, equilibration time t_y appears to have an extremely wide range of applicability to skeletal systems, from a few days for calcium in young puppies to many tens of years for radium in man (Figure 15).

Discussion

The power function model is now complete. Having started with the three parameters ηk, b, and ϵ, and having related them to metabolic parameters through the BCL equation, we now find that the behavior of the model can, under certain conditions, be equally well determined by three characteristic times, the turnover time ϵ of the initial pool, the crossover time t_x, and the body's equilibration time t_y. The behavior of the model can be summarized by geometry on log-log graph paper (Figure 11), and it is often more convenient to use these graphical relationships than the power function expressions on which they are based.

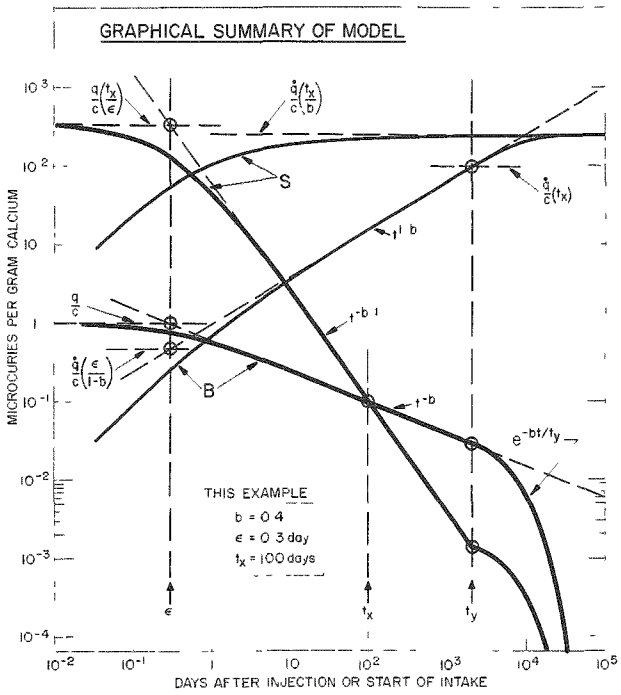

Figure 11

Graphical summary of the model: body specific activity, B, and serum specific activity, S, following a single intravenous injection, q, (descending curves) or following the start of a continuous injection at rate $\dot{q}$ (rising curves). (q/c is plotted equal to 1 μc/g calcium, $\dot{q}/c$ equal to 1 μc/day/g calcium. c is body calcium in grams.)

Note particularly that when, after a single injection, the tracer has equilibrated within the body so that S and B are exponential functions, S and B are far from equal. This means that the body will act as a single compartment despite the fact that on a microscopic scale the distribution of radioactivity may be far from uniform.

Now, how can this model be used to plan and to interpret experiments upon skeletal systems? First, it provides a simple means for comparing existing data from different types of experiments. Second, it provides an estimate for the concentrations of a tracer that might be found in a future experiment. The model probably will never be able to answer currently practical questions such as how to remove lethal amounts of radioactivity from the skeleton, but it does provide an additional tool which may help to solve such problems.

An example of the first use occurs in the study of the retention of radium in the human body. Long-term studies of the uptake of radium in persons exposed to a higher-than-normal level of radium in their drinking water[21] may provide a direct measurement of the equilibration time. Current measurements of the radium content of the blood of radium-dial painters 30 to 40 years after their ingestion of radium are being compared with Expression (9). This should lead to better estimates of the excretion factor, η, for radium in man, which in turn may help us to understand the short term retention of radium and its possible relation to the high accretion rates reported by Bauer et al.,[2] for barium in man and in rat. Such an intercomparison of data may clarify the mechanism by which radium is held in bone at the level of the individual bone crystal.

As examples of the second use of the model, a number of predictions can be made. When the power function parameter b is as small as 0.2, the equilibration time should become short enough to be readily observable. It might become useful in the prediction of radiation dose. Ironically, the predicted equilibration time for radium in dogs that were about 1.3 years old at injection, based on the data shown in Figure 3, is so short that there is a clear contradiction between data and model: about a year after injection B should start to fall noticeably below and S to rise noticeably above the power function lines. This disagreement is probably due to dependence of R upon the age at injection and hence, due to partial failure of postulate (IV), but exponential behavior of B and S is now expected for these dogs.

No such exponential behavior is yet apparent in the data for radium in man at even 20-29 years after radium intake.[22] But this does not contradict the theory because the best estimate of equilibration time for radium in man is very much longer than for radium in dogs (Figure 15).

The most startling prediction of the theory is that the level of radium in human serum 40 years after radium intake should be only

one hundredth the body average. In other words, B/S should be the order of 100. Preliminary confirmation of this large factor has now been obtained.[23] Whether it will now be possible to observe an exponential trend in B and S for radium in man remains to be seen. The difference between the power function and the exponential function is probably not detectable except at times as long as $2(t_y)$, and t_y itself is not yet known accurately for man.

Surprisingly, the model works quite well for a rapidly-growing puppy (Figure 4) during a period of time in which one might have expected quite rapid changes in physiological state. The reason seems to be that rapidly-growing animals have a very high accretion rate A_5, and this, the model shows (Figure 8), is accompanied by a very small value of b. Thus, although b may be changing with time, it is so nearly zero that the changes are not significant. This suggests that the complete model - the power function together with the exponential termination - may be tested not only many years after injection of the tracer (as for radium in man) but also within the first year in growing puppies and adult dogs. There is an inverse correlation between accretion rate and equilibration time which should produce a peculiar anomaly in the retention of an alkaline earth radioisotope, as shown in Figure 12. The retention at about a year after injection should be less in very young puppies and in older dogs than it is in puppies with intermediate accretion rates. Actually, pertinent data now being submitted for publication by C. F. Decker, L. A. Kaspar, and W. P. Norris of this Laboratory played a large part in suggesting this effect. Of course the model cannot be expected to hold through the adolescence of these puppies because their growth rates then drop so markedly.

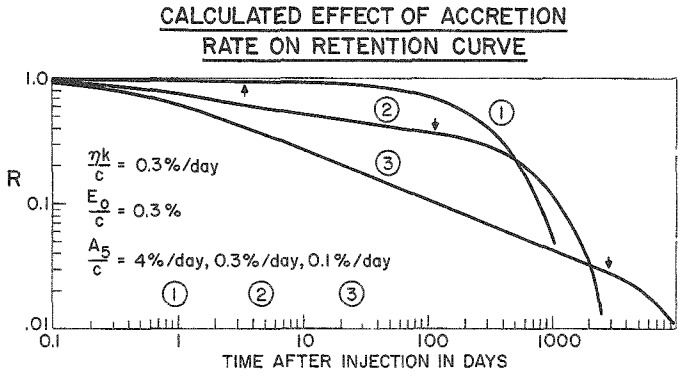

Figure 12

The effect of accretion rate A_5 upon the shape of the retention curve according to the present model. A high accretion rate reduces the slope b so that initially there is high retention, but it also reduces equilibration time t_y (indicated by the arrows) so that retention becomes exponential thereafter. This effect should be observable in young puppies as compared to older dogs. The rapid decrease of accretion rate at adolescence would arrest the exponential fall in retention, an effect not included in the model.

The extent to which the postulate of age-invariance (IV) is an adequate description for the adult human body will probably be determined eventually by direct experiment. But in the meantime, the extensive data for the uptake of Sr^{90} in man as a result of the testing of nuclear weapons gives evidence in favor of age-invariance. Kulp and Schulert[4] found that there was practically no age-dependence of the quantity of Sr^{90} in hundreds of adult skeletons from New York City. Thus, the time integral of R (Expression 17) appears to be independent of age over a period of several years after injection. The rise in the concentration of Sr^{90} in the food during the period from the beginning of testing until the time of observation can be simulated in the model by integration of Expression (7). When F is chosen to fit the observed specific activity of the food, the observed specific activity of the body can be well-approximated by the power-function model (Figure 13). Fortunately, the values of the parameters which give a good fit to the fallout data are approximately the same as those which fit data for the retention of Sr^{85} in man (Figure 7). These parameter values are also approximately equal to those which yield the accepted values for accretion rate A_5 and exchangeable pool E_5. Thus, the theory appears to be capable of interrelating a number of different experimental approaches to skeletal metabolism.

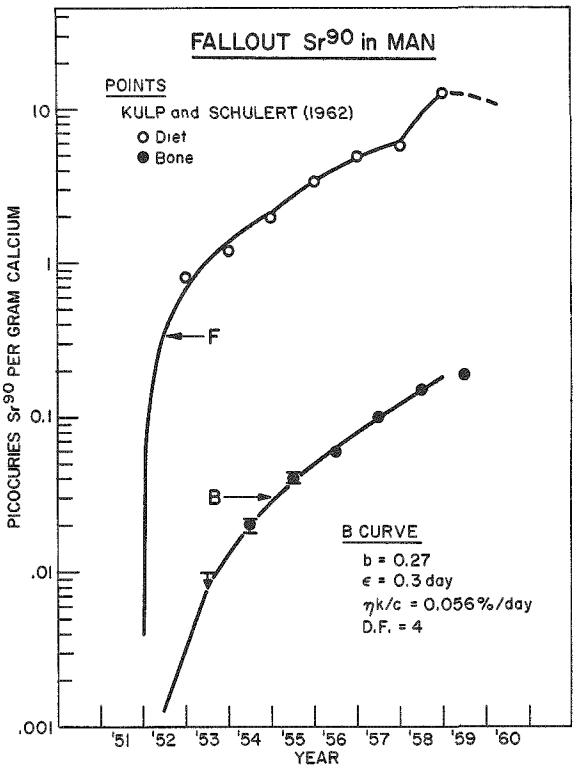

Figure 13

Data for Sr^{90} in the diet and in whole skeletons from New York City [Kulp and Schulert[4]]. Curve B is given by Expression (21) in the appendix, to appear in a subsequent report.

Terminology

Because several previously-non-overlapping fields are involved, considerable effort has been made to simplify and yet conform to the accepted usage of letter symbols. In this paper, F is for food, S is for serum, B is for body, and R is for retention. The quantity q and the rate $\dot{q}$ of introduction of a radioisotope into the serum correspond to their electrical analogues, charge and current. Similarly, c stands for body calcium or capacity. A and E have been given a personality by Bauer. R and b are familiar in the power function world (but here b itself is positive). η is an excretion factor, μ an absorption factor, t a time, e is 2.718, and ϵ is the small time which is usually neglected in the final mathematical expression. The parameter ϵ is similar to, but not identical with, Tyler's γ and Heaney's θ (it's usually smaller than γ or θ): θ must satisfy S, γ must

satisfy R, but ϵ must satisfy R, S, A, and E. All the expressions are dimensionally correct, so that units need not be specified; the suggested unit merely helps to fix ideas. Symbols which represent functions of time are capitalized, while constants or physiological parameters are lower case. When a capital letter has a subscript, it refers to the particular time in days given by the subscript. F, S, and B all stand for activities per unit weight of calcium and do not imply how, or during what length of time, the alkaline earth radioisotope has been introduced into the body; on the other hand, R refers to the body's fractional retention of the radioisotope as a function of time following a single injection into the serum or central exchange.

Possible Significance of the Power Function

To base a model upon the power function with only pragmatic justification leaves one with a feeling of dissatisfaction. Data can often be fitted more closely by other more complicated functions, such as a series of polynomials or a series of exponential functions. The exponential function, through its appearance in the phenomenon of radioactive decay and in the mathematical solutions of compartmental models, has acquired physiological respectability, and it is sometimes forgotten that it is only a statistical approximation to the behavior of a system. In particular, the exponential function is a statistical property of a system as observed with a tracer which has equilibrated within the system. The power function may also be a statistical property of a system, observable when the time of observation with a tracer after its injection is much less than the time necessary for equilibration within the system. Power function, here, is meant to indicate the form $R = \epsilon^b(t+\epsilon)^{-b}$ because only to this dimensionally-correct form would one expect to attach significance.

Now, if retention of bone-seekers were the only instance in which the power function has appeared, one would hesitate to speculate. There appears to be no reason why a skeletal system, no matter how complex, should have the required correlation between the sizes of deposit and their rates of transfer. But curiously, the power function turns up in other fields which deal with complex systems. There is the decay of radioactivity in a mixture of fission products as a function of time since their production in a nuclear explosion.[24] There is the diffusion of a tracer into a continuous medium.[25] Even the experimental curves of the frequency of the use of a word as a function of its rank in the frequency scale in a number of different languages have been well fitted by the power function.[26] Of course, one might fall back on the familiar adage that all data approximate straight lines on log log paper, but surely this does not apply to data which cover four or five orders of magnitude in two dimensions. Furthermore, the retention of Sr^{85} as a function of time following injection in men which have decidedly abnormal metabolism is <u>not</u> closely represented by the power function model (Figure 14).

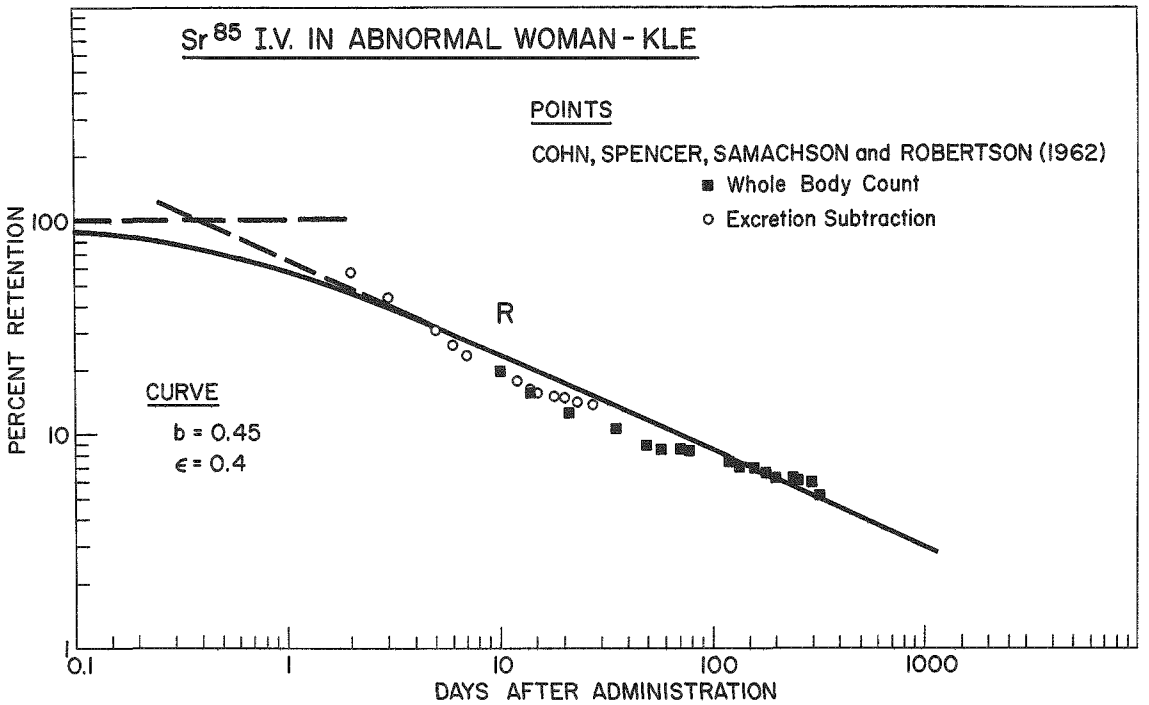

Figure 14

Data for Sr^{85} retention in a woman with extremely high urinary calcium (514 mg/day) from Cohn et al.[14] (Patient Code KLE.) and Spencer and Samachson.[13]

It is an interesting possibility that the power function may be the natural description for the behavior of a tracer in a complex system whose component sizes have evolved by growth under the dynamic control of the same mechanisms and constraints that now determine the internal rates of transfer. In short, the power function may be a statistical property of optimum systems.

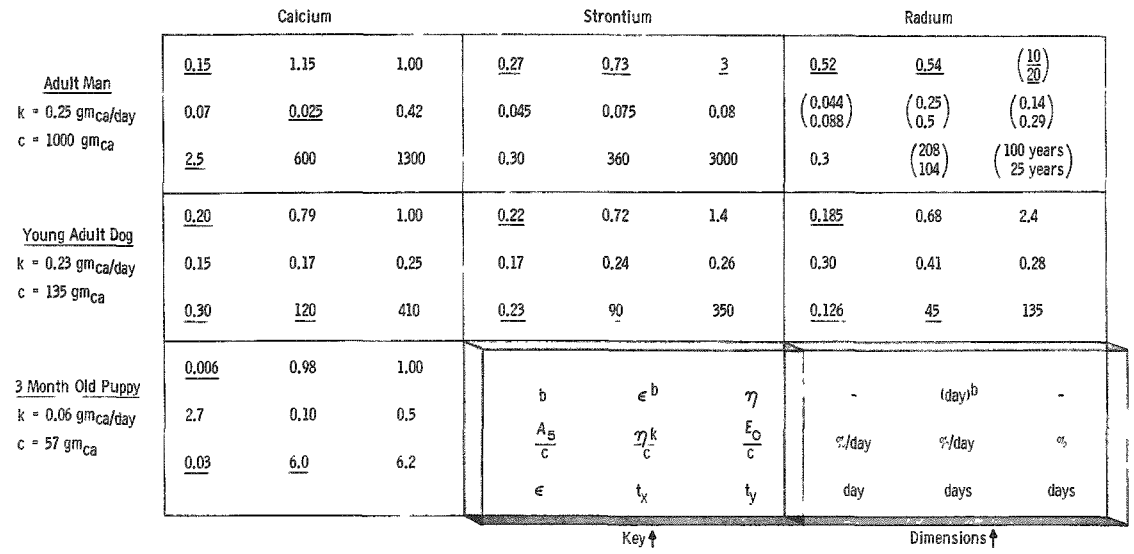

Figure 15

Sample values for the parameters. Symbols and dimensions appear in corresponding positions in the two squares at the bottom right of figure. The numbers in each square were calculated from those underlined.

Data for Ca^{45} in puppy come from Lee et al.[12] (Figure 4); for Ca^{45} in young adult dogs from Maletskos[8] (until 100 days after injection); for Sr^{90} in 1.3 year old beagles from Stover et al.[27] (until 2 years); and for Ra^{226} in 1.3 year old beagles from Van Dilla et al.[11] (Figure 3). The model represents these data for B and S within 20-30% from 0.01 day onwards, except that t_y appears to be too short at least for radium because no departure from the power function lines is apparent by 1000 days. This may result from the age-dependence of retention reported by Glad et al.[28]

The values for calcium in man have been chosen to approximate the normal serum-urine curve of Heaney and Whedon[5] (Figure 6); the values for strontium in man approximate the retention curve of Cohn et al.[14] as in Figure 7 - the value of η was estimated from Spencer et al.;[29] the values for radium in man are based on b and ϵ^b as given by Norris et al.,[30] together with two estimates of η that yield reasonable values of A_5, t_x, and t_y. The values of t_x for man may overestimate the actual crossover time by a factor of two because of the kind of departure from power function retention shown in Figure 7. The model appears to be less accurate for man than for dogs, particularly for strontium serum-urine data [Bishop et al.[31]].

References

1. Norris, W. P., S. A. Tyler and A. M. Brues. Science 128, 456 (1958).

2. Bauer, G. C. H., A. Carlsson and B. Lindquist. Mineral Metabolism, Vol. 1, Part B., ed. C. L. Comar and F. Bronner. Academic Press, New York, 1961.

3. Tyler, S. A. Argonne National Laboratory Biological and Medical Research Division Semiannual Report, July through December 1957. ANL-5841, p. 132.

4. Kulp, J. L. and A. R. Schulert. Science 136, 619 (1962).

5. Heaney, R. P. and G. D. Whedon. J. Clin. Endrocrinol. and Metab. 18, 1246 (1958).

6. Bryant, F. J. and J. F. Loutit. Report AERE-R-3718 (1961).

7. McLean, F. C. and M. R. Urist. Bone. University of Chicago Press, Chicago, 1961.

8. Maletskos, C. J. PhD Thesis, Massachusetts Institute of Technology, 1954.

9. Bauer, G. C. H. and R. C. Ray. J. Bone and Joint Surg. 40A, 171 (1958).

10. Aubert, J. P. and G. Milhaud. Biochim. Biophys. Acta 39, 122 (1960).

11. Van Dilla, M. A., B. J. Stover, R. L. Floyd, D. R. Atherton and D. H. Taysum. Radiation Res. 8, 417 (1958).

12. Lee, W. R., J. H. Marshall and H. A. Sissons, in preparation, 1963.

13. Spencer, H. and J. Samachson, unpublished data, 1963.

14. Cohn, S. H., H. Spencer, J. Samachson and J. S. Robertson. Radiation Res. 17, 173 (August 1962).

15. Cohen, J. C., C. J. Maletskos, J. H. Marshall and J. B. Williams. J. Bone and Joint Surg. 39A, 561 (1957).

16. Marshall, J. H., Jennifer Jowsey and R. E. Rowland. Radiation Res. 10, 243 (1959).

17. Marshall, J. H. In Bone as a Tissue, ed. K. Rodahl et al. McGraw-Hill, New York, 1960. p. 144.

18. Rowland, R. E. Radiation Res. 15, 126 (1961).

19. Bauer, G. C. H., A. Carlsson and B. Lindquist. Kungl. Fysiograf. Sällskap. Förhandl. (Lund) 25, 1 (1955).

20. Brues, A. M. and S. A. Tyler. Atompraxis 5, 253 (1959).

21. Stehney, A. F. and H. F. Lucas. Proc. First Intern. Conf. on Peaceful Uses of Atomic Energy. United Nations, Geneva, 1955. Vol. 11, p. 49.

22. Marinelli, L. D. Radiology 78, 544-552 (1962).

23. Lucas, H. F., C. E. Miller and L. A. Barrer, unpublished data, 1963.

24. Way, K. and E. P. Wigner. Phys. Rev. 73, 1318 (1948).

25. Barrer, R. M. Diffusion in and through Solids. Cambridge University Press, Cambridge, 1951. pp. 45-46.

26. Brillouin, L. Science and Information Theory. Academic Press, New York, 1962. pp. 44-47.

27. Stover, B. J. and D. R. Atherton. Proc. Soc. Exptl. Biol. Med. 99, 201 (1958).

28. Glad, B. W., C. W. Mays and W. Fisher. Radiation Res. 12, 672 (1960). (footnote)

29. Spencer, H., Margaret Li, J. Samachson and D. Laszlo. Metabolism 9, 916 (1960).

30. Norris, W. P., T. W. Speckman and P. F. Gustafson. Am. J. Roentgenol. 73, 785 (1955).

31. Bishop, M., G. E. Harrison, W. H. A. Raymond, A. Sutton and J. Rundo. Intern. J. Radiation Biol. 2, 125 (1960).

DECAY-TIME APPARATUS

O. J. Steingraber and I. B. Berlman

The apparatus developed by one of the authors[1] was designed to measure the decay time of organic scintillation crystals, plastics, and solutions. A special feature of this system is its ability to accept pulses random in time and amplitude, and, therefore, excitation of the scintillation material can be obtained from either α particles, β particles, or uv radiation.

The α and β sources are deposited on stainless steel rods and housed in miniature cells similar to those described in Reference 2. Small cells are used so that only a small region of the photocathode is exposed to radiation to reduce the time dispersion of each pulse. The strength of the source was specifically chosen to minimize counting time.

For excitation by pulsed uv radiation, special hydrogen flash lamps were built. Since the mean half-width of the discharge is a function of both the electrode spacing and the hydrogen pressure, closely spaced (8-15 mils) tungsten electrodes were linearly positioned in the tube, and the tubes were filled to a pressure just below atmospheric pressure. The brightest and most stable operating tubes were constructed with one electrode having a blunt hemispherical tip (positive) and the other electrode a pointed (45°) tip (negative). After the sparking potential had been reached, the operating voltage was in the region of 2600 volts. It is estimated that 10^8 photons are emitted per pulse.

Figure 16 shows the pulse contour of a flash from a hydrogen tube using a neutral filter as seen by the 56 UVP photomultiplier tube. It is believed that the half-width of the flash itself is less than a nanosecond and the half-width of 3.2 nanosecond, as shown in the figure, is primarily the contribution of the impulse response function of the apparatus. Note should be taken that there is essentially no ringing beyond the main pulse.

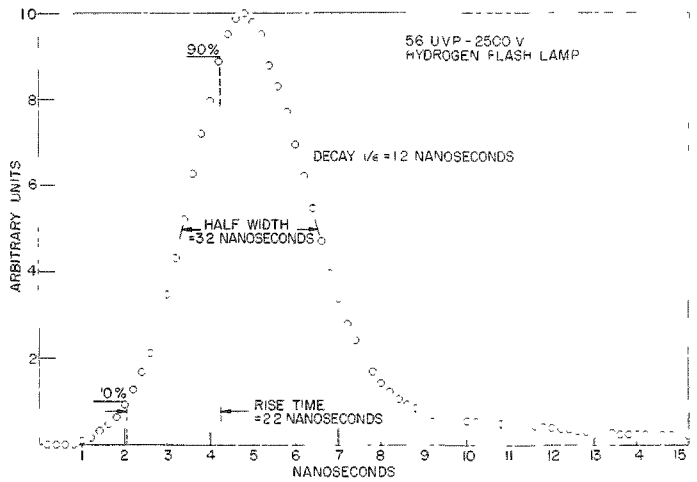

Figure 16

Pulse contour of a flash from a hydrogen tube using a neutral filter as seen by the 56 UVP photomultiplier tube

The pulse contour of a stilbene crystal excited by α and β particles is shown in Figure 17. The mean decay time of this crystal is 4.6 nanoseconds. This value compares favorably with that obtained by another technique, which employs a pulsed electron beam.[3] A slight variation in short decay times with photomultiplier voltage remains as yet unresolved.

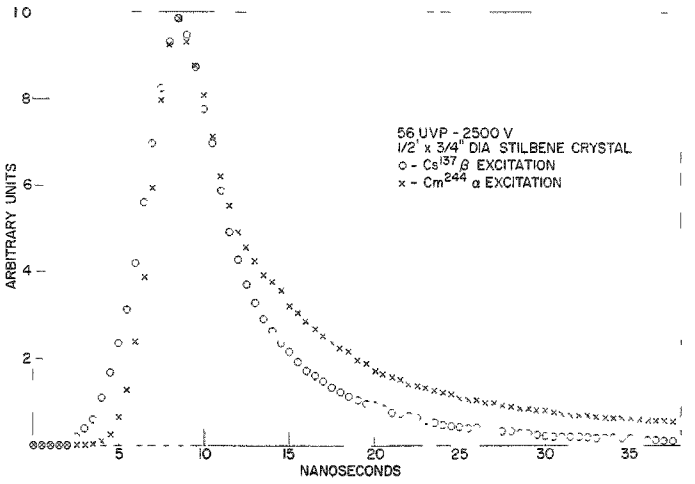

Figure 17

The pulse contour of a stilbene crystal excited by α and β particles

We wish to thank B. G. Oltman for his assistance in filling the hydrogen flash lamps and Dr. Robert K. Swank for some illuminating discussions.

References

1. O. J. Steingraber. "System for Recording Pulse Shapes. Preliminary Report." Argonne National Laboratory Radiological Physics Division Semiannual Report, July through December 1961. ANL-6474, pp. 14-21.

2. I. B. Berlman. "Luminescence in a Scintillation Solution Excited by α and β Particles and Related Studies in Quenching." J. Chem. Phys. 34, 598-603 (1961).

3. R. K. Swank, H. B. Phillips, W. L. Buck and L. J. Basile. "Decay Times of Scintillators." I.R.E. Trans. NS-5, 183-187 (1958).

NANOSECOND FLUORESCENCE DECAY-TIME MEASUREMENTS*

I. B. Berlman

Abstract

A new versatile apparatus has been used to measure the fluorescence decay times of four series of related compounds, each dissolved in an appropriate solvent. The solutes were excited directly by pulsed monochromatic radiation, and the pulse contour of the emitted radiation was recorded. Molecular types were 1) simple polynuclear compounds, such as diphenyl, p-terphenyl, etc; 2) compounds with condensed benzene rings, e.g., naphthalene, anthracene, etc; 3) oxadiazole compounds; and 4) oxazole compounds. All the solute molecules chosen have a high fluorescence quantum yield. The oxadiazole compounds as a class have very fast decay times with BBD [2,5-di-(4 biphenylyl)-1,3,4 oxadiazole] having the fastest decay time of all the compounds tested, 0.9 nsec. In fact, this decay time is the shortest reported to date. Generally, the longer the molecule the shorter the fluorescence decay time.

*To be presented at American Physical Society Meeting, March 25-28, 1963, St. Louis, Missouri.

A STUDY OF THE α/β RATIO IN LIQUID ORGANIC SCINTILLATION SOLUTIONS*

I. B. Berlman

Abstract

The relative intensity of the light pulses produced by α and β particles in a scintillating solution of 2,5 diphenyloxazole (PPO) in xylene has been investigated as a function of the solute concentration. Below a solute concentration of 2 g/l. the α/β ratio is related in an inverse manner to the PPO concentration. From these data the dynamic quenching parameter has been calculated.

Some of the factors which generally influence the α/β ratio in a liquid scintillation solution are discussed. Since the value of the α/β ratio in an organic liquid scintillating solution is usually less and in certain cases appreciably lower than in an organic solid scintillator, it is reasonable to assume that dynamic quenching by the transient radiation products produced by an alpha particle takes place during the excitation lifetime of the solvent and the solute. Corroborative experimental evidence demonstrates the inverse dependence of the α/β ratio on the lifetime of the solvent and/or the solute.

Finally various solvents, with similar characteristics, such as viscosity, etc., each having 8 g/l. of PPO as the solute, have been selectively tested with the viewpoint of investigating the relationship between sensitivity to transient radiation damage and the α/β ratio. Preliminary results are presented.

*Paper presented at International Congress of Radiation Research, Harrogate, England, Aug. 6-10, 1962.

A MEASUREMENT OF THE PHOTOLUMINESCENT QUANTUM YIELD OF LIQUID SCINTILLATORS. A PRELIMINARY REPORT

W. R. Anderson and I. B. Berlman

(Reported by W. R. Anderson*)

Introduction

When ultraviolet light falls on a scintillating solution, some or all of the photons in the beam are absorbed and fluorescence emission takes place. Many investigators have attempted to determine the ratio between the number of photons emitted and the number absorbed, i.e., the quantum efficiency of various scintillators, but the difficulty of the measurement has created fairly large uncertainties in the results.[1,2] Ideally, if the fluorescence emission were distributed uniformly in all directions and the exciting light could be scattered also uniformly by some medium, the ratio between the amounts detected in a particular direction, as in Figure 18, would be the ratio between totals. Although the emission from fluorescent solutions is approximately uniform,[1] that emitted from scatterers is in general non-uniform; hence the two measurements cannot be compared directly. However, there are ways of getting around this difficulty, and we decided to investigate two of those mentioned in the literature. One involves use of a so-called "integrating" sphere,[3] common in photometry measurements.[4,5] The scatterer and the fluorescent sample are illuminated in succession at the center of a sphere having a highly diffusing interior surface. Through multiple reflection the sphere homogenizes the light, so that the luminosity of the interior surface is a measure of the total flux. The other involves an analysis of the degree of polarization of the radiation of both the scatterer and the fluorescent solution in the direction of the detector.[2] The degrees of polarization, the ratio of measured intensities, and the ratio of total fluxes bear a known relationship to each other.

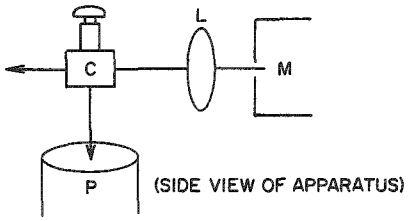

Figure 18

Apparatus for measuring fluorescence emitted from the cell (side view). C is the transparent cell containing scatterer (glycogen in water) or fluorescent sample. L is the quartz lens. M is the Hilger and Watts monochromator with Hg lamp. P is the detector, (a 6903 photomultiplier and an electrometer).

Method I. Use of Integrating Sphere

If a light source is placed inside a sphere the interior surface of which is perfectly diffusing, the interior becomes uniformly illuminated,

*University of Illinois, Chicago, Illinois.

whether or not the source emits uniformly in different directions, and the luminosity of the surface at any point is proportional to the total emission from the source.[3,4,5] We are using this principle in the arrangement indicated in Figure 19. The scatterer and the fluorescent sample are contained in standard quartz cylindrical spectrograph cells 10 mm thick and 22 mm in diameter. Two different spheres have been tried, one made from a hollow white plastic dime-store baseball, and the other machined from Teflon, both with an inside diameter of $2\frac{1}{2}$ in. and entrance and exit apertures $\frac{3}{8}$ in. wide x $\frac{5}{8}$ in. high. Actually, the equivalent of three spheres was tested, since the baseball was tried both uncoated and coated with a smoked layer of MgO.

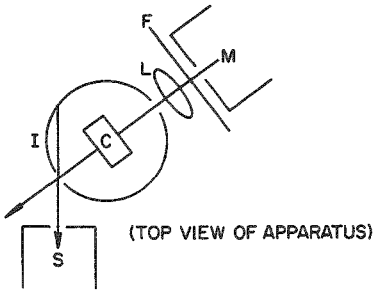

Figure 19

Apparatus for measuring fluorescence reflected from integrating sphere (top view). C is a transparent cell, F is a band-pass filter, I is an integrating sphere, L is a quartz lens, M is a monochromator with Hg lamp and S is a detector (Beckman DK2 spectrophotometer).

The ideal spherical surface is one which will 1) create uniform luminosity, and 2) reflect highly at all wavelengths involved. The first condition is required, but one has difficulty determining whether it has been achieved. Although removal of the top quarter of the spheres showed fairly uniform luminosity and thus indicated possible fulfillment of the first requirement, the results (see Table 1 and Discussion of Results) cast doubt on this. The second condition is desirable but not required since a relative diffuse reflection factor can be determined and the calculations can take the variation in this factor into account. The factor is determined from two measurements made with the Beckman DK2 spectrophotometer, the first using the cell containing the scatterer in the arrangement of Figure 19, and the second with the monochromator beamed directly into the DK2. Readings are recorded at the wavelength at which the Hg monochromator source produces bright lines. The ratio between the two responses, if one assumes perfect scattering by the scatterer, is the relative diffuse reflection factor at each wavelength. Results for the three spheres are given in Figure 20. The uncoated baseball is seen to have been a poor reflector in the ultraviolet region and the MgO-coated sphere only slightly better. The latter result was

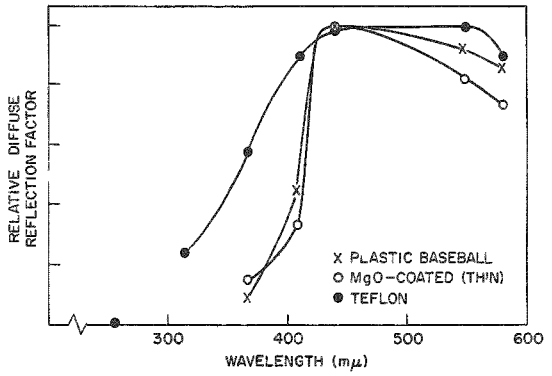

Figure 20

Wavelength response from various reflecting surfaces on the integrating sphere

unexpected and is very likely attributable to the use of too thin a coating of MgO; tests with heavier layers are planned. Teflon does much better; its reflection factor is at a constant high value from 560 to 460 mμ, then drops gradually, but at 313 mμ is still 0.24 of its maximum. No inference should be made from Figure 20 concerning the comparative absolute reflection abilities of the surfaces since the curves are not comparable in this respect.

Following the lead of Weber and Teale,[2] we are using an aqueous solution of glycogen as the scatterer. The suitability of a scatterer is easily tested, since the fraction of a beam scattered by an ideal scatterer varies inversely as the fourth power of the wavelength.[2,6,7] The total fractional attenuation (apparent absorption) of a beam is then given by

$$1 - T = F_S + F_A = k\lambda^{-4} + 0 = k\lambda^{-4} \qquad (1)$$

where T is the fraction transmitted, F_S and F_A are the fractions scattered and (truly) absorbed, respectively, k is a proportionality constant for the particular solution, and λ is the wavelength. When the scatterer is satisfactory, a plot of (1 - T) against λ^{-4} is a straight line through the origin since F_A exists only for an imperfect scatterer. Plots of (1 - T) against λ^{-4} as obtained on our DK2 for the glycogen in use at present (Eastman 590) indicate that the material is failing to meet this requirement, possibly because of impurities. How greatly our results are affected by this situation is difficult to determine.

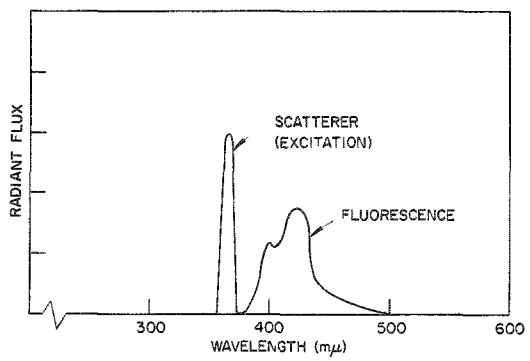

Figure 21

Spectrogram of fluorescence radiation of sample and of exciting radiation

The principal measurement is made with the arrangement of Figure 19. The monochromatic beam falls first on the scatterer and an "energy" curve is obtained on the DK2; then the scatterer is replaced by the fluorescent sample and a second curve obtained. A typical pair of "energy" curves is given in Figure 21. The ratio of the "areas" under the two curves, after taking into account the transmittance of the solution, the reflection factor of the sphere, and the spectral sensitivity of the spectrophotometer (determined previously) is the quantum efficiency of the sample. In the present trials involving a mercury arc excitation at 366 mμ, an Eastman 18A filter is used in the beam to suppress stray light. Let:

N_0 = photon flux of monochromatic exciting beam incident on cell

$\Delta N'$ = photon flux at detector from scatterer

ΔN = photon flux at detector from fluorescent sample

T_0' = fraction of incident beam transmitted by scatterer (and therefore lost)

T_0 = fraction of incident beam transmitted by fluorescent sample (and therefore lost)

k = relative diffuse reflection factor of sphere (luminosity per unit incident flux)

k_0 = relative diffuse reflection factor of sphere at wavelength of exciting light

$\overline{k}$ = relative diffuse reflection factor of sphere (average) over the wavelengths of the fluorescence

s = relative sensitivity of DK2 (number of photons in unit wavelength bandwidth per unit reading of DK2)

s_0 = same at wavelength of exciting light

y' = ordinate of DK2 curve for scatterer

y = ordinate of DK2 curve for fluorescent sample

λ = wavelength of light

q = quantum efficiency of sample

The average relative diffuse reflection factor $\overline{k}$ of the fluorescence can be defined as $\int y \cdot s \cdot d\lambda / \int y \cdot s \cdot k^{-1}\, d\lambda$, where the integrals refer to the fluorescent "energy" curve of Figure 21. The ratio of photon fluxes at the spectrophotometer may be expressed two ways: first, in terms of the quantum efficiency,

$$\frac{\Delta N}{\Delta N'} = \frac{N_0 (1 - T_0) \overline{k}\, q}{N_0 (1 - T_0') k_0} = \frac{(1 - T_0) \left(\int y \cdot s \cdot d\lambda / \int y \cdot s \cdot k^{-1}\, d\lambda\right) q}{(1 - T_0') k_0} \quad , \qquad (2)$$

and second, in terms of the spectrophotometer readings,

$$\frac{\Delta N}{\Delta N'} = \frac{\int y \cdot s \cdot d\lambda}{s_0 \int y' \cdot d\lambda} \quad . \qquad (3)$$

Then from (2) and (3),

$$q = \frac{(1 - T_0') \int y \cdot s \cdot k^{-1}\, d\lambda}{(1 - T_0)\, s_0\, k_0^{-1} \int y' \cdot d\lambda} \qquad (4)$$

which is the ratio of corrected "areas" under the DK2 curves. Results obtained thus far are given in Table 1.

Table 1

Results to date

Trial no.	Fluorescent solution		Glycogen scatterer	Excitation wavelength, (λ_0)	Integrating-sphere method		Polarization-analysis-method
	Material	Fraction of excitation absorbed, ($1 - T_0$)	Fraction of excitation scattered, ($1 - T_0'$)		Sphere used	q	q
1	Anthracene in hexane	0.96	0.75	366 mμ	Uncoated baseball	0.31	0.45
2	Anthracene in hexane	0.99	0.68	366 mμ	Teflon	0.17	0.31

Some comparison values from the literature:

Anthracene in hexane (very dilute) 0.31 [Weber and Teale[2]]

Anthracene in benzene (very dilute) 0.24 [Bowen and Wokes[1]]

Anthracene crystals 0.80-0.83 [Borison and Vishnevski[3]]

Method II. Polarization-Analysis Technique

Weber and Teale[2] show that the ratio between the total fluxes from the scatterer and the fluorescent sample, can be determined if the intensities at right angles to the exciting beam, as in Figure 18, as well as the extents of polarization in that direction, are known. They show that

$$\frac{\text{Ratio of total fluxes (fluorescent sample to scatterer)}}{\text{Corresponding ratio of measured intensities at right angles}} = \frac{3 + p}{3 + p'} \qquad (5)$$

where p is the polarization of the fluorescent sample and p' that of the scatterer. The polarizations are defined by $(I_\perp - I_{||})/(I_\perp + I_{||})$ where (see Figure 18) $I_\perp$ is the intensity of the component with electric vector perpendicular to the direction of the exciting beam and $I_{||}$ that of the component with vector parallel. Since polaroid film is unsuitable as an analyzer, for it transmits poorly below 400 mμ,[8] we have copied Weber and Teale and constructed a quartz-plate analyzer. It consists of a stack of 8 plates, each 1 mm thick, separated by 1-mm air spaces. The index of refraction $\underline{n}$ of fused quartz varies from 1.49 at 300 mμ to 1.46 at 600 mμ;[9] therefore, the angle of incidence for maximum effect over this range (i.e., Brewster's angle, equal to arctan $\underline{n}$) varies from 56.1° to 55.6°. It is fortunate that the setting is not critical and that the effect changes little over several degrees because it was intended that the plates be inclined to produce an angle of 56°; but because of the refraction effect, not taken into account in the design of the assembly, the angle turns out to be about 59°. The principle of operation is indicated in the sketch of the

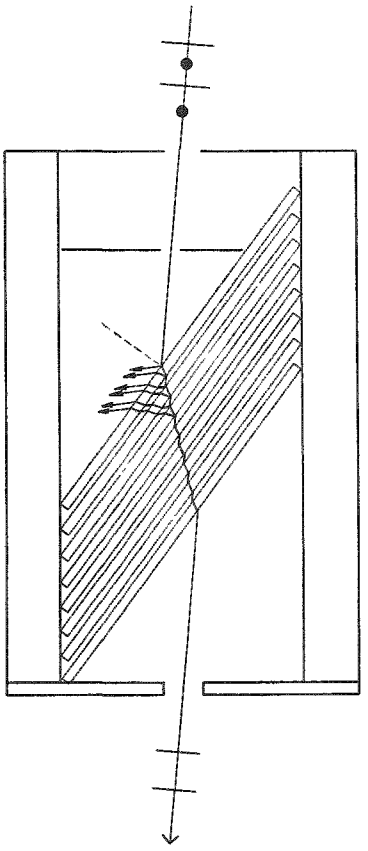

Figure 22

Diagram of uv polarizer made of quartz plate

assembly in Figure 22. Ideally, any component with electric vector perpendicular to the page (the so-called "s-component," with vector perpendicular to the plane of incidence)[10] is progressively extinguished by partial reflection at each interface, as illustrated at the top plates, while most of the component parallel to the page (the "p-component") is transmitted. Data on reflection and transmission were not found for quartz, but the following data for glass (n = 1.55) 3° above Brewster's angle was used as a first approximation.

	p-component	s-component
Fraction transmitted at each interface[11]	99.9%	80.7%
Fraction left after eighth plate	$(0.999)^{16}$ = 98.4%	$(0.807)^{16}$ = 3.2%

In practice, the portions reflected upwards are partially re-reflected downwards, and so on, so that a whole series of incompletely-polarized overlapping multiple images are formed at the base in addition to that desired, and the separation of the two components is less effective than that predicted from the calculation. With three $\frac{3}{16}$ in. circular stops in place, as indicated, our device passes 19% as much plane-polarized light when in the "extinction" position as when in the "transmission" position. This percentage ought to be reduced considerably by the addition of a fourth stop, just below the bottom quartz plate. Greater spacing between the plates would have increased the image displacements; $\frac{1}{4}$ in. has been suggested.[10] Actually, the analyzer need not be a 100% polarizer; all that is needed is that one know how efficient it is, so that two simply-solved simultaneous equations can be set up relating the true intensities to the pair of intensity readings obtained. Let: T_0, T_0', p, p', ΔN, $\Delta N'$, and λ be as previously defined and:

λ_0 = wavelength of exciting light

J_λ = relative radiant energy flux of fluorescence spectrum per unit wavelength bandwidth

F = photomultiplier current produced by fluorescent sample

S = photomultiplier current produced by scatterer

r = relative response of photomultiplier (current per unit radiant energy flux)

r_0 = relative response of photomultiplier at the wavelength of exciting light

h = Planck's constant

c = velocity of light in vacuum

Let us assume that a spectrum J_λ against λ is available for the fluorescent sample. Since the relative number of photons received at the photomultiplier from the fluorescent sample is $\int J_\lambda(\lambda h^{-1} c^{-1})d\lambda$ and the total current produced is $\int J_\lambda \, r d\lambda$, the average relative sensitivity of the photomultiplier (photon flux per unit current) is $\int J_\lambda \, \lambda d\lambda / hc \int J_\lambda \, r d\lambda$. The corresponding relative sensitivity towards light from the scatterer is λ_0 / hcr_0. The quantum efficiency can then be determined from

$$q = \frac{1 - T_0'}{1 - T_0} \cdot \frac{3 + p}{3 + p'} \cdot \frac{\Delta N}{\Delta N'} = \frac{1 - T_0'}{1 - T_0} \cdot \frac{3 + p}{3 + p'} \cdot \frac{F}{S} \cdot \frac{\int J_\lambda \, \lambda d\lambda / hc \int J_\lambda \, r d\lambda}{\lambda_0 / hc \, r_0} \qquad (6)$$

The quantities T_0 and T_0' are obtained from transmittance measurements on the spectrophotometer, the quantities F and S from a 6903 photomultiplier (as in Figure 18) in an electrometer circuit, and the quantities p and p' from the same apparatus, with the quartz-plate analyzer interposed between the cell and the photomultiplier. The cells used are the same ones described in connection with the integrating-sphere method. The response (r against λ) of the 6903 tube has been determined previously. Many fluorescent spectra (J_λ against λ) are obtainable from the literature; however, we ran our own curve for anthracene, using the spectrophotometer curve obtained from the arrangement of Figure 19 and took into account the varying sphere reflection factor and the spectral response of the spectrophotometer. Results to date are incorporated in Table 1.

Discussion of Results

The results in Trial 1 are questionable since they were obtained before good techniques had been established. Those in Trial 2 can be looked at more seriously. Although the result by the polarization-analysis method gives results identical to those obtained by Weber and Teale, this does not per se establish the superiority of that method. The known uncertainty in both of our results is still high; moreover, since Weber and Teale used a very dilute and we an almost 100% absorbing solution, the technical quantum efficiencies might reasonably be expected to differ. We are confident that with further study of the problem the reliability of each method can be improved considerably.

References

1. E. J. Bowen and F. Wokes. Fluorescence of Solutions. Longmans, Green and Co., London (1953). p. 22.

2. G. Weber and F. W. J. Teale. Trans. Faraday Soc., 53, 646 (1957).

3. M. D. Borison and V. N. Vishnevski. Bull Akad. Nauk USSR, Physical Ser. 20 (4) 459 (1956).

4. J. W. L. Walsh. Photometry. Constable and Col, London, 2nd ed. (1953). pp. 137, 141, 158, and 257-272.

5. E. V. Condon and H. Odishaw. Handbook of Physics. McGraw-Hill, New York (1958). pp. 6-48 to 6-51.

6. H. C. Van de Hulst. Light Scattering by Small Particles. John Wiley & Sons, New York (1957). p. 83.

7. E. V. Condon and H. Odishaw. Handbook of Physics. McGraw-Hill, New York (1958). p. 6-124.

8. American Inst. of Physics Handbook. McGraw-Hill, New York (1957). p. 6-44.

9. Handbook of Chemistry and Physics, Chemical Rubber Publ. Co., Cleveland, 31st ed. (1949). p. 2286.

10. G. K. T. Conn and G. K. Eaton. J. Opt. Soc. Am., 44, 553 (1954).

11. Handbook of Chemistry and Physics. Chemical Rubber Publ. Co., Cleveland, 31st ed. (1949). p. 2288.

DISSOCIATIVE ATTACHMENT OF SUBEXCITATION ELECTRONS IN LIQUID WATER, AND THE ORIGIN OF RADIOLYTIC "MOLECULAR" HYDROGEN*

Robert L. Platzman

Abstract

An electron in liquid water having kinetic energy, T, greater than 6.8 eV loses energy by electronic excitation so quickly that its attachment to a water molecule has negligible probability. However, subexcitation electrons ($T \leqq 6.8$ eV) are moderated at a rate which permits appreciable attachment. The only subexcitation attachment process is

$$H_2O + \epsilon^- \rightarrow OH + H^- \quad ;$$

its cross-section, $Q_{att}(T)$, has threshold at 4.8 eV and peak at 6.0 eV. The H^- formed thereby reacts immediately by

$$H^- + H_2O \rightarrow OH^- + H_2 \quad .$$

This reaction sequence, which is established experimentally in the vapor phase and should proceed just as effectively in the liquid, produces molecular hydrogen directly, i.e., not by combination of two hydrogen atoms (currently the accepted explanation). The 100-eV yield, $g_{att}(H^-) = g_{dir}(H_2)$, is calculated by integration of the attachment probability in dT, $N \cdot Q_{att}(T) \cdot v \cdot (-dT/dt)^{-1}$, from threshold to a particular subexcitation-electron energy, and thereafter over the subexcitation-electron spectrum, $g_T(\epsilon^-)$. (Here N = density of water molecules and $\frac{1}{2}mv^2 = T$.) The rate of moderation, $-dT/dt$, is obtained by adding to the Debye energy-loss the comparable energy-loss to vibrational modes, computed from experimental absorption-coefficients for infrared radiation. It is found that $g_{dir}(H_2) \approx 0.2 \pm 0.1$. This result is comparable to the experimental $g(H_2) \approx 0.4$ for γ radiation, and shows that the mechanism does contribute to the observed molecular yield. Other implications concern the effect of temperature on radiolysis, isotope effects, $G(H_2)$ in ice, and the character and initial spatial distributions of radicals assumed in diffusion kinetics.

*Presented at International Congress of Radiation Research, Harrogate, England, Aug. 6-10, 1962.

COSMIC-RAY NEUTRON BACKGROUND RESEARCH. HEXAFLUOROBENZENE SCINTILLATOR

Jacob Kastner and B. G. Oltman

As pointed out by Marinelli,[1] maximum response of the "twin" scintillation fast neutron detector[2,3] is obtained when one of the solutions has a relatively low proton-electron ratio. Williams and Hayes at Los Alamos[4] employed hexafluorobenzene, which contains no hydrogen at all and yet was claimed to be comparable to fluorinated xylene in regard to light yield.

Recently this rare compound became available as a special product of the Imperial Smelting Company.* The light yield of the raw material as received has been determined using the technique described by Grismore and Oltman.[5] The pulse height of 0.26 relative to xylene which we obtained is in agreement with the value of 0.23 determined by the Los Alamos group (presumably not bubbled with N_2).[6] The good yield attests to the minimum 0.97 purity claimed by the manufacturer.

References

1. L. D. Marinelli. Argonne National Laboratory Radiological Physics Division Semiannual Report, July through December, 1960. ANL-6297, p. 49.

2. I. B. Berlman and L. D. Marinelli. Rev. Sci. Instr. 27, 858 (1956).

3. I. B. Berlman, R. Grismore and B. G. Oltman. Rev. Sci. Instr. 31, 1198 (1960).

4. D. L. Williams and F. N. Hayes. U.S.A.E.C. Report, LA-2375.

5. R. Grismore and B. G. Oltman. Argonne National Laboratory Radiological Physics Division Semiannual Report, July through December, 1960. ANL-6297, p. 45.

6. F. N. Hayes, et al. U.S.A.E.C. Report, LAMS-2455, p. 130.

---

* Imperial Smelting Corporation Limited, Avonmouth, England. The material arrived in Chicago within a week of the order and spent spent 3 weeks in customs.

STUDIES OF LOW ACTIVITY PHOTOTUBE MATERIALS

H. A. May and P. E. Hess

Part I

The radioactivity of several types of contemporary photomultiplier tubes, and of many of their component parts, has been previously reported and the low residual activity of quartz-envelope tubes noted.(1) Since these tubes are produced in small quantity, with rather long delivery times, and are quite expensive, it was not feasible to break up one or more of them in order to count the various parts and determine more precisely the location and amount of their radioactivity. Parts of several experimental tubes have since been obtained through the courtesy of Dr. Jack Sharpe, of EMI Industries, Ltd. A description of the samples which have been counted follows:

1. Two graded seals, consisting of a glass cylinder some 5 cm in outside diameter by 3 cm long, with consecutive rings of an undetermined number of glasses, their expansion coefficients apparently grading from that of quartz to Kodial. Total sample weight 42 g.
2. Three tube bases or "presses," each consisting of 15 small Kovar pins sealed into a Kodial glass disc. Total sample weight 48 g.
3. Glass cylinder originally fused to one of the tube bases, thus apparently having thermal expansion properties similar to Sample 2 above, presumably Kodial. Sample weight 30 g.

All samples were crushed into small bits in order to improve the counting geometry. No attempt was made to separate the Kovar pins included in Sample 2 from the adhering pieces of glass since all previous experience indicates that the metal is free of activity. The samples were sealed in small polyethylene bags and counted directly in contact with the 0.010-inch thick steel "window" of the crystal. A low background 7-inch diameter by $3\frac{1}{2}$-inch crystal having one-half-inch integral mercury shielding was employed. An additional two inches of bismuth were placed within the standard 8-inch Fe cave and the whole surmounted by a plastic scintillator some 24 inches in diameter, operated in anticoincidence with the crystal in order to provide some further reduction in the background rate arising from meson interactions in the shielding. The net integral background over our standard energy band of 30 keV to 1.575 MeV under these conditions was 321 ± 5.3 cpm. The quoted uncertainty represents the rms deviation from the mean of four background runs, and is due to small gain shifts rather than statistical uncertainties. The observed net counting rates and quantities calculated therefrom are summarized in Table 2.

Table 2

Radioactivity analysis of selected phototube components

Sample	1 (graded seals)	2 (bases)	3 (Kodial ring)
Net weight, g	42	48	30
Net cpm	56 ± 1.6	86 ± 1.4	70 ± 1.5
Cpm/g	1.33	1.79*	2.34
Estimated cpm per tube	28	29	-
Cpm in K^{40} peak	11.6	26.3	22.3
Estimated K content, g	0.64	1.5	1.24
K content, %	1.5	3	4
Cpm estimated due to radium	21.6	trace quantity only	
Radium content,** curies	$2.5 + 2 \times 10^{-11}$		

* The sample includes the weight of the Kovar pins; the data must be interpreted accordingly.

** Radium-226, assuming complete radon retention and equilibrium with gamma-emitting daughters.

Discussion

No attempt has been made to count these samples in a geometry simulating that which exists in actual use. However, the findings seem to be quite consistent with previous reports of the activity of whole tubes. Although we have assumed that fused quartz was completely free of naturally radioactive elements, this generalization may not be wholly justified. A potassium content of 0.005% as measured by flame photometry has been reported from samples of one commercial supplier.(2) In a 5-inch diameter phototube, containing approximately 400 g of quartz, this would result in the emission of about 40 photons per minute, and, hence, a readily detectable background contribution would result. We have had no opportunity to investigate this directly. An additional contribution would obviously arise from the beta-particle emission, dependent upon the geometry and materials between the quartz and the detecting crystal.

A potassium-free glass has been developed by the Corning Glass Company under an AEC contract.(3) The fabrication of this glass into usable phototubes has presented many problems, due to the gradual vitrification during working, so that it now appears that use of a multiple graded

seal to a pressed base of conventional Nonex glass may be necessary. The practical reduction in radioactivity which will be realized with such construction appears to be much less than was desired. The utility of K^{40} counting as a direct method of potassium analysis in glass and the significance of potassium content in construction of counter tubes has received some attention in the German technical press.[4-6] Whether further efforts will be forthcoming, paralleling and possibly extending the work by Corning, remains to be seen.

Part II

Since the metals employed in electron tube structures, namely copper, iron, nickel, tungsten, molybdenum, Kovar, etc. are found to contain less radioactivity than glass by at least several orders of magnitude, some consideration should be given to the feasibility of manufacturing low-level photomultiplier tubes without any glass whatsoever. Construction utilizing a metal shell, quartz or sapphire window, and ceramic insulators for the internal multiplier structure supports and for lead-through of external leads, appears to be entirely feasible with existing techniques. Methods of making ceramic-to-metal seals are well established[7] and should not introduce any activity. The thermal expansion characteristics of sapphire more nearly match those of appropriate metals;[8] however, its greater cost and the tendency toward cleavage may be a disadvantage. Direct quartz-to-metal seals by active metal soldering has been reported,[9] as has an indium soldering technique for quartz-to-glass bonding.[10] The radioactivities of some materials involved in such construction have been determined and are shown in Table 3. The following is a more detailed description of the samples. A single sapphire boule approximately 7 cm in diameter was obtained from the Linde Company.* This was in an unpolished, as-grown condition. Alternate sample and background runs were made in the previously described low-background facility for a total counting time of 300 minutes each, with aged air flowing to eliminate radon fluctuations.

The Nuvistor type of receiving tube construction introduced by RCA employs a thin ceramic disc base, which supports and spaces the tube electrodes. Some of the supporting leads extend through the base and serve as connecting leads, the whole being made vacuum tight by means of metallized and brazed areas about each pin. The entire assembly is sealed to a metal shell in a similar manner. Samples of these ceramic bases have been counted. The first determination was made on a 8.7-g sample consisting

*It is a pleasure to acknowledge the assistance of Mr. F. McGuire, Jr., Crystal Products Division, Linde Company, who generously loaned the sapphire to us.

for the most part of bases removed from defective Nuvistor tubes. Subsequently, a larger number of virgin bases was obtained in order to allow a determination at a more significant counting level.* The net counting rate observed from these samples appears to be roughly the same as that of other ceramic parts we have examined in the past.

Table 3

Net activity of materials for proposed low-activity phototubes

Sample	Net weight, g	Background*	Background + Sample	Sample, net	Net cpm/g
1. Sapphire boule	190	374.1 ± 4.1	372.7 ± 2.6	-	-
2. Ceramic bases, RCA (Nuvistor)	8.7	314.8 ± 1.4	334.5 ± 0.9	19.7 ± 1.9	2.3
3. Ceramic bases, RCA (Nuvistor)	26.0	355.7 ± 1.0	378.1 ± 0.6	22.4 ± 1.2	0.9
4. Ceramic insulators** DuMont type	44.5	354.4 ± 0.6	401.2 ± 1.9	46.8 ± 2.1	1.1
5. Alumina tubes, Morganite	278	442.6 ± 1.6	453.9 ± 1.3	11.3 ± 1.6	0.04

*Variations in background reflect slightly different shielding arrangements since these measurements were spread over a time interval of about a year and other experiments were in progress concurrently. Anticoincidence detectors were in operation for Sample 2 only.

**Data previously reported in Reference 1, p. 94. Mass of sample reported erroneously in that report and repeated here for comparison.

A 99.7% alumina ceramic, in the form of thermocouple tubes, was also counted. This sample was of "Triangle RR" grade, manufactured by the Morganite company of England. Because of the high purity and the fact that the sintering process employed in manufacture requires a temperature in the neighborhood of 1700°C, it was hoped that the residual radioactivity would be very low. That this is true may be seen from comparison of the counting rates observed, as tabulated in Table 3.

Discussion

The demands of a constantly expanding electronics industry for vacuum tubes capable of extremely high-power output at frequencies of 10 kmc and above has led to development of a large number of specialized ceramics falling into four broad categories.(11) These are known as high alumina, forsterite, steatite, and zircon-talc. The composition of each

*The interest and assistance of Mr. W. J. Zimmerman of the Electron Tube Division, Radio Corporation of America, in supplying us with these parts is gratefully acknowledged.

may be varied widely in order to obtain the desired physical characteristics, such as vacuum-tight crystalline structure or a particular thermal expansion coefficient or dielectric constant. The temperature at which the ceramic "matures" or takes on its ultimate microstructure, consisting of various crystalline forms in a vitreous matrix, and the dimensional stability during the firing process are important considerations also. The range of compositions which are typical of each group is illustrated below (Table 4).

Table 4

Range of compositions for typical electrical ceramics

	Compound			
	Alumina	Forsterite	Steatite	Zircon-talc
Composition, %				
Al_2O_3	90 - 95			
Kaolin	3 - 5		10	
Ball clay	2 - 5	3 - 10		7 - 10
Talc	1 - 3	50 - 80	70 - 90	20 - 40
$Mg(OH)_2$		10 - 40		
$BaCO_3$		6 - 7	5 - 8	
BaF_2		10		5 - 10
Bentonite		3 - 5		3 - 5
Feldspar			10	
Zircon ($ZrO_2 \cdot SiO_2$)				40 - 80
Typical linear thermal expansion coefficient (25° - 300°), x 10^{-6}	5.1 - 6.2	9	6.5 - 7.8	5.5*
Typical firing temperature, °C	1600 - 1750	1200 - 1450	1350	1300

*This provides the closest match to Kovar or Fernico.

The point to the above discussion is that all of these formulations include natural clay products in varying amounts, consisting principally of aluminum and magnesium silicates and varying in crystalline form and in the extent of trace elements contained by reason of the geochemistry of the original deposit. Hence, readily detectable amounts of potassium, radium and thorium are to be expected. The ceramic Nuvistor bases are known to fall into the Forsterite class, characterized by the predominance of magnesium orthosilicate.

As opposed to these silicate-based materials, which are essentially only improvements and refinements on age-old porcelain, the Morganite material represents a single-phase metal-oxide ceramic, formed into a compact mass by a sintering process. Since extremely high temperatures are required for this, as for the flame growing of the synthetic sapphire (also pure alumina, of course), it is likely that the low radioactivity which we observe is the result of volatilization of contaminating trace elements during processing, rather than of high purity of the source materials. Further investigation of this point is planned.

References

1. H. A. May. Argonne National Laboratory Radiological Physics Semiannual Report, July through December 1959. ANL-6104, pp. 89-95.

2. Dr. Jack Sharpe, EMI Electronics, Ltd., personal communication.

3. Correspondence regarding Contract AT(30-1) 2505, May, 1960, issued by AEC New York Operations Office, New York.

4. H. Gebauer. Kerntechnik 2, 121-123 (1960).

5. H. Drost and H. Pupke. Exptl. Tech. Physik 7(1), 20-26 (1959)

6. K. Barth. Silikat Tech. 11, 554-558 (December 1960).

7. S. S. Cole and G. C. Sommer. IRE Trans. CP-8 (4), 151 (1961).

8. R. D. Olt. Electronics 32(49), 110 (December 4, 1959).

9. M. E. Knoll. Rev. Sci. Instr. 32, 83 (1961).

10. S. Pakswer and J. Dowd. Rev. Sci. Instr. 33, 780 (1962).

11. L. Navias. J. Am. Ceram. Soc. 37, 329 (1954).

NEUTRON PRODUCTION IN MASSIVE SHIELDS AND EFFECT UPON THE LOW-ENERGY GAMMA-RAY BACKGROUND

H. A. May

I. Introduction

An extended series of experiments has been carried on over the past three years designed to elucidate the contribution of cosmic-ray phenomena to the background of low-energy gamma rays observed in large sodium iodide crystals inside massive shields. The experiments and their results have been described in our semiannual reports,[1,2] and in several other publications.[3,4] At first we tacitly assumed that some portion of the background which did not originate from the crystal detector itself (including the photomultiplier tube) or from the shielding material originated from interactions of cosmic rays with the shield. Since the mu-mesonic component is the most penetrating, it was surmised that this component was mainly responsible and hence, that charged particle detectors of suitable geometry and efficiency in anticoincidence should be capable of eliminating the cosmic ray contribution completely. Extensive measurements with GM tube arrays and large plastic scintillators have shown that this goal could be approached but not completely attained since the background suppression provided by them did not equal the suppression obtainable in measurements performed at large depths.

Since evaporation neutrons are produced by capture of low-energy negative muons, or as the result of direct nuclear interaction by fast muons, it was at first thought that the inadequacy of the anticoincidence techniques was a result of the relatively long time periods required for neutron thermalization and capture in high-atomic-number materials. Further evidence lending support to our conviction that locally-produced neutrons are present in significant numbers has been presented by Parker.[5] A similar conclusion was reached by Grinberg and Le Gallic.[6]

From further inquiry into cosmic-ray phenomena, it became apparent that other processes which are also capable of generating evaporation neutrons must be taken into consideration. Information on such processes and their relative importance in this particular situation may be found in the extensive literature of cosmic-ray physics; the relevant facts, however, are all but concealed by the very extent of the literature, the welter of experimental detail, and by the predominant interest of the cosmic-ray physicist in primary phenomenology. Extensive summaries, such as those of Rossi[7] and the monograph on mesons by Thorndike[8] have been found particularly comprehensive. A summary of cosmic-ray and neutron physics appropriate to an understanding of low-energy gamma-ray production in the environment is in preparation. For the present, we shall state in simplified form and without complete documentation, the principal conclusions of such a summary.

II. Cosmic-Ray Physics

Near sea level, the penetrating or hard component of cosmic radiation consists almost entirely of muons, having a rest mass of 210 electron masses or 105.6 MeV. The incident particle flux, from all directions, on a unit sphere is about 1.7×10^{-2} cm^{-2} sec^{-1}, the ratio of positively to negatively-charged particles being about 1.25. The energy spectrum reaches a maximum at around 0.6 BeV, with a mean energy of 1.8 BeV. Energy loss is primarily by ionization and amounts at minimum ionization to some 1.2 MeV/g/cm^2 in air, or 1.8 MeV/g/cm^2 in dense materials. When brought to rest, the muon may either decay or be captured; the former alternative (represented as $\mu^{\pm} \rightarrow e^{\pm} + 2\nu$) is the only one possible for the positive muon because the Coulomb barrier prevents a capture approach to the nucleus. The most probable energy of the decay electrons is around 45 MeV. In the case of negative muons, the processes of capture and decay are equally probable in a material of $Z_{eff} = 12$, but capture predominates in heavier materials such as iron or lead. Before nuclear capture, the muon is trapped briefly in a Bohr orbit and hence a mesonic x-ray is emitted. The K_α line occurs with at least 80% probability, releasing 1.55 MeV in iron or 6.0 MeV in lead. Nuclear capture results in excitation of the nucleus, leading to the evaporation of one or two neutrons, with energies ranging from one to ten MeV, while the major portion of the energy is carried off by neutrino emission, and at most 10 MeV by de-excitation gamma photons. Direct nuclear interaction by penetrating mesons also occurs, releasing a greater average number of evaporation neutrons.

Nuclear interactions may also be produced by the so-called nucleonic component of cosmic rays, which at sea level is composed predominately of high energy neutrons, and protons. Although their numbers are less than the total meson flux by an order of magnitude, these nucleons interact much more readily, being characterized by a mean free path of some 150 g/cm^2. The total number of evaporation neutrons produced is determined by the interaction cross section, which is approximately geometrical (and hence, varies as $A^{2/3}$), and by the multiplicity or average number of neutrons released per interaction by the excited nucleus. This number is approximately 3 in iron and 6.5 in lead;[9] since this value increases with energy of the incident particle, these numbers may depend upon any bias inherent in the experimental methods of measurement. The energy spectrum of the nucleonic component extends into the BeV region, and hence is capable of producing nuclear cascades, i.e., of locally generating nucleons with energies exceeding 100 MeV or so. Since the excited nuclei of each generation lose energy by evaporation of several neutrons, the observed multiplicity depends upon the thickness of the interacting medium.

Neutrons may also be produced in shielding materials by the "soft" or electron-photon cascade component containing gamma rays with energies exceeding the threshold for the γ-n process. The cross section for the photonuclear effect shows the well-known giant resonance at approximately 20 MeV in iron. The extent to which this process contributes to neutron production in a massive shield is determined by the attenuation of the "soft" component in building material surrounding it. The typical range of a em shower particle is of the order of one radiation length, or about 25 g/cm^2 in concrete. However, an investigation of extensive air showers showed that some 3% of the particles were capable of penetrating 10 cm of lead. Hence, one should expect photonuclear reactions to contribute to the neutron production.

The fast neutrons, regardless of their origin, lose energy rapidly by elastic and inelastic scattering. In iron, the latter process is possible only above the 840 keV threshold and results in emission of a de-excitation photon of the same energy. The inelastic process contributes 37 percent of the total cross section when averaged from 4 MeV to threshold. The root mean square distance traveled by a neutron in being slowed from 4 MeV to thermal energies, as calculated from Fermi age theory, is about 65 cm in iron;* hence, it is apparent that escape from the customary shielding thickness is appreciable. The neutrons which are thermalized in the Fe shield are characterized by an absorption mean free path (actual trajectory) of 4.7 cm, or a diffusion length of 1.3 cm. The gamma spectrum resulting from thermal neutron capture in iron extends from 300 keV to 10 MeV, with major lines at 364 keV, 1.63, 1.72, 5.91, 6.01 and 7.64.

The transport cross section of neutrons and their inelastic scattering cross section in high atomic number materials, such as lead, mercury, and bismuth, differ widely and will not be discussed further.

The average time required by a fast neutron to become thermalized, and to be captured, is of some interest. This may be readily calculated

---

* By way of comparison, the same quantity is about 16 cm in water and 185 cm in lead.

for hydrogenous materials, but in denser materials, and particularly in the range of medium atomic numbers, effects associated with the binding energy and thermal energy of the lattice are significant in the region of a few keV energy, and are not amenable to simple theory.(10) The values which are given in Table 5 are experimental for the most part. In particular, the time to reach an energy of one electron volt in iron is extrapolated from recent Russian data for the time to reach 4.9 eV;(11) the probable error is unknown. However, the orders of magnitude are undoubtedly correct and serve to indicate the problems inherent in the use of anticoincidence devices.

Table 5

Time constants associated with energy loss of fast (3 MeV) neutrons in shielding materials

Material	Time to reach 1 ev, μsec	Thermalization time constant, μsec	Diffusion time, μsec
H_2O	1.3	6	210
Fe	110	??	22
Pb	430	900	910

We may summarize this section, then, by noting that some fraction of all cosmic particles is energetically capable of producing evaporation neutrons in the usual shielding materials. This may be minimized by the use of materials with low atomic mass since the probability of meson decay becomes appreciably greater and the neutron multiplicity less.

III. Implications of Theory

From this brief discussion, it may be inferred that efficient reduction of the major portion of the cosmic-ray contribution may best be accomplished by removal of the nuclear interacting component by a suitable shielding layer of material with low atomic mass. The required thickness of suitable materials is illustrated in the accompanying table (Table 6).

If these materials can be provided free of radioactivity, they can serve also as conventional gamma-ray shields. Such materials have indeed been proposed, and in a few cases used, as gamma shields(12-16) but apparently without a full realization of their properties. The total shield thickness might well then be chosen so that the density of low-energy photons produced by inelastic scatter and by capture of evaporation neutrons at the

inner layer of the shield is comparable to the photon density arising from residual radioactivity. It may be worth while to point out that once the nuclear component has been reduced to the point that meson interactions in the shield predominate, the advantages of materials with low atomic number become far less compelling, for in this case, as we have seen, the neutron multiplicity is appreciably smaller. The removal or reduction of neutron effects by anticoincidence devices will still be greatly simplified by the rapid thermalization which is characteristic of light elements.

Table 6

Thickness of typical shield materials vs. attenuation of cosmic-ray nucleons

Attenuation				
I/I_0 =	0.37	0.135	0.05	0.011
Thickness (mean free paths)				
	1	2	3	4.5
Thickness (meters) of Material				
H_2O	1.5	3.0	4.5	6.7
Soil (ρ = 1.5 to 1.8)	0.85-1.0	1.7-2.0	2.5-3	3.8-4.5
Ordinary concrete (ρ = 2.3)	0.65	1.3	2.0	2.9

Note: The mean free path of the nuclear component is only slightly dependent upon mass number, but may be weakly dependent upon the energy of the nucleon. Values ranging from 120 to 180 g/cm^2 are found in the literature; here, a mean value of 150 g/cm^2 has been used.

It should be noted that the influence of the type and total mass of building construction materials overlying a low-level shield may have an appreciable effect upon the ultimate background count obtainable therein, and attempts to compare such figures for shields of comparable dimensions at different locations must take this into consideration. As an example, we present some data on background counting rate in a shield located in the Food and Container Institute, U. S. Army Quartermaster Depot, Chicago.*

*We are indebted to Major J. P. Berg and Captain O. P. Snyder of the Quartermaster Corps for their generous assistance in obtaining these data.

The shield consists of a section of a 16-inch naval gun barrel, cast in 1917, machined to an average wall thickness of 11 inches. End plates of 10-in. armor plate were fastened in place and the entire assembly lined with $\frac{1}{4}$ inch of selected, low activity lead.

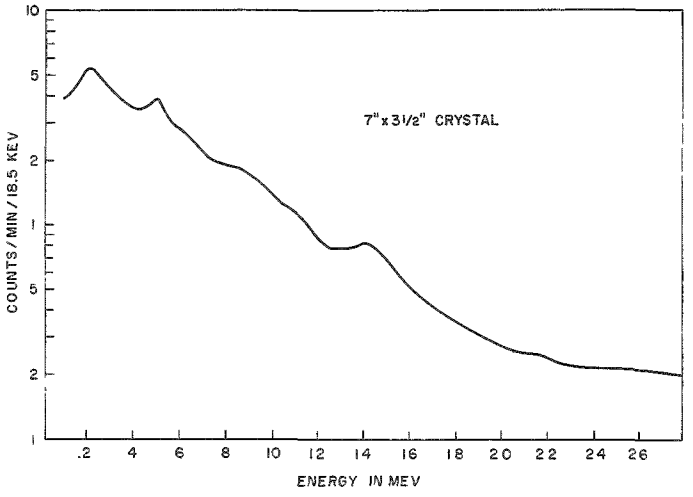

Figure 23

Background spectra in 16-inch naval gun barrel shield, Food and Container Institute, U. S. Quartermaster Depot

Within this shield, the integral counting rate of a low background 7-inch x $3\frac{1}{2}$-inch crystal with quartz EMI phototube attached over the energy region from 30 keV to 1.575 MeV was found to be 417 ± 5 cpm.* This may be compared with a typical figure of 390 cpm in our 8-inch thick shield. That the difference cannot be caused by radioactivity in the gun barrel is indicated by the extremely smooth spectrum obtained (see Figure 23), which shows no evidence of the presence of thorium or radium chains.

The gun barrel was located on the top floor of the building with 7 inches of reinforced concrete overhead, whereas our basement location has 14 inches of overlying concrete. The difference in overlying building materials of 39 g/cm^2 is exactly equivalent to the extra 2 inches of iron in the top slab of the gun barrel shield. Thus the net attenuation of the nuclear-interacting component is the same. The higher mass number of iron results in increased evaporation neutron production in this medium. A quantitative assessment of the resultant photon flux within each shield, and of the similar though smaller effects in the shield walls, appears to be extremely difficult and of doubtful accuracy. The observed difference in counting rates is in the right direction, consistent with these qualitative arguments. However, it must be admitted that this may be entirely fortuitous.

IV. Experiment

A crude experiment bearing upon the effect of background neutrons was performed in our laboratory by surrounding the 7 x $3\frac{1}{2}$-inch low-background crystal with approximately 15 cm of paraffin and replacing some of the outer iron shielding with lead. The 8-inch thick iron cave previously employed in many of these studies[1] was located at grade level with only a thin aluminum roof overhead. When the central space was filled

* The quoted probable error results from an estimate of the uncertainty in the low-energy cutoff. Counting statistics alone, for two runs of 100 minutes and 250 minutes, result in a probable error of approximately ±1 cpm.

with paraffin, the net increase in a 110-keV band centered at 2.23 MeV, was 5.4 counts per minute.* The change in the shape of the spectra was definitely above statistical error.

The cave construction is such that the square steel plates forming the top can be readily removed without disturbing the sides or the door. All but one of the top plates were removed and the space filled with lead bricks; the volume of iron thus replaced was about 6% of the total shield. In the presence of this lead the net increase due to paraffin in the same band was now 8.6 cpm. Table 7 summarizes the observed data:

Table 7

Observed integral counting rates for certain shielding arrangements designed to demonstrate neutron effects

Shielding	Energy band	
	60 keV - 3.2 MeV	2.17 - 2.28 MeV
Fe - paraffin	747 ± 1.5 cpm	24.30 ± 0.27 cpm
Fe alone	671 ± 1.0 cpm	18.90 ± 0.17 cpm
Difference	76 ± 1.85 cpm	5.4 ± 0.32 cpm
Fe, Pb and paraffin	810 ± 1.2 cpm	26.9 ± 0.21 cpm
Fe and Pb alone	668 ± 1.0 cpm	18.41 ± 0.17 cpm
Difference	142 ± 1.6 cpm	8.5 ± 0.27 cpm

Two major physical processes can produce the observed increase in background counting rate when paraffin is added. Many of the fast neutrons which emerge from the inner iron surfaces are thermalized, the rms distance traveled in paraffin to reach thermal energy from an original energy of 3 MeV being about 13.5 cm.[18] Since the thermal diffusion length in paraffin is of the order of 2.5 cm, most of these will also be captured by the hydrogen, emitting a 2.225-MeV photon. The fraction which diffuse back into the iron are captured near its inner boundaries because the iron diffusion length is only 1.3 cm. Thus, the mean distance

* The existence in the background of such a hydrogen capture peak produced by cosmic-ray neutrons alone was first reported by Ellett and Brownell.[17] In their case the hydrogen was present in the form of a large plastic scintillation anticoincidence detector.

In the first attempt, blocks of paraffin were piled about the crystal, filling the cave as nearly as possible, but this resulted in a greatly increased counting rate at low energies. A difference spectrum demonstrated fission product contamination, presumably from repeated handling of the blocks during previous experiments. Hence fresh paraffin was obtained, which had been stored for several years in unopened packages so that any short lived fission product contamination which might have been present at time of manufacture would have decayed out. Thin stainless containers were fabricated; two end sections 38 x 38 x 16 cm thick, and a center section 38 x 38 x 35 cm, with a cylindrical piece cut out of the center to accommodate the crystal and preamplifier. These were filled with clean paraffin and sealed, permitting repeated handling with minimum precautions against surface contamination.

which an iron capture gamma ray must travel before being detected by the crystal is reduced, and hence, the number detected is increased. The reduction of path length in iron and substitution of a high probability of Compton scattering in the paraffin further alter the shape of the observed spectrum.

However, the effects at cosmic-ray flux levels are not large enough to yield a statistically smooth difference spectrum in any reasonable time interval. In order to assess these effects further, a series of background runs has been made under a shield capable of removing the nuclear interacting component without reducing the meson flux too greatly. The site was provided by the earth mound over the ring-shaped building which will house the main accelerating magnets of the Argonne Zero Gradient Synchrotron, now under construction. Figure 24 shows a plan view of the instrument access tunnel leading from the high bay magnet assembly and test building into the ring, together with a portion of the ring itself. The tunnel is 24 feet wide by 16 feet high, and is provided with heavy-duty rails embedded in the floor. An 8-inch thick iron cave, previously used in many of these studies, was placed upon a small flat car, and thus it could be quickly and readily moved from the assembly building, where only a thin steel roof was overlying, into the region of maximum shielding indicated in the figure. The directly-overlying shielding in this location, as shown on the elevation, Figure 25, consists of 3 feet of normal density concrete and about 25 feet of earth. Unfortunately, this thickness is not uniform because of the approximately 35° slope of the overlying earth mound. The reduction in earth thickness with zenith angle in one direction should be roughly compensated for by the increase in the opposite direction.

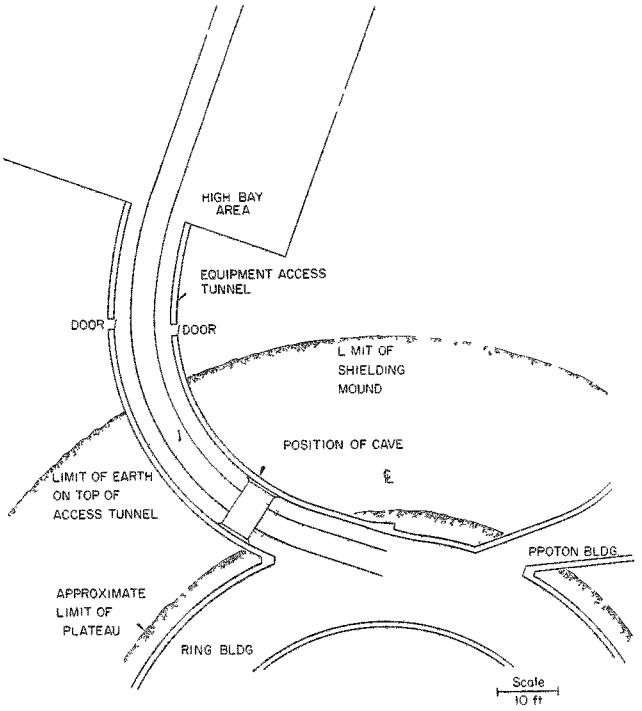

Figure 24

Plan of ZGS ring and high bay assembly buildings and interconnecting access tunnel

The ease with which the equipment could be moved into the tunnel contributed significantly to the success of the experiments since the transfer could be affected without disturbing the crystal inside the cave or turning off any electronic equipment, thus minimizing gain shifts between comparative data runs.

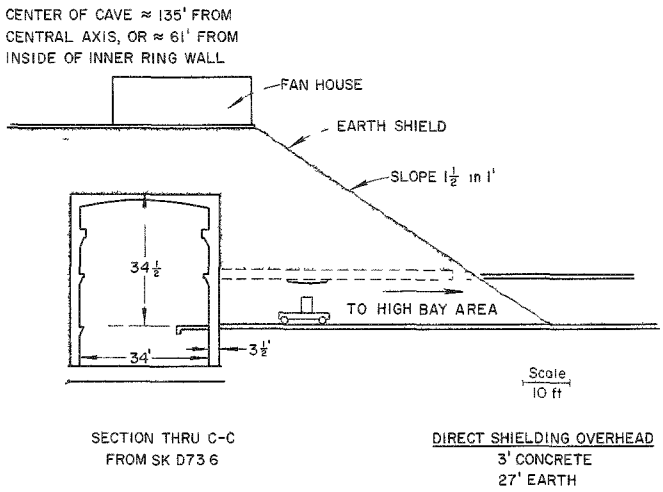

Figure 25

Elevation of instrument access tunnel and section of ring.

Spectral data were accumulated from 30 keV to 6 MeV with a 7 x $3\frac{1}{2}$ inch low-background NaI crystal within the cave. Also, the muon through-peak at about 42 MeV was recorded. As an indication of the neutron flux within the shield, the crystal was surrounded with paraffin, as described above, and the increase in counting rate was noted in an energy band from 2.1 to 2.35 MeV, centered about the hydrogen radiative capture line.

To confirm independently the presence of neutrons a second identical set of containers was filled with borated paraffin, the boron concentration (commercial grade borax) of which produced a 95% probability for thermal neutron capture in the boron. Additional runs were made in the Radiological Physics Division's calibration garage in order to assess and extend the reliability of these data (limited by the restricted time available at the ZGS site) and to determine whether the normal fluctuations in cosmic-ray intensity with time, over the period of about eight months during which data were accumulated, might have any effect upon our observations. As shown by data in the table, the locations are in most respects comparable.

Under these circumstances, the results tabulated in Table 8 and represented by the spectra of Figure 26 were observed. The shape of the spectra shown in Figure 26 clearly illustrate the removal of the H capture peak at 2.23 MeV and the appearance of the B^{10} capture peak (480 keV) following the substitution of the borated paraffin.

Table 8

Summary of background gamma-ray counting rates in small iron cave, at selected sites

Location	ZGS, high bay	Bldg. 203 calib. garage	Bldg. 203 basement	ZGS tunnel	Chicago water tunnel
Total shield overhead	0	0	80 g/cm^2	1460 g/cm^2	1.6 x 10^4 g/cm^2
Calculated relative intensity-mesons	1.0	1.0	0.92	0.34	0.013
-nucleons	1.0	1.0	0.58	0.001	none
			Counts per minute		
I. Meson peak	128	125	114	46	1.8 ± 0.1
Meson peak, relative rate	1.0	1.0	0.90	0.36	0.014
II. 4.5 to 6 MeV					
a) no paraffin	23.6	22.8	16.9 ± 0.2	9.2	0.63 ± 0.01
b) plain paraffin	-	21.0	14.4 ± 1.0	-	-
c) borated paraffin	-	17.6	13.3 ± 1.0	-	-
relative rate*		1.0	0.73	0.40	-
III. 3 to 4.5 MeV					
a) no paraffin	45	42.5	34.1	23.7	2.95 ± 0.1
b) plain paraffin	-	42.4	31.0 ± 0.15	-	-
c) borated paraffin	-	35.0	29.4 ± 0.2	-	-
relative rate*		1.0	0.79	0.54	-
IV. 2.1 to 2.35 MeV					
a) no paraffin	9.0	9.8	7.1 ± 0.25	3.53	2.06 ± 0.1
b) plain paraffin	12.7 ± 0.6	14.3 ± 0.2	9.9 ± 0.1	3.24 ± 0.1	-
c) borated paraffin	7.67 ± 0.2	9.2 ± 0.2	6.6 ± 0.1	3.1 ± 0.1	-
relative rate*	1.0	1.14	0.81	0.35	-

*Mean of relative rates, calculated for conditions "a," "b" and "c."

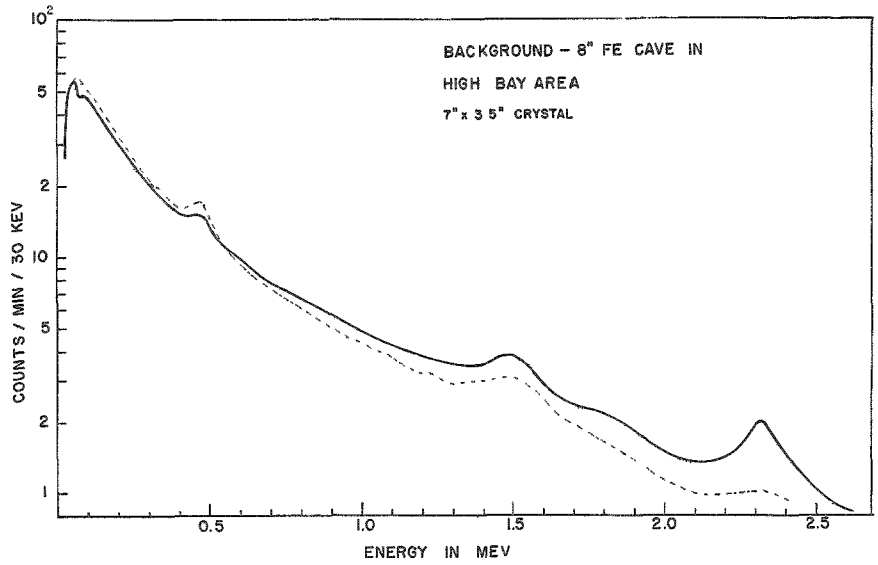

Figure 26

Background spectra in 8-inch Fe cave, alone (·····), with plain paraffin (——) and borated paraffin (—·—·—·), showing 2.2-MeV capture peak.

Discussion

A quantitative analysis of these results in terms of neutron moderation and capture within the shield or the materials surrounding the crystal appears extremely difficult.*

However, certain qualitative arguments and conclusions are not without significance. The gamma rays detected by the crystal in the 3- to 6-MeV region are well above those emitted by any naturally-occurring isotopes, and hence, must arise from neutron effects, or from the cascade photons produced by meson knock-on or decay processes.

The relative number of mesons striking the shield at each location, as calculated from the results of Wilson,(19) are in excellent agreement with the observed ratio of counting rates in the meson through-peak. The relative intensity of the nucleon flux may be calculated from the known interaction mean free path of the nuclear cascades. We represent these quantities by f_μ and f_n respectively. Let the observed net counting rate within the iron shield due to both components, under a given thickness x of overlying material, in the energy band ΔE at E, be represented by $C(x,\Delta E,E)$. To the extent that the "intrinsic" radioactivity of the crystal and iron shield has not changed over the interval of more than three years during which the data of Table 7 have been accumulated, $C(x,\Delta E,E)$ may be known by subtracting the observed rate in the Chicago water tunnel (Column 6) from the corresponding entries at lesser depths.** One might then assume that $C(x,\Delta E,E)$ is of the form:

$$C(x,\Delta E,E) = k[\alpha(\Delta E,E)\, f_\mu + \beta(\Delta E,E)\, f_n]\, C(0,\Delta E,E)$$

and hope to be able to determine the relative values of α and β, i.e. the relative contributions of the meson and nucleonic components. These proportionality constants depend on: 1) the fraction of incident cosmic-ray particles at depth x which interact in the iron shield; 2) the mean number

---

*A description of the neutron energy spectrum and flux as a function of spatial coordinates, resulting from a known source spectrum and spatial distribution, may be determined in theory by a solution of the Boltzmann transport equation. The practical difficulties involved when even simple boundary value conditions are imposed are well known. An approximate solution has been obtained by the use of an electronic computer code developed for use in reactor calculations, in which the rectangular parallelepiped geometry of the shield is approximated by a hollow sphere of equal volume. The evaporation neutron spectrum was represented by that portion of the fission spectrum falling between 3 and 10 MeV, with an average energy of 4 MeV. With these results, and the appropriate interaction cross sections, a calculation of the spatial distribution of inelastic scatter and capture gamma rays which result will be sought. Whether a meaningful analysis can be made remains to be seen.

**There is some evidence that this "intrinsic" activity at the lower energies has indeed become less. Mercury has been introduced and removed several times from the integral shielding compartment; the crystal has been recanned, and a different phototube has been coupled to it. However, at these energies, the change is expected to be slight. Another possible cause for a change is from the thorium alpha activity which produces diffuse peaks in the spectrum at about 3.2 and 5.5 MeV. No direct information is available on a possible change in the intensity of these anomalies with time.

of neutrons produced by these interactions, 3) the number and energy spectrum of photons arising, either from the primary interactions directly, or accompanying the transport and capture of neutrons, and 4) the energy degradation and absorption processes which relate the spectrum of photons emerging from the inner shield wall to the initial production spectrum represented by the preceding term. It is apparent that all these factors are spatially dependent as well, and hence, that values for α and β would be extremely difficult even to approximate directly from the flux and energy spectrum of mesons and nucleons The constant k represents the crystal efficiency (interaction ratio × photofraction × a mean geometrical absorption factor) for detecting an emergent photon of energy E

The data of Table 8 when so analyzed give the following results

Energy region	Depth from surface	
	x = 80 g/cm^2	x = 1460 g/cm^2
3.0 - 4.5 MeV	αk = 0.58 βk = 0 42	αk = 1.5 indeterminate (f_n = 0)
4.6 - 6.0 MeV	k = 0.42 βk = 0.58	αk = 1.5 indeterminate

These results suggest that with small amounts of shielding (80 g/cm^2), the penetrating mesons and nucleonic component are approximately equally effective in generating low energy photons. whereas those mesons which interact after penetrating 1460 g/cm^2 of earth are roughly three times as effective as the mesons at the surface The explanation for this effect. if real, is not apparent.*

Consider now the counting rates in the 2.2-MeV hydrogen capture region in the presence of paraffin. In this region, a mean increase of about 19% is observed when the Fe shield is located in the Building 203 calibration garage as compared to the ZGS high bay building This difference could not be caused by neutrons from the Van de Graaff accelerator in Building 208, located in direct line of sight some 320 feet to the west of us since data were taken only when this was known to be shut down. The effect is believed to be real, but no satisfactory explanation is available at present.

* The median energy of cosmic mesons present beneath this shield thickness is approximately 2.7 BeV (versus 1.8 BeV at the surface), and hence, the fraction which are brought to rest and captured in the shield should be less. The neutron multiplicity per meson capture is independent of initial meson energy. If such experimental data were available for a number of absorber thicknesses, so that analysis showed αk and βk to vary with depth in a consistent manner, we might consider the results to be significant. For the present, while they may be consistent with the physical processes involved, their significance remains uncertain.

The presence of locally-generated neutrons in substantial numbers in the high bay and Building 203 basement locations is documented by the increased counting rate in the 2.2-MeV region when the crystal is surrounded by paraffin, and by the sharp reduction upon substitution of borated paraffin. The virtual disappearance of these changes below 1460 g/cm^3 of shielding show that very few neutrons are being produced in the shield at that depth and that these effects arise predominantly from the nucleonic component.

These conclusions are supported by measurements taken with a paraffin-shielded BF_3 tube, or "long counter," at each of the locations. Because of the low natural rates encountered, strong measures were taken to insure that the electronic background of the system, arising from spurious line noise or direct pickup of radiated energy of a pulse nature, was completely eliminated The natural background of the stainless steel counter tube itself, due to internal alpha emitters,[20] was in some cases an appreciable fraction of the total observed rate. Table 9 shows these results.

Table 9

Summary of background counting rates in BF_3 "long counter"

Location	Gross count rate,* cpm	Net count rate,* cpm
ZGS, high bay	0 643 ± 0.036	0.472 ± 0 037
Building 181	0.554 ± 0.041	0.383 ± 0 042
Garage, Hinsdale	0.570 ± 0.011	0.400 ± 0 014
Building 203 basement	0.432 ± 0 027	0.261 ± 0.028
Building 203, in Fe room	0.545 ± 0 023	0.374 ± 0.025
ZGS, access tunnel	0 174 ± 0 015	0 003 ± 0.017
BF_3 tube in cadmium (tube background)	0 171 ± 0.009	

*Errors shown are 0.9 confidence level

The rows labeled "Building 181" and "Garage, Hinsdale" are believed to be truly proportional to the local cosmic-ray neutron flux in the 0.1- to 10-MeV region at the earth's surface. The first location was in a small frame building (181) about 2000 feet from locations where occasional exponential experiments are conducted, and 2300 feet from the reactor CP-5 No time-dependent fluctuations in counting rate were observed, however The counting rate is seen to be identical, within statistics, to that observed at the author's garage, a typical frame structure seven miles distant from the laboratory or any known man-made source of neutrons The counting rate in the ZGS high bay area appears to be slightly higher for reasons

unknown. This location is about 1250 feet from the power reactor EBWR, but the large mound of earth remaining from excavation of the ZGS site lies in a direct line of sight, so that it is difficult to assess the significance of the observation. The results in Building 203 basement seem to show a rise in fast neutron flux within the iron room, as expected by the higher Z of Fe compared to concrete but in contradiction with some earlier preliminary measurements made by Grismore.(2)

The reduction in counting rate within the ZGS access tunnel is perhaps the most prominent and gratifying feature of the experiments; it is in agreement with the previous conclusions concerning the virtual absence of any local neutron flux at this location. The gamma-ray figures of Table 7 relate to evaporation neutrons generated within the iron shield, whereas the "long counter" is insensitive for the most part to the very high energy nucleonic component per se but does respond to evaporation neutrons arising from interactions in the surrounding concrete and earth materials of low mean multiplicity. More direct measurement of the nucleonic component might be accomplished by providing some material with high atomic number as a neutron producer about the detector, thus approximating the standard Simpson neutron monitor(21) on a smaller scale.

A most practical aspect of this work is the background reduction in the gamma-ray flux in the 60-keV to 1.6-MeV region, where most naturally-occurring gamma rays are found. The observed rates in this band, taken concurrently with the data already discussed, are tabulated in part in Table 10.

Table 10

Location	Integral counting rate, 60 keV to 1.575 MeV, cpm (no mercury in housing, no paraffin surrounding)
ZGS, high bay (April-May, 1962)	556 ± 15
Building 203, calibration garage (September-October, 1962)	569 ± 14
Building 203, basement (1959-1961)	435 ± 10
ZGS, access tunnel (April-May, 1962)	340 ± 6
Chicago water tunnel (September, 1958)	380 ± 10

Each number is the result of several experiments, and the uncertainties, calculated from the observed deviations from the mean, are due primarily to energy calibration shifts; the resulting variance is many times that due counting statistics alone. The first, second and fourth entries of

Table 10 were taken over a period of a few months, during which the "intrinsic" activity of the crystal and shield was believed to be constant; the Chicago water tunnel experiments were performed in 1958, and, as noted above, intrinsic changes in activity may have occurred since, accounting for the inconsistency in the last two entries. The substantial reduction in the low energy region due to the elimination of the nucleonic component within the ZGS tunnel is clearly demonstrated.

At higher energies (>3 MeV), however, the data of Table 8 indicate that the meson component, increasing as it does from 1.4 to a substantial 36% of the surface value between the depths 1.6×10^4 and 1.46×10^3 g/cm^2, apparently contributes most of the crystal background at the lesser depth.

Many of the experimental details and much of the data reduction involved in these experiments were performed by Paul Hess. The assistance of the Particle Accelerator Division in making facilities in the ZGS building available, and in particular, the help of Don Roy, is gratefully recognized. Above all, the unfailing interest and helpful discussions of Mr. L. D. Marinelli have made this report possible.

References

1. H. A. May. Argonne National Laboratory Radiological Physics Division Semiannual Report, July through December 1958. ANL-5967, p. 145.

2. R. Grismore, B. G. Oltman, and L. D. Marinelli. Argonne National Laboratory Radiological Physics Division Semiannual Report, January through June 1959. ANL-6049, p. 6.

3. L. D. Marinelli, C. E. Miller, H. A. May, and J. E. Rose. Radioactivity in Man, ed. G. Meneely. Charles C. Thomas, 1961. pp. 16-30.

4. H. A. May and L. D. Marinelli. Proc. IAEA Symp. on Whole Body Counting, Vienna, June 12-16, 1961. International Atomic Energy Agency, Vienna, 1962. pp. 15-36.

5. R. P. Parker. Nuclear Instr. and Methods 8, 339 (1960).

6. B. Grinberg and T. LeGallic. Intern. J. Appl. Radiation and Isotopes 12, 104-117 (1961).

7. B. Rossi. Revs. Mod. Phys. 20, 537 (1948).

8. A. M. Thorndike. Mesons, A Summary of Experimental Facts. McGraw Hill, 1952.

9. K. W. Geiger. Can. J. Phys. 34, 288 (1956).

10. G. von Dandel and N. G. Sjostrand. Progress in Nuclear Energy, Ser. 1, Vol. 2, ed. D. J. Hughes, J. Sanders and J. Horowitz. Pergamon Press, 1958. p. 183.

11. A. I. Isakov. Soviet Physics JETP 14 (4), 739 (1962).

12. R. C. McCall. Health Physics 2, 304 (1959).

13. H. W. Wilson, D. E. Watt and D Ramsden. Intern. J. Appl. Radiation and Isotopes 10, 156 (1961).

14. W. H. Johnston. (Wm. Johnston Laboratories, Inc., Baltimore, Md.) personal communication.

15. G. Maycock and J. Vennart. Nature 182, 1545 (1958).

16. N. Rasmussen. Radium and Mesothorium Poisoning, Dosimetry and Instrumentation. MIT Progress Report, AECU-3504 (May 1957).

17. W. H. Ellett and G. L. Brownell. Nuclear Instr. and Methods 7, 56 (1960). See also, K. G. McNeill, and L. D. Davis. Can. J. Phys. 40, 732 (1962).

18. Mary J. Stanley. Two Group Constants for Reactor Materials. U.S. Atomic Energy Commission Report APEX-369 (1958) p. 38.

19. V. C. Wilson. Phys. Rev. 53, 337 (1938).

20. O. W. Bilharz. BF_3 Counter Background Study. U. S. Atomic Energy Commission Report KAPL-M-OWR-1 (1962).

21. J. A. Simpson, W. Fonger and S. B. Treiman. Phys. Rev. 90, 934 (1953).

OBSERVATION OF BACKGROUND IN A LARGE WATER SHIELD

H. A. May

The efficacy of low atomic number shielding materials is attested to by recent and preliminary studies made in a water-shielded human counter just completed at the Veterans Administration Hospital, Iowa City, Iowa.(1) It consists of a cylindrical steel tank 23 feet in diameter by 19½ feet in height, which is filled with filtered, singly distilled and deionized water. A cylindrical room 7 feet in diameter and 8 feet high is supported near the center with access from a basement laboratory being afforded via a passageway which has a 180° turn to provide baffling. The shielding in this direction is not seriously compromised, and a massive steel door is avoided. The shield is underground, the upper surface being approximately two feet below grade. By locating the shield outside, but in the angle formed by two wings of the ten-story hospital building, shadow shielding from penetrating cosmic radiation is provided.

The low-energy background within the room was measured with the 7- x 3½-inch crystal facing downward and raised from the floor about two inches only, a position necessitated by lack of any permanent crystal support. Because of the altered sensitivity to radon daughters within the room, a somewhat lower counting rate should result than when the crystal is suspended in the center of the room, a location typical of normal whole body counting. The surface of the iron had not as yet been sand blasted or lined with lead. Comparable data were obtained in our iron room No. 2 (lead lined) under similar geometry, and the two spectra are shown in Figure 27. The difference in shape and structure at low energies is typical of such shieldings; the almost constant ratio of counting rates above about 600 keV is noteworthy. The integral counting rate from 30 keV to 1.6 MeV is 443 ± 6 cpm in the water shield versus 539 ± 7 cpm in our steel room. Because of the difference in shielding afforded by surrounding structures and of the uncertainties concerning surface contamination, it is perhaps premature to attach great significance to these numbers. To what extent this marked difference will be enhanced by sandblasting and lining the water-shielded room remains to be demonstrated.

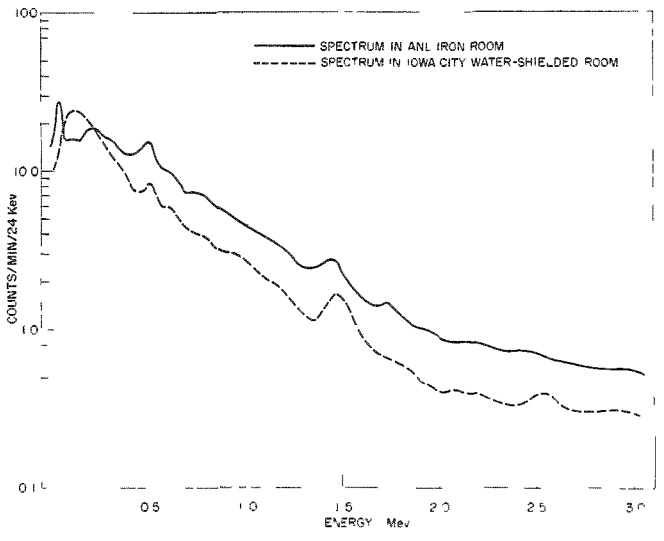

Figure 27

Background of 7- x 3-1/2-inch crystal No. 1 (no Hg in housing)

The absence of any marked 2.2-MeV thermal neutron capture peak in the water shield is somewhat unexpected. The fast neutron flux within this shield, as indicated by long counter data obtained with the same equipment mentioned above, is very low, being approximately only 14% of that in our iron room.

If the interaction between the protective vinyl coating applied to the tank and the water is small enough to permit turning off the recirculating ion exchanger, a further reduction in background might be obtained by borating the water. It has also been suggested that the Cerenkov radiation arising from mesons traversing the tank could be used to provide a useful anticoincidence signal. The only convenient place to couple a phototube to the water volume is through a three-foot-diameter standpipe which extends above grade, but since this is off-center, the uniformity of response over the tank area may seriously limit the practical application of such a scheme. Further experiments are planned in cooperation with the Verterans Administration personnel.

Acknowledgement

I am indebted to Dr. Richard Peterson, William Cook and Eugene Weiner of the Veterans Administration Hospital, Iowa City, for making their facilities available to us, and for their unfailing hospitality.

Reference

1. R. E. Peterson, E. V. Weiner, and W. Cook. Evaluation of a Water Shield Whole-Body Counter. Proc. Second Symp. on Radioactivity in Man, held at Northwestern University Medical School, September 5-7, 1962, in press.

EFFECT OF SILVER HALIDE CONTENT ON THE FILM DOSIMETRY OF A Sr^{90}-Y^{90} APPLICATOR*

Amrik S. Chhabra**

Abstract

Different dilutions of G5 Ilford emulsion have been used in Lucite for depth dose measurement of radiations emitted by a Sr^{90}-Y^{90} β-ray applicator and compared to results obtained with a Failla extrapolation chamber. The response of emulsion with normal silver content is quite satisfactory in the β-ray region, but it is too sensitive in the bremsstrahlung region by a factor of $\approx$40. The response of emulsions in which the AgBr: gelatin ratio is decreased by as much as a factor of five approaches somewhat that of the ionization chamber, in fair agreement with calculations based on Greening's formulation, but it is still too high for accurate dose measurements in regions where the contribution from bremsstrahlung is of the order of a few percent. Values of 2250 and 460 eV were found for the energy required to produce a developable grain.

Apparatus

A camera, shown in Figure 28, was used for exposure of the G5 emulsion films of 1- x 3-inch size. The gelatin/silver ratio as supplied by the manufacturer were 1, 2, 4 and 8 times the normal.† The emulsion in each case was 10μ thick and mounted on acetate-base film of 5/1000-inch thickness. The film slides, sandwiched between blackened Lucite absorbers at different depths, were stacked up into their holder in the camera and held in position by two screws set in the bottom rotating plate. The Sr^{90}-Y^{90} β-applicator could be brought on top of the film and absorber stack by

*This work was made possible through the financial support of the International Cooperation Administration under the exchange programme, and the laboratory facilities provided by the Radiological Physics Division of the Argonne National Laboratory.

**On leave from the Atomic Energy Establishment, Trombay, Bombay, India.

†The values of silver bromide determined chemically by extraction in nitric acid and titration with potassium thiocyanate were found to be 3.575 (normal), 1.841, 1.032 and 0.834 mg/cm^2. These values have been used in this paper as the correct ones although they are somewhat at variance with manufacturer's specifications.

rotating the top plate holding the source. To cover the wide range of exposure, each type of film was exposed in three different batches, each covering successively depths of 0-5; 4-8, and 7-18 mm; and times of exposure were adjusted as to give optical density within workable range. A control film, exposed to a standard Sr^{90}-Y^{90} calibrator, as given in Dudly's chapter,(1) consisting of Sr^{90}-Y^{90} in plaster of Paris, and developed in D-19 simultaneously with the other films, was used to provide the relevant density versus exposure curve. The density of the films, up to a range of six, was measured in an Ansco color densitometer, Model-12, with an aperture of 3-mm diameter. The Sr^{90}-Y^{90} β-applicator of stainless steel mounting was used at a distance of 6.35 mm from the top surface of the Lucite absorbers for all ionization and emulsion measurements.

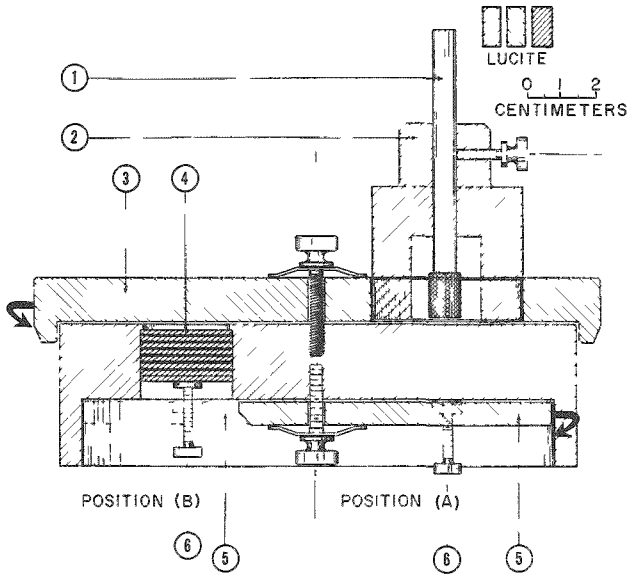

Figure 28

Diagram of the camera used for film exposure to beta-ray applicator.

1. Sr^{90}-Y^{90} applicator.
2. Applicator holder.
3. Top rotating plate used to bring the source on top of film stack.
4. Stack of Lucite absorbers and films positioned in the holder.
5. Bottom rotating plate to cover and hold the film stack from the bottom side.
6. Screws to hold the stack in position.

The absolute depth-dose measurements were made with a Failla extrapolation ion chamber with Lucite plates coated with Aquadag and of adjustable gap width. The collecting electrode, made by scratching a circle of 3-mm diameter at the center of the bottom plate, was connected to a vibrating reed electrometer (Applied Physics Corporation, Model-30) of maximum sensitivity of 10^{-17} amp. In the β-region, depth dose measurements were made with the constant deflection method employing a suitable resistor; in the bremsstrahlung region, the rate of charge collection method was used. Further details on the depth-dose measurements made with the extrapolation chamber will be found in Chhabra's paper published in Radiology.(2)

Results and Discussion

Figure 29 shows the results of depth-dose measurements in Lucite made with the extrapolation chamber, G5 and NTB stripping emulsion (10μ thick) of normal gelatin/silver ratio. It should be noticed that both

NTB and G5 start getting too sensitive at ≈6 mm depth, well before the end of the β-ray region which continues down to about 10 mm. Beyond this depth, in the bremsstrahlung region, both films are too sensitive by a factor of ≈40 compared to the response of the extrapolation chamber.

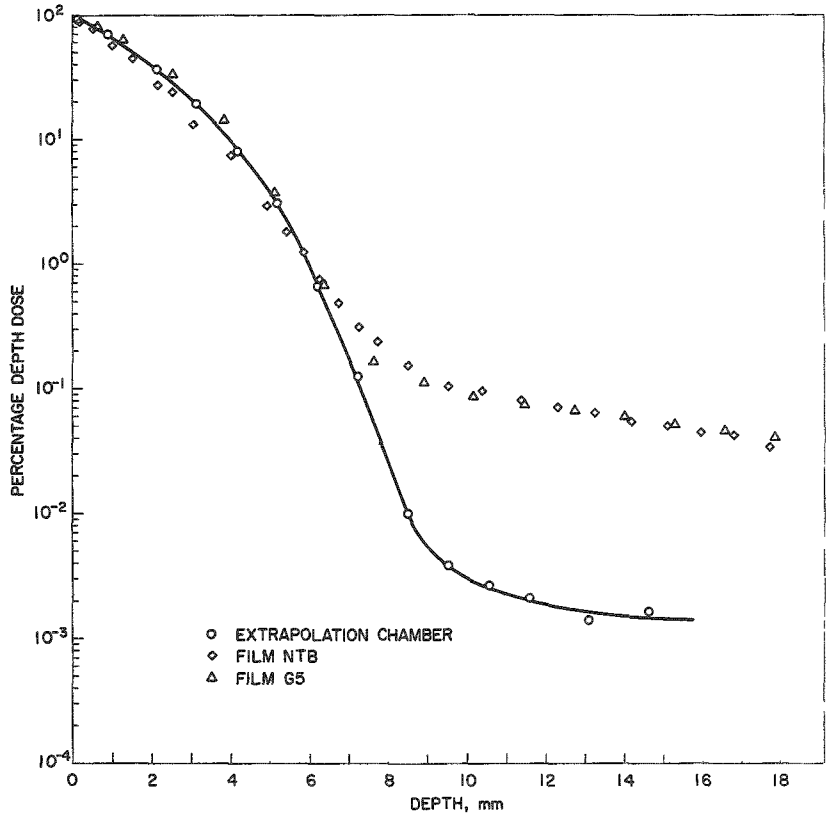

Figure 29

Comparison of depth-dose curves taken in Lucite with extrapolation chamber, Film NTB (Eastman Kodak) and G5 (Ilford)

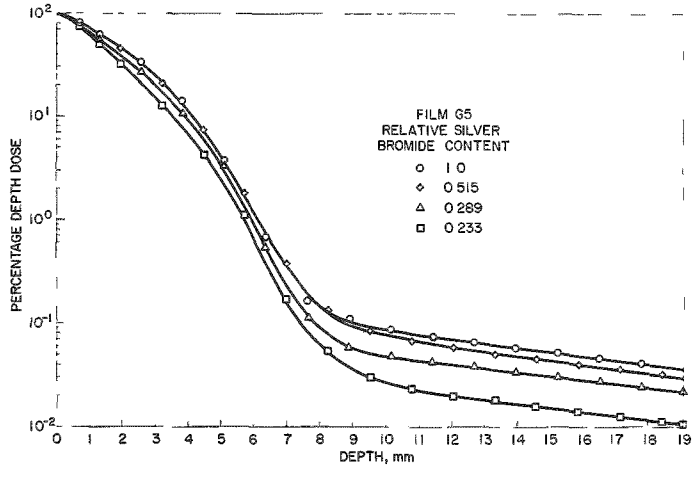

Figure 30

Depth-dose curves in Lucite taken with G5 emulsion of different gelatin/silver ratios

In Figure 30 are shown depth-dose curves for the G5 emulsion, with gelatin/silver ratios of normal, and 2, 4 and 8 times the normal, all curves being normalized to the dose at the surface. As the silver content of the emulsion is decreased there is a mild improvement in the response of the film throughout the region of β-rays and a much more pronounced one in the bremsstrahlung region.

This result can be predicted by using calculations developed by Greening[3] who assumes that the photographic effect is proportional to the energy absorbed by the AgBr in the emulsion and calculates this energy by the following expression:

$$\frac{\text{Ergs/g of AgBr}}{\text{Ergs/g of air}} = \frac{[(\tau + \sigma_a)/\rho]\ \text{AgBr}}{[(\tau + \sigma_a)/\rho]\ \text{air}} \times F_1F_2F_3 + 0.71 \quad . \qquad (1)$$

This formula leads to the energy absorbed in the AgBr of the emulsion as compared to that in air by correction of their mass energy absorption coefficients $(\tau + \sigma_a)/\rho$.* The factor F_1 takes into account the energy of fluorescent x rays emitted by AgBr which are not utilized by the emulsion. The factor F_2 corrects for the energy lost through secondary electrons leaving the thin emulsion sheet, and F_3 the energy lost by the grain to the gelatin of the emulsion itself. The last term, equal to 0.71, represents the relative energy gain by the silver bromide through secondary electrons produced in gelatin and the surrounding material of low atomic number. The factor F_3 effectively takes into account the gelatin to silver ratio of the emulsion, whereas F_2 is dependent on the thickness, or more strictly speaking, on the density of the emulsion which in turn determines the range of the secondary electrons These correction factors have been calculated in detail by Greening and are tabulated in his paper.

The calculated curves of Figure 31 show energy absorption relative to that in air for emulsions of different silver bromide content but of same thickness (10μ) and photon energies of 248, 103, 62, 41 and 31 keV. The experimental points, derived from the bremsstrahlung region (≈12 mm depth) of the depth-dose curves in Figure 30, are normalized with the value of 28.1

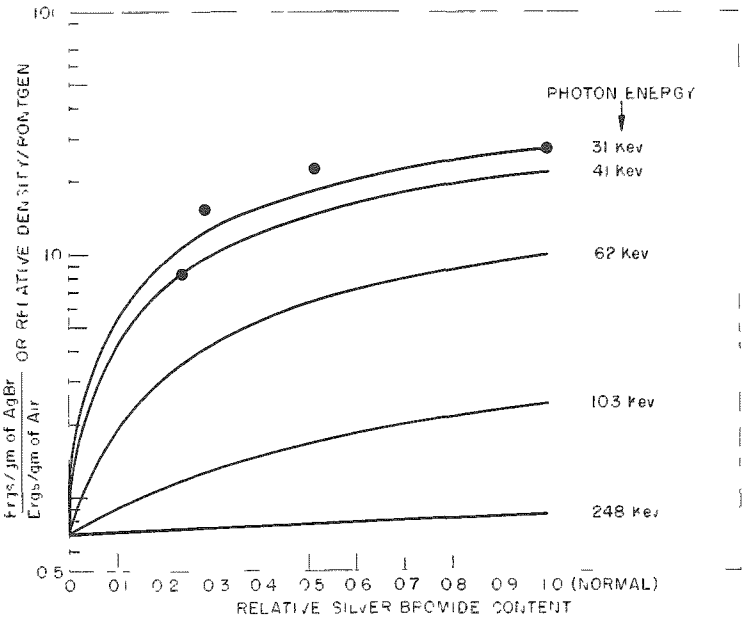

Figure 31

Calculated response of G5 emulsions (Greening's formulation) as a function of silver bromide content. Photon-energies of 250, 100, 62, 40 and 30 keV. The experimental points, ●, from Figure 30 in the bremsstrahlung region (at depth of ≈12 mm) lie fairly close to the curve for 30 keV

*τ is the linear photoelectric absorption coefficient, σ_a the Compton recoil absorption coefficient and ρ the density of the material.

for normal silver bromide content. This number is equal to 40 x 0.71, the value 40 being derived from the ratio of curves in Figure 29 and the value of 0.71 obtained by Greening's analysis; they indicate an effective bremsstrahlung energy of about 30 keV. The experimental curve should hit the ordinate at a value of about 2.2; this limit, calculated in the appendix for an emulsion with a single grain of 0.3μ diameter exposed to an effective γ energy of 40 keV, is the lowest value one could achieve unless the grain size itself is reduced. This limit is always reached in practice when the secondary electron produced in AgBr has range equal to the average distance between two grains.

The experimental points seem to be in fair agreement with the theoretical curve; and the latter suggests that a reduction of silver bromide content by a factor of about 20 would reduce the film response to bremsstrahlung by only a factor of 13. This would leave the film still too sensitive by a factor of ≈3.5. However, in the 40- and 100-keV γ-energy region, the same reduction would leave the film too sensitive only by a factor of 2.5 and 1.3 respectively.

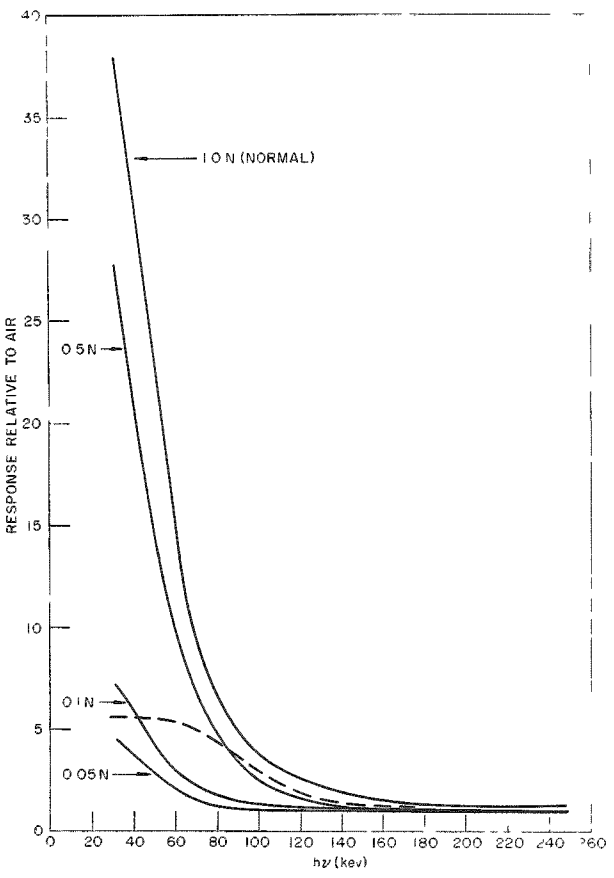

Figure 32

Response of film relative to air against photon energy for different silver bromide content (normal, and 1/2, 1/10, and 1/20th normal). The dotted curve gives the ratio of response of films with normal and 1/10th normal silver bromide content as a function of photon energy.

The curves in Figure 32 show the calculated response of the film relative to air against gamma energy for normal, 1/2, 1/10 and 1/20th normal silver bromide content. Since this relative response is strongly dependent on AgBr content, the presence of bremsstrahlung at a given point within the medium can be detected by measuring the relative response of a "normal" and, say, 1/10 normal emulsion; the values of this relative response are shown in Figure 32 by the dotted line to which the absolute value of the ordinates applies. It should be realized also that since this curve applies only to the presence of monochromatic photon radiation, it is of limited use unless some independent estimate is made of the relevant photon energy.

Exposure versus density curves for the different G5 emulsions are shown in Figure 33. These films,

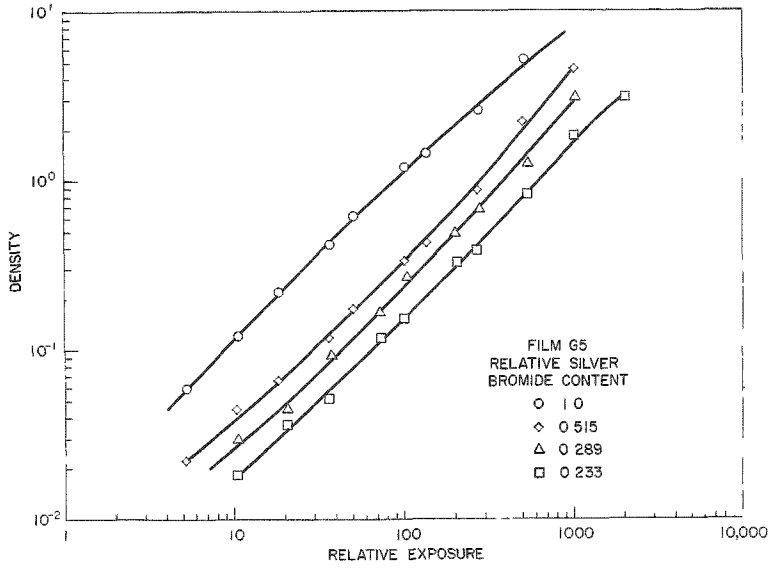

Figure 33

Density versus exposure curves for four different concentrations of silver bromide in G5 emulsion, obtained with standard Sr^{90}-Y^{90} calibrator.

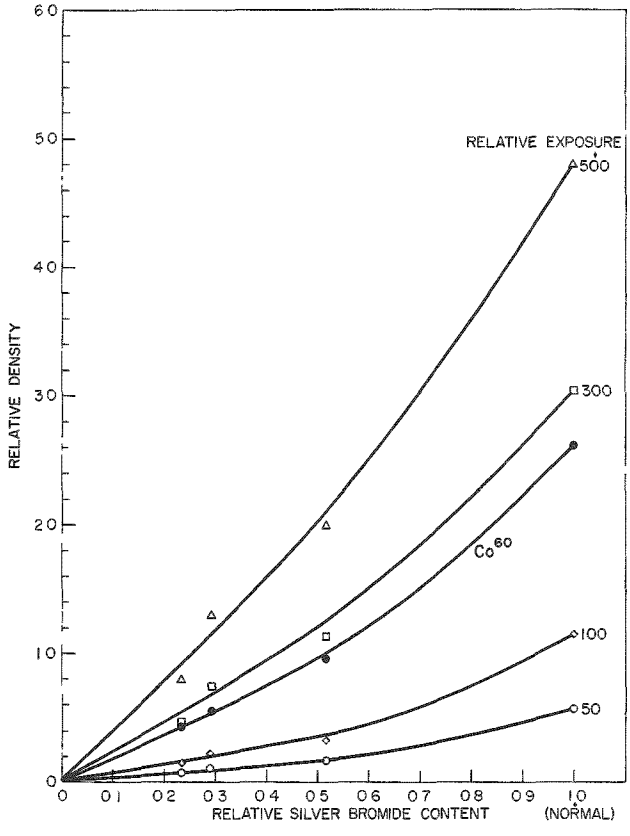

Figure 34

Photographic response of G5 emulsion to beta rays (open points) and Co^{60} gamma rays (black dots) as a function of silver bromide content. Each beta-ray curve corresponds to one particular exposure.

exposed to a standard Sr^{90} calibrator and simultaneously developed in D-19 for 5 minutes and fixed for 10 minutes, exhibit, to a first approximation, a fairly linear response, irrespective of AgBr concentration. From these curves one could draw, for different exposures, the relative response of the film to beta rays as a function of relative AgBr content, as shown in Figure 34. These curves are linear and pass through the origin in the region of low silver content; their slopes, however, increase as the silver content is increased. This could be due to multiple scattering of beta rays inside the emulsion, which effectively increases their path length and, correspondingly, the photographic effect. In Figure 34 is also shown a curve for identical Co^{60} γ-ray exposure of the normal and "diluted" films sandwiched between 3 mm of Lucite absorber. This curve follows the same trend as that

for beta rays, thereby indicating that the photoelectric effect for these high-energy gammas is negligible.

For beta-ray dosimetry, a reduction in silver bromide would be beneficial since it would reduce the "high Z" multiple scattering but, as already mentioned for exact evaluation of γ-ray dose, use of two films of different dilutions would always be desirable for it would give some information on the nature of the dose absorbed in tissue.

Calculation of energy required by a developable grain

From the simultaneous measurement of β- and bremsstrahlung depth doses with the extrapolation chamber and the photographic emulsions, the mean energy $\overline{E}$ required by the emulsion grain to become developable was calculated for emulsions type NTB and G5. The number of grains developed per cm^2 (n) determined through the film density (D) measurement by the relation:

$$D = ka\ n \tag{2}$$

where

$k = \log_{10} e$

a = average area of a developed grain (mean diameter of both NTB and G5 emulsion grain is about 0.3μ).

The energy absorbed in silver bromide through beta-particle exposure was determined from the stopping power of silver bromide relative to Lucite and the absorbed dose measured by the extrapolation chamber. Thus the mean energy ($\overline{E}\,\beta$) spent per grain made developable follows from:

$$\overline{E}_\beta = A\ \frac{\text{dose in rads (Lucite)} \times S_{AgBr}}{n}\ \text{eV} \tag{3}$$

where

S_{AgBr} = stopping power of silver bromide relative to Lucite

and

A = constant, which takes care of the amount of silver bromide per square cm and conversion from 100 ergs to eV.

In the bremsstrahlung region the energy absorbed in silver bromide was determined from the absorbed dose in Lucite, as measured with the extrapolation chamber, and the calculated relative absorptions shown in Figure 31. The mean energy ($\overline{E}_\gamma$) spent per grain made developable could then be determined from the relation

$$\overline{E}_\gamma = A \frac{\text{dose in rads (Lucite)} \times 1/S_{(\text{Lucite})} \times f}{n} \text{ eV} \qquad (4)$$

where

$$S_{\text{Lucite}} = \frac{(\tau + \sigma_a)/\rho \text{ Lucite}}{(\tau + \sigma_a)/\rho \text{ air}} \times \text{stopping power of Lucite relative to air}$$

(The first term giving the ratio of mass absorption coefficient for Lucite and air is very close to unity.) f = factor obtained from ordinates of Figure 31 for effective photon energy of ≈30 keV. A and n being the same as in the relation for beta rays.

The values of $\overline{E}_\beta$ and $\overline{E}_\gamma$ thus calculated for film NTB were respectively 2300 and 2205 eV (avg 2250) and for film G5, were about 480 and 450 eV (avg 460). These results are at variance with some conclusions drawn by Malinowski[4] who states that the mean energy spent per grain made developable by x rays or ionizing particles is dependent only on geometrical dimensions of the emulsion grain. In our measurements, two emulsions NTB and G5, both having grains of the same average diameter showed relative sensitivities differing by a factor of five following either beta- or gamma-ray exposure. Our values for NTB are of the order of other published or calculated values.[5,6]

I wish to express my sincere thanks to L. D. Marinelli for suggesting the problem and for directing the course of this work. My thanks are also due to Dr. G. Failla for the use of his extrapolation ionization chamber and to R. E. Rowland for the use of darkroom facilities. Special thanks are due to Dr. J. E. Rose for the kind permission to work in the Radiological Physics Division.

APPENDIX: ENERGY ABSORPTION OF 40-KEV PHOTONS BY A SINGLE GRAIN OF AgBr SURROUNDED ON ALL SIDES BY GELATIN AND OTHER MATERIAL OF LOW Z

The energy absorbed in a single grain of AgBr relative to air is given by the relation

$$\frac{\text{Ergs/g of AgBr}}{\text{Ergs/g of Air}} = \frac{(\tau + \sigma_a)/\rho \text{ AgBr}}{(\tau + \sigma_a)/\rho \text{ Air}} \times F_1 F_2 + 0.71 \qquad (5)$$

where the various terms are as explained before. The factor F_2 is now the fraction of energy retained inside the grain.

Assuming isotropic distribution of electrons and their straight trajectories, the average path length in a spherical grain of radius r is given equal to $\frac{2}{3}$ r. From the relation between the range R and the energy E of an electron given by the formula $R = C \cdot E^{1.74}$, the fraction of the original energy retained by the electron after travelling a fraction p of its range is calculated to be: $(1-p)^{1/1.74}$.(3) The fractional energy F_2, spent inside the grain is thus equal to $\{1 - (1-p)^{1/1.74}\}$. The fraction p is given by the average path length ($\frac{2}{3}$ r = 0.1μ) divided by the total range R of the electron in AgBr. R was determined from the ranges given by Lea(7) for tissue divided by the density of AgBr (6.47 g/cm^3).

For an x-ray energy of 40 keV, the percentage of electrons of different energy groups given by Greening(3) and their ranges in tissue and AgBr and the fractional energy retained in the grain are shown in Table 11. The over-all retention of energy inside the grain (factor F_2) will be given by the sum of the values noted in the table after each is properly weighed by the number of electrons in that group. The factor F_2, for the photon energy of 40 keV and grain diameter equal to 0.3μ, is thus calculated to be 0.05. From the ratio of the mass absorption coefficient of AgBr to air equal to $\frac{12.2}{0.241}$ and factor F_1 = 0.598, as given by Greening,(3) the energy absorption in the silver bromide grain relative to air is found to be 2.2. It may be pointed out here that the value of F_1 as calculated by Greening for a normal emulsion should be a little lower for the present case because almost all the fluorescent radiation will escape. This may reduce the above value by about 10%.

Table 11

The division of total number of electrons, their respective energy and range in tissue and AgBr, released in silver bromide between the silver and bromide photo, Auger and recoil electrons, for 40-keV photon energy. The last row gives the fraction of energy of electron of the particular group retained in the AgBr grain of 0.3μ diameter.

	Ag photo	Br photo	Ag Auger	Br Auger	Recoil		Ag photo	Br photo	Ag Auger	Br Auger	Recoil
Percentage of total number of electrons	48	28	18	6	0	Range in AgBr, μ (6.47 g/cm^3)	0.875	2.30	2.01	0.656	-
Electron energy, keV	15.8	27.8	25.5	13.5	-	Fraction of energy retained inside the grain = $1-(1-p)^{1/1.74}$	0.068	0.0256	0.0291	0.0905	-
Range in tissue, μ (1 g/cm^3)	5.6	14.9	13.0	4.25	-						

F_2 = (0.068 x 0.48 + 0.0256 x 0.28 + 0.0291 x 0.18 + 0.0905 x 0.06) = 0.05.

References

1. Dudley, R. A. "Photographic Film Dosimetry," in Radiation Dosimetry. Academic Press, New York, 1956 Chapter 7, p. 300.

2. Chhabra, Amrik S. "Sr^{90}-Y^{90} Beta-Ray (and Bremsstrahlung) Depth-Dose Measurements in Lucite. Radiology 79, 1001-1007 (1962).

3. Greening, J. R. "The Photographic Action of X-rays." Proc. Phys. Soc. 64 B, 977 (1957).

4. Malinowski, J. "On the Mechanism of the Photographic Action of X-rays." Z. Phys. Chem. 204, 276-285 (1955).

5. Poddar, R. K. "Sensitivity of the Photographic Emulsion to Beta Spectra and its Dependence on Their Average Energy." Radiation Res. 11, 498-508 (1959).

6. Marinelli, L. D. "Radiation Dosimetry of Internally Administered Beta-Ray Emitters: Status and Prospects." Radiology 63, 656-661 (1954).

7. Lea, D. E. "Actions of Radiations on Living Cells." Cambridge University Press, Cambridge, 1946, p. 24.

EFFECT OF LONG DECAY CHAINS ON THE COUNTING STATISTICS IN THE ANALYSIS OF RADIUM^{224} AND RADON^{222}

H. F. Lucas, Jr. and D. A. Woodward*

I. Introduction

The very low concentrations of Th^{228} and Ra^{226} found in normal human bone require counting times of 6-20 hours to attain reasonable statistical accuracy. In the procedures used, the respective daughters Ra^{224} and Rn^{222} are each separated from the parent, purified and then assayed by alpha counting.[1,2] The counting systems have efficiencies of 0.50 and 0.85 counts per alpha for the Ra^{224} and the Rn^{222} series respectively.[1,3]

For these or any radioactive series, the number of counts are distributed according to the Poisson law only for counting intervals that are much shorter than the mean life of all of the nuclides being counted and when the solid angle subtended by the detector is very much less than 100%.[4] Consequently, the standard deviation in the count is not accurately estimated by the square root of the number of counts. A method is desired to estimate accurately the variance in the number of observed counts, one which is as simple to apply as if the number of counts were distributed according to the Poisson law.

Let us suppose that we have a defective counting instrument which always records exactly 2.60 counts for every true input count. If we then observe N counts on this instrument, the standard deviation of N is estimated by $\sqrt{2.60\ N}$. Similarly in the counting of the long decay chains in which the mean life of some of the nuclides is very short compared to the counting interval, and in which the solid angle subtended by the detector is very large, there is a very high probability of observing a count not only from the parent but also each of the daughters. Thus, one might expect that the standard deviation of the count could be estimated by an expression such as $\sqrt{JN}$, where J is the ratio of the observed count to that from the parent atoms.** Thus, in our case, J can have values between 1 and 4 for the Ra^{224} and between 1 and 3 for the Rn^{222} series, respectively.

The problem of estimating the standard deviation of the observed count from long decay chains has been of concern for a long time. Adams[5] in 1933 applied a derivation of the probability law to the counting of alpha particles from Th^{232} in equilibrium with its daughters. Lindeman[6] in an

---

* Applied Mathematics Division.

** This meaning of J is accurate only for counting times very short compared to the mean life of the parent.

attempt to remove the approximations and limitations of the method of Adams used a different approach. Unfortunately, both failed to include in their calculations the pertinent experimental parameters.*

Huybrechts[8] has included in his derivation the solid angle subtended by the detection device, as well as the detection efficiency. His calculations assume that a nuclear emulsion was used as the detection device and that the counting interval was 30 days for the U^{238}, Th^{232}, or Th^{228} series in equilibrium with their daughters.

Preliminary calculations confirmed that the short half-lives of the daughters of Ra^{224} and Rn^{222} had a greater effect on the estimate of the standard deviation of the count than it had for the case of Th^{232} in equilibrium with its daughters. Moreover, the magnitude of this effect would vary with time after parent-daughter separation. The value of J has been calculated as a function of each of three of the possible variables which affect its value: a, the counting interval, b, the time after parent-daughter separation, and c, the solid angle subtended by the detection device. All calculations were made with an IBM-704 computer and the following method.

II. Method

Each alpha particle emitted in the radioactive decay series initiated by the decay of the parent atom (Ra^{224} or Rn^{222} in the present case) may result in an observed count Let M be the number of parent atoms initially in the sample, i.e at the time of purification, and N be the total observed count in a given measurement. Suppose that all atoms in the same state of the decay scheme are equally likely to be counted. Then it follows that the decay of any one family (parent atom together with its daughters) is as likely to be counted as the decay of any other family. Thus the number of counts resulting from one family has the same mean number, μ, of observed counts and variance σ^2 as that from any other family. Consequently, the variance of the total observed count N is $M\sigma^2$ and the mean of N is $M\mu$.

We wish to estimate the value $M\sigma^2$ which is the variance in the total number of observed counts. If we let $J = \sigma^2/\mu$, then NJ is an unbiased estimator of $M\sigma^2$ because the mean of NJ is $M\mu J = M\sigma^2$. In addition, the variance of the estimator NJ (the variance of the estimate of the variance of the number of observed counts) is $M\sigma^2 J^2$ which we estimate by NJ^3.

Let $q(0), q(1), q(2) \ldots q(h)$ be the probabilities that 0, 1, 2, ... h counts, respectively, are obtained from the α decay of a family. If H is the maximum number of α counts per family, then $q(h) = 0$ for $h > H$. The variance σ^2 in the number of counts resulting from the decay of a single family is

* A further criticism of the method of Lindeman as well as a very complete discussion of this problem will be found in Reference 7.

$$\sigma^2 = \left[\sum_{h=0}^{H} h^2 q(h)\right] - \mu^2 \qquad (1)$$

where the mean number μ of observed counts per family is

$$\mu = \sum_{h=0}^{H} hq(h)$$

and

$$J = \sigma^2/\mu$$

The problem then is to calculate the probabilities q(0), q(1), ... , q(H). Let t_1 be the time elapsed between purification and the start of counting and let Δt be the length of the counting interval. Let the parent state be E(0) and the subsequent states to which it decays be E(1), E(2), . . . E(K), k = 0, 1, 2 . . . K. Let E(K) be stable. This scheme is sufficient since "branching" may be ignored for alpha counting in either the Ra^{224} or Rn^{222} series. Let P(i, j; t) be the probability that an atom in state E(i) at t = 0 will be in state E(j) at time t. From the Bateman equation,[9]

$$P(i,j;t) = \begin{cases} \left\{\sum_{k=i}^{j-1} \frac{\lambda_k e^{-\lambda_k t}}{\lambda_j - \lambda_k} \left[\prod_{\substack{b=i \\ b\neq k}}^{j-1} \frac{\lambda_b}{\lambda_b - \lambda_k}\right]\right\} + \left[\prod_{b=i}^{j-1} \frac{\lambda_b}{\lambda_b - \lambda_j}\right] e^{-\lambda_j t}, & \text{if } j > i \\ e^{-\lambda_i t}, & \text{if } i = j \\ 0, & \text{if } i > j \end{cases} \qquad (2)$$

where

λ_k = decay constant of state E(k)

and

$\lambda_K = 0$.

Let D(i, j; h) be the probability that h is the number of counts recorded for an atom which was in state E(i) at time t_1 and in state E(j) at time $t_1 + \Delta t$. A typical history of an atom is that it was in state E(0) at t = 0, state E(i) at T = t_1, and state E(j) at t = $t_1 + \Delta t$. The probability that this is the history and that h counts were recorded is given by the product

$$P(0, i; t_1) \cdot P(i, j; \Delta t) \cdot D(i, j; h) \qquad (3)$$

Since an atom can have only one history, the histories of all atoms are mutually exclusive. Hence, the probability of h counts is the sum of expression (3) over all histories, i.e.,

$$q(h) = \sum_{i=0}^{K} \sum_{j=i}^{K} P(0, i; t_1)\ P(i, j; \Delta t)\ D(i, j; h) \qquad (4)$$

The value of D(i, j; h) is determined by the experiment. For the case being considered here, the counting device is only sensitive to alpha particles, and the fraction of the total solid angle subtended by the sensitive volume (the geometrical efficiency) is known. If the sample being counted is sufficiently thin, then little self-absorption occurs and all alpha particles will have the same probability, d, of being counted. Since both the alpha proportional counter and the radon counter have a detection efficiency for alphas of approximately 100%, the value of d will be approximately equal to the experimental efficiency of 0.50 and 0.85 counts per alpha for the Ra^{224} and Rn^{222} series respectively.

Let the number of α particles emitted between state E(i) and E(j) be A(i, j), which is obtained by counting within the decay scheme (Table 12). Then D(i, j; h) is the probability of exactly h successes in A(i, j) independent trials, that is,

$$D(i, j; h) = \binom{A(i, j)}{h} d^h (1-d)^{A(i, j)-h} \qquad (5)$$

where

$$\binom{A}{h} = \begin{cases} \dfrac{A(A-1)\cdots(A-h+1)}{1\cdot 2 \cdots h}, & \text{if } h \le A \\ 0, & \text{if } h > A \end{cases}$$

is a binomial coefficient and d for our instruments is the efficiency of the counting device.

Table 12

Decay scheme of Ra^{224} and Rn^{222}

State	Ra^{224}		Rn^{222}	
	Nuclide	λ_k (hr^{-1})	Nuclide	λ_k (hr^{-1})
E(0)	Ra^{224} α	7.934×10^{-3}	Rn^{222} α	7.550×10^{-3}
E(1)	Em^{220} α	4.579×10^{1}	Po^{218} α	1.369×10^{1}
E(2)	Po^{216} α	1.579×10^{4}	Pb^{214} β	2.131×10^{0}
E(3)	Pb^{212} β	6.515×10^{-2}	Bi^{214} β	1.558×10^{0}
E(4)	Bi^{212} α	6.874×10^{-1}	Po^{214} α	2.40×10^{7}
E(5)		0	Stable*	

* The alpha decay is slow enough to be neglected for the usual values of t and Δt.

The value of J used in estimating the variance (and hence the standard deviation) of the count may be calculated from Eqs. (1), (2), (4), and (5), when all alpha particles are equally likely to be counted. As an example consider the Ra^{224} series. Let t_1 = 2 hr, Δt = 1 hr, d = 0.470 and N = 20.* From Table 12, we see that four alphas are emitted from five states; hence H = 4 and K = 5. The solution of Eq. (4) for the case h = 4 yields

$$q(4) = \sum_{i=0}^{5} \sum_{j=i}^{5} P(0, i; 2) \cdot P(i, j; 1) \cdot D(i, j; 4) \quad . \tag{6}$$

From Eq. (5) we see that D(i, j; 4) = 0 unless A(i, j) ≥ 4. From Table 12, A(i, j) cannot be greater than 4 and A(i, j) = 4 only if i = 0 and j = 5. Thus, from Eq. (5)

$$D(0, 5; 4) = d^4(1-d)^0 \left(\frac{4 \times 3 \times 2 \times 1}{1 \times 2 \times 3 \times 4}\right) = d^4 \tag{7}$$

and

$$q(4) = P(0, 0; 2) \cdot P(0, 5; 1) \cdot d^4$$

Equation (2) is used to calculate P(0, 0; 2) and P(0, 5; 1). Similarly, q(3), q(2), and q(1) may be calculated as above. For this case where the efficiency d = 0.47 and the number of counts N = 20, we find:

$$\mu = \sum_{h=0}^{4} hq(h) = 0.0112620 \quad . \tag{8}$$

and

$$\sigma^2 = \left[\sum_{h=0}^{4} h^2 q(h)\right] - \mu^2 = 0.0213583$$

$$J = \frac{\sigma^2}{\mu} = 1.89649$$

$$\sigma_N = \sqrt{JN} = 6.2$$

and

$$\sigma_N^2 = NJ \pm \sqrt{NJ^3}$$

$$= 37.9 \pm 11.6$$

* In this example it was assumed that the background of the counting device was zero.

III. Discussion

The value of J in the long decay chains is a function of many variables; of these the counting interval, the time after parent-daughter separation, and the solid angle of the counting device have been evaluated. Because of the very wide range of these experimental conditions, it is useful to determine how each affects the value of J.

A. Variation of J with Counting Interval.

The effect of the counting interval Δt on the value of J is shown in Figure 35 for the Ra^{224} and Rn^{222} series. For these calculations the time from purification to start of the count was held constant at t_1 = 1.0 hr and the efficiency was 0.47 for the Ra^{224} and 0.92 for the Rn^{222} series, respectively. For the Rn^{222} series, the value of J is seen to increase from 1.04 to 2.50 as the counting interval increases from 0.01 to 7 hr and then to decrease to 1.44 for a counting interval of 100 hr. These changes in J as the counting interval increases illustrate that: a) J ≈ 1 when the counting interval is much shorter than the respective half-lives of Rn and its daughters; b) J increases to a maximum as the counting interval becomes much longer than the half-lives of the daughters but remains shorter than that of radon; and c) J decreases from this maximum as the counting interval becomes much longer than the longest half-life.

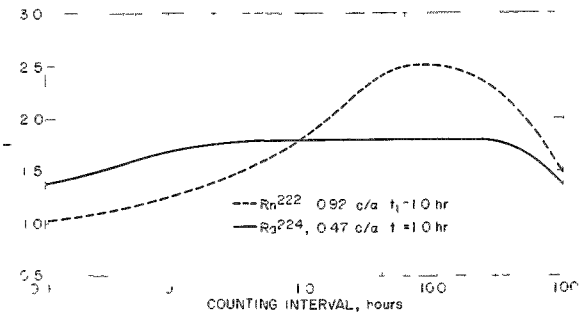

Figure 35

Variation of J for Ra^{224} and Rn^{222} with counting interval

A similar explanation follows for the Ra^{224} series when the difference in the decay scheme is taken into account. The very large range of counting intervals over which the value of J is constant at 1.80 is very convenient since it encompasses all normally encountered counting intervals. Thus, for this series, a single value can be used in all calculations.

B. Variation of J with Solid Angle.

The dependence of J on solid angle (and hence efficiency) is shown in Figure 36 for the Ra^{224} and Rn^{222} series. For these calculations, the time of the count was held constant at t_1 = 1 hr after separation from daughters, and the counting interval was Δt = 10 hr. For both series, the value of J increases from a low of about 1.0 to a high of about 3 as the efficiency varies from 0.01 to 1.00. Significantly large values of J are obtained

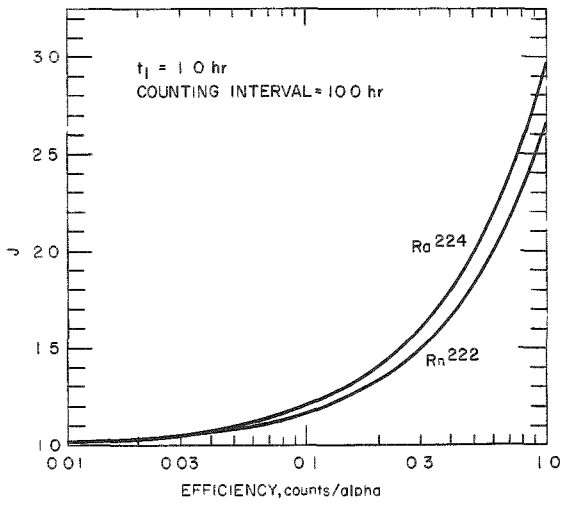

Figure 36
Variation of J for Ra^{224} and Rn^{222} with efficiency.

for efficiencies of 0.3 to 0.9, which are commonly attained in alpha counting of these nuclides. Curves calculated for other normally-encountered counting intervals and times after separation of daughters give similar results, as would be expected from Figure 35.

C. Variation of J with Time after Separation from Daughters.

The effect of a delay between the time of separation of Ra^{224} and Rn^{222} from their daughters and the start of counting is shown in Figures 37 and 38, respectively. For both series, the value of J remains relatively constant for times after separation ranging from 0.1 to 1000 hr provided the counting interval is short compared with the half-life of either Ra^{224} or Rn^{222}. At longer counting intervals, such as 1000 hr, the value of J ranges from 0.53 to 2.35 for the Ra^{224} series and from 0.090 to 2.83 for the Rn^{222}. Similar curves are obtained for other values of detection efficiency.

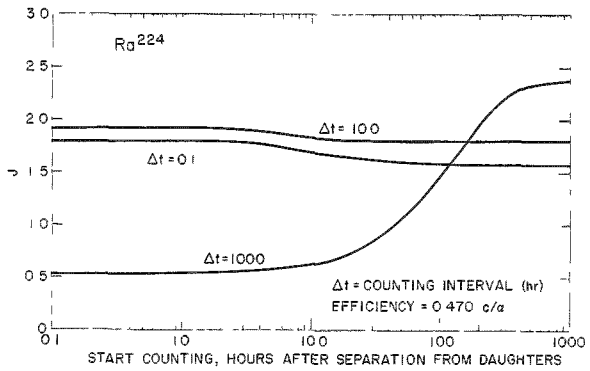

Figure 37
Variation of J for Ra^{224} for counting intervals beginning at various times after separation from daughters.

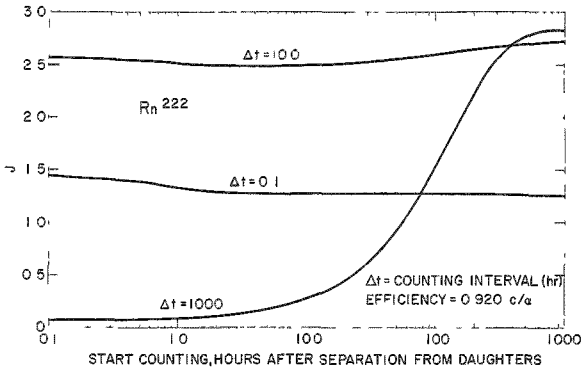

Figure 38
Variation of J for Rn^{222} for counting intervals beginning at various times after separation from daughters.

The value of J for other counting intervals, times after separation and for efficiencies of 0.250, 0.500 and 0.853 are respectively summarized in Tables 13 through 15 for the Ra^{224} and in Tables 16 through 18 for the Rn^{222} series. From these data it is possible by interpolation quickly to estimate the value of J appropriate to various experimental conditions.

Table 13

Variation of J for radium-224. Efficiency = 0.250

TIME AFTER SEPARATION	COUNTING INTERVAL (HOURS) 0.001	0.010	0.100	1.000	2.000	5.000	10.000	20.000	100.000	1000.000
0.0001	1.0519	1.2126	1.4572	1.4924	1.4933	1.4975	1.5028	1.4927	1.1952	0.7504
0.0010	1.0642	1.2142	1.4558	1.4923	1.4932	1.4974	1.5028	1.4927	1.1952	0.7504
0.0100	1.1241	1.2231	1.4452	1.4911	1.4926	1.4972	1.5027	1.4926	1.1952	0.7504
0.1000	1.1686	1.2315	1.4274	1.4886	1.4910	1.4962	1.5018	1.4919	1.1951	0.7507
0.2000	1.1690	1.2316	1.4271	1.4882	1.4905	1.4954	1.5010	1.4912	1.1951	0.7512
0.3000	1.1690	1.2315	1.4269	1.4878	1.4899	1.4946	1.5002	1.4905	1.1950	0.7516
0.4000	1.1689	1.2314	1.4267	1.4874	1.4894	1.4938	1.4993	1.4897	1.1950	0.7521
0.5000	1.1688	1.2313	1.4264	1.4869	1.4887	1.4931	1.4985	1.4890	1.1949	0.7525
0.6000	1.1687	1.2311	1.4261	1.4864	1.4881	1.4923	1.4977	1.4883	1.1949	0.7529
0.7000	1.1686	1.2309	1.4258	1.4858	1.4874	1.4914	1.4968	1.4876	1.1948	0.7534
0.7000	1.1686	1.2309	1.4258	1.4858	1.4874	1.4914	1.4968	1.4876	1.1948	0.7534
0.8000	1.1684	1.2307	1.4254	1.4852	1.4868	1.4906	1.4960	1.4868	1.1948	0.7538
0.9000	1.1683	1.2305	1.4250	1.4846	1.4861	1.4898	1.4952	1.4861	1.1947	0.7543
1.0000	1.1681	1.2303	1.4246	1.4840	1.4853	1.4890	1.4943	1.4854	1.1947	0.7547
2.0000	1.1660	1.2273	1.4190	1.4769	1.4776	1.4806	1.4861	1.4784	1.1944	0.7592
3.0000	1.1634	1.2238	1.4124	1.4690	1.4695	1.4724	1.4783	1.4717	1.1942	0.7638
4.0000	1.1607	1.2201	1.4056	1.4611	1.4616	1.4646	1.4709	1.4656	1.1943	0.7686
5.0000	1.1581	1.2165	1.3990	1.4536	1.4541	1.4573	1.4641	1.4599	1.1945	0.7734
6.0000	1.1557	1.2131	1.3927	1.4466	1.4472	1.4506	1.4578	1.4546	1.1950	0.7784
7.0000	1.1534	1.2100	1.3870	1.4401	1.4407	1.4444	1.4520	1.4498	1.1957	0.7835
8.0000	1.1513	1.2071	1.3816	1.4341	1.4348	1.4387	1.4466	1.4454	1.1965	0.7886
9.0000	1.1494	1.2044	1.3767	1.4285	1.4293	1.4334	1.4417	1.4413	1.1976	0.7939
10.0000	1.1476	1.2019	1.3721	1.4234	1.4242	1.4285	1.4372	1.4376	1.1988	0.7993
11.0000	1.1459	1.1996	1.3679	1.4186	1.4196	1.4240	1.4330	1.4342	1.2001	0.8047
12.0000	1.1444	1.1975	1.3640	1.4143	1.4153	1.4199	1.4291	1.4311	1.2016	0.8102
13.0000	1.1430	1.1956	1.3604	1.4102	1.4113	1.4160	1.4256	1.4282	1.2032	0.8158
14.0000	1.1416	1.1937	1.3570	1.4065	1.4076	1.4125	1.4223	1.4256	1.2050	0.8214
15.0000	1.1404	1.1921	1.3539	1.4030	1.4041	1.4092	1.4193	1.4233	1.2068	0.8271
16.0000	1.1393	1.1905	1.3511	1.3998	1.4010	1.4062	1.4165	1.4211	1.2088	0.8328
17.0000	1.1382	1.1890	1.3484	1.3968	1.3980	1.4034	1.4139	1.4192	1.2108	0.8386
18.0000	1.1372	1.1877	1.3459	1.3940	1.3953	1.4008	1.4116	1.4174	1.2129	0.8444
19.0000	1.1363	1.1864	1.3436	1.3914	1.3927	1.3983	1.4094	1.4158	1.2151	0.8502
20.0000	1.1355	1.1853	1.3414	1.3890	1.3903	1.3961	1.4074	1.4144	1.2174	0.8560
30.0000	1.1295	1.1770	1.3263	1.3721	1.3739	1.3809	1.3943	1.4065	1.2428	0.9148
40.0000	1.1263	1.1727	1.3183	1.3635	1.3656	1.3738	1.3894	1.4061	1.2708	0.9725
50.0000	1.1246	1.1703	1.3140	1.3589	1.3615	1.3709	1.3885	1.4094	1.2990	1.0276
60.0000	1.1237	1.1690	1.3117	1.3566	1.3596	1.3702	1.3897	1.4144	1.3263	1.0794
80.0000	1.1229	1.1679	1.3096	1.3550	1.3587	1.3714	1.3944	1.4258	1.3766	1.1729
100.0000	1.1226	1.1676	1.3091	1.3548	1.3592	1.3738	1.3998	1.4369	1.4263	1.2533
1000.0000	1.1225	1.1674	1.3091	1.3582	1.3662	1.3917	1.4352	1.5054	1.6771	1.7221

Table 14

Variation of J for radium-224. Efficiency = 0.500

TIME AFTER SEPARATION	COUNTING INTERVAL (HOURS) 0.001	0.010	0.100	1.000	2.000	5.000	10.000	20.000	100.000	1000.000
0.0001	1.1037	1.4252	1.9144	1.9849	1.9865	1.9949	2.0057	1.9855	1.3905	0.5007
0.0010	1.1284	1.4283	1.9116	1.9846	1.9864	1.9949	2.0056	1.9855	1.3905	0.5007
0.0100	1.2482	1.4462	1.8903	1.9822	1.9851	1.9944	2.0053	1.9853	1.3904	0.5007
0.1000	1.3373	1.4630	1.8549	1.9772	1.9821	1.9923	2.0036	1.9838	1.3902	0.5014
0.2000	1.3381	1.4631	1.8541	1.9764	1.9810	1.9908	2.0020	1.9824	1.3901	0.5023
0.3000	1.3380	1.4630	1.8538	1.9756	1.9799	1.9893	2.0003	1.9809	1.3900	0.5032
0.4000	1.3378	1.4628	1.8534	1.9747	1.9787	1.9877	1.9987	1.9795	1.3899	0.5041
0.5000	1.3376	1.4625	1.8529	1.9738	1.9775	1.9861	1.9970	1.9780	1.3899	0.5050
0.6000	1.3374	1.4622	1.8523	1.9727	1.9762	1.9845	1.9953	1.9766	1.3898	0.5059
0.7000	1.3372	1.4619	1.8516	1.9716	1.9749	1.9829	1.9937	1.9751	1.3897	0.5068
0.7000	1.3372	1.4619	1.8516	1.9716	1.9749	1.9829	1.9937	1.9751	1.3897	0.5068
0.8000	1.3369	1.4615	1.8508	1.9705	1.9735	1.9813	1.9920	1.9737	1.3896	0.5077
0.9000	1.3366	1.4610	1.8500	1.9693	1.9721	1.9796	1.9903	1.9722	1.3895	0.5086
1.0000	1.3363	1.4606	1.8492	1.9680	1.9707	1.9780	1.9887	1.9708	1.3894	0.5095
2.0000	1.3320	1.4547	1.8380	1.9537	1.9552	1.9612	1.9722	1.9567	1.3887	0.5185
3.0000	1.3268	1.4475	1.8248	1.9379	1.9390	1.9448	1.9565	1.9435	1.3884	0.5277
4.0000	1.3215	1.4401	1.8111	1.9222	1.9232	1.9292	1.9418	1.9311	1.3885	0.5371
5.0000	1.3163	1.4330	1.7979	1.9072	1.9083	1.9147	1.9282	1.9197	1.3891	0.5468
6.0000	1.3114	1.4262	1.7855	1.8932	1.8943	1.9012	1.9156	1.9092	1.3900	0.5567
7.0000	1.3068	1.4199	1.7739	1.8801	1.8815	1.8888	1.9040	1.8996	1.3914	0.5669
8.0000	1.3026	1.4141	1.7632	1.8681	1.8696	1.8773	1.8933	1.8907	1.3931	0.5773
9.0000	1.2987	1.4088	1.7533	1.8570	1.8586	1.8668	1.8834	1.8826	1.3952	0.5878
10.0000	1.2951	1.4038	1.7442	1.8468	1.8485	1.8570	1.8744	1.8752	1.3976	0.5985
11.0000	1.2918	1.3992	1.7358	1.8373	1.8391	1.8481	1.8660	1.8684	1.4003	0.6094
12.0000	1.2887	1.3950	1.7280	1.8285	1.8305	1.8398	1.8583	1.8622	1.4032	0.6205
13.0000	1.2859	1.3911	1.7208	1.8205	1.8225	1.8321	1.8512	1.8565	1.4065	0.6316
14.0000	1.2833	1.3875	1.7141	1.8130	1.8151	1.8250	1.8446	1.8513	1.4099	0.6429
15.0000	1.2808	1.3841	1.7079	1.8060	1.8083	1.8184	1.8386	1.8466	1.4136	0.6542
16.0000	1.2786	1.3810	1.7021	1.7996	1.8019	1.8124	1.8330	1.8423	1.4175	0.6657
17.0000	1.2765	1.3781	1.6968	1.7936	1.7960	1.8067	1.8279	1.8384	1.4216	0.6772
18.0000	1.2745	1.3754	1.6918	1.7880	1.7905	1.8015	1.8231	1.8348	1.4258	0.6888
19.0000	1.2727	1.3729	1.6872	1.7828	1.7854	1.7967	1.8187	1.8316	1.4302	0.7004
20.0000	1.2710	1.3705	1.6829	1.7780	1.7807	1.7922	1.8147	1.8287	1.4347	0.7121
30.0000	1.2590	1.3540	1.6525	1.7443	1.7478	1.7618	1.7887	1.8131	1.4857	0.8296
40.0000	1.2527	1.3454	1.6366	1.7269	1.7313	1.7477	1.7788	1.8123	1.5416	0.9450
50.0000	1.2493	1.3407	1.6280	1.7179	1.7230	1.7419	1.7771	1.8188	1.5980	1.0552
60.0000	1.2474	1.3381	1.6233	1.7132	1.7192	1.7404	1.7794	1.8287	1.6526	1.1589
80.0000	1.2457	1.3358	1.6193	1.7099	1.7173	1.7428	1.7888	1.8515	1.7531	1.3458
100.0000	1.2452	1.3351	1.6181	1.7097	1.7184	1.7475	1.7995	1.8737	1.8406	1.5065
1000.0000	1.2450	1.3349	1.6182	1.7164	1.7324	1.7833	1.8704	2.0107	2.3541	2.4443

Table 15

Variation of J for radium-224. Efficiency = 0.853

TIME AFTER SEPARATION	COUNTING INTERVAL (HOURS) 0.001	0.010	0.100	1.000	2.000	5.000	10.000	20.000	100.000	1000.000
0.0001	1.1769	1.7253	2.5599	2.6802	2.6830	2.6974	2.7157	2.6812	1.6662	0.1482
0.0010	1.2191	1.7307	2.5551	2.6797	2.6827	2.6973	2.7156	2.6812	1.6662	0.1482
0.0100	1.4234	1.7611	2.5189	2.6756	2.6806	2.6964	2.7151	2.6809	1.6661	0.1483
0.1000	1.5754	1.7899	2.4584	2.6671	2.6754	2.6929	2.7121	2.6784	1.6657	0.1495
0.2000	1.5767	1.7901	2.4571	2.6657	2.6736	2.6903	2.7093	2.6759	1.6656	0.1510
0.3000	1.5766	1.7898	2.4566	2.6644	2.6717	2.6877	2.7065	2.6735	1.6654	0.1525
0.4000	1.5763	1.7895	2.4559	2.6629	2.6697	2.6850	2.7037	2.6710	1.6653	0.1540
0.5000	1.5760	1.7890	2.4550	2.6612	2.6676	2.6823	2.7009	2.6685	1.6651	0.1555
0.6000	1.5756	1.7885	2.4540	2.6595	2.6654	2.6796	2.6980	2.6660	1.6649	0.1571
0.7000	1.5752	1.7879	2.4528	2.6576	2.6631	2.6768	2.6952	2.6635	1.6648	0.1586
0.7000	1.5752	1.7879	2.4528	2.6576	2.6631	2.6768	2.6952	2.6635	1.6648	0.1586
0.8000	1.5747	1.7873	2.4515	2.6557	2.6608	2.6740	2.6924	2.6611	1.6646	0.1601
0.9000	1.5742	1.7865	2.4501	2.6536	2.6584	2.6712	2.6895	2.6586	1.6645	0.1616
1.0000	1.5736	1.7858	2.4487	2.6515	2.6560	2.6684	2.6867	2.6561	1.6643	0.1631
2.0000	1.5663	1.7757	2.4297	2.6270	2.6296	2.6398	2.6586	2.6322	1.6632	0.1785
3.0000	1.5575	1.7635	2.4070	2.6001	2.6019	2.6118	2.6318	2.6095	1.6626	0.1942
4.0000	1.5484	1.7509	2.3838	2.5733	2.5750	2.5852	2.6067	2.5885	1.6628	0.2103
5.0000	1.5396	1.7387	2.3612	2.5477	2.5495	2.5604	2.5835	2.5690	1.6637	0.2269
6.0000	1.5312	1.7271	2.3400	2.5237	2.5257	2.5375	2.5620	2.5511	1.6654	0.2438
7.0000	1.5234	1.7164	2.3203	2.5015	2.5038	2.5163	2.5422	2.5347	1.6677	0.2611
8.0000	1.5163	1.7065	2.3020	2.4810	2.4835	2.4967	2.5239	2.5196	1.6706	0.2788
9.0000	1.5096	1.6974	2.2852	2.4620	2.4648	2.4787	2.5071	2.5057	1.6742	0.2968
10.0000	1.5035	1.6889	2.2696	2.4446	2.4475	2.4621	2.4917	2.4931	1.6782	0.3151
11.0000	1.4978	1.6811	2.2552	2.4284	2.4316	2.4468	2.4774	2.4815	1.6828	0.3337
12.0000	1.4926	1.6739	2.2419	2.4135	2.4169	2.4326	2.4642	2.4708	1.6879	0.3525
13.0000	1.4878	1.6672	2.2296	2.3997	2.4032	2.4196	2.4521	2.4612	1.6934	0.3715
14.0000	1.4833	1.6610	2.2182	2.3869	2.3906	2.4075	2.4409	2.4523	1.6993	0.3907
15.0000	1.4791	1.6553	2.2077	2.3750	2.3789	2.3963	2.4306	2.4442	1.7056	0.4101
16.0000	1.4752	1.6500	2.1978	2.3640	2.3681	2.3859	2.4211	2.4369	1.7123	0.4296
17.0000	1.4716	1.6450	2.1887	2.3538	2.3580	2.3763	2.4123	2.4302	1.7192	0.4493
18.0000	1.4683	1.6404	2.1802	2.3443	2.3487	2.3674	2.4042	2.4242	1.7264	0.4690
19.0000	1.4652	1.6361	2.1723	2.3355	2.3400	2.3591	2.3968	2.4187	1.7339	0.4889
20.0000	1.4623	1.6321	2.1650	2.3272	2.3319	2.3514	2.3899	2.4138	1.7417	0.5088
30.0000	1.4418	1.6040	2.1132	2.2697	2.2757	2.2996	2.3455	2.3871	1.8286	0.7093
40.0000	1.4311	1.5892	2.0861	2.2401	2.2476	2.2756	2.3287	2.3858	1.9240	0.9061
50.0000	1.4252	1.5812	2.0714	2.2247	2.2335	2.2657	2.3257	2.3969	2.0201	1.0941
60.0000	1.4220	1.5768	2.0634	2.2167	2.2269	2.2630	2.3296	2.4138	2.1133	1.2710
80.0000	1.4192	1.5729	2.0565	2.2111	2.2238	2.2672	2.3457	2.4527	2.2848	1.5899
100.0000	1.4183	1.5717	2.0545	2.2107	2.2255	2.2753	2.3640	2.4906	2.4341	1.8641
1000.0000	1.4179	1.5713	2.0547	2.2222	2.2495	2.3364	2.4849	2.7243	3.3102	3.4639

Table 16

Variation of J for radon-222. Efficiency = 0.250

TIME AFTER SEPARATION	COUNTING INTERVAL (HOURS)									
	0.001	0.010	0.100	1.000	2.000	5.000	10.000	20.000	100.000	1000.000
0.0001	1.0090	1.0309	1.1569	1.3092	1.3791	1.4321	1.4277	1.3876	1.1024	0.7527
0.0010	1.0089	1.0306	1.1562	1.3091	1.3790	1.4320	1.4277	1.3875	1.1024	0.7527
0.0100	1.0080	1.0278	1.1499	1.3082	1.3784	1.4317	1.4275	1.3874	1.1023	0.7527
0.1000	1.0052	1.0186	1.1225	1.3001	1.3725	1.4286	1.4258	1.3865	1.1021	0.7529
0.2000	1.0047	1.0167	1.1143	1.2922	1.3658	1.4252	1.4240	1.3854	1.1020	0.7531
0.3000	1.0045	1.0160	1.1103	1.2847	1.3595	1.4220	1.4222	1.3845	1.1019	0.7534
0.4000	1.0043	1.0155	1.1069	1.2777	1.3535	1.4189	1.4205	1.3836	1.1018	0.7536
0.5000	1.0042	1.0151	1.1038	1.2713	1.3481	1.4161	1.4190	1.3828	1.1017	0.7539
0.6000	1.0041	1.0146	1.1007	1.2654	1.3431	1.4135	1.4176	1.3820	1.1017	0.7543
0.7000	1.0039	1.0142	1.0979	1.2601	1.3387	1.4111	1.4163	1.3813	1.1017	0.7546
0.7000	1.0039	1.0142	1.0979	1.2601	1.3387	1.4111	1.4163	1.3813	1.1017	0.7546
0.8000	1.0038	1.0138	1.0953	1.2554	1.3347	1.4090	1.4151	1.3807	1.1017	0.7549
0.9000	1.0037	1.0135	1.0929	1.2512	1.3312	1.4071	1.4141	1.3801	1.1018	0.7553
1.0000	1.0037	1.0131	1.0908	1.2475	1.3281	1.4054	1.4131	1.3796	1.1018	0.7557
2.0000	1.0032	1.0115	1.0798	1.2285	1.3118	1.3965	1.4083	1.3773	1.1036	0.7604
3.0000	1.0031	1.0110	1.0770	1.2238	1.3078	1.3943	1.4073	1.3773	1.1062	0.7657
4.0000	1.0030	1.0109	1.0764	1.2227	1.3070	1.3940	1.4074	1.3779	1.1091	0.7712
5.0000	1.0030	1.0109	1.0762	1.2225	1.3068	1.3940	1.4077	1.3786	1.1119	0.7766
6.0000	1.0030	1.0109	1.0762	1.2225	1.3069	1.3942	1.4081	1.3794	1.1148	0.7821
7.0000	1.0030	1.0109	1.0762	1.2225	1.3069	1.3944	1.4085	1.3801	1.1177	0.7874
8.0000	1.0030	1.0109	1.0762	1.2226	1.3070	1.3946	1.4089	1.3809	1.1205	0.7928
9.0000	1.0030	1.0109	1.0762	1.2226	1.3071	1.3948	1.4093	1.3816	1.1234	0.7981
10.0000	1.0030	1.0109	1.0762	1.2226	1.3072	1.3950	1.4096	1.3824	1.1262	0.8034
11.0000	1.0030	1.0109	1.0762	1.2227	1.3072	1.3952	1.4100	1.3831	1.1289	0.8086
12.0000	1.0030	1.0109	1.0762	1.2227	1.3073	1.3954	1.4104	1.3838	1.1317	0.8138
13.0000	1.0030	1.0109	1.0762	1.2228	1.3074	1.3956	1.4108	1.3846	1.1344	0.8189
14.0000	1.0030	1.0109	1.0762	1.2228	1.3075	1.3958	1.4112	1.3853	1.1372	0.8240
15.0000	1.0030	1.0109	1.0762	1.2228	1.3076	1.3961	1.4115	1.3861	1.1399	0.8291
16.0000	1.0030	1.0109	1.0762	1.2229	1.3076	1.3962	1.4119	1.3867	1.1425	0.8342
17.0000	1.0030	1.0109	1.0762	1.2229	1.3077	1.3963	1.4123	1.3874	1.1452	0.8392
18.0000	1.0030	1.0109	1.0762	1.2229	1.3078	1.3965	1.4126	1.3881	1.1478	0.8441
19.0000	1.0030	1.0109	1.0763	1.2230	1.3079	1.3967	1.4130	1.3888	1.1505	0.8490
20.0000	1.0030	1.0109	1.0763	1.2230	1.3079	1.3969	1.4133	1.3895	1.1531	0.8539
30.0000	1.0030	1.0109	1.0763	1.2234	1.3086	1.3986	1.4168	1.3961	1.1780	0.9008
40.0000	1.0030	1.0109	1.0763	1.2237	1.3093	1.4002	1.4199	1.4022	1.2011	0.9443
50.0000	1.0030	1.0109	1.0764	1.2240	1.3099	1.4017	1.4229	1.4079	1.2225	0.9846
60.0000	1.0030	1.0109	1.0764	1.2243	1.3105	1.4031	1.4256	1.4131	1.2424	1.0219
80.0000	1.0030	1.0109	1.0764	1.2248	1.3115	1.4056	1.4305	1.4225	1.2779	1.0887
100.0000	1.0030	1.0109	1.0765	1.2252	1.3123	1.4078	1.4347	1.4306	1.3085	1.1462
1000.0000	1.0030	1.0110	1.0767	1.2279	1.3176	1.4208	1.4603	1.4801	1.4956	1.4981

Table 17

Variation of J for radon-222. Efficiency = 0.500

TIME AFTER SEPARATION	COUNTING INTERVAL (HOURS) 0.001	0.010	0.100	1.000	2.000	5.000	10.000	20.000	100.000	1000.000
0.0001	1.0180	1.0618	1.3138	1.6184	1.7581	1.8641	1.8555	1.7751	1.2047	0.5055
0.0010	1.0178	1.0612	1.3124	1.6182	1.7580	1.8640	1.8554	1.7751	1.2047	0.5055
0.0100	1.0161	1.0556	1.2998	1.6164	1.7569	1.8634	1.8551	1.7749	1.2047	0.5055
0.1000	1.0104	1.0373	1.2449	1.6002	1.7449	1.8572	1.8516	1.7729	1.2043	0.5058
0.2000	1.0093	1.0335	1.2286	1.5843	1.7317	1.8504	1.8479	1.7709	1.2040	0.5062
0.3000	1.0089	1.0320	1.2205	1.5694	1.7189	1.8439	1.8444	1.7690	1.2038	0.5067
0.4000	1.0086	1.0310	1.2139	1.5554	1.7070	1.8378	1.8411	1.7672	1.2036	0.5073
0.5000	1.0084	1.0301	1.2075	1.5425	1.6961	1.8321	1.8380	1.7655	1.2035	0.5079
0.6000	1.0081	1.0292	1.2015	1.5308	1.6863	1.8269	1.8351	1.7640	1.2034	0.5085
0.7000	1.0079	1.0284	1.1958	1.5202	1.6774	1.8222	1.8326	1.7626	1.2034	0.5092
0.7000	1.0079	1.0284	1.1958	1.5202	1.6774	1.8222	1.8326	1.7626	1.2034	0.5092
0.8000	1.0077	1.0276	1.1906	1.5108	1.6695	1.8180	1.8302	1.7614	1.2034	0.5099
0.9000	1.0075	1.0269	1.1859	1.5025	1.6624	1.8142	1.8281	1.7603	1.2035	0.5106
1.0000	1.0073	1.0263	1.1817	1.4951	1.6562	1.8108	1.8263	1.7593	1.2037	0.5114
2.0000	1.0064	1.0229	1.1596	1.4569	1.6237	1.7929	1.8165	1.7547	1.2071	0.5208
3.0000	1.0061	1.0221	1.1541	1.4475	1.6156	1.7886	1.8146	1.7546	1.2124	0.5314
4.0000	1.0061	1.0219	1.1528	1.4454	1.6139	1.7879	1.8148	1.7558	1.2181	0.5423
5.0000	1.0061	1.0218	1.1525	1.4450	1.6137	1.7881	1.8154	1.7573	1.2239	0.5533
6.0000	1.0061	1.0218	1.1524	1.4450	1.6137	1.7884	1.8162	1.7588	1.2297	0.5641
7.0000	1.0061	1.0218	1.1524	1.4450	1.6139	1.7888	1.8170	1.7603	1.2354	0.5749
8.0000	1.0061	1.0218	1.1524	1.4451	1.6140	1.7892	1.8177	1.7618	1.2411	0.5856
9.0000	1.0061	1.0218	1.1524	1.4452	1.6142	1.7896	1.8185	1.7633	1.2467	0.5962
10.0000	1.0061	1.0218	1.1524	1.4453	1.6143	1.7900	1.8193	1.7648	1.2523	0.6067
11.0000	1.0061	1.0218	1.1524	1.4454	1.6145	1.7904	1.8200	1.7662	1.2579	0.6172
12.0000	1.0061	1.0218	1.1525	1.4454	1.6147	1.7908	1.8208	1.7677	1.2634	0.6276
13.0000	1.0061	1.0218	1.1525	1.4455	1.6148	1.7912	1.8216	1.7691	1.2689	0.6379
14.0000	1.0061	1.0218	1.1525	1.4456	1.6150	1.7915	1.8223	1.7706	1.2743	0.6481
15.0000	1.0061	1.0218	1.1525	1.4457	1.6151	1.7919	1.8230	1.7720	1.2797	0.6582
16.0000	1.0061	1.0218	1.1525	1.4457	1.6153	1.7923	1.8238	1.7734	1.2851	0.6683
17.0000	1.0061	1.0218	1.1525	1.4458	1.6154	1.7927	1.8245	1.7748	1.2904	0.6783
18.0000	1.0061	1.0218	1.1525	1.4459	1.6156	1.7930	1.8252	1.7762	1.2957	0.6882
19.0000	1.0061	1.0218	1.1525	1.4460	1.6157	1.7934	1.8260	1.7776	1.3009	0.6981
20.0000	1.0061	1.0218	1.1525	1.4460	1.6159	1.7938	1.8267	1.7790	1.3061	0.7078
30.0000	1.0061	1.0219	1.1526	1.4467	1.6173	1.7973	1.8335	1.7922	1.3560	0.8016
40.0000	1.0061	1.0219	1.1526	1.4474	1.6186	1.8005	1.8399	1.8044	1.4022	0.8885
50.0000	1.0061	1.0219	1.1527	1.4480	1.6198	1.8035	1.8457	1.8157	1.4451	0.9691
60.0000	1.0061	1.0219	1.1528	1.4486	1.6209	1.8063	1.8512	1.8263	1.4848	1.0439
80.0000	1.0061	1.0219	1.1529	1.4496	1.6229	1.8112	1.8609	1.8450	1.5559	1.1775
100.0000	1.0061	1.0219	1.1530	1.4504	1.6247	1.8155	1.8693	1.8612	1.6169	1.2923
1000.0000	1.0061	1.0219	1.1535	1.4558	1.6352	1.8417	1.9207	1.9602	1.9913	1.9962

Table 18

Variation of J for radon-222. Efficiency = 0.853

TIME AFTER SEPARATION	COUNTING INTERVAL (HOURS)									
	0.001	0.010	0.100	1.000	2.000	5.000	10.000	20.000	100.000	1000.000
0.0001	1.0308	1.1054	1.5354	2.0550	2.2934	2.4742	2.4594	2.3223	1.3493	0.1563
0.0010	1.0304	1.1043	1.5330	2.0547	2.2932	2.4741	2.4594	2.3223	1.3493	0.1563
0.0100	1.0274	1.0949	1.5115	2.0515	2.2912	2.4730	2.4588	2.3219	1.3492	0.1563
0.1000	1.0178	1.0636	1.4178	2.0239	2.2709	2.4624	2.4529	2.3186	1.3485	0.1568
0.2000	1.0159	1.0571	1.3900	1.9969	2.2482	2.4508	2.4466	2.3151	1.3480	0.1576
0.3000	1.0152	1.0546	1.3762	1.9715	2.2265	2.4397	2.4405	2.3119	1.3476	0.1585
0.4000	1.0147	1.0529	1.3649	1.9476	2.2062	2.4293	2.4349	2.3088	1.3473	0.1594
0.5000	1.0143	1.0514	1.3541	1.9256	2.1876	2.4196	2.4296	2.3060	1.3471	0.1604
0.6000	1.0139	1.0499	1.3437	1.9055	2.1708	2.4108	2.4248	2.3034	1.3470	0.1615
0.7000	1.0135	1.0484	1.3340	1.8875	2.1556	2.4028	2.4204	2.3010	1.3470	0.1627
0.7000	1.0135	1.0484	1.3340	1.8875	2.1556	2.4028	2.4204	2.3010	1.3470	0.1627
0.8000	1.0131	1.0471	1.3252	1.8714	2.1421	2.3955	2.4164	2.2989	1.3470	0.1639
0.9000	1.0128	1.0459	1.3171	1.8572	2.1301	2.3891	2.4128	2.2970	1.3472	0.1652
1.0000	1.0125	1.0448	1.3100	1.8446	2.1195	2.3833	2.4096	2.2953	1.3475	0.1665
2.0000	1.0109	1.0391	1.2722	1.7795	2.0640	2.3527	2.3930	2.2875	1.3534	0.1825
3.0000	1.0105	1.0377	1.2628	1.7635	2.0503	2.3454	2.3897	2.2874	1.3624	0.2006
4.0000	1.0104	1.0374	1.2606	1.7599	2.0473	2.3442	2.3900	2.2894	1.3721	0.2192
5.0000	1.0104	1.0373	1.2601	1.7592	2.0469	2.3445	2.3911	2.2919	1.3820	0.2379
6.0000	1.0104	1.0373	1.2600	1.7591	2.0470	2.3451	2.3924	2.2945	1.3918	0.2564
7.0000	1.0104	1.0373	1.2600	1.7592	2.0473	2.3457	2.3937	2.2971	1.4016	0.2748
8.0000	1.0104	1.0373	1.2600	1.7594	2.0475	2.3464	2.3951	2.2996	1.4113	0.2930
9.0000	1.0104	1.0373	1.2600	1.7595	2.0478	2.3471	2.3964	2.3022	1.4209	0.3111
10.0000	1.0104	1.0373	1.2601	1.7596	2.0481	2.3478	2.3977	2.3047	1.4305	0.3291
11.0000	1.0104	1.0373	1.2601	1.7598	2.0483	2.3484	2.3990	2.3072	1.4400	0.3469
12.0000	1.0104	1.0373	1.2601	1.7599	2.0486	2.3491	2.4003	2.3097	1.4494	0.3646
13.0000	1.0104	1.0373	1.2601	1.7600	2.0489	2.3497	2.4016	2.3122	1.4587	0.3822
14.0000	1.0104	1.0373	1.2601	1.7602	2.0491	2.3504	2.4029	2.3146	1.4680	0.3996
15.0000	1.0104	1.0373	1.2601	1.7603	2.0494	2.3510	2.4041	2.3171	1.4772	0.4170
16.0000	1.0104	1.0373	1.2601	1.7604	2.0496	2.3517	2.4054	2.3195	1.4863	0.4341
17.0000	1.0104	1.0373	1.2601	1.7606	2.0499	2.3523	2.4066	2.3219	1.4954	0.4512
18.0000	1.0104	1.0373	1.2602	1.7607	2.0502	2.3529	2.4078	2.3242	1.5044	0.4681
19.0000	1.0104	1.0373	1.2602	1.7608	2.0504	2.3536	2.4091	2.3266	1.5133	0.4849
20.0000	1.0104	1.0373	1.2602	1.7609	2.0507	2.3542	2.4103	2.3290	1.5222	0.5016
30.0000	1.0104	1.0373	1.2603	1.7621	2.0531	2.3601	2.4220	2.3514	1.6073	0.6615
40.0000	1.0104	1.0373	1.2604	1.7633	2.0553	2.3656	2.4328	2.3723	1.6861	0.8098
50.0000	1.0104	1.0373	1.2605	1.7643	2.0574	2.3707	2.4428	2.3917	1.7593	0.9473
60.0000	1.0104	1.0373	1.2606	1.7653	2.0593	2.3755	2.4521	2.4096	1.8271	1.0748
80.0000	1.0104	1.0373	1.2608	1.7670	2.0627	2.3840	2.4688	2.4416	1.9483	1.3027
100.0000	1.0104	1.0373	1.2609	1.7685	2.0657	2.3912	2.4831	2.4692	2.0525	1.4987
1000.0000	1.0104	1.0374	1.2618	1.7775	2.0837	2.4359	2.5707	2.6381	2.6911	2.6996

IV. Summary

In the counting of long decay chains, it is often necessary to use counting intervals that are long with respect to the half-life of the individual members of the series. With modern instrumentation the efficiency may be very nearly 100%. Consequently, the approximations normally used for estimating the statistical counting error are not valid. A method has been presented by which the variance of the observed count can be easily calculated for any long decay chain. The effects of the counting interval, the efficiency, and the delay of start of counting relative to the time of separation of Ra^{224} and Rn^{222} from their respective daughters have been presented. The counting interval and the efficiency were found to produce significant effects for both the Ra^{224} and the Rn^{222} series. A simple and convenient method has been presented to correct for this effect by the use of a quantity J which can be calculated for a given experimental condition.

Very great thanks are due Mr. Daniel F. Carson of the Applied Mathematics Division for writing and revising the computer program. Thanks are also due Dr. Andrew F. Stehney for bringing this problem to our attention.

References

1. A. F. Stehney, D. E. Wallace, F. H. Ilcewicz. Argonne National Laboratory Radiological Physics Division Semiannual Report. January through June, 1956. ANL-5596, p. 12.

2. H. F. Lucas, Jr. Argonne National Laboratory Radiological Physics Division Semiannual Report, July through December, 1960 ANL-6297, p. 55.

3. H. F. Lucas, Rev. Sci. Inst. 28, 680 (1957).

4. G. Friedlander, J. W. Kennedy. Introduction to Radiochemistry. John Wiley and Sons, Inc., New York, 1949, p. 207.

5. N. I. Adams, Jr. Phys. Rev. 44, 651 (1933).

6. H. Lindeman. Physica 21, 589 (1955).

7. A. Jaffey. A Survey of Statistics Useful in Measurements with Special Application to Nuclear Measurements. John Wiley and Sons, New York, to be published. Ch. 5.

8. M. Huybrechts. Nuovo Cimento 6 (4), 811-31 (1957).

9. H. Bateman. Proc. Camb. Phil. Soc. 15, 423 (1910).

RaD (Pb^{210}) IN THE HUMAN SKELETON. ESTIMATES OF THE EXPONENT OF THE RETENTION FUNCTION, THE SKELETAL CONTENT AND THE DOSE RATE IN PEOPLE WITH HIGH RADIUM CONTENT*

Richard B. Holtzman, Ph.D.

Abstract

Based on measurements of the RaD contents in bone specimens from human subjects possessing large body burdens of Ra^{226} (~1 μc), estimates were made of: 1) the exponent of the power function ($R = At^{-b}$) for the retention of RaD in the skeleton, 2) the total skeletal content of the long-lived member of the Ra^{226} decay chain, RaD (Pb^{210}), by whole body counting of the Ra^{226}, and 3) the effective dose rate from the RaD decay chain relative to that of Ra^{226}.

The RaD content was determined in each of 12 samples of bone from seven subjects whose Ra^{226} body content ranged from 0.4 to 10.5 μc and who had carried these burdens from 24 to 36 years. The analyses were performed by wet ashing the bone in nitric and perchloric acids, converting to hydrochloric acid solution and plating the RaD decay product, RaF (Po^{210}), onto a silver disc which was alpha counted. Ra^{226} was determined by the Rn emanation method.

The measurements of the RaD/Ra^{226} ratios on each of several sets of samples from given individuals indicated the RaD was formed at the location of Ra^{226} decay. Using the values of: 1) Rn retention in vivo of 0.4, 2) Rn retention during storage of 1.0, 3) the exponent of the power function describing the Ra^{226} retention of 0.52, and 4) no RaD injected originally, it was possible to estimate that the exponent of the power function describing the RaD retention was 0.10. This is comparable to the value of 0.14 derived from the data of Kehoe et al.[1] on stable Pb metabolism which were taken on a single individual over a period of 14 months. Thus, after determination of this b and given the other constants, it then becomes possible to calculate at any time, the total skeletal RaD content from the Ra^{226} content, the latter value obtainable by whole-body counting. RaD urinary excretion data were found to be of little value in determination of the whole-body RaD content.

Thirty years after acquisition of the Ra^{226} burden the effective dose rate due to the RaD decay chain is about 8% of that from the Ra^{226} decay chain, while calculation shows that, averaged over a 25- to 40-year period,

*Work in Progress: Radiology 80, 122-123 (January 1963).

the RaD rate is about 5% that of the Ra^{226}. During the 5- to 50-year period after acquisition, the RaD rate is a constant (±10% of the 30-year value). Thus, for a 30-year Ra^{226} body content of 1 μc, (skeletal dose rate of about 10 rad/day), the RaD dose rate is about 0.6 rad/day with a resultant accumulated dose of about 6000 rad.

Reference

1. R. A. Kehoe, J. Cholak, D. M. Hubbard, K. Bambach and R. R. McNary. J. Ind. Hyg. Toxicol. 25, 71 (1945).

NATURAL AIRBORNE RADIOACTIVITY RaD (Pb^{210}) AND RaF (Po^{210}) IN THE HUMAN BODY AND ENVIRONMENT*

Richard B. Holtzman

Abstract

RaD and RaF in the human body have been measured and found to contribute a significant fraction of the total natural radiation dose to the human skeleton. The parent nuclide RaD, like H^3, C^{14} and Rn^{222}, was found to enter the environment mainly as an airborne activity, that is, it enters the body by direct inhalation and by atmospheric deposition onto vegetation which is subsequently consumed.

The RaD content of the body was extrapolated from measurements on small samples of bone from about 100 individuals. Sixty percent of the RaD is in the skeleton and fairly uniformly distributed therein. The RaD content is representative of the dose in that the daughter, RaF, which produces most of the dose, is in radioactive equilibrium with the parent. The average concentrations were 0.146 pc RaD/g ash and 0.037 pc Ra^{226}/g ash in these samples. On the average, the concentration was greater in trabecular than in cortical bone, 0.184 pc/g and 0.105 pc/g ash, respectively; and, on the average, men had higher concentrations than women, 0.161 pc/g ash compared to 0.119 pc/g ash. No regional correlations were apparent in our data, and the content in Chicago people was found to vary over more than a factor of 5. There is evidence, however, that some arctic residents possess body contents of RaD 5 to 10 times the average.

Calculations using some of the metabolic parameters of lead and RaD showed that food and air were the major sources of the RaD in the body. Integrated values of RaD consumption were determined from fecal analyses and the average daily amount of RaD leaving (and entering) the body was determined from analysis of urine. A few foods were also measured. Analogous to the exceptionally high Sr^{90} and Cs^{137} concentrations found in arctic regions, some foods from these regions were also found to be high in RaD.

The total dose rate due to RaD is about twice that due to Ra^{224} and about equal to that of Ra^{226} + Ra^{228} combined. The total rate is estimated at about 48 mrem/year, of which 12 are due to Ra^{226}, 12 to Ra^{228} and 24 to RaD. The Sr^{90} dose rate in 13-year-old children is about 1/7 the average RaD dose.

*Presented at meeting of the Society of Nuclear Medicine at Iowa City, Iowa, November 11, 1962; to be published in Health Physics.

THE TRANSLOCATION OF RADIUM DAUGHTERS TO THE SKELETONS OF THOROTRAST PATIENTS*

L. D. Marinelli and H. F. Lucas, Jr.

Introduction

Although evidence that thorium daughters separate from Thorotrast deposits in humans has been sought before, it remained for Stenstrom[1] to establish in 1941 "that some elements of the thorium series were eliminated to a considerable extent from the tissues." In the postwar period both Rotblat and Ward[2] and Rundo[3,4,5] reported the results of more precise measurements on the radioactive equilibrium status of the thorium chain in liver, spleen and a few other tissues. Hursh et al.[6] in 1957 published detailed analyses of Th^{232} contents in several tissues, with some indications of Th^{228} contents, and measured the excretion rate of the radium isotopes up to several months after injection. From these studies and various types of measurements at our Laboratory,[7,8] sporadically described in our semi-annual reports,[9,10,11] has emerged a rough picture of the physical and metabolic problems involved. It has been established that approximately 90% of Th^{232} of the body is deposited in the liver and spleen.

The Radioactivity of the Skeleton

In this paper we shall concern ourselves principally with the radioactivity in the skeleton, and to a much more limited extent with the radioactivity of the active bone marrow which, potentially, may lead to greater tangible damage. Before proceeding, we wish to emphasize the necessity of distinguishing raw bone containing marrow from bone per se. The radioactive content of trabecular bone containing marrow is much the greater and, when extrapolated to the whole skeleton, it occasionally leads to absurd values, as shown in Table 19 (item 2); it also varies radically from sample to sample. The only tenable explanation is that the bone-enclosed marrow (present in varying and indeterminate amounts) accumulates from the very beginning considerable $Th^{232}O_2$. Radiometric analysis suggests, however, that the daughters, Ra^{228} and Th^{228}, many decades after injection, are still present therein, but in quantities definitely lower than expected from undisturbed radioactive growth (items 4 and 6, Table 19).

The data concerning the radioactivity of trabecular bone cleaned with ethylenediamine and of cortical bone (devoid of red marrow) are more consistent among themselves despite the variety of methods of analysis employed but, as shown in Table 20, they are not too numerous. They show a striking uniformity in the amount of the original Th^{232} in the skeleton, especially in

*Presented at the Tenth International Congress of Radiology, Montreal, Canada, August 26 - September 1, 1962.

Table 19

The activity of Th^{232}, Ra^{228} and Th^{228} in the entire skeleton as obtained from extrapolation of measurements of samples of fresh trabecular bone containing marrow. Activity of injected Th^{232} = 100

ITEM	PATIENT CODE	DURATION OF BURDEN	SPECIMEN AND WEIGHT	TIME BETWEEN BIOPSY ANALYSIS	TOTAL SKELETAL ACTIVITY AS % OF INJECTED Th^{232}			THOROTRAST INJECTED cc	METHOD OF ANALYSIS	REF.
					Th^{232}	Ra^{228}	Th^{228}			
(1)	M.H.	17 D	CANCELLOUS BONE 97 mg ASHED	-	6.0	-	-	75	SPECTROCHEMICAL	(6)
(2)	04-105 (S.B.)	9 D	RIBS 46 g FRESH	3.300 D	(118) (100%)	(81) (68%)	(80) (67%)	48	γ-RAY SPECTROSCOPY RADIOAUTOGRAPH	(9)
(3)	No. 2 (a)	15-20 Y	BODY OF VERTEBRA 12 g FRESH	15 D	-	7.5	8.4	20	RADIOCHEMICAL	(13)
	(b)		HEAD OF FEMUR 2.7 g FRESH	180 D	-	2.9	2.6			
(4)	No. 1 (a)	20 Y	STERNUM BONE 1.41 g FRESH	200 D	34 (100%)	6.7 (20%)	5.9 (17%)	60	RADIOCHEMICAL	(13)
	(b)		1.35 g FRESH	1.7 Y	-	5.7	6.7			
(5)	A.D.	19 Y	CANCELLOUS BONE 25 mg ASH	-	26.4	-		75	SPECTROCHEMICAL	(6)
(6)	04-103 (J.J.C.)	15 Y	RIB 1.47 g ASH	ZERO	32.7 (100%)	11.0 (33%)	3.3 (10%)	50	RADIOCHEMICAL α-SPECTROMETRY	ANL

EXTRAPOLATION TO Th^{232} IN EQUILIBRIUM AT INJECTION (SKELETAL WEIGHT EQUALS 10% BODY WEIGHT).

Table 20

The activity of Th^{232}, Ra^{228} and Th^{228} in the entire skeleton as obtained from extrapolation of measurements of clean trabecular or cortical bone. Activity of injected Th^{232} = 100

ITEM	PATIENT CODE (AGE)	DURATION OF BURDEN	SPECIMEN AND WEIGHT	TIME†	TOTAL SKELETAL ACTIVITY AS % OF INJECTED Th^{232}			THOROTRAST INJECTED cc
					Th^{232}	Ra^{228}	Th^{228}	
(A)	04-101 R.C. (53)	18 y	MOLAR TOOTH 0.9 g ASHED	350 d	0.50	-	1.68	10
(B)	A.D. (85) (a)	19 y	COMPACT BONE 830 mg ASH	-	0.56	-	-	75
	(b)		TRABEC. BONE 4.2 μg FRESH	1 y	-	-	1.74	
(C)	M.H. (58)	17 d	COMPACT BONE 20 mg ASHED	-	0.56	-	-	75
(D)	04-102 M.W. (32) (a)	16 y	VERTEBRAL BONE 1.9 g ASH	60-90 d	-	5.5	4.2	(75)*
	(b)		0.2 mg FRESH		-	-	3.7	
(E)	04-104 NO. 284 (75) (a)	26.5 y	TRABEC. TIBIA 4.9 g ASH (B-3)	ZERO	0.82	1.15	1.19	10
	(b)		TRABEC. FEMUR 6.07 g ASH (B-5)	ZERO	0.77	0.77	1.17	
	(c)		CORTICAL FEMUR 3.04 g ASH (B-6)	ZERO	0.4	0.63	0.72	
	(d)		4.4 g ASH (B-1a)	ZERO	0.40*	0.63	0.75	
	(e)		CORTICAL TIBIA 6.56 g ASH (B-2)	ZERO	0.46	0.96	0.74	
	(f)		5.51 g ASH	ZERO	-	-	0.92	
(F)	04-103 J.J.C. (37) (a)	15 y	CORTICAL FEMUR 7.6 g FRESH	2.3 y	-	1.5	1.8	50
	(b)		5.4 g FRESH	2.0 y		2.3	3.4	
	(c)		2.4 g ASH	ZERO	0.44	0.88	0.90	
	(d)		VERTEBRAE** 3.32 g DRY	2.0 y		6.7	4.3	
	(e)		RIB (INORGANIC) 1.45 g ASH	ZERO	5.4	7.1	3.3	

* ASSUMED VALUE. ** CONTAMINATED IN JAR BY VERY ACTIVE SAMPLES OF LIVER AND SPLEEN.
† TIME (POST-BIOPSY) TO WHICH SKELETAL ACTIVITY REFERS.

compact bone, and definitely larger amounts of radioactivity in trabecular bone, even when it has been cleaned with EDA.* The last two cases (E and F) show ratios of activities in the two types of bone which seem fairly uniform for any one type of bone and for any one patient.

Worthy of note is the fact that, in any one bone sample shown in Table 20, Th^{228} is not always higher than Ra^{228}, and then by not much more than 30%, suggesting that translocated Th^{228} does not migrate en masse from the reticulo-endothelial system (R.E.S.) to the skeleton. It is more likely instead that most of the Th^{228} found in bone is born in bone mineral from the decay of its parent Ra^{228}.

In Table 21 we have gathered all the data concerning our most thoroughly studied patient and have compared the activity of Th^{228} found in bone with that expected therein if the deficiency of Th^{228} in the R.E.S., as indicated by the liver biopsy, had been transferred totally to bone. At best, the data are equivocal in the sense that only the values of Th^{228} found in trabecular bone are high enough to approach the value expected from a substantial migration of Th^{228} from the R.E.S; yet these experimental Th^{228} values in bone are not high enough to account also for the Th^{228} produced by the Th^{232} and the Ra^{228} found in bone at time of autopsy. Of interest is the marrow value and its lack of equilibrium, directly demonstrated for the first time.

Table 21

Case 04-103. 14-year burden. ~50 cc injection

Tissue	Th^{232}	Ra^{228}	Th^{228}	Ra^{224}	Remarks
cortical femur	.44	.9-2.3	.9-3.4	?	} extrapolated to 2,800 gm of ash
trabecular vert. (e.d.)	-	6.7	4.3		
trabecular rib (e.d.)	5.4	7.1	3.3		
liver	100	41 59	36 5		R.E.S. equilibrium released in circulation
marrow (active)	4.4 (100)	.63 (14.4)	.08 (1.8)		calculated from organic fraction of rib
skeleton (theor.)	0	.87	.87		from R.E.S. (Ra^{228})
skeleton (theor.)	0	0	5.00		from R.E.S. (Th^{228})
skeleton (theor.)	.44	1.31	6.31		if Th^{232} in bone is in equilibrium
skeleton (theor.)	.44	.87	5.87		if Th^{232} in bone is not in equilibrium

} analysis of tissues

It is unfortunate that no data are now available about the presence of Ra^{224} and its short-lived daughters in the living skeleton of the Thorotrast patient. Evidence that Ra^{224} is circulating has been obtained by direct assay

*These values bracket the recent measurements of Turner, et al.[13]

of blood and excreta.[5,6] From what is known from Ra^{226} elimination at later times, this element should be responsible for most of the dose in bone, as illustrated in Table 22 where all the range of dosimetric data is summarized: if our guess is right, Ra^{224} should account for more that 90% of the skeletal dose. It is obvious that direct assay of the shorter lived daughters in the skeleton of Thorotrast patients is essential to the clarification of the issue.

Table 22

Dosimetry of 20 cc thorotrast injection
(440 nCi of Th^{232})

Element	Contents in nCi		Dose-rate rads y^{-1}		
	Bone		Bone		Red Marrow
	Compact	Trab. (e.d.)	Compact	Trab.	
Th^{232}	1.8-2.5 (5)	3.4-24 (2)	20-27	37-260	1.8 min. (L.D.M.) 11.0 (J.B.H.) 42.0 (J.R.)
Ra^{228}	2.8-5 (2)	3.4-31 (3)	~0	~0	
Th^{228}	3.2-4.0 (3)	4.6-14.6 (4)	47-58	67-210	
Ra^{224}*	66(?)		1000(?)		
Thoron + daughters	60(?)		3400(?)		

*Direct Ra^{224} measurements from bone urgently needed; value shown derived from whole-body excretion of Ra^{224} and late metabolic data on Ra^{226}.

( )Number of patients.

The Marrow

Before leaving Table 22 we should glance at the column indicating roughly the dose-rate to the marrow. The wide range of 1.8 to 42 rads per year is indicative of what happens when extrapolations are made from very few samples. The lowest value was obtained by us from a few milligrams of marrow extracted from a rib; the largest value was obtained by assuming that 10% of Th^{232} goes to the marrow and stays there at about 50% equilibrium.

The presence of some leukemia cases in both the Danish and Swedish series of registered cases makes it imperative that the marrow dose-rate be determined much more accurately at various times after injection. From the epidemiological point of view the dosage estimates of Table 23 are interesting but in dire want of accuracy. We restrict ourselves to remarking that the doses involved in various tissues are of the order of 15 to 1000 times background and that these doses are being delivered at low dose rates. These are in a range of great interest from the standpoint of protection at the radiation worker's level.

Table 23

Estimates of radiation doses in Thorotrast patients
(20 cc injection)

Tissue	Radioactive Source	Average Dose Rate rads per year	R.B.E.	Accumulated Rems (20 years)	Reference
Skeleton	Th^{232} + daughters	1.4 - 3.0	4-10	112-600	Reynolds, et al. (1958)
Marrow	Th^{232} + daughters	1.2 - 2.9	4-10	96-580	Hursh (1957) Rundo (1955)
Bronchi	Thoron + daughters	12 - 19	4-10	960-3800	Rundo (Oct. 1958)
Lungs	"	0.8 - 1.9	4-10	64-380	Rundo (Oct. 1958)
Liver	Th^{232} + daughters	27	4-10	2100-5400	Rundo (Feb. 1958)
Spleen		71	4-10	5700-14000	Rundo (Feb. 1958)

Physiological Implications

It should be realized that the Thorotrast patient also offers unique opportunities to students of bone physiology. Into his circulation several elements are injected at constant rate for long periods of time. If we focus our attention on the radium isotopes, Ra^{228} and Ra^{224}, we realize that if we can establish their content in bone we can also evaluate both short- and long-term transport parameters quite directly.

From the retention function of Ra^{226} in humans and knowledge of the equilibrium status of the thorium chain in the R.E.S. system it is possible to make some predictions as to the translocation of Ra^{228} and Ra^{224} to the skeleton. However, from comparison of the experimental information gathered by Rotblat, Rundo and Hursh on the R.E.S. with that attained by us on the skeleton prediction is possible only with Ra^{228}. This is illustrated in Figure 39. The solid lines represent the total skeletal contents of Ra^{228} to be expected by assuming the limits of retention found by Norris et al.[12] The agreement is fair at late times; no experimental information is available at early ones, yet at the local level it is intriguing to speculate as to why, under this seemingly constant infusion, Ra^{228} is more concentrated in clean trabecular than in compact bone. Is it artifact or is it of physiological significance? Could it be due to the capillaries holding on to the colloidal particles of Thorotrast?

Of late, many physical techniques useful to these studies have been developed in our Laboratory and elsewhere. In the proper hands these

investigative tools have been fruitful and have established the existence of long-term exchange in bone, hitherto unsuspected, and have proved capable of revealing physiological events in bone which have occurred many years before observation.

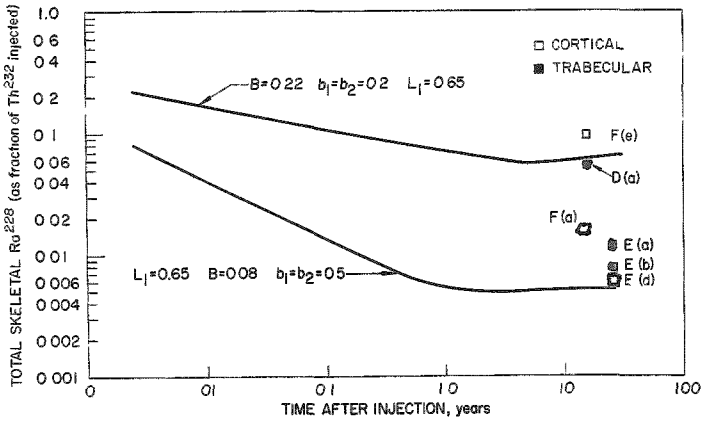

Figure 39

Comparison between experimental and theoretical values of the skeletal activity ratio of Ra^{228} to that of Th^{232}.

B = Ra^{228}/Th^{232} in injected material

L_1 = Ra^{228} / Th^{232} in reticulo-endothelial system (R.E.S.)

t = time in days; b = a constant

Assumed retention, R, of injected Ra^{228}

$$R = B\,(1-b_1)\,t^{-b_1}$$

Assumed fractional retention of Ra^{228} released into circulation by washout of R.E.S.

$$R_2 = (1-L_1)\,(1-b_2)\,t^{-b_2}$$

The samples, F(e), etc. are described in Table 20.

Conclusions

It is our earnest hope that, true to their tradition of concern with the untoward effects of radiation, radiologists throughout the world will intensify their study of Thorotrast patients especially from the epidemiological point of view. In this effort the essential cooperation of public health authorities cannot fail since it is becoming increasingly evident that some quantitative data on man must be obtained and that the time to obtain it is now, because the populations of interest are disappearing because of natural causes.*

*An earlier, but more detailed, treatment of this observation has been published elsewhere.[14]

References

1. W. Stenstrom. Elimination of radioactive elements by patients and rabbits after injection of Thorotrast. Radiology 37, 698-704 (1941).

2. J. Rotblat and G. Ward. The radioactivity from Thorotrast and its retention in tissues. Phys. Med. Biol. 1, 125-137 (1956).

3. J. Rundo. The radioactivity of Thorotrast. Phys. Med. Biol. 1, 138-146 (1956).

4. J. Rundo. Radiation dosage from Thorotrast. Transactions of IX Intern. Congr. of Radiology, Munich, Germany, July 23-30, 1959. George Thiem Verlag, Stuttgart, 1961, pp. 1258-1265.

5. J. Rundo. Measurements and dosimetry of radioactive isotopes deposited within the human body, with special reference to collodial thorium dioxide, following intravenous injection. Ph.D. Thesis, University of London, 1958.

6. J. B. Hursh, L. T. Steadman, W. B. Looney and M. Colodzin. The excretion of thorium and thorium daughters after Thorotrast administration. Acta Radiol. 47, 481-498 (1957).

7. D. E. Wallace. Argonne National Laboratory, private communication (1961); Argonne National Laboratory Radiological Physics Division Semiannual Report, January through June 1961. ANL-6398, pp. 51-70.

8. D. P. Krause. Argonne National Laboratory, private communication (1961).

9. C. E. Miller and L. D. Marinelli. Preliminary study on the retention of Th^{232} daughters following Thorotrast injections. Argonne National Laboratory Radiological Physics Division Semiannual Report, July through December 1958. ANL-5967, pp. 103-104.

10. L. D. Marinelli and A. F. Stehney. Radioactivity in bones of patients injected with Thorotrast. Argonne National Laboratory Radiological Physics Division Semiannual Report, July through December 1958. ANL-5967, pp. 105-106.

11. C. E. Miller. Study of Thorotrast in humans, Argonne National Laboratory Radiological Physics Division Semiannual Report, July through December 1957. ANL-5829, pp. 154-155.

12. W. P. Norris, T. W. Speckman and P. F. Gustafson. Studies of the metabolism of radium in man. Am. J. Roentgenol. 73, 785-802 (1955).

13. R. C. Turner, J. M. Radley and W. V. Mayneord. The α-ray activity of human tissues. Brit. J. Radiol. 31, 397-406 (1958). (p. 404, case 4).

14. L. D. Marinelli and H. F. Lucas. Translocation of thorium daughters to bone. Some Aspects of Internal Irradiation. Pergamon Press, London, 1962. pp. 499-515.

GEOLOGICAL OCCURRENCE OF NATURAL RADIUM-226 IN GROUND WATER OF ILLINOIS*

Grover H. Emrich,** and Henry F. Lucas, Jr.

The concentration of naturally-occurring radium-226 in the northern half of Illinois forms a consistent areal pattern for each of the Cambrian and Ordovician aquifers. Maximum data now available are for the St. Peter Sandstone (Middle Ordovician), and this paper relates particularly to that unit. Low Ra^{226} concentrations occur in north-central Illinois, a recharge area, and along a part of the Illinois River, an area of discharge. The Ra^{226} content increases slowly down the regional hydraulic gradient to a line corresponding to the northern edge of the Pennsylvanian outcrop, south of which it increases rapidly.

The natural source of Ra^{226} is decay of uranium-238. Its concentration in Illinois ground water may have two possible causes. First, the Ra^{226} content may reflect the length of time the water has been in contact with the formation. If this is true, relatively low concentrations would be found in areas of recharge or in areas of natural or artificial discharge where piezometric gradients steepen and water velocities increase, an explanation that would account for the relative local decrease in Ra^{226} content in the cones of depression near Chicago. Second, the uranium may have been slowly flushed by ground water from the areas of recharge and deposited farther down the hydraulic gradient. Thus, the Ra^{226} content would be controlled by the distribution of uranium in the sediments.

---

*Presented by G. H. Emrich at the meeting of The Geological Society of America, Houston Texas, Nov. 12-14, 1962.

**Illinois Geological Survey

CORRELATION OF THE Ra^{228} AND Ra^{226} CONTENT OF MAN WITH THAT OF THE FOOD AND WATER OF HIS ENVIRONMENT*

H. F. Lucas, Jr., D. E. Wallace, A. F. Stehney
and F. H. Ilcewicz

Abstract

An extensive study of the naturally occurring concentrations of Ra^{226}, Ra^{228} and Th^{228} in normal human bone, food and potable waters has been made. The relative contribution of food and water to man's skeletal content can be separately determined since many of the municipal water systems in the midwestern United States contain sufficient radium to increase the body content as much as twenty times the average of that obtained from food alone.

The Th^{228}/Ra^{228} ratio has been determined in adult bone of individuals undergoing life-long, continuous, constant exposure to Ra^{228}. This was accomplished by an initial extraction and determination of Th^{228} which, repeated after a one- or two-year growth period, provided a direct measure of the Ra^{228} content. The Th^{228}/Ra^{228} ratio has been found to be essentially unity for adults. The variation of this ratio with age will be discussed.

Average whole-body contents from food sources of 40% Ra^{226} and 12% Ra^{228} were found. This corresponds to 20 and approximately 8 times the average daily intake respectively. For life-long, continuous, constant intake, whole-body retention of Ra^{226} from water corresponds to 50 times the activity in a single liter; retention of Ra^{228} from water is approximately one-third that of Ra^{226}.

The Ra^{228}/Ra^{226} ratio in the bone and the drinking water of individuals known to consume water from wells with high radium content will be used to estimate the mean residence time of radium in trabecular and cortical bone.

*Presented at International Congress of Radiation Research, Harrogate, England, Aug. 6-10, 1962.

A CYTOGENETIC STUDY OF SOME RADIUM DIAL-PAINTERS AND THEIR PROGENY*

Neil Wald,** Charles E. Miller, Wayne H. Borges**
and Jip Kim**

Abstract

The ingestion of radium by women employed in painting watch dials with luminous paint in the early decades of this century has produced a human population group undergoing continuous internal radiation exposure. In the course of long-term surveillance of members of this group by Argonne National Laboratory, an incidental observation has been that a number of their progeny exhibit various abnormalities which might stem from genetic transmission.

Cytogenetic methodology now permits the direct observation of numerical and morphological abnormalities in human blood cell chromosomes. Association of chromosomal aberrations with various congenital anomalies, with previous external radiation exposure, and with some forms of leukemia which are also increased in incidence following radiation exposure has been reported.

It was considered of interest to determine, first, whether any cytogenetic abnormalities were present in the blood cells of persons exposed to long-term internal irradiation from radium; and, second, whether any cytogenetic evidence could be found for a possible relationship between a significant maternal body-burden of radium and anomalies in the progeny.

In an initial study, two dial-painters and their progeny and the progeny of two other dial-painters were examined. One of the dial-painters studied had developed an osteogenic sarcoma. Abnormalities among the progeny included mongolism, cerebral palsy, dwarfism, coarctation of the aorta, multiple unilateral anomalies, omphalocele, multiple miscarriages and familial recurrent infections. Pedigrees, estimates of radium body-burdens and cumulative critical organ radiation dosages, and the nature and frequency of chromosome aberrations observed, are presented in detail.

---

*Presented at International Congress of Radiation Research, Harrogate, England, August 6-10, 1962.

**University of Pittsburgh, Graduate School of Public Health.

PATTERNS OF RADIUM RETENTION IN MICE AS RELATED TO MAN*

Asher J. Finkel** and Charles E. Miller

Abstract

The evaluation of the long-term effects of internal deposition of radium requires an understanding of the pattern of isotope retention in the organism. Retention of radium in mice was followed by means of whole-body γ-ray spectroscopy after the material was administered by a single intravenous injection. On the assumption that continuous feeding is essentially equivalent to multiple daily injections, the power functions describing the retention of radium and radon daughters after a single intravenous injection have been integrated to predict retention after periods of continuous feeding. This integration was performed for feeding times of various lengths and was accomplished with the aid of an electronic computer. These calculations produced curves that closely agreed with those acquired experimentally when mice were fed radium for the same periods of time and then measured for radium content periodically. This correspondence of theoretical and observed values for both radium and radon daughters justifies the integration of single injection data to predict the long-term retention after finite periods of injestion of radium and, by analogy, of strontium. The validity of retrospective estimations of maximum body burdens of radium in persons studied many years after ingestion or injection is also fortified by these studies. Long-term effects of radium deposition are more properly correlated with such estimates of maximum body burdens than with current body contents measured many years after administration.

*Presented at International Congress of Radiation Research, Harrogate, England, August 6-10, 1962.

**Health Division.

THE LATE EFFECTS OF RADIUM DEPOSITION IN HUMANS*

Robert J. Hasterlik,** Asher J. Finkel† and Charles E. Miller

Abstract

Within the past four years, 261 persons who were formerly employed in the luminous-dial industry or who received radium therapeutically have been measured for radium burden. Two hundred and thirty represent cases previously unreported in the literature; the remainder are earlier cases recently restudied. Current body burdens which range from less than 0.001 μc to 10 μc, have been arbitrarily divided into those less than 0.001 μc (23 cases), those between 0.001 and 0.01 μc (36 cases), those between 0.01 and 0.1 μc (102 cases), those between 0.1 and 1 μc (60 cases), and those above 1 μc (40 cases). One hundred and sixty-two cases, therefore, have body burdens clustered within an order of magnitude above and below the permissible body burden of 0.1 μc. Of the 261 measured, skeletal radiographic studies and evaluations have been done on 232. Systematic criteria for grading the severity of the radiographic lesions have been developed. Radiographic changes range from those barely detectable, such as slight coarsening of the trabecular pattern, to those of advanced severity, such as aseptic necrosis, pathological fracture, and bone malignancy. A high degree of correlation exists between the current body-burden of radium and the degree of radiographic change. The determination of a point on this continuum of radiographic changes which represents clinically significant disease or disability has been an important consideration. Fourteen patients developed one or more malignancies casually related to the presence of radium in the skeleton. These data constitute the fruits of an intensive effort to acquire information from a much larger radium-bearing population than has hitherto been studied.

---

*Presented at International Congress of Radiation Research, Harrogate England, August 6-10, 1962.

**Argonne Cancer Research Hospital, University of Chicago.

†Health Division.

RECOVERY FROM RADIATION-INDUCED CLEAVAGE DELAY IN GAMETES OF ARBACIA PUNCTULATA*

Patricia McClement Failla

Exposure to ionizing radiation of either the egg or sperm of Arbacia punctulata retards quantitatively the time of first cleavage of the fertilized egg.(1,2) Early experiments by Henshaw demonstrated that the magnitude of the radiation-induced cleavage delay decreases with the length of time during which the irradiated eggs remain in sea water after irradiation but before insemination.(1,2) Henshaw found this decrease to be exponential with time and termed the phenomenon "recovery." No such recovery could be demonstrated in irradiated sperm which consists mostly of nuclear material. It has been assumed, therefore, that certain cytoplasmic components are necessary for the recovery mechanism to operate.

During a recent reinvestigation of aspects of this recovery process, it was found that the recovery rate of irradiated eggs in sea water was independent of oxygen.(3) When irradiated eggs were kept, prior to fertilization, in deoxygenated sea water the same decrease in cleavage delay was observed as when they were in fully aerated sea water for the same period. It was decided, therefore, to look for recovery in irradiated sperm by allowing the sperm to enter the egg and then blocking cell division for various lengths of time by the removal of oxygen. This technique demonstrated that indeed recovery does occur in irradiated sperm if the sperm is inside the egg during the recovery period. The methods used and results obtained are described below.

The criterion of effect was the amount of delay in the time of first cleavage of fertilized eggs induced by exposure of either the eggs or sperm to a dose of 10,000 roentgens. The cleavage times were measured from the time of fertilization to the time when 50% of the eggs had cleaved. The cleavage times are considered to be good to about ± 1 minute; hence, the cleavage delay values are accurate to about ± 2 minutes. The dose was delivered by a 5,000-curie cesium-137 gamma-ray unit at a rate of 5,000 r/min.

For the investigation of sperm recovery, irradiated and unirradiated sperm from the same animal were used to fertilize normal eggs in test tubes. Within a few minutes after fertilization, nitrogen was started bubbling through the fertilized egg suspensions. Samples were removed thereafter at various intervals to finger bowls of fresh sea water, and

*Work performed at the Marine Biological Laboratory, Woods Hole, Massachusetts. Science 138, 1341-1342 (1962).

cleavage times were measured. The cleavage times of the unirradiated, nitrogen-treated samples were compared with the normal control cleavage time to give values for the prolongation of the cell division cycle caused by the removal of oxygen. These nitrogen-induced prolongations are plotted as "recovery period" intervals on the abscissa in Figure 40. The time delays of first cleavage induced by the exposure of the sperm to 10,000 r are plotted on a logarithmic scale on the ordinate.

The results of two experiments shown in Figure 40 illustrate the two types of recovery curve observed. In 2 out of 4 cases, the radiation-induced cleavage delay decreased exponentially with recovery time as in curve A. In the other two, there was an initial sudden drop followed by a slower exponential decline as in curve B. The similarity in the terminal slopes of curves A and B is coincidental; the recovery rates of sperm from different animals usually vary somewhat.

It was then decided to apply the same technique to irradiated eggs and to compare the curves for eggs allowed to "recover" before and after fertilization. The results of two such experiments are shown in Figure 41. In the case of the unfertilized eggs the recovery period represents the time interval between irradiation and fertilization; for the fertilized eggs,

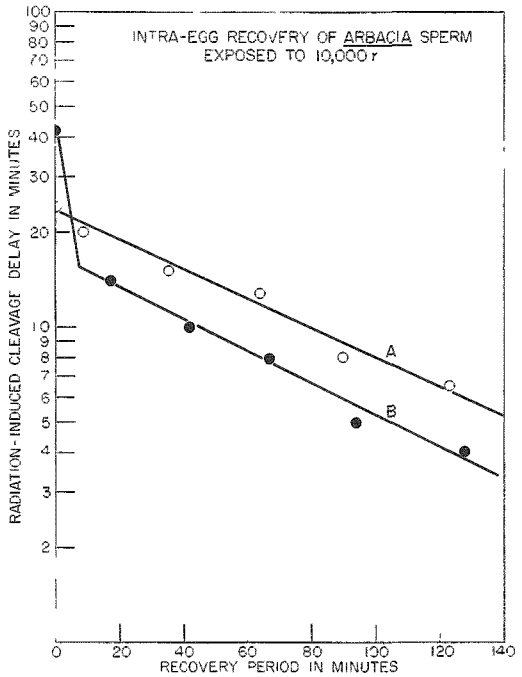

Figure 40

The decrease in cleavage delay for irradiated Arbacia sperm as a function of time-interval cell-division process retarded by nitrogen treatment. Curves A and B show results of two experiments and represent the two types of response found.

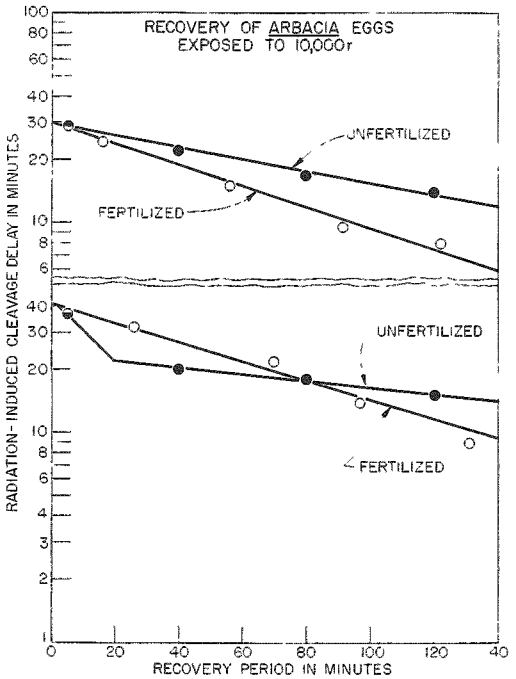

Figure 41

The decrease in cleavage delay for irradiated Arbacia eggs. See text for definitions of recovery period in the case of fertilized and unfertilized eggs. Results of two experiments are shown indicating the types of response found.

inseminated immediately after irradiation, it represents the time cell division was retarded by exposure to nitrogen. The same two forms of recovery curve were found as with irradiated sperm, and in four experiments all four possible combinations of the two curve shapes were observed. In each case, however, the terminal portion of the recovery curve for the fertilized eggs was steeper. It appears, therefore, that the kinetics of the pre- and post-fertilization recovery processes in irradiated eggs from the same animal differ and that the post-fertilization process is somewhat more efficient.

The cleavage delay induced by exposure of Arbacia gametes to radiation has been interpreted as the time required for the zygote to repair or replace some (nuclear?) substance necessary for cell division which was destroyed by the radiation.(4) Since recovery from this delay was demonstrated in unfertilized eggs but not in sperm, it was postulated that some cytoplasmic component was essential for repair. The experiments described above confirm this view since they demonstrate that recovery can take place in irradiated sperm if the sperm is inside the egg where it can presumably mobilize the required resources for repair. It has also been shown, however, that the recovery mechanism which operates in the irradiated unfertilized egg is not necessarily the same in the zygote. It is planned to apply the technique used in these experiments to investigate further recovery and other aspects of radiation damage in Arbacia gametes.

References

1. P. S. Henshaw. Studies of the effect of roentgen rays on the time of first cleavage in some marine invertebrate eggs. I. Recovery from roentgen-ray effects in Arbacia eggs. Am. J. Roentgenol. 27, 890-898 (1932).

2. P. S. Henshaw. Further studies on the action of roentgen rays on the gametes of Arbacia punctulata. Am. J. Roentgenol. 43, 899-933 (1940).

3. Patricia Failla. In vivo and in vitro recovery or irradiated gametes of Arbacia punctulata. Radiation Res. 17, 767-773 (November 1962).

4. D. E. Lea. Actions of Radiations on Living Cells, 1st ed., The Macmillan Co., New York, 1947.

PERIODIC EVENTS IN BONE

D. J. Simmons

Biologic clocks have been the subject of several recent symposia,[1-3] and an extensive body of information is available in the literature concerning the timing of physiological and biochemical events in a wide variety of tissues. Preliminary studies using the colchicine method suggested that the mitotic activity of chondrocytes in the distal and proximal epiphyseal plates of the femur and tibia respectively was subject to a diurnal periodicity.[4] These findings were confirmed autoradiographically by the use of tritiated thymidine as a marker for DNA synthesis.[5] This technique allowed more detailed study of the cyclic activity of chondrocytes. Counts of colchicine mitoses and thymidine-labeled cells, however, failed to show definitive periodic changes in populations of osteoblasts and their precursor cells. The experiment to be described is a preliminary attempt to determine whether the functional activity of bone cells differs within a single 24-hour period.

Method

Thirty-eight albino rats, Sprague Dawley Strain, weighing 45-50 g each, were singly housed and maintained for two weeks under a photoperiod of 12 hours (09:00-21:00) alternating with twelve hours of darkness (21:00-09:00) and at a temperature of 73-75°F. Food and water were supplied ad libitum, and intentional disturbance was limited to 09:00-09:30 when the cages were attended. The animals were weighed 24 hours prior to experimentation, and groups and subgroups were established according to their weight-gain performance during the two-week conditioning period. The rats weighed 150-175 g at the time they were used. Nineteen animals were given intravenous injections of 1.5 μc Sr^{85}/100 g body weight in 0.1 ml distilled water via the tail vein between 09:20-11:00 (Day group); a second series (Night group) was injected between 21:00-22:30. Subgroups of 4-5 rats were sacrificed by decapitation at 2-3, 4, 8 and 12 hours after receiving the tracer dose, and 2-3 ml of blood and the femora were obtained from each animal. The blood was centrifuged, and aliquots of serum were assayed in a well-type scintillation counter. The left femora were radiographed and divided into distal epiphyseal-metaphyseal and shaft segments. The segments were ashed, weighed, and assayed in the same way as the blood samples.

The findings have been plotted in Figure 42, and the data have been expressed as μc Sr^{85}/g Ca. Bone ash was assumed to be 38% calcium, and serum calcium was taken as 10.3 mg %.[6]

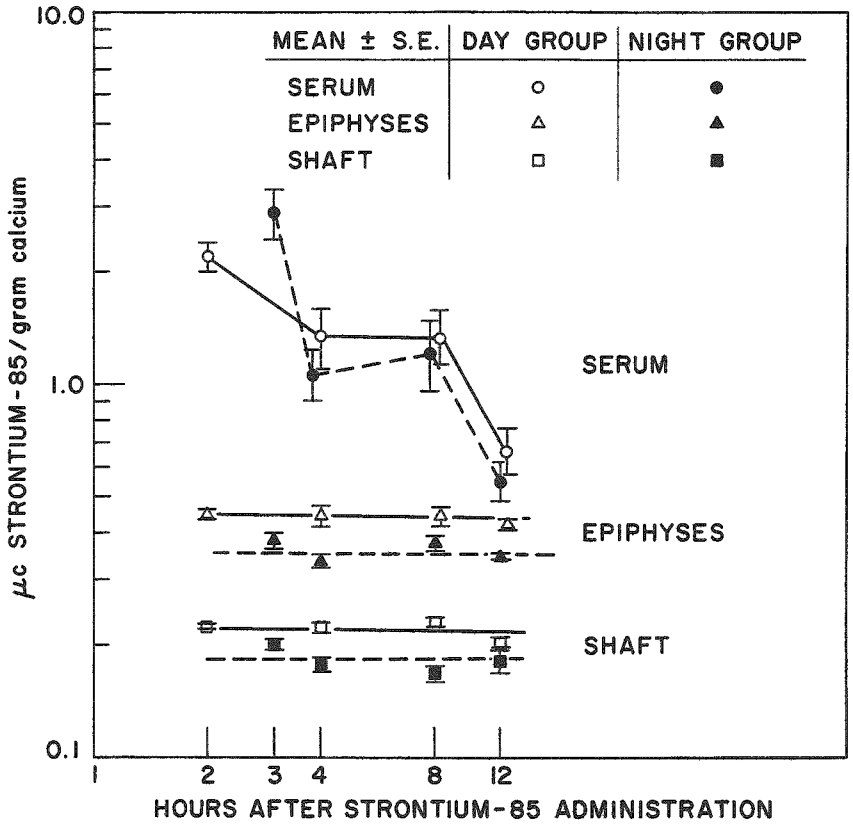

Figure 42

Retention of strontium-85 in serum and bone of rats

Results

The 2- to 3-hour serum samples reveal that the disappearance of Sr^{85} from blood is initially more rapid in animals injected during the day. However, day-night values are not significantly different from 4-12 hours after tracer administration. The early depletion of serum strontium-85 is reflected by the significant differences in tracer content of both epiphyseal and shaft segments at 2-3 hours, and the specific activities in bone remain relatively constant thereafter despite the decreasing serum activity. The day bone values are slightly, but consistently, higher than the night values (circa 10-20%) throughout the experimental period.

Discussion

Although strontium is handled differently from calcium by the body in terms of intestinal and kidney discrimination, its uptake and retention in bone is at least in part dependent upon the presence of a calcifiable

organic matrix, collagen, produced by osteoblasts. Adrenal hormones are known mitotic inhibitors, and their relation to diurnal periodic events has been stressed by Halberg;[1] periods of maximum adrenal mitotic activity and corticosteoid production generally correspond to the hours when these activities are minimal in most other tissues, and adrenal hormones have long been known to suppress bone matrix formation[7] and mineralization.[8] The proof that the diurnal cycle established for cartilage and perhaps, in these experiments, for bone cells is adrenal-regulated is not yet established. The corresponding and early changes in the specific activities of serum and bone and the relative constancy of the bone values thereafter indicates that the effect is not due to the differential excretion of strontium via the urine; although the strontium excretory component is unknown, the urinary calcium-to-strontium ratio is very constant,[9] and urinary calcium levels are not subject to diurnal fluctuations in man.[10] It is believed, therefore, that the results reflect the degree of collagen formation during the light-dark periods. The fact that periodic changes in populations of osteoblasts undergoing DNA synthesis could not be detected by cell counts[5] is probably due to the very small size of the potentially replicative population and to the errors inherent in a census of a non-uniform tissue, the cells of which are undergoing rapid modulations.

References

1. F. Halberg, E. Halberg, C. P. Barnum and J. J. Bittner. Photoperiodism and Related Phenomena in Plants and Animals, ed. Withrow. Am. Assoc. for Advancement of Science, Washington, D. C., 1959. pp. 803-878.

2. Cold Spring Harbor Symposia on Quantitative Biology, 25 (1960).

3. Rhythmic Functions in the Living Systems, ed. W. Wolf. Ann. N. Y. Acad. Sci. 98, 753-1326 (1962).

4. D. J. Simmons. Nature 195, 82-83 (1962).

5. D. J. Simmons. Clinical Orthopaedics No. 24, 176-189 (1963).

6. W. Ponsold, G. Luft and H. Seipalt. Natur wissenschaften 49, 88-89 (1962).

7. G. Vaes and G. Nichols, Jr. Endocrinology 70, 890-901 (1962).

8. J. D. Gonin and H. Fleisch. Helv. Physiol. Acta 20, 23-25 (1962).

9. C. L. Comar, R. H. Wasserman, S. Ullberg and G. A. Andrews. Proc. Soc. Exptl. Biol. Med. 95, 386-391 (1957).

10. R. C. Manchester. J. Clin. Invest. 12, 995-1008 (1933).

THE RETENTION OF Ba^{133} IN BEAGLES

R E Rowland

This report supplements an earlier report on the whole-body retention of Ba^{133} in two beagles which has now been measured for 1,000 days.(1) The plasma concentration had been measured during the first 14 days following the injection in both dogs; in one of them a measurement has now been made at more than 1,000 days after injection.

Dog A22B was 8 months old (245 days) and weighed 7.2 kg at time of injection. (Weight 1,000 days later was 7.5 kg) This dog received 6.1 μc Ba^{133}. Dog 576 was at least four years old at the time of injection, weighed 10.1 kg, and received an injection of 10 μc Ba^{133}. Complete details of the injection solution and technique of measurement will be found in the earlier report.(1)

The fractional retention of the barium tracer is tabulated in Table 24 and shown in graphical form in Figure 43. It will be noted that the data cannot be fitted with a single straight line on the log-log plot, yet the deviation from a power function is not marked over this time interval.

Table 24

Fractional retention of Ba^{133}

Days from injection	Dog 576	Dog A22B
0	1.0	1.0
20	0.49	0.667
34	0.423	0.583
41	0.418	0.583
48	0.414	0.604
83	0.376	0.510
139	0.333	0.461
188	0.308	0.406
293	0.253	0.362
363	0.225	0.353
454	0.214	0.320
693	0.174	0.282
995	0.155	0.294

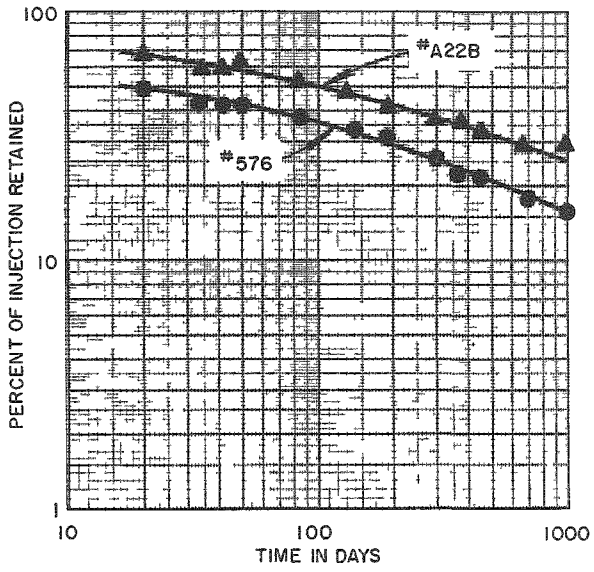

Figure 43

The fractional retention of Ba^{133} in two beagles plotted as a function of time

The plasma data are listed in Table 25. The Ba^{133} concentration for the last observation was determined by gamma-ray analysis of 420 ml

of plasma, using an aliquot of the original injection solution.* The plasma was collected over a ninety-day period (days 1,002 through 1,093) by taking approximately 150 ml of whole blood from dog A22B every two weeks, separating the plasma, measuring it, and storing it until a sufficient quantity had been obtained for analysis.

Table 25

Blood specific activity

Time	% Injected dose/mg Ca		Time	% Injected dose/mg Ca	
	Dog 576	Dog A22B		Dog 576	Dog A22B
1 hr	0.283	0.253	3 days	0.0118	0.00359
6 hr	0.117	0.0631	7 days	0.0038	0.00166
24 hr	0.0515	0.0176	14 days	0.0011	0.000628
2 days	0.0204	0.00883	(1002-1091 days)	-	$(86 \pm 16) \times 10^{-7}$

The specific activity of the plasma is shown in graphical form in Figure 44, in terms of percent of injected dose per gram of calcium. It is evident from the last measurement that the slope of the Ba^{133} concentration in plasma does not follow the initial slope over the entire 1,000 day interval.

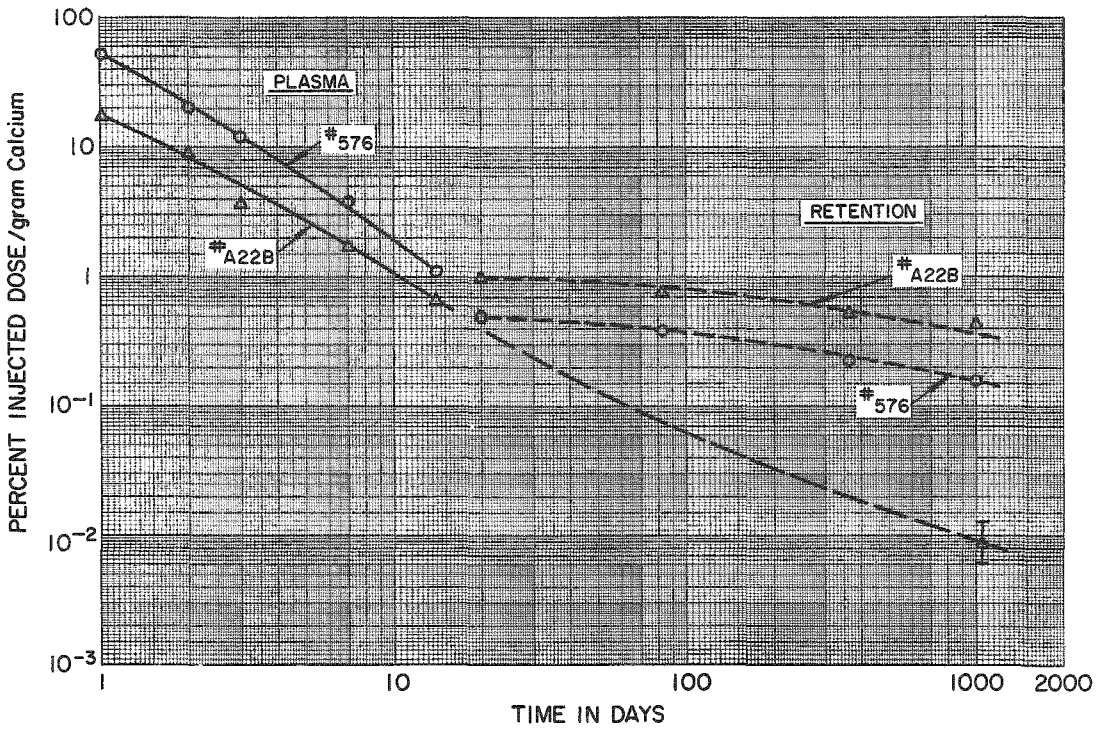

Figure 44

The Ba^{133} concentration in the plasma of two beagles plotted as a function of time. Also shown in the same units, percent of injected dose per gram calcium, are the skeletal retention values. Note that the plasma concentration drops below the average skeletal concentration by 10 days after injection for dog A22B, and by 30 days for dog 576.

*We are indebted to H. F. Lucas, Jr., for the gamma-ray analysis of the blood sample.

Figure 44 also shows the retention of Ba^{133} in the two dogs, expressed in the same units as the plasma concentration. It has been assumed that the skeleton of dog 576 contains 100 grams of calcium, and that of dog A22B, 70 grams. This type of plot shows the relationship between the specific activity of the plasma and that of the skeleton. The specific activity of the plasma does not fall below that of the skeleton for 10 days for the younger dog, and 30 days for the older animal. However, the plasma concentration does keep falling further and further below the skeleton with the passage of time. If the retention, R_t, were accurately described by a power function, then the plasma concentration would be expected to be described by another power function. That is, if $R_t = at^{-b}$, the excretion, dR/dt, would be given by $dR/dt = ct^{-b-1}$, where t is time after administration and a, b, and c are constants. Since the isotope excreted can be assumed to have gone via the blood, the plasma concentration would be expected to follow a power function of the form t^{-b-1}.

In these dogs, since the retention is observed to drop faster than a power function, excretion must be occurring at a higher rate than that expected from a power function. It follows that the plasma concentration must be higher than expected, and this seems to be the case here.

The significant point here, however, is the fact that, 1,000 days after the isotope was administered, the plasma specific activity is a factor of fifty below that of the skeleton.

Reference

1. R. E. Rowland. Retention and plasma clearance of the alkaline earth elements. Argonne National Laboratory Radiological Physics Division Semiannual Report, July through December 1959. ANL-6104, pp. 34-47.

RADIUM IN HUMAN TEETH: A QUANTITATIVE AUTORADIOGRAPHIC STUDY*

R. E. Rowland**

This study of radium in human teeth was undertaken to determine the distribution of this radioelement in the dental tissues many years after medical or occupational exposure. Dudley has suggested that the total body content of a person contaminated with radium could be estimated from the radium content of a single tooth, and it appears from his measurements that the uncertainty involved in such an estimate is not much greater than a factor of two.(1) It would be most remarkable if the radium content of a tooth should give a representative measure of the radium content of the entire skeleton, for it has been shown that the radium content of equivalent bone samples (i.e., one gram) may vary as much as a factor of ten.(2) It is of interest to determine whether this observed correlation in teeth is fortuitous or is a metabolically significant observation.

Methods and Materials

Teeth from three radium cases were studied.

Case 03-473: (Dial-painter, female)

A former dial-painter who had painted for two years when she was 19 to 21 years old. An impacted mandibular 3rd molar was removed at age 55, following removal of a bone sequestrum from the left mandible six months before. Her total-body radium content was determined at this time by whole-body counting to be 1.2 μc Ra^{226}.(3)

Case 03-201: (Radium acquired therapeutically; female)

No precise information is available about the source of this woman's radium; we have assumed that it was acquired therapeutically about 35 years ago. An impacted mandibular 3rd molar was removed at age 52; no bone is available. The total radium content of this woman was determined at this time by whole-body counting to be 3.0 μc Ra^{226}.(3)

---

*Accepted for publication in Archives of Oral Biology.

**Present address: Department of Radiation Biology, School of Medicine and Dentistry, University of Rochester, Rochester, N. Y.

Case 03-998: (Dial-painter, female)

This woman painted watch dials for a six-year period (1917 to 1923) when she was 27 to 33 years old. Her death occurred in 1925, at age 35; the autopsy report stated "severe anemia, with purpura, petechiae, buccal sepsis, early jaw necrosis and red bone marrow." The mandible, with 10 teeth, and a portion of the femur were obtained from a museum jar in which they had been stored dry. Although early estimates of the total radium content of this patient ranged from 90 to 180 μc,[4] recent studies of these bone samples indicate that the terminal content was in the range of 5 to 20 μc Ra^{226}, in addition to an equal amount of the shorter-lived Ra^{228}, which had been present originally.[5] Two teeth, the left canine and the left 2nd molar, were studied autoradiographically, while all ten were measured to determine their Ra^{226} content.

Each tooth included in this study was sealed, individually, within a glass vial and the gamma-ray spectrum of each recorded immediately and again a month later. From these two measurements, the total Ra^{226} content and the radon retention of each tooth was determined.

The teeth studied autoradiographically were first embedded in methyl methacrylate and then cut into longitudinal sections 150 or 200 microns thick. To facilitate subsequent comparison with the autoradiographs, microradiographs were taken of each section (17.5 kv x rays, Eastman Kodak spectroscopic plates 649-0). Three different autoradiographs were then made from each section:

1) An appropriate exposure (3 to 120 days) on an alpha-track plate to produce an autoradiograph from which alpha-track counts could be made to determine the microscopic radium concentrations.

2) A long exposure (1-4 months) on a beta-sensitive plate to produce a visible image of the radium distribution in the tooth.

3) A stripping-film autoradiograph (2-month exposure) to yield high-resolution localization of the radium deposits within the tooth.

The radium concentrations found in various portions of the teeth were evaluated by counting the number of tracks per unit area in the autoradiographs. These counts were expressed as radium concentrations per gram of calcium, using an average alpha particle range of 6.3 mg/cm^2, radon retention values of 40% for the bone sections and 75% for the tooth sections, and calcium concentrations of 24.4%, 27%, and 36% by weight, respectively, for bone, dentin and enamel.[6]

Results

The radium content of each tooth studied in detail and of all ten teeth from Case 03-998 are tabulated in Table 26. For comparison with the skeleton (10^3 g Ca) the radium content of each tooth is expressed in terms of grams of calcium by assuming that the calcium content of a tooth is 28% by weight. This comparison is made in Table 27.

Table 26

Gamma-ray measurements of teeth from radium cases

Case	Tooth	Total activity, pc Ra^{226}	Weight, g	$\frac{pc}{g}$	$\frac{pc}{g\ Ca}$	Radon retention in vitro, %
03-473	Mandibular 3rd molar	2100	1.20	1750	6150	75
03-201	Mandibular 3rd molar	1510	1.45	1040	3730	44
03-998	Right canine	859 ± 8	1.022	840	3000	76
	Left canine	1318 ± 12	1.013	1300	4640	71
	Right lateral incisor	570 ± 7	0.477	1190	4250	75
	Left lateral incisor	595 ± 6	0.317	1880	6680	59
	Right first premolar	659 ± 8	0.799	825	2960	70
	Left first premolar	519 ± 7	0.715	725	2600	54
	Right second premolar	485 ± 4	0.398	1220	4360	62
	Left second premolar	711 ± 8	0.932	765	2710	66
	Right second molar	1623 ± 11	1.939	840	3000	68
	Left second molar	1614 ± 12	1.970	820	2930	60
03-998	Total	8953	9.582	935	3300	

Table 27

Comparison of the specific activity of the teeth and the skeleton

Case	Specific activity		Ratio: tooth/skeleton
	Tooth pc/g Ca	Skeleton pc/g Ca	
03-473	6150	1200	5.1
03-201	3730	3200	1.2
03-998 (10 teeth)	3300	(10000)*	(0.3)*

*Based on a body content of 10μc.

The significance of these measurements will be discussed below.

Case 03-473: (Exposure at age 19 to 21 years)

The autoradiographs of the sections from this tooth indicate that dentin was being formed at the time of exposure to radium (Figure 45b). On the microradiograph (Figure 45a) cross hatching is employed to indicate the portion of the dentin which has given rise to this autoradiographic image. The dark lines in the autoradiograph, adjacent to a grey band, are interpreted to indicate that the original exposure to radium was at a high concentration for a short time, but that over the rest of the exposure period the intake was at a lower level.

When the tooth section is exposed to the autoradiographic plate for a longer period (Figure 45c), it is evident that radium is present in other portions of the tooth. In addition to the deposit in the forming dentin, deposits in the following locations are visible:

1) immediately under the surface of the enamel,

2) in the dentin which was formed before the exposure to radium,

3) in the dentin formed after the exposure to radium.

The radium concentrations measured in this tooth are tabulated in Table 28. The distribution in the pre-existing dentin, observed to decrease with depth, is shown in graphical form in Figure 46. This graph shows, in addition, the maximum hotspots and the average diffuse level observed in the small bone sample, and the magnitude of the concentration under the enamel surface.

Table 28

Radium concentrations measured in bones and teeth

Case	Number and type of deposition	Bone pc/g Ca	Dentin pc/g Ca	Enamel pc/g Ca
03-473	Hotspots	13,500	84,000 22,000	-
	Diffuse	740	380-1250	900
03-201	Hotspots	-	404,000	-
	Diffuse	(1500 ± 750)	210-3030	1700
03-998	Hotspots	88,700	63,000	-
	Diffuse	1,880	300-17,200	880

(a)

(b)

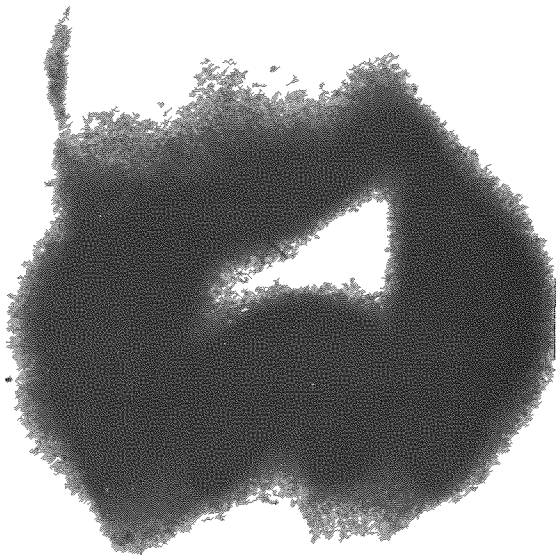

(c)

Figure 45

A 200-micron thick section cut from the mandibular third molar of Case 03-473. a) A microradiograph; b) an autoradiograph exposed for one month; and c) an autoradiograph exposed for four months. The outline of the autoradiographic darkening of (b) has been indicated on the microradiograph (a) with cross hatching.

5mm

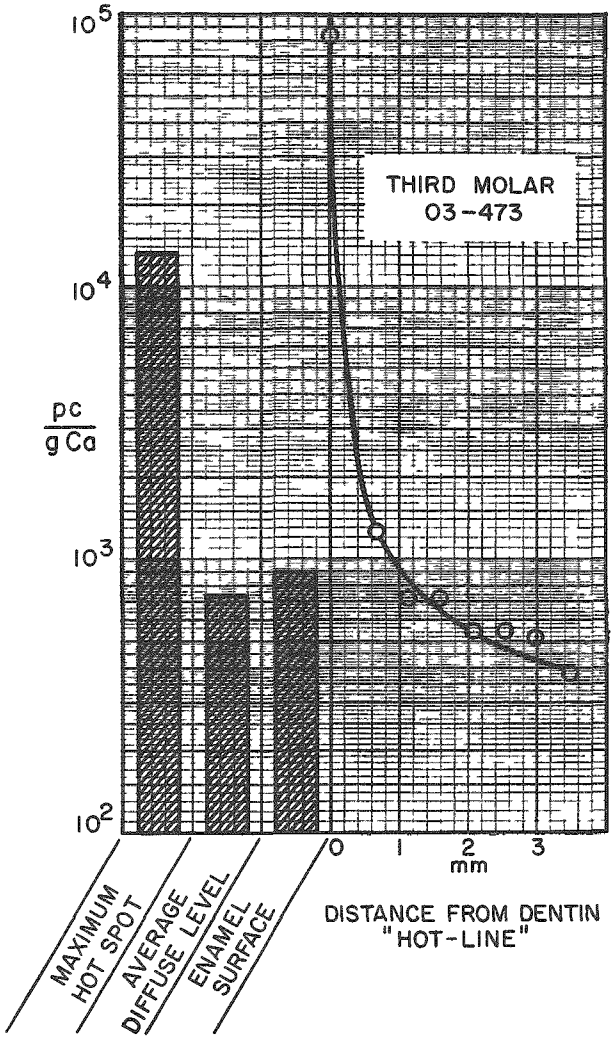

Figure 46

Comparison of the radium concentrations observed in the bone and tooth of Case 03-473. The maximum hotspot and the average diffuse level measured in the bone, and the enamel surface concentration are shown as histograms; the radium concentration in the dentin is plotted as a function of the distance from the dentin hot-line.

Case 03-201: (Exposure during late teens?)

The assumption as to the age at which this woman received radium is verified by the autoradiographs of the tooth sections. A narrow line of darkening, 50-250 microns wide, is present in the autoradiograph (not illustrated) of the dentin between the pulp cavity and the enamel. Since the 3rd molar has completed its crown formation and started root formation by age 17 (95th percentile),[7] it is likely that this girl was in her late teens when she received radium. The narrow line of darkening, actually resolvable into two narrow lines, suggests that she received two courses of treatment which lasted not more than a few months; the route of administration was probably intravenous.

The radium concentrations in this tooth are illustrated graphically in Figure 47. No bone was available for comparison; however, a diffuse

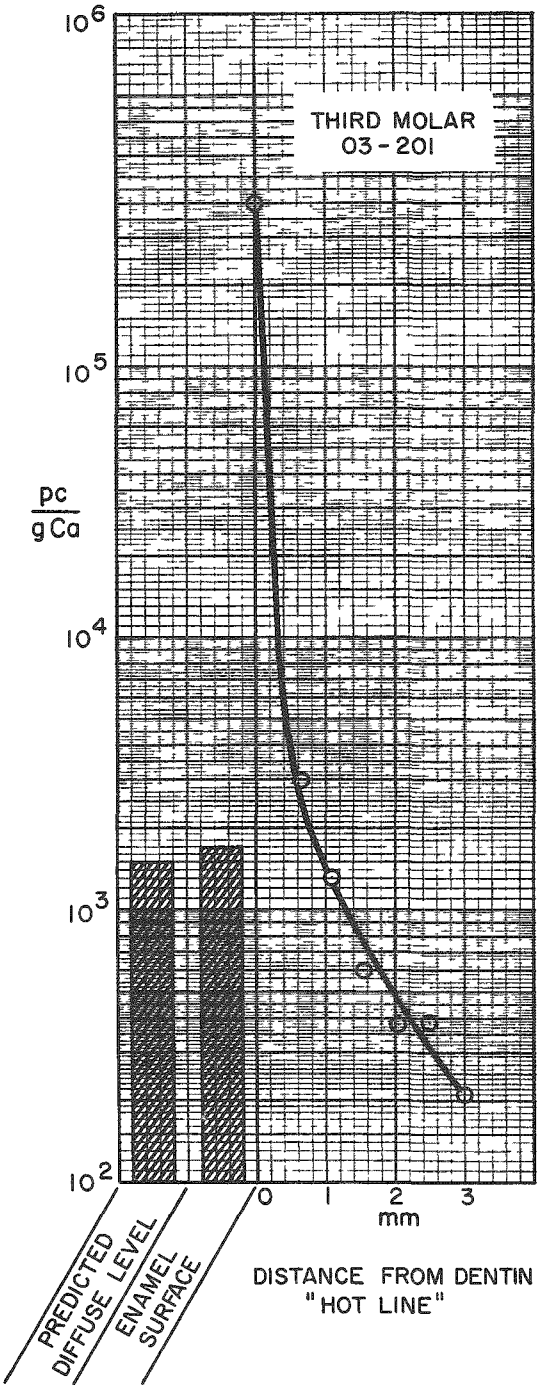

Figure 47

Comparison of the radium concentrations observed in the tooth of Case 03-201. A predicted diffuse level, as described in the text, is also shown for comparison.

distribution, predicted on the basis of the body content, is shown. This prediction is based on the observation that the diffuse level is approximately one half of the uniform label, i.e., that concentration obtained by dividing the skeletal radium content by the skeletal mass.[8]

Case 03-998: (Exposure over a six-year period, from age 27 to 33 years)

In spite of the age of this woman at exposure, dentin was being formed in the left second molar (Figure 48). In addition to the dentin deposit, a longer autoradiograph (Figure 48c) illustrates the same distributions listed for Case 03-473. In the canine tooth (Figure 49) no growth of dentin took place, so that the entire label was in the pre-existing dentin and the enamel surface. However, in both the molar and the canine tooth an intense deposit of radium is present in the outermost layer of the cementum which covers the roots. This deposit is equal in specific activity to that observed in the dentin, suggesting that this layer of cementum was probably formed during the exposure to radium. The measured specific activities are shown in graphical form in Figure 50.

A small disk of enamel, lying on the surface of the dentin between the two roots of the 2nd molar is visible in the microradiograph (Figure 48a). Enamel in this location is not unusual,[9] but it is mentioned here because it is highly radioactive, and thus is known to have been formed during this six-year period.

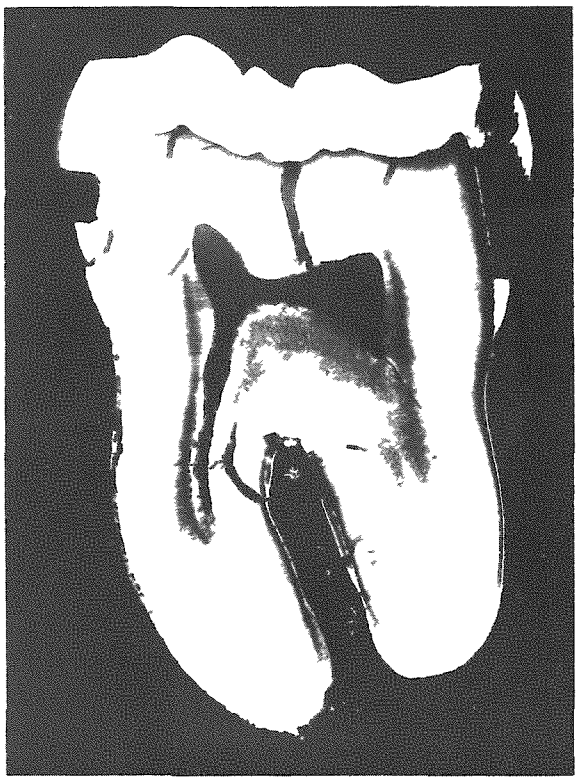

(a)

(b)

(c)

5 mm

Figure 48

A 150-micron thick section cut from the left second molar of Case 03-998. a) A microradiograph, b) a seven-week autoradiograph, and c) a four-month autoradiograph.

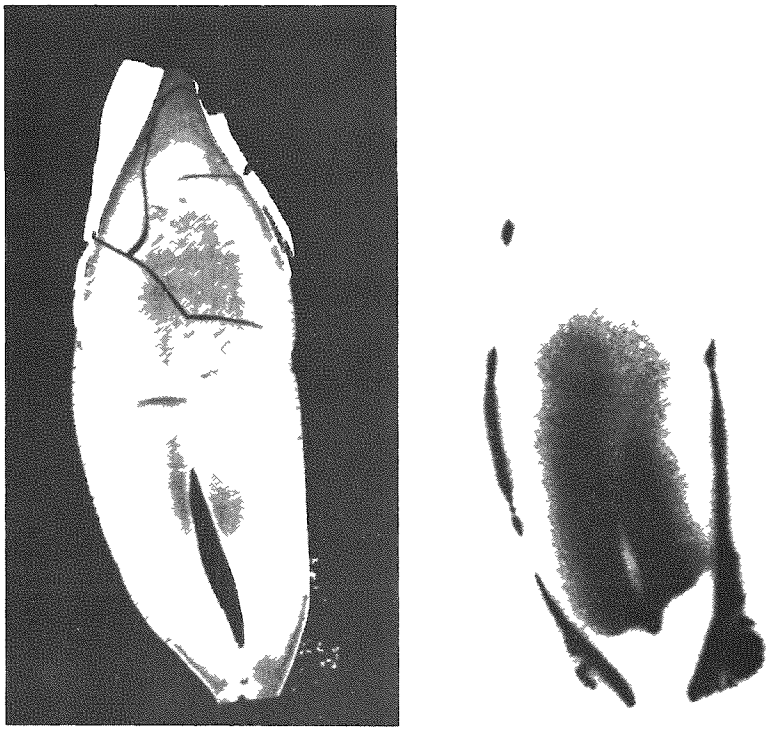

1 cm

Figure 49

A 150-micron thick section cut from the left canine tooth of Case 03-998. a) A microradiograph, and b) a four-month autoradiograph.

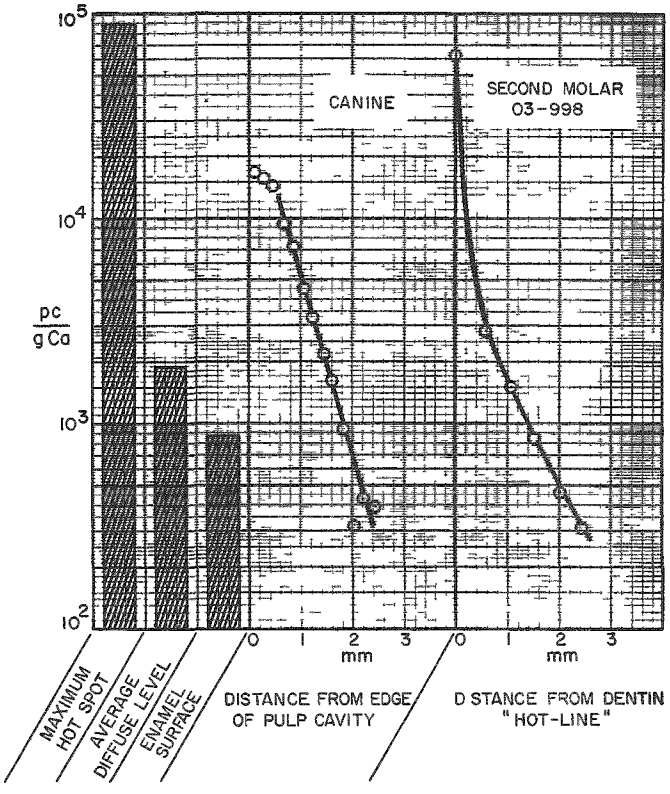

Figure 50

Comparison of the observed radium concentrations in the teeth of Case 03-998 with the concentrations in bone. The deposit in the dentin of the canine tooth was measured from the edge of the pulp cavity, while this distribution in the second molar was measured from the hot-line in the dentin.

Discussion

The autoradiographs of these teeth indicate that a significant quantity of radium has been deposited within the dental tissues. This observation is in agreement with the studies of the radium content of teeth from radium cases that have been made at MIT[1] and at Argonne.[10] These studies have shown that such teeth usually contain a radium-to-calcium ratio of the same order of magnitude as the skeleton; the MIT study suggested that the ratio

$$\frac{(Ra/Ca)\ \text{tooth}}{(Ra/Ca)\ \text{skeleton}} \simeq 0.3$$

with a range of 0.10 to 0.73.

On the basis of the present study this conclusion should be modified to apply only to teeth that were mature at the time of exposure. In those teeth which were still being formed when radium was present the above ratio may be as large as 5 to 1 (Table 27). The reason, of course, lies in the high uptake of the isotope in the forming dentin, as illustrated in Figure 45. Even in mature teeth a considerable range is to be expected, for the radium-to-calcium ratio of a given tooth will depend upon the ratio of dentin to enamel and the ratio of buried dentin to dentin adjacent to the pulp cavity in that tooth, and will be influenced by the amount of bone and cementum attached to the tooth when the measurement is made.

These observations give rise to the basic question: by what process does this isotope enter the dentin of a mature tooth, or the pre-existing dentin of a forming tooth? Could this be a manifestation of a long-term exchange process?

The ability of the dental tissues to acquire trace elements by an exchange process is well known. An autoradiograph of a tooth from a radium-dial painter which appears to illustrate this uptake has been published.[11] Previous to this the ability of pre-existing dentin to acquire lead from the blood supply had been described.[12] The most striking demonstration of this exchange capacity was provided by Sognnaes et al.,[13] who, using monkeys, described the uptake of P^{32} in the dental tissues at short time intervals after administration. Indeed, they showed that the P^{32} in the dentin decreases with depth in a manner similar to the approximately exponential decrease shown here for radium (Figures 46, 47 and 50).

Thus, it is evident that these isotopes can enter the teeth quickly and remain there for long periods, just as is the case in bone. It is paradoxical that, even after a 30-year residence in dentin, Ra^{226} should show a distribution in depth so similar to that of P^{32} at very short times. A deposition resulting from an exchange process, which operates rapidly enough to be seen in minutes, might be expected to be drastically altered after many years.

It is instructive to compare the magnitude of the dentin deposit with the equivalent deposition in bone, the so-called diffuse distribution. It is evident from Figure 46 that the dentin within 1 mm of the pulp cavity (or the edge of the pulp cavity at the time the radium was in the blood) contains as much, or more, radium per gram of calcium as is found in the diffuse distribution in bone. Further in depth the dentin contains less activity than the bone; in this respect it should be recalled that few regions in bone are more than a few hundred microns from the blood supply, while portions of the dentin may be 10 to 40 times this distance. In each tissue there exists a microscopic distribution system, the canaliculae in bone and the dentin tubules in the dentin. This distribution system could provide a rate-limiting step in the process of distributing these tracers in depth.

When the dentin tubules no longer transport fluids, such as is the case when they become filled with mineral deposits (sclerosis), exchange phenomena would no longer take place within the affected region. If the stoppage occurred before the radium were present, no uptake of the isotopic tracer would take place; note that this appears to have been the situation in the lower portion of the root of the canine tooth from 03-998 (Figure 49). If such occlusion occurred after the isotope had been deposited within the dentin, no further removal by exchange would take place.

Let us consider an alternative mechanism for the deposition of these isotopes within the dentin, namely, that they indicate a net gain of mineral in these regions. This implies that the dentin must be continually increasing in density. The sclerotic process, mentioned above, is an example of such an increase, and may account for a portion of the uptake of such tracers. Yet, the fact that all of the teeth examined in all of the studies mentioned have shown uptake of isotopic tracers, independent of the age of the teeth, strongly suggests that the bulk of this uptake must be due to long-term exchange and not to a gain of additional mineral.

It can be concluded from this study that when Ra^{226} is present in the blood, it will be incorporated within the teeth. It will be deposited in those regions in which new mineral is being formed, and will, to a lesser extent, enter those portions of the mineral previously formed. In the pre-existing dentin this deposit decreases exponentially in magnitude with distance from the blood supply. In the enamel a deposit is present along the outer surface; if there is also a deposition in depth within the enamel it is much less intense, for it was not visible in the teeth studied here.

The processes described above may be expected to apply to the other members of the alkaline-earth family, namely calcium, strontium, and barium. Thus, mature teeth can, by virtue of their ability to acquire these elements by exchange processes, be expected to give a reliable indication of the amount of contamination of the entire skeleton following exposure to the radioactive forms of any of these elements.

It is of interest to note that the radium concentration in small samples of bone in which no appositional growth had taken place during the exposure to radium, and thus would contain only a diffuse label without any hotspots, would provide a valid method of estimating the radium content of the entire skeleton. The uncertainties inherent in extrapolating radium concentrations measured in small bone samples to the entire skeleton arise from the continual removal and replacement processes at work in normal bone. The teeth, in contrast, once their growth is finished, provide a stable environment in which isotopes acquired by long-term exchange processes remain undisturbed.

It is thus understandable why the observed gamma-ray measurements of the teeth correlate so well with the total skeletal content. It should also be evident that quantitative autoradiographic measurements of the teeth could yield even better estimates of the total skeletal content of an alkaline-earth isotope deposited within the skeleton.

The teeth in this study were acquired through the efforts of Drs. A. J. Finkel, C. E. Miller and L. D. Marinelli, of this Laboratory, and Dr. R. J. Hasterlik, of the Argonne Cancer Research Hospital.

References

1. R. D. Evans. Reliability of teeth as indicators of total-body Ra burden. Annual Progress Report, Radioactivity Center Massachusetts Institute of Technology (May 1960). pp. 5-12.

2. W. P. Norris, W. P. Speckman and P. F. Gustafson. Studies of the metabolism of radium in man. Am. J. Roentgenol. 73, 785-802 (1955).

3. C. E. Miller. Unpublished measurements, 1962.

4. H. S. Martland. Occupational poisoning in manufacture of luminous watch dials. J. Am. Med. Assoc. 92, 466-552 (1929).

5. R. E. Rowland. Detailed autoradiographic and microradiographic studies of bone from human radium cases. Argonne National Laboratory Radiological Physics Division Semiannual Report, January through June 1961. ANL-6398, pp. 5-23.

6. R. F. Sognnaes. Dental aspects of the structure and metabolism of mineralized tissues. In: Mineral Metabolism, I-B, (Ed. C. L. Comar and F. Bronner). Academic Press, New York, 1961, pp. 677-741.

7. S. M. Garn, A. B. Lewis and D. L. Polacheck. Variability of tooth formation in man. Science 128, 1510 (1958).

8. R. E. Rowland and J. H. Marshall. Radium in human bone: the dose to microscopic volumes of bone. Radiation Research 11, 299-313 (1959).

9. M. A. Rushton and B. E. Cooke. Oral Histopathology. Livingstone, Edinburgh, 1959. p. 24.

10. C. E. Miller and J. B. Corcoran. Estimation of radium body-content of exposed humans from the activity of extracted teeth. Argonne National Laboratory Radiological Physics Division Semiannual Report, January through June 1960. ANL-6199, pp. 68-70.

11. J. C. Aub, R. D. Evans, L. H. Hempelmann and H. S. Martland. The late effects of internally-deposited radioactive materials in man. Medicine 31, 221-329 (1952).

12. J. C. Aub, L. T. Fairhall, A. S. Minot and P. Rexonikoff. Lead poisoning. Medicine 4, 1-250 (1925).

13. R. F. Sognnaes, J. H. Shaw and R. Bogoroch. Radiotracer studies on bone, cementum, dentin and enamel of Rhesus monkeys. Am. J. Physiol. 180, 408-420 (1955).

LOCAL DISTRIBUTION AND RETENTION OF RADIUM IN MAN*

R. E. Rowland**

The distribution and retention of radium in bone are governed by the metabolism of bone itself. If we understand the mineral phase of bone, its formation, exchangeability, and removal, we are well on the way to an understanding of the behavior of radium in bone.

The terminal distribution of radium in human bone serves to illustrate several phases of bone metabolism. In order to understand the terminal picture, we must first review the initial processes by which radium was deposited in bone.

The Deposition of Radium in Bone

The first step in the process is the behavior of radium in the blood. Following an intravenous injection of radium, the plasma concentration, initially high, continually falls with the passage of time. No studies have been made of the behavior of radium in human blood, but the process is undoubtedly similar in pattern to that which occurs in the dog. Figure 51 shows the relationship between the specific activity (ratio of radium to calcium) of the blood and the skeleton of the beagle. These curves were derived from the published data of Van Dilla et al.[1] They illustrate an extremely important point, namely, that the specific activity of the blood eventually drops below that of the skeleton, and continues to fall relative to the skeleton. Whether or not this process continues for as long as a human lifetime remains to be seen. However, as long as the total-body retention is adequately described by a power function, the blood plasma concentration should also be described by a power function, giving the type of behavior illustrated here.

All of the processes by which radium is transferred from the blood to the bone mineral, or transferred from bone mineral to the blood, are dependent upon the specific activity of the plasma and the mineral itself. For example, in the process of new bone formation, radium is incorporated in the newly-formed mineral at the same concentration (radium to calcium) as it exists in the blood.[2] Thus, bone mineral formed the day of the injection contains more radium than subsequently formed mineral. The intense

---

*Presented at IAEA Scientific Meeting on the Diagnosis and Treatment of Radioactive Poisoning, Vienna. October 15-19, 1962.

**Present Address: Department of Radiation Biology, School of Medicine and Dentistry, University of Rochester, Rochester, New York.

radium deposits produced by this prompt incorporation of radium into the mineral have been termed "hotspots." This process is the same a week, month, or year after the radium injection, but the specific activity of the newly-formed mineral is dependent upon the time after injection that it was formed.

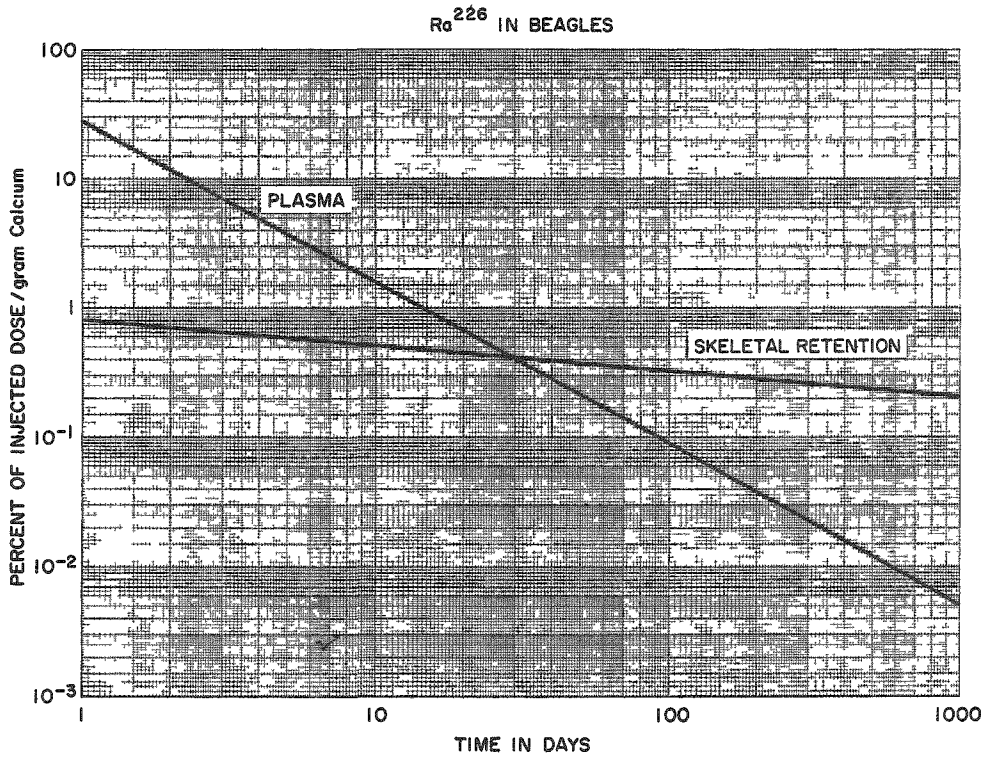

Figure 51

The specific activity of the blood plasma and the skeleton of beagles as a function of time. These curves were derived from the published data of Van Dilla et al.[1] They were obtained by expressing the retention and the plasma concentration data in the same units, per cent of injected dose per gram calcium. The radium was assumed to be entirely in the skeleton, and the skeleton was considered to contain 100 grams of calcium. The plasma data were transformed by assuming 10 mg of calcium per 100 mg of plasma.

The hotspots formed following a single injection of radium differ from those observed in human radium cases, for the latter were usually exposed to radium for a considerable length of time. In a forming osteon, a single radium injection will show as a ring of alpha tracks, corresponding to the bone formed soon after the injection. Extended exposure, to medical administration or oral ingestion, will produce wide bands of radium-labeled bone and completely labeled osteons, such as is shown in Figure 52.

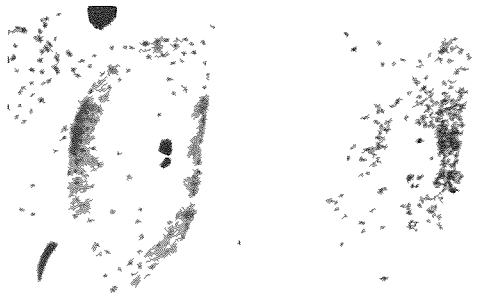

Figure 52

A micoradiograph and a stripping-film autoradiograph of a single osteon completely labeled with radium. It is from one of the Elgin State Hospital cases (03-118) who had received 41 weekly injections of Ra^{226}. The bone section is 100 microns thick; the autoradiograph was exposed for 55 days.

While the specific activity of the blood plasma is higher than that of the skeleton, any processes that transfer calcium-like atoms from the blood to the existing mineral must result in the deposit of radium in the bone mineral. Such processes, often called exchange processes, are of considerable importance in distributing radium throughout the skeleton. At short times after radium administration, the pattern of exchange-deposited radium continually changes; such early changes have been described and illustrated by Lacroix.(3) It is important to recognize that all of the bone mineral reached by the circulating fluids acquires radium by these exchange processes.

When an autoradiograph is made of a radium-labeled bone, essentially all of the mineral is seen to contain radium. A gross autoradiograph of the radium in a human femur is shown in Figure 53. This bone section is from a woman who had painted watch dials for a two-year period 35 years before her death. The hotspots here have been overexposed in order to show the diffuse distribution; this term has been applied to the distribution of the radium throughout the bulk of the bone mineral.

Figure 53

A microradiograph and an autoradiograph of a complete cross section from the femur of a radium-dial painter (Code 03-407). This woman tipped her brush in her mouth for a two-year period when she was 19 to 21 years old. The sample was obtained at death 35 years later. The body burden was 1.45 μc; the autoradiograph was exposed for 1 year on an Eastman Kodak autoradiographic Type A plate.

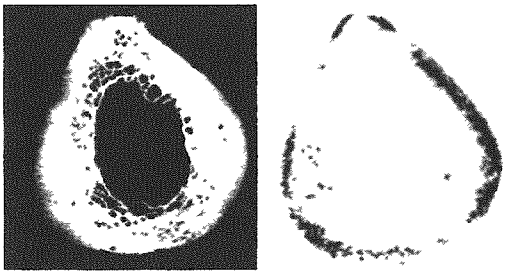

While exchange processes probably account for most of the diffuse distribution in bone, it is important to realize that other processes also can label bone so that the radium is indistinguishable in magnitude from the exchange deposits. For example, as was pointed out above, new bone formation, if it takes place when the blood has fallen to the appropriate specific activity, will result in a radium deposition equivalent to the diffuse distribution.

Another process by which bone acquires radium is termed secondary mineralization. When an osteon is first formed, its mineral density is low. With the passage of time, of the order of months or even years, the mineral density increases. This addition of mineral to a previously-formed structure will result in the incorporation of radium into the structure if the secondary mineralization process takes place while the blood plasma specific activity is elevated.

A year or so after the exposure to radium has terminated, all of the bone in the body will be labeled. Hotspots will indicate the new bone growth that took place during the exposure period, while exchange, secondary mineralization, and new bone formation together will have deposited radium in all the remaining mineral. By this time the short-term exchange deposits will have disappeared; the isotope remaining will be relatively well fixed within the skeleton.

The Removal of Radium from the Skeleton

What processes can now remove radium from the skeleton? Obviously resorption of bone, by osteoclasts, will remove the mineral and hence the radium. Is this the only process by which radium can be removed?

Let us recall that the retention, R, of radium has been described by a power function of the form[4]

$$R_t = 0.54t^{-0.52}$$

A power function gives a straight line when plotted on log-log paper, but if we consider the loss of radium from the skeleton in equal time increments, the loss decreases with the passage of time. For example, of the radium in the body one year after an I.V. injection, 31% will be lost during the subsequent year. During the next year, the loss will be only 18% of the amount present at the start of the year. Similarly, between the 5th and 6th year, 15% will be lost, between the 10th and 11th year 5%, and between the 20th and 21st year, 2.8% will be lost. Could resorption account for this decreasing rate of loss?

It could if the resorption process were age dependent, so that decreasing resorption rates could be expected with increasing age. However, we must first recall that, with the limited data available, the power function is essentially age independent. Also, according to the work of Jowsey,[5] resorption rates seem to stay constant through early adulthood, then increase with advancing age. Thus, we conclude that the power function could not result from changes in the rate of bone resorption.

With a constant rate of resorption, perhaps the decreasing rate of loss of radium is due to the fact that there is little radium left to resorb

after the first few years, so that most of the resorption process does not remove radium-labeled bone. If this were the correct interpretation, the observed retention would be described by an exponential rather than a power function. However, an even more convincing argument is visible in Figure 53. Recall that this is the radium distribution remaining many years after acquisition; it is obvious that very little radium has been removed from this section by resorption. This picture, incidentally, is typical of most autoradiographs of radium bones many years after acquisition. It is evident, then, that very little of the labeled bone has been removed by resorption.

How, then, is radium released from bone? If resorption is relegated to a minor role in the removal process, what other mechanism is left? The answer lies in the diffuse distribution. The radium was acquired by all the mineral of the skeleton by some kind of exchange process. If bone can acquire this isotope by exchange, surely it can lose it by the same process. When we speak of exchange processes, it is natural to think of fairly rapid processes. Such processes exist; there are highly labile regions that quickly acquire radium or other alkaline earth isotopes. However, these labile regions also lose these isotopes rather quickly. In the long-term picture we are interested, not in these short-term processes, but rather in processes with relatively long time constants.

It has been shown in the dog[2] that the specific activity of radium concentrations in both hotspots and the diffuse distribution decrease in magnitude during the first year following incorporation of radium into bone. While this direct measurement describes the behavior of radium in canine bone at relatively short times after incorporation, there exists another argument which lends weight to this mechanism.

It is known that the diffuse distribution constitutes a sizeable fraction of the total skeletal content. Measurements have shown that the average skeletal radium concentration (total radium divided by total skeletal mass) is only twice as great as the average diffuse level in terminal radium cases.[6] Likewise, in the dog the diffuse level was also observed to be about half the average skeletal concentration a few years after the administration. Generalizing from these observations, we conclude that the magnitude of the diffuse distribution is closely related to the total skeletal content. Thus the diffuse level must drop in magnitude in a fashion similar to the total body content.

Release of radium from the skeleton is, thus, governed by two processes, resorption and exchange. The resorption process removes discrete volumes of bone and liberates the radium therein to the blood stream, while exchange processes remove radium and calcium from all of the mineral of the skeleton. The former thus leaves a clear mark, at least if new bone replaces the resorbed volume, for if the plasma concentration of radium has

fallen as postulated, the replacement mineral is relatively radium free. Exchange, however, leaves no record of its removal of radium; it can only be deduced to have occurred from the retention and skeletal distribution data.

Microscopic Distribution of Radium in Bone

Having discussed the mechanisms of uptake and release of this element from the skeleton, now let us turn our attention to the microscopic distribution of radium as it exists terminally. For such studies we depend upon microradiographs of the bone sections, stripping-film autoradiographs, and the quantitative analysis of alpha-track plates.

Quantitative evaluation of the radium concentrations in bone provides a powerful tool for the unraveling of the metabolic processes at work in bone. Complete details of the transformation from alpha-track counts into radium concentrations will be found in a previous publication;[6] it suffices here to state that hotspots and diffuse distributions can be evaluated from the track counts. A brief list of some measured value is shown in Table 29.

Table 29

Some typical measured radium concentrations

Patient	Terminal radium burden, μc	Average skeletal concentration, pc/mg	Method of acquisition	Maximum hotspot, pc/mg	Average diffuse, pc/mg	Ratio: hotspot to diffuse	Ratio: diffuse to average conc.
03-996	8	1.3	Dial painter	9	0.28	32	0.22
01-008	8	1.3	Dial painter	16	0.54	30	0.42
03-995	7	1.0	Dial painter	30	0.32	94	0.32
03-648	2.7	0.49	Dial painter	15	0.38	40	0.78
			The Elgin State Hospital Cases				
03-117	1.2	0.17	45 Number of weekly I.V. injections: 10 μc Ra^{226} each	12	0.080	150	0.47
03-118	3.6	0.66	41	16	0.15	107	0.23
03-109	0.8	0.15	18	13	0.060	218	0.40
03-119	0.6	0.12	7	14	0.054	263	0.45

The first finding of importance from radium cases relates to the diffuse distribution. The comparison between the diffuse level and the total radium content of the skeleton is best made by calculating the radium concentration in bone that would exist if all the skeletal radium were uniformly distributed throughout the bone. This uniform label, or average skeletal concentration, is obtained by dividing the total radium content by the bone mass; bone mass has been assumed to be 7,000 grams for a 70-kg man, or 10% of the body weight, if the latter were accurately known. It was surprising to find, as has been mentioned above, that the diffuse level was

approximately one-half of the uniform label. While these measurements were made on cortical bone, all trabecular bone studied to date shows the same diffuse labeling in non-hotspot areas. These observations thus indicate the importance and magnitude of the diffuse distribution in bone.

Another significant parameter calculated from the quantitative measurements is the hotspot-to-diffuse ratio. The ratio has been observed to range from a low of 16 to a high of over 250; its magnitude is related to the length of exposure to radium. In order to be countable, a hotspot distribution must cover an area of bone the dimensions of which are about three times the length of an alpha-track range. Thus in an osteon the intense deposit must be 80 or 90 microns wide, corresponding in general to an exposure period of 6 to 10 weeks. The hotspot concentrations cannot be obtained from simple track counts for exposure periods shorter than this.

The Elgin State Hospital cases illustrate nicely the decreases in this ratio with increasing exposure times. In Table 29 these cases are listed separately; note that the ratio ranges from 263 for an eight-week exposure to 107 for the 41-week exposure. Note also that dial-painters have, in general, lower values of this ratio than do those medically exposed. This is a consequence of exposure time; medical administration was usually for a shorter time than industrial exposure.

The intensity of the hotspots in the Elgin State Hospital cases is of great usefulness in estimating radium intake rates for other cases. This group, who received weekly injections of 10 μc Ra^{226}, is seen (Table 29) to have hotspot concentrations of about 14 pc/mg bone terminally. Knowing that 10 μc per week produced 14 pc/mg bone (seen 25 to 30 years later), we can estimate the intake rate for any other measured terminal concentration, as long as we know the isotope was received intravenously.

It is apparent that these cases in which the quantity of radium administered and the route of administration are accurately known are of great value to us. As more information becomes available describing the discrimination against orally acquired radium, these Elgin cases will be of even more importance.

Before leaving the subject of quantitative evaluation of radium concentrations, it should be pointed out that while the diffuse distribution is related to the total body content, which in turn is dependent upon the total quantity of radium acquired, the hotspot concentrations are not related to the body content of radium. These concentrations depend only upon the rate at which this isotope was acquired. The concentration of radium in the blood during the time a bone volume was formed determines the ra ium concentration within that volume. This is illustrated by comparing hotspot concentrations found in two cases with widely different body contents, such as 01-008 and 03-119, in Table 29. Here the body burdens are 8 and 0.6 μc,

respectively, a difference greater than a factor of ten, while the hotspot concentrations are 9.0 and 14 pc/mg bone, respectively, with the higher concentration in the case with the lower body burden. Case 01-008 painted for over a year and acquired a considerable body content as a consequence, but the rate of intake (from orally acquired radium to the blood) never equaled the rate of intake experienced by case 03-119, 10 μc Ra^{226} per week, I.V., for 7 weeks.

Deductions from the Terminal Distribution

From observation of stripping-film autoradiographs and quantitative evaluation of alpha-track counts from terminal bone sections, a great deal of information can be obtained about the original exposure to radium. For example, the length of exposure can be estimated in two different ways. The first is the hotspot-to-diffuse ratio; comparison of the measured ratio with those obtained from the Elgin cases allows an estimate to be made of total exposure time. This can be verified to some extent by the stripping-film autoradiographs; for the width of the radium label in the hotspots is time dependent. Three months is required for the average human osteon to form; an exposure time less than this will leave the osteons partially labeled, while a much longer exposure will leave most osteons that were formed during this period fully labeled.

Age at the time of exposure can be inferred if growth in a given location can be correlated with age. An excellent example is the tooth; if dentin was being formed while the radium was acquired, a graphical history of the acquisition is visible in the autoradiographs of the dentin.(7)

An estimate of the total body content can be made, if it is not known, from the diffuse distribution. Since the diffuse distribution has been observed to be about one-half of the average skeletal concentration, the latter, and hence, the total body content, can be obtained from such a measurement. The uncertainty in this kind of estimate is about a factor of two, large, yet of considerable value if no other estimate is available.

Even the rate of acquisition can be inferred from these studies; for this we recall that the Elgin cases had hotspot concentrations, terminally, of about 14 pc/mg bone. Since they received 10 μc Ra^{226} per week intravenously, any observed hotspot concentration can be expressed in terms of an intravenous input rate. To obtain an estimate in the case of ingested radium, it is necessary to know the magnitude of the discrimination against radium in the absorption process. Estimates of this factor vary from 4 to 10 for man. Thus the 30-pc/mg hotspots observed in Case 03-995 suggest that this dial-painter ingested from 80 to 200 μc of Ra^{226} per week while painting.

Figure 54 will be employed to demonstrate a case in which the value of the detailed terminal measurements is readily apparent. This shows a gross autoradiograph of the radium distribution in the bone of a patient with a relatively low burden, 0.4 μc Ra^{226}. This woman had a bone tumor, and thus, this is one of the lowest pure Ra^{226} burdens known to have produced a tumor. The distribution of radium within the bone section is seen to be very unusual, for only a portion of the mineral is heavily labeled. The diffuse level in the intensely labeled portion of the bone is characteristic of a total content of 2.4 μc, not 0.4 μc as measured. Evidently considerable resorption and replacement of bone has taken place, with the result that most of the bone present when the radium was acquired has been removed. Examination of the stripping-film autoradiographs leads to the conclusion that the radium was acquired over a short time interval, for the hotspot osteons are not fully labeled but rather contain narrow rings of alpha tracks. This conclusion is supported by the hotspot-to-diffuse ratio of 180, characteristic of about a 12-week exposure. The hotspot concentrations are three times as intense as found in the Elgin cases, suggesting 30 μc Ra^{226} per week if it was obtained intravenously.

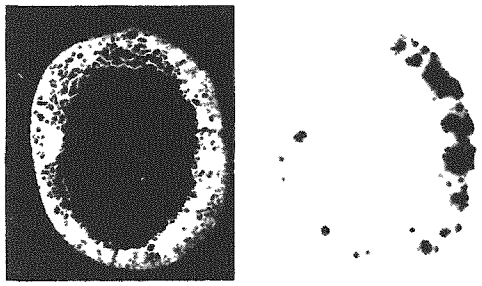

Figure 54

A microradiograph and an autoradiograph of a cross section of the femur from Case 03-216. The microradiograph indicates a rather porotic bone, yet in many locations where bone is present very little darkening can be observed on the autoradiograph. This kind of a distribution has not been seen previously; it may be interpreted as having had most of the radium-labeled bone removed by remodeling, or as indicating that some portions of the bone did not originally acquire radium at the same rate as other portions.

From these observations we conclude that this woman, with no record of industrial exposure, received her radium medically, probably via the intravenous route. She received about 360 μc of Ra^{226} over a 12-week period probably no later than the middle or late 1920's, at least 30 years before her death. The normal rate of loss, i.e., the power function prediction, would leave about 1.6 μc after 30 years. This quantity is certainly within the carcinogenic range. Thus the detailed study of the radium distribution has changed the basic question in this case from one concerning unexpected toxicity to one concerning an unusually large clearance of the radium.

Conclusion

The skeleton is known to be the site of deposition of many radioelements when they are introduced into the mammalian body. However, it is evident that it is not sufficient to characterize a radioactive body burden

by describing the total content of the skeleton. As we inquire into the details of the skeletal distribution, it becomes apparent, at least in the case of the alkaline-earth radioelements, that bone metabolism itself must be understood before one can hope to relate such concepts as radiation dose and the resulting damage.

We have seen that the terminal distribution of radium within the human skeleton bears an intimate relationship to both the original distribution and the metabolic processes at work in bone during the period this isotope was carried. It has also been shown that from the terminal distribution considerable information can be obtained about the acquisition of radium. The importance of such information should not be underestimated, for it may hold the key to otherwise inexplicable differences between the terminal body content and the observed toxicity of the alkaline-earth radioisotopes.

References

1. M. A. Van Dilla, B. J. Stover, R. L. Floyd, D. R. Atherton and D. H. Taysum. Radium (Ra^{226}) and radon (Em^{222}) metabolism in dogs. Radiation Res. 8, 417-437 (1958).

2. R. E. Rowland. Microscopic metabolism of Ra^{226} in canine bone and its bearing on the radiation dosimetry of internally deposited alkaline earths. Radiation Res. 15, 126-137 (1961).

3. P. Lacroix. Autoradiographic study of bone with Ca^{45}, In Radioisotopes and Bone, ed. P. Lacroix and A. Budy. Davis, Philadelphia, 1962. pp. 51-66.

4. W. P. Norris, T. W. Speckman and P. F. Gustafson. Studies of the metabolism of radium in man. Am. J. Roentgenol. 73, 785-802 (1955).

5. J. Jowsey. Age changes in human bone. Clinical Orthopoedics 17, 210-217 (1960).

6. R. E. Rowland and J. H. Marshall. Radium in human bone: The dose in microscopic volumes of bone. Radiation Res. 11, 299-313 (1959).

7. R. E. Rowland. Radium in human teeth: A quantitative autoradiographic study. Arch.Oral Biol., in press and this report, p 116.

HIGH-RESOLUTION AUTORADIOGRAPHIC AND MICRORADIOGRAPHIC STUDIES OF BONE AND TEETH FROM HUMAN RADIUM CASES*

R. E. Rowland**

Abstract

Radium burdened individuals constitute the only large group who have carried a radioactive contaminant internally for long times. While these cases have been extensively studied in recent years, the only method by which their radium insult can be expressed is in terms of their body content today, rather than in terms of the quantity of radium acquired.

This shortcoming can be alleviated in part with the information that can be developed from quantitative autoradiographic studies of the microscopic distributions of radium in bone and teeth. These studies yield information on the rate of intake of radium during the period of exposure, and in some cases on the length of time the individual was exposed to radium; under ideal conditions even the age at which the isotope was acquired can be estimated. It is felt that the autoradiographic and microradiographic studies are of considerable value in determining the toxicity of internally deposited radium; their relevance in the determination of permissible levels is discussed.

* Presented at X International Congress of Radiology, Montreal, August 26 - September 1, 1962.

** Present address: Department of Radiation Biology, School of Medicine and Dentistry, University of Rochester, Rochester, N. Y.

SKELETAL RETENTION OF THE ALKALINE EARTH RADIOISOTOPES AND BONE DOSIMETRY*

R. E. Rowland**

In order to evaluate the dose delivered to bone tissue by internally-deposited radioisotopes of the alkaline earth family, it is necessary to understand the mechanisms that release these isotopes from bone. It has been postulated that processes other than direct resorption of bone mineral must be of importance in the over-all removal of these isotopes from bone, particularly in the adult animal.[1,2] The purpose of this report is to describe the experimental studies that have shown the validity of this assumption and to indicate how the results may be applied to the problems of dosimetry.

In order to avoid semantic difficulties, it is necessary to define a few of the terms that will be employed. The first of these is resorption. By resorption is meant the process by which a distinct volume of bone mineral and matrix is removed from bone. Often, but not necessarily, this process is followed by the apposition of new bone; the process of new bone formation which results in an increase of mineral volume. It is these two processes that are referred to when the general term, bone turnover, is employed. In contrast to the above terms, exchange processes are those which do not involve changes in mineral volume. By exchange is meant any process involving equal and opposite rates of transfer of atoms to and from a single microscopic volume of bone mineral.

When we consider the dosimetry of the alkaline earth isotopes in bone, the nuclear characteristics of each, such as the physical half-life, type of decay, and the energy of the emitted radiation, are of paramount importance. However, there exist basic similarities between the members of this chemical family when they are deposited in bone. The work of the Radiobiological Laboratory at the University of Utah has demonstrated the similarity of the retention of Sr^{90} and Ra^{226} in beagles,[3,4] while other laboratories have shown that in this species Ca^{45} and Ba^{133} are also retained in a similar manner.[5] The retention of all, in the adult beagle, can be described by a power function of the form

$$R_t = at^b \quad ,$$

---

* Presented at University of Utah, College of Medicine, Symposium on Some Aspects of Internal Irradiation, Heber, Utah, May 8-11, 1961. Pergamon Press, Oxford, 1962 pp. 455-469.

** Present address: Department of Radiation Biology, School of Medicine and Dentistry, University of Rochester, Rochester, New York.

where R_t is the fractional retention at any time t (in days) after an intravenous injection of one of these isotopes, a is the fractional retention at one day, and b has a value close to -0.2. While the emphasis hereafter will be on the similarities of these radioisotopes in bone, and as a consequence they will all be considered together, it must not be forgotten that the actual dosimetric patterns that result from these isotopes are vastly different. When the term isotope is subsequently used, it will refer to a radioisotope of one of the above mentioned elements, and will indicate an application where apparently identical results would be obtained with any of the above mentioned tracers.

In Figure 55 is illustrated a practical problem in dosimetry. Here is an autoradiograph, with an accompanying microradiograph, of the distal end of the tibia of a 16-month old beagle.* The isotope is Sr^{90}, acquired orally; feeding started in utero and continued to 450 days of age, at a constant rate of Sr^{90} per gram of calcium. The dog was sacrificed 21 days after the Sr^{90} was discontinued.

If this animal had lived for several years after the Sr^{90} feeding had been stopped, the total accumulated dose or the dose rate at a given time to a specific volume of tissue might well represent a problem for the radiobiologist to solve. Before such a calculation can be made, the mechanism of removal of the isotopes from bone must be known.

If resorption were the only process that could release an isotope from bone, then, with the passage of time, autoradiographs of bones such as this one would be identical in photographic density, but lighter patches would be present, corresponding to locations in which resorption had occurred. The important point is that, wherever original bone remained, the specific activity of the isotope in the bone mineral would be unchanged.

On the other hand, if exchange alone were responsible for the loss of the isotope, then subsequent autoradiographs would be identical to this one, but they would require longer exposures to produce the same autoradiographic darkening. That is, the specific activity of the isotope in the bone mineral would have decreased with the passage of time.

The concept that isotopes may be lost from bone by exchange processes is not new; indeed, most workers have realized that the diffuse uptake of an isotope into pre-existing bone could not indicate a net transfer of mineral into these regions. This distribution itself, and in particular, the quantitative studies of its magnitude which indicated that it represents about one half of the total skeletal content of a deposited isotope,[6,7] have given a clear indication of the significance of exchange processes in the deposition and retention of isotopes in the skeleton.

---

*Dog 5S3, from AEC Project No. 6, School of Veterinary Medicine, University of California, Davis.

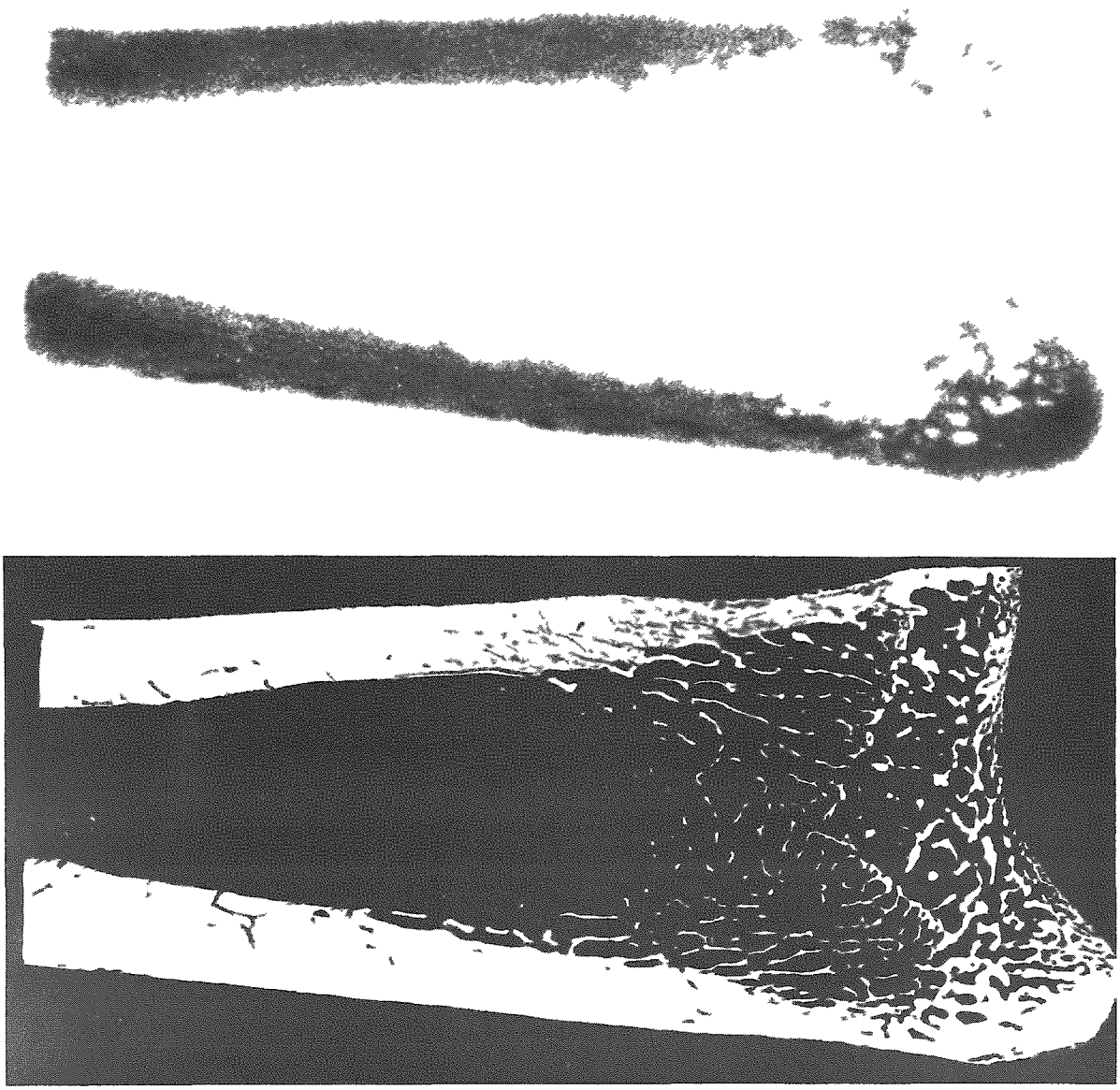

Figure 55

A microradiograph and an autoradiograph of a longitudinal section cut through the distal end of the tibia of a dog which had been fed a constant ratio of Sr^{90}/g Ca. Feeding of the isotope started in utero and continued until the dog was 450 days old, the animal was sacrificed 21 days after Sr^{90} was removed from the diet.

Less is known regarding the retention of these isotopes after they have been fixed in the skeleton by the process of new mineral formation. Turning our attention again to Figure 55, it should be noted that, while this autoradiograph illustrates a uniform distribution of the isotope throughout the bone mineral, much like a diffuse distribution produced in bone by exchange, actually the isotope was originally incorporated everywhere by the process of new mineral formation. Thus, for the case in question, we need to know how isotopes deposited by growth processes are removed from bone.

A study has been made to determine the processes by which isotopes, deposited in bone by either exchange or growth, are removed with the passage of time. Since this work will be reported in full elsewhere,(8) it will simply be briefly summarized here.

An adult dog was given equal injections of Ra^{226} once a week for a period of eight weeks. Four weeks after the last injection a front limb was removed by amputation; one year later the dog was sacrificed. Quantitative autoradiographs were made from the bone sections in order to compare the Ra^{226} at amputation to that existing at time of sacrifice. This study was designed so that a comparison of the specific activity of the tracer (Ra^{226}) in two distributions, the regions of exchange and the regions of growth, could be made at two different times. The results indicated that, over the one-year interval, the specific activity decreased in both distributions.

The amount of the decrease is quite significant, and can best be compared with the decrease in the total skeletal burden of the dog. The actual content of the dog was not determined, but the power law retention formula indicated that the Ra^{226} content at sacrifice (ignoring the missing limb) would have been 66% of the content at the time of amputation. However, a comparison between two bones (the radii) was made, which indicated that the one removed at sacrifice contained 74 ± 5% as much Ra^{226} per gram as the one removed by amputation. The autoradiograph study showed that the autoradiographic hotspots (which correspond to areas of appositional bone growth) decreased over this time interval to 66 ± 12% of their original level, and that the diffuse (exchange labeled bone) decreased to 75 ± 15% of the original level.

The fact that the diffuse distribution did not lose as much activity as the hotspots does not imply that the exchange rate is lower for this distribution. The explanation lies in the magnitude of the blood specific activity. At the time of amputation the specific activity (Ra^{226}/g Ca) in the diffuse distribution was less than the specific activity (Ra^{226}/g Ca) of the blood, so that exchange between blood and bone would still be increasing the diffuse concentration. Exchange would not be expected to decrease the diffuse level until the activity in the blood had dropped below the level in the bone; this did not occur until two months after the amputation. Thus, even with equal exchange rates, we would expect to find less loss from the diffuse distribution in this particular study.

Perhaps the most significant finding from this work has been, not simply that both distributions lost activity by exchange processes, but rather, the magnitude of the losses. These observed losses (exchange losses) were large enough to account for almost all of the loss of activity from this dog, thus implying that bone resorption must play only a small role in the removal of these isotopes from the skeleton.

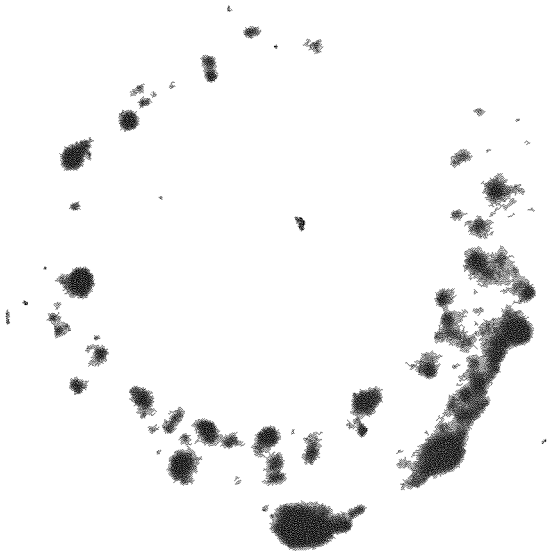

Figure 56

An autoradiograph of a 100-μ-thick section cut from the femur of a dog which had received a single injection of mixed Sr^{87} and Sr^{90} as an adult 10-1/2 years before death.

Yet, on further consideration, this is not a surprising result, for studies on the distribution of isotopes in bone at long times after injection have indicated that no great amount of resorption has taken place. Consider the autoradiograph shown in Figure 56; this is from a 100-μ-thick section from the femur of a dog that carried Sr^{90} for $10\frac{1}{2}$ years after receiving, as an adult, a single injection of mixed Sr^{89} and Sr^{90}.* It can be seen, from the uniformity of the autoradiograph, that little bone turnover has taken place after the isotope was deposited.

From the studies on the radium-dial painters we are familiar with the fact that autoradiographs of bone sections from these individuals show little evidence of bone turnover. Figure 57 illustrates the maximum turnover, as indicated by autoradiographic analysis, that has been seen

Figure 57

An autoradiograph of a 100-μ-thick section cut from the humerus of a radium-dial painter who had acquired mixed Ra^{226} and Ra^{228} as the result of a two-year exposure 41 years before death. The diffuse distribution here indicates that extensive bone turnover has taken place. The section is not markedly osteoporotic; i.e., bone exists in all of the locations where little autoradiographic darkening is seen.

*Bone from dog QA142 was kindly supplied by Dr. M. Finkel. This animal was given mixed Sr^{89} and Sr^{90} on 2/22/1946, as part of a program of toxicity studies carried on by the Biological and Medical Research Division of Argonne National Laboratory.

in our studies on human cases at Argonne. This autoradiograph is from a 100-μ-thick bone section from the humerus of a 57-year-old dial-painter who had painted for a two-year period 41 years before death. Considerable non-uniformity is visible in this autoradiograph, indicating regions where turnover has occurred, yet the turnover rate could not have been more than about 2 or 3% per year to leave as much unaltered bone as is visible here.

Let us now turn our attention to the dosimetric implication of these results Both distributions, exchange and appositional growth, have been shown to lose activity with time, but can we characterize the time rate of loss? A clue is given by the observations that have indicated that the magnitude of the diffuse distribution is related to the total skeletal content of an isotope. Such observations have been made in dogs, from a few weeks to several years after the isotope was acquired, and in human radium cases, at observation times of twenty to forty years.(7) Hence it is suggested that the loss of activity from this (diffuse) distribution can be described by a function of the same form that describes the total retention, which in the case of beagles is a power function with an exponent of about -0.2. Although it is not conclusively proved by our data, it seems reasonable to assign a similar rate of loss to the hotspots, i.e., the regions in which the isotope has been deposited by growth.

Thus, from a terminal autoradiograph from which the quantity of an isotope per unit mass of bone in specific regions has been determined, it is possible to calculate the concentration of the isotope that existed in that location at any previous time. While the ability to make such a calculation is not necessary for studies in which the isotope has been in bone for only a short time, it does become important for those cases in which the isotope has been in bone for many years. Consider for example the autoradiograph of Figure 56· the concentration of isotope per gram of bone that must have existed one month after the injection would have been 2.7 times as great as observed terminally. The case illustrated in Figure 57, at the end of the two-year period of exposure as a dial-painter, would have contained about 4.5 times as much radium per unit volume of bone than is indicated by its autoradiograph if the loss of radium from humans is described by the function(9)

$$R_t = 0.54\, t^{-0.52} \quad .$$

The dose delivered to a volume of tissue from a concentration of an isotope in a microscopic volume of bone is described by a function of the form

$$\frac{dD}{dt} = K\, q_t \quad .$$

Here the dose rate, dD/dt, is in rads per day; K is an appropriate constant, and q_t is the observed concentration (μc/g bone) in the bone

mineral at the time of observation. The total accumulated dose to the tissue in question over the entire time interval the isotope has been in the bone is then

$$D = \int_0^{t_s} K\, q_t\, dt$$

where t_s (in days) is the time interval between the acquisition of the isotope and the observation of the bone section.

If this expression is evaluated on the basis that exchange losses do not occur, so that the concentration (q_t) of the isotope in bone decreases only as the result of radioactive decay, then

$$D = \int_0^{t_s} K\, q_0\, (e^{-\lambda t})\, dt \quad .$$

Here q_0 is the original concentration of the isotope in bone, and λ is the decay constant of the isotope in question. Integration of this expression yields

$$D = K\, q_0\, \frac{1 - e^{-\lambda t_s}}{\lambda} \quad .$$

If the half-life is so long that decay need not be considered, this reduces to

$$D = K\, q_0\, t_s \quad .$$

When we allow the original concentration of the isotope in bone to decrease by both decay and exchange losses, and if exchange losses are postulated to follow a power law, such that

$$q_t = q_0\, t^b\, e^{-\lambda t}$$

then

$$D = \int_0^{t_s} K\, q_0\, t^b\, e^{-\lambda t}\, dt \quad .$$

This integration yields

$$D = K\, q_0\, \frac{\Gamma_{\lambda t}\,(b+1)}{\lambda^{b+1}}$$

where $\Gamma_{\lambda t}\,(b+1)$ is the incomplete gamma function. For the case when the half-life is very long, this expression becomes

$$D = K\, q_0\, \frac{t_s^{b+1}}{b+1} \quad .$$

Since, when evaluating bone tissue dose, the actual concentration seen is a terminal one, these equations are most logically compared with each other in terms of the terminal concentration, q_t, of the isotope.

Case I: No loss by decay or exchange;

$$D = K\, q_t\, t_s \quad .$$

Case II: Loss by decay but not by exchange;

$$D = K\, q_t\, \frac{1 - e^{-\lambda t_s}}{\lambda_e^{-\lambda t_s}} \quad .$$

Case III: Loss by exchange but not by decay;

$$D = K\, q_t\, \frac{t_s}{b + 1} \quad .$$

Case IV: Loss by both exchange and decay;

$$D = K\, q_t\, \frac{\Gamma_{\lambda t}\,(b+1)}{t_s^b \,.\, e^{-\lambda t_s} \,.\, \lambda^{b+1}}$$

From a comparison of Cases I and III it can be seen that for a long-lived isotope, such as Ra^{226}, the accumulated dose, calculated from a terminal distribution, will be greater by a factor of $1/(b+1)$ when loss by exchange is considered than when it is ignored, independent of the time of observation. If $b = -0.5$, as appears to be the case for Ra^{226} in human beings,(9) the accumulated dose is a factor of two greater than the product of the terminal dose rate times the number of days the isotope was carried.

Table 30

Evaluation of the incomplete gamma function

b	t_s (years)	$\Gamma_{\lambda t}\,(b+1)$
-0.2	10	0.3662
	20	0.5769
	30	0.7245
-0.25	10	0.4209
	20	0.6432
	30	0.7940
-0.3	10	0.4865
	20	0.7205
	30	0.8752

In Table 30 the values of the incomplete gamma function have been tabulated for use with Sr^{90}. Three different values of the exponent b have been included in the calculations, to bracket the values obtained for this element in man and dog, and three different observation times included, to range from long-term dog studies to the potential human problem.

As a demonstration of the magnitude of the errors that would be introduced in the calculation of accumulated dose to a bone tissue volume as a consequence of the failure to consider loss of an isotope by exchange or by decay, a series of dose calculations are listed in Table 31, based on the isotope Sr^{90}. Here the calculations from an observed terminal concentration of Sr^{90} in bone are compared, when calculated by means of the four cases considered above. Observation times of 10, 20, and 30 years are employed, for three values of the exponent b, namely -0.2, -0.25, and -0.3. The results obtained by Case IV are assigned a value of unity in the table, and the values obtained by the alternative methods are expressed in terms of the value of Case IV.

Table 31

Comparison of the values of accumulated dose

b	t_s (years)	Case I	Case II	Case III	Case IV
-0.2	10	0.69	0 79	0.87	1.0
	20	0.60	0 78	0.75	1.0
	30	0.52	0.77	0.65	1.0
-0.25	10	0.65	0 74	0.87	1.0
	20	0.56	0 73	0.75	1.0
	30	0.48	0 72	0.64	1.0
-0.3	10	0 60	0 69	0.86	1.0
	20	0 52	0 68	0.74	1.0
	30	0 44	0 66	0.64	1 0

This compilation of values serves two purposes. First, it demonstrates, for Sr^{90}, that failure to consider loss by exchange can introduce errors which are of the same magnitude as the errors introduced by the failure to consider the loss by radioactive decay Second, it provides a method for the rapid calculation of total accumulated dose. For example, consider an observation of the terminal concentration of Sr^{90} in a dog which had carried the isotope for ten years A Case I calculation, which is simply the product of the terminal concentration and the number of days the isotope was carried, ignores both kinds of loss, decay and exchange. However, it is very easy to perform and if the appropriate exponent for exchange loss is assumed to be b = - 0 2 the value obtained is seen to be 69% of the value that would have been obtained by the rigorous approach of Case IV. Since the calculations involving the incomplete gamma function are quite involved, this comparative approach to the accumulative dose calculations is to be preferred

While the purpose of this presentation is to relate the problems of skeletal dosimetry to the mechanism of isotope release from bone, a comment about total-body retention appears to be in order. Obviously, the

loss by exchange of these isotopes from the skeleton must have a bearing on the manner in which the total body loses activity with time. Empirically it has been observed that the change in retention with time is well described by a power function. Perhaps it had better be stated that exchange losses from the skeleton are described by a power function, and that as long as this is the predominant removal process, the total retention can also be described by such a function. However, when losses by resorption become comparable in magnitude to losses by exchange, then the total retention should be expected to deviate from the power law.

When will this occur? Unfortunately, very few data on the rate of resorption are available. Our radium studies have indicated that resorption rates of the order of 1% per year were required to explain the uniformity of the autoradiographs of human bone sections.(10) Since, after resorption releases activity from bone, a certain fraction of this activity is redeposited, it is evident that the total release of an isotope by resorption will be less than the rate of resorption. It is of interest to note that, even after a burden time of 30 years, the release of Ra^{226} from the skeleton is predicted to be of the order of 1.5% per year; hence, unless metabolic disturbances were to increase the process of resorption, it appears that even then release by exchange is still the predominant removal process.

Conclusions

Alkaline earth isotopes are incorporated into bone by two processes, bone growth and exchange, and lost therefrom by two similar processes, bone resorption and exchange. In the adult animal (dog and man have been specifically studied), exchange processes are the predominant mechanism for the release of these isotopes.

Since these concepts imply that the concentration of an isotope everywhere in bone is decreasing in magnitude with time, the terminal concentration of activity does not characterize the concentration that was present in the identical location at previous time. It is suggested that these changes in concentration may be described by a power function. Calculations have been performed, based on this hypothesis, to indicate how the dose rate at any previous time, and also the total accumulated dose over the entire exposure, can be determined from a terminal observation of the dose to a particular volume of tissue.

References

1. R. E. Rowland, J. Jowsey, and J. H. Marshall. Structural changes in human bone containing Ra^{226}. Proc. Geneva Conf. on Peaceful Uses of Atomic Energy. United Nations, New York, 1958. Vol. 22, pp. 242-246.

2. J. H. Marshall, R. E. Rowland, and J. Jowsey. Microscopic metabolism of calcium in bone. V. The paradox of diffuse activity and long-term exchange. Radiation Res. 10, 258-270 (1959).

3. C. W. Mays, D. H. Taysum, and W. Fisher. Annual Progress Report, Radiobiological Laboratory, Coll. Med., Univ. of Utah (March 31, 1958). pp. 139-146.

4. M. A. Van Dilla, B. J. Stover, R. L. Floyd, D. R. Atherton, and D. H. Taysum. Radium (Ra^{226}) and radon (Rn^{222}) metabolism in dogs. Radiation Res. 8, 417-437 (1958).

5. R. E. Rowland. Argonne National Laboratory Radiological Physics Division Semiannual Report, July through December, 1959. ANL-6104, pp. 34-47.

6. J. S. Arnold, W. S. S. Jee, and K. Johnson. Observations and quantitative radioautographic studies of calcium-45 deposited in vivo in forming Haversian systems and old bone of rabbit. Am. J. Anat. 99, 291-313 (1956).

7. R. E. Rowland and J. H. Marshall. Radium in human bone: the dose in microscopic volumes of bone. Radiation Res. 11, 299-313 (1959).

8. R. E. Rowland. Microscopic metabolism of Ra^{226} in canine bone and its bearing upon the radiation dosimetry of internally deposited alkaline earths. Radiation Res., in press.

9. W. P. Norris, T. W. Speckman, and P. F. Gustafson. Studies of the metabolism of radium in man. Am. J. Roentgenol. 73, 785-802 (1955).

10. R. E. Rowland. Late observations of the distribution of radium in the human skeleton, In Radioisotopes in the Biosphere, ed. R. S. Caldecott and L. S. Snyder. University of Minnesota, Minneapolis, 1960. pp. 339-353.

THE EFFECTS OF ATMOSPHERIC STABILITY AND HORIZONTAL SHEAR ON THE ACCUMULATION AND DIFFUSION OF RADON

John E. Pearson* and Harry Moses

1. Introduction

Studies of the vertical and temporal distributions of natural atmospheric radon have been made in a previous test series at the Argonne National Laboratory.(1) These studies have resulted in new data on the natural radioactivity of the atmosphere and in an increased interest in the possibility of using radon data to indicate the behavior of materials released to the atmosphere from a ground area source.

As radon studies may provide a helpful approach to the problem of air pollution from an area source, it was decided to conduct an additional series of tests in conjunction with accurate measurements of wind and temperature profiles.

2. Experimental Equipment

Temperature, wind speed, and part of the radon measurements were made from various levels on a portable, triangular, aluminum tower which was 31.5 cm on a side and about 16.5 meters high (see Figure 58). Arms made from 3.81-cm outside diameter aluminum pipe supported the sensing devices (see Figure 59). Temperatures were measured and radon samples were collected at locations 122 cm from the tower. Wind speeds were measured at a distance of 167 cm from the tower. Sensing devices were located at the following six levels above the ground: 0.5, 1, 2, 4, 8, and 16 meters.

The ground around the tower (within 1,000 ft) is fairly level;(2) the slopes are gradual; elevation changes are limited to plus or minus seven ft, except for a steepening descent toward a ravine to the southeast (see Figure 60). The 1,000-ft circle is almost without trees; a small clump of 20-ft saplings stands in a shallow hollow about 125 ft to the north, and a line of similar trees runs down the slope to the southeast. In the southwesterly direction, the nearest trees, full grown oaks, are 1,200 to 1,400 ft away. The ground cover of coarse grass and weeds was mowed regularly and was 4 to 16 cm in height within 100 ft of the tower. At 300 ft to the west-southwest was the 150-ft meteorological tower of open steel-work construction and at about 600 ft to the west was the Meteorology Building, a gable-roofed structure, 14 ft high and about 30 ft wide as viewed from the tower.

*Resident Research Associate, Argonne National Laboratory, Summers of 1960 and 1961, and Professor of General Engineering, University of Illinois, Urbana, Illinois.

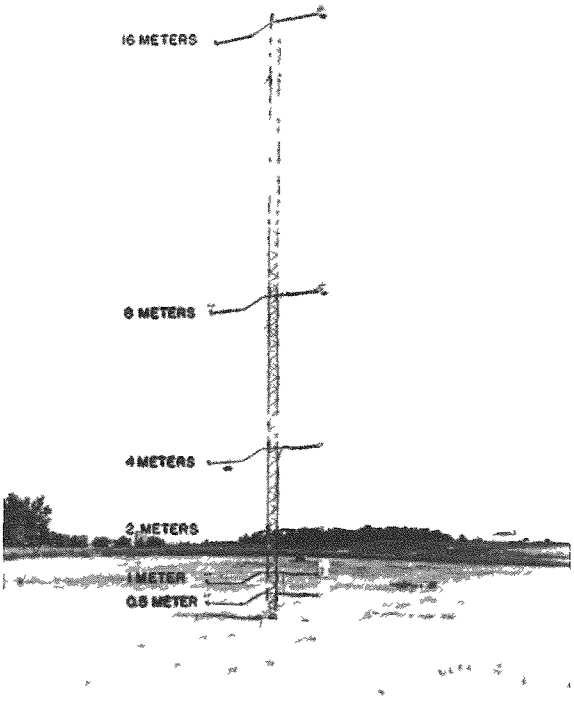

Figure 58

The 16-meter meteorology tower

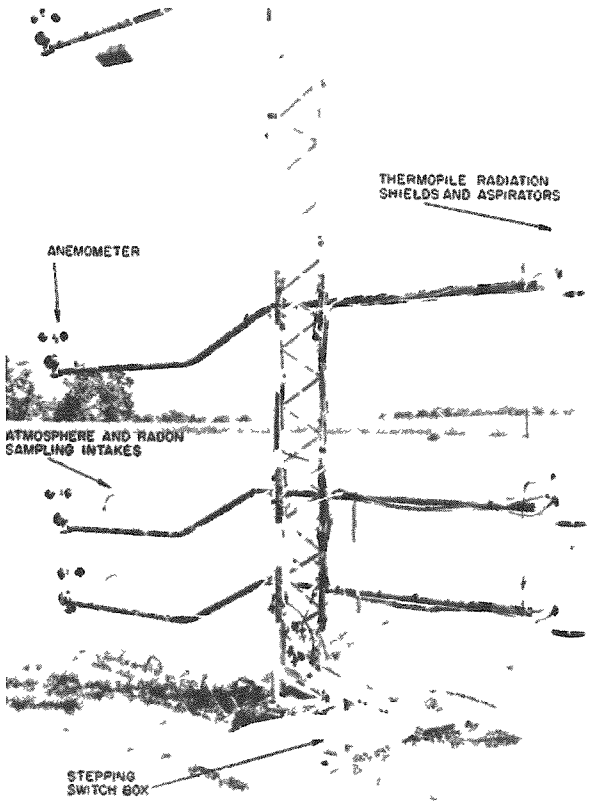

Figure 59

The instruments on the portable meteorology tower

Figure 60

The Argonne National Laboratory Meteorological Site and surrounding territory with contours

Scale 1" = 880 ft

Contours are at 5 ft intervals

the land slopes inward from that contour

ponds where the land slopes inward from the outer contour

a cemetery

8, 9, 16, 17 section number on the map

739, 743, 750, etc. elevations

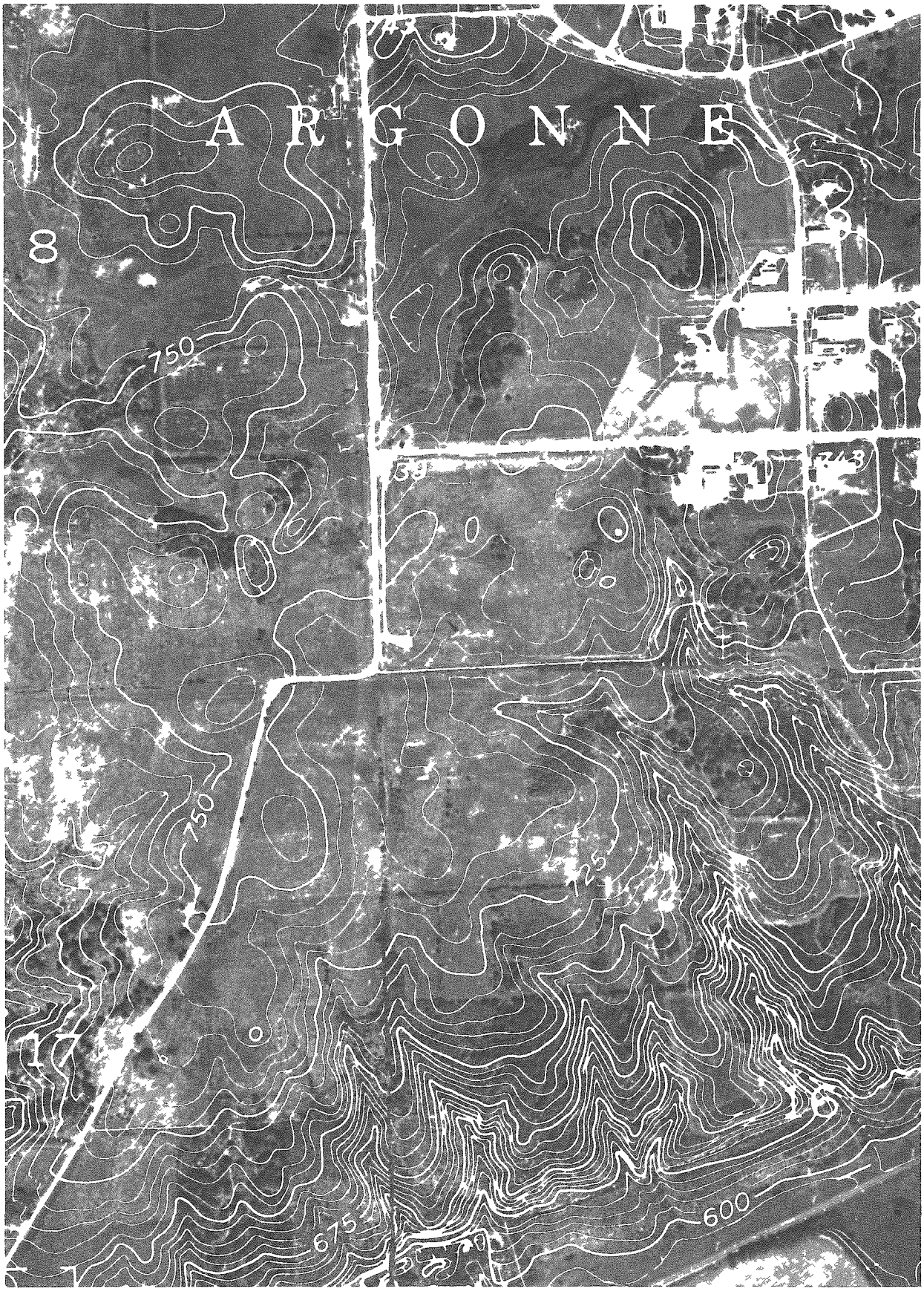
ARGONNE
8
750
675
600

Wind-speed measurements were made by individually-calibrated, cup anemometers manufactured by C. F. Cassela & Company, Ltd. of London (see Figure 59). Rotation of an anemometer cup opened and closed an electrical contact, and the total number of pulses for each counter was indicated on a register in the radon shed (see Figure 61). To check their performance, the six anemometers were mounted on poles at the same elevation above the ground. The poles were placed in a straight line approximately normal to the direction of wind flow. The positions of the anemometers on the poles were changed three times during the course of 17 twenty-minute tests. Wind velocities varied on the different tests from 4.2 to 8 meters per second. Velocities measured by the instruments were compared with the average velocity for each test. Individual values remained within one percent of the average values in 95 cases out of 102. Some of the variation may have been due to lack of uniformity of natural wind or to air-flow interference between the anemometers. For example, it was found that for all cases studied, the outside anemometers read slightly lower than those nearer to the center.

Temperatures between measurement levels at the tower were obtained with thermopile pairs mounted within two concentric, aspirated cylinders to protect them from the direct radiant energy of the sun or surroundings (see Figure 59). The thermopile pairs included twelve copper-constantan thermocouples made of #26 B & S gauge wire. Six junctions at the end of each pile were imbedded in paraffin located in the last two centimeters of closed Pyrex glass tubes 8-mm outside diameter and 5 cm long. All wire was contained in vinyl plastic tubing and tinned-copper braid shielding. The emf's of the thermopile pairs were scanned by a gold-plated stepping switch in a box in the ground at the base of the tower (see Figure 59). The switch was wired to scan as follows:

a) Pair #1 (8 to 16m)
b) Pair #2 (4 to 8m)
c) Pair #3 (2 to 4m)
d) Pair #4 (1 to 2m)
e) Pair #5 (0.5 to 1m)
f) Reference voltage (approx. 115 microvolts)
g) Pair #1 (8 to 16m)
h) Pair #2 (4 to 8m)
i) Pair #3 (2 to 4m)
j) Pair #4 (1 to 2m)
k) Pair #5 (0.5 to 1m)
l) Zero reference (short circuit)

Each of the 12 positions was scanned for 5 seconds for a total of 60 seconds per cycle. Thus two readings were made of each significant level every minute. Since each run was 20 minutes long, a total of 40 temperature-difference readings for each layer was obtained.

The output of the thermopiles was fed to a strip-chart recorder (Minneapolis-Honeywell Electronik potentiometer, one-half second full-scale response). The recorder was equipped to record zero input at the

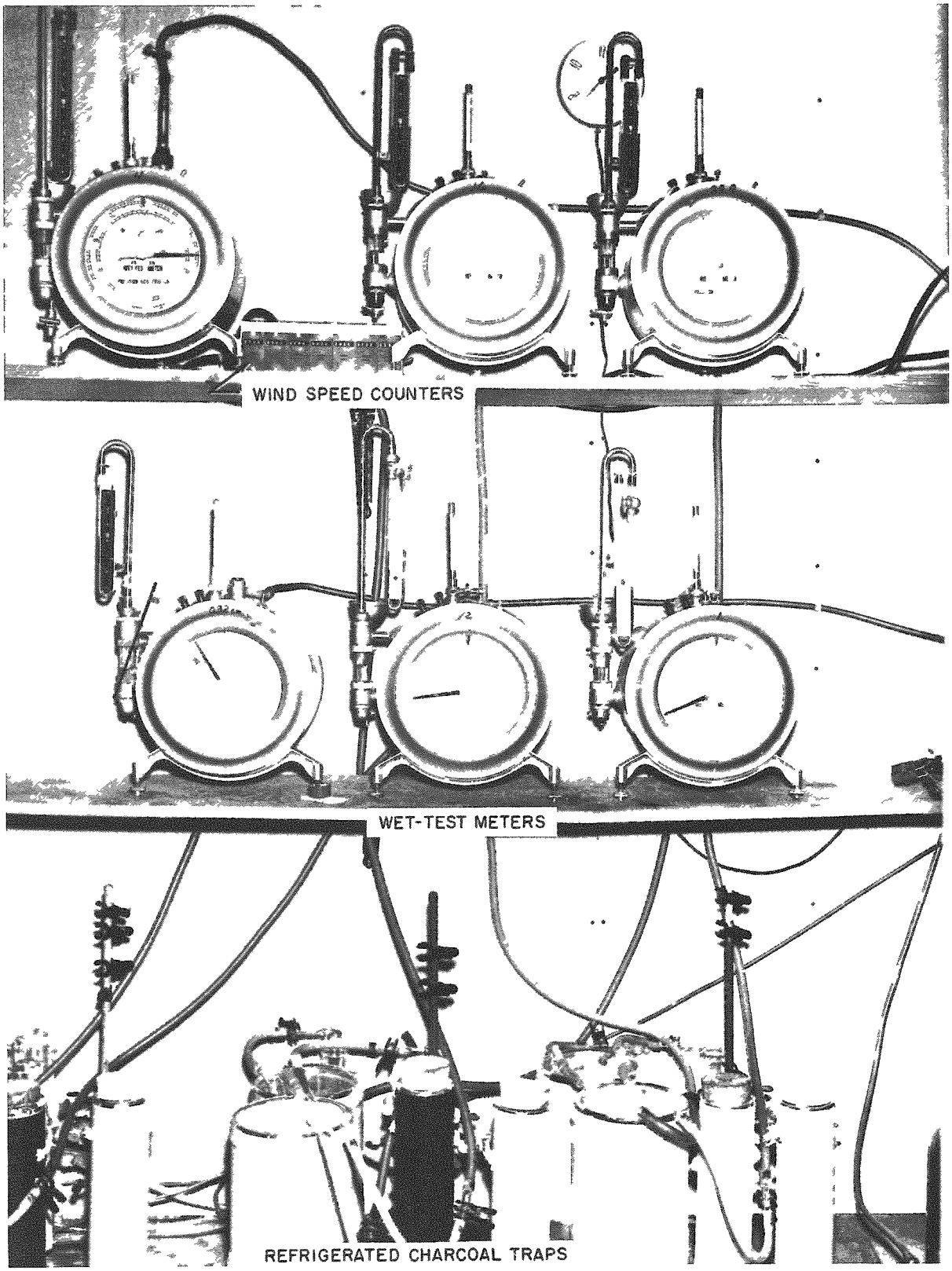

Figure 61

Field apparatus for measuring radon, showing wind-speed counters, wet-test meters and refrigerated charcoal traps.

center of the scale and plus or minus 500 microvolts at the chart edges. One microvolt corresponded to one chart unit. The recorder was further equipped with a Datex analog-to-digital converter which in turn fed a Datex-Monroe Data/Log for recording chart readings during the last second of each temperature-reading interval.

Calibrations of the thermopiles were made with water baths (E. H. Sargent & Co., constant temperature water baths). Bath temperatures were thermostatically controlled to within 0.01°C and were measured with Beckman differential thermometers. Bath temperatures were varied through the range of temperatures expected during operations (i.e., from 16 to 30°C). The calibration indicated the thermopiles were suitable for the experiment since 93% of the measurements obtained fell within 0.016°C of the National Bureau of Standards curves of emf vs. temperature for copper-constantan. The largest variation was 0.033°C.

Lag coefficients, time required for the temperature differences to be reduced to 1/e of their original value, for the thermopiles in water baths were determined. Coefficients were found for increasing and for decreasing temperatures. The variation in the worst case was 1.7 seconds. Lag coefficients reported below are based on average values for both increasing and decreasing temperatures:

Pair #1 - 15.2 seconds
Pair #2 - 13.6 "
Pair #3 - 15.5 "
Pair #4 - 13.0 "
Pair #5 - 12.0 "

In order to obtain data on the standard deviation of the wind direction, which are related to the atmospheric diffusion rate, a Gelman-Gill, fast-response bivane was mounted one meter above the ground in the vicinity of the tower and its motions were recorded on a pair of Esterline-Angus 0-1 milliampere recorders, one for azimuth and one for vertical angle.

Meteorological measurements regularly made by the Argonne Meteorology Group were available for this study. They included wind directions and speeds to 45.7 meters above the ground; temperature differences to 43.9 meters; dew points to 39.9 meters; soil temperatures to 8.84 meters below ground surface; atmospheric pressure; intensity of solar radiation; and net radiation flux. Equipment used to measure these variables has been described previously.[1,2]

For the present study radon and air mixtures were collected at 1 cm above the ground at the base of the portable tower, at 0.5, 1, 4, and 16m on the portable tower, and at 40m on the 150-ft meteorological tower. The

mixture was drawn in either Tygon or copper tubing of 8-mm diameter from the point of collection to a wooden enclosure housing various instruments used in this study. When copper tubing and Tygon were used side by side to compare diffusion of radon through the tubing walls, the results indicated no apparent difference.

Samples, collected at the various levels, were sucked through traps containing Drierite and Ascarite, to remove water vapor and CO_2, through two water traps cooled with dry ice, at approximately -78.5°C, and finally through dry-ice-cooled radon traps containing 7 grams of activated cocoanut charcoal (see Figure 62). Each level was provided with a pump ahead of a wet-test meter which operated at a small positive pressure (3.5 cm of water or less). The volume of air handled was measured with these wet-test meters manufactured by Precision Scientific Company, and in all cases the volume was corrected to standard temperature and pressure.

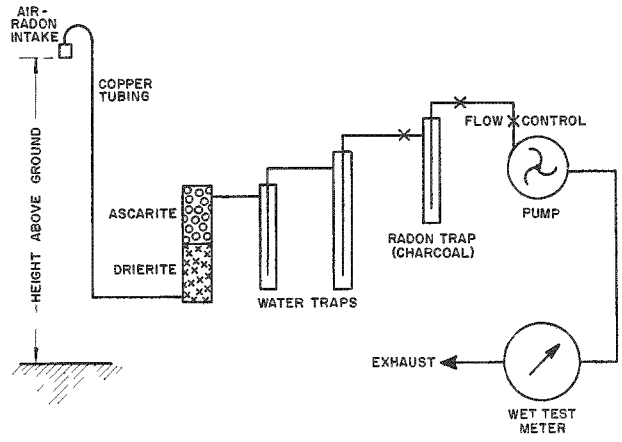

Figure 62

A schematic diagram of the radon collection apparatus

The radon traps were removed to a laboratory where the radon was transferred to counter bottles and the activity determined as described previously.[1,3]

3. Experimental Procedures

Observations of temperatures, wind speeds, other meteorological parameters, and samples of radon were taken for 20-minute periods at $1\frac{1}{2}$-hr intervals for tests of approximately 24-hr duration. Twenty-four-hour tests were made on 8-9, 15-16, 23-24 June and 30 June-1 July, 7-8, 14-15, 20-21, 28-29 July, and 4-5 August. Measurements of radon concentrations were made in only five of the nine tests, along with average temperatures and wind speeds.

The data were placed on IBM punch cards to faciltate analysis and study. The following code was used.

Card Column	Data
1-3	Number to identify the test period
4,5	year
6,7	month
8,9	day
10,11	hour
12,13	minute
14,15	hour code
16-19	height in cm
20	± temperature sign
21-24	temperature in degrees C to the nearest hundredth of a degree
25	± wet bulb temperature sign
26-29	wet bulb temperature in degrees C to the nearest hundredth of a degree
30-33	wind speed in m sec^{-1} to the nearest hundredth of a meter per second
34-39	radon concentration in pc $liter^{-1}$ to the nearest tenth of a milliliter
40-42	relative humidity in percent (at 1m level only)
43,44	wind direction in tens of degrees
45-47	standard deviation of azimuth to the nearest tenth of a degree (bivane data)
48-50	standard deviation of elevation to the nearest tenth of a degree (bivane data)
51-53	average sunshine in langleys min^{-1} to the nearest hundredth of a langley
54	± radiation flux sign
55-57	radiation flux in langleys min^{-1} to the nearest hundredth of a langley
58-60	soil temperature at 1 cm below surface in degrees C to the nearest tenth of a degree
61-63	soil temperature at 10 cm below surface in degrees C to the nearest tenth of a degree

Card Column	Data
64-66	barometric pressure in in. Hg (20 omitted) to the nearest hundredth of an inch
67,68	visibility in miles
69	visibility in fractions of a mile: 0 = 0, 1 = $\frac{1}{16}$, 2 = $\frac{1}{8}$, 3 = $\frac{3}{16}$, 4 = $\frac{1}{4}$, 5 = $\frac{5}{16}$, 6 = $\frac{3}{8}$, 7 = $\frac{1}{2}$, 8 = $\frac{5}{8}$, 9 = $\frac{3}{4}$
70	weather or obstruction: 0 = none, 1 = smoke, 2 = light rain, 3 = rain, 4 = thundershower, 5 = ground fog in patches, 6 = fog
71	obstruction to visibility: 0 = none, 1 = smoke, 2 = haze
72	cloud cover: 0 = none, 2 = scattered, 5 = broken, 9 = overcast
73,74	basic profile deck number (No. 71).

4. Wind Speed, Temperature, and Radon Profiles

Data for the test period of 28-29 July 1960, a rather typical day in July, were plotted in three dimensional form as shown in Figure 63. In all cases the vertical axis represents height above earth's surface in meters, and the axis to the right represents Central Standard Time. The maximum temperature at one meter was 89°F at 1430 and the minimum was 64°F. The test period began with a clear sky which changed to scattered clouds by the time of the 1230 run. Scattered clouds changed to broken by 1600 and overcast at 1730, after which they returned to scattered by 1900 and to clear on the next observation and for the remainder of the test period. Visibility was in the 10-mile-and-over range until 0400 on 29 July when it dropped to $\frac{1}{4}$ mile in fog. This condition gradually improved to 4-mile visibility at the end of the test period.

The top portion of Figure 63 shows the variation of wind speed with elevation and time. In almost all cases the wind speed increased with elevation. However, during the period between midnight and 0400 on the 29th the speed at 100 cm exceeded that at 200 cm, and in one case it exceeded that at 400 cm. The very weak winds in this period may have been caused by air drainage. At such low velocities, however, the accuracy of the data are subject to question. Also evident, in this portion of Figure 63, is the variation of wind speed with time: the speed increased until 1430 and then decreased rapidly during the remainder of the afternoon, with weak winds during the clear night.

The central portion of Figure 63 indicates the variation of temperature with elevation and time. Maximum temperatures are apparent at 1430 as is the decrease of temperature with height during the daytime. The development of inversion conditions during the hours of darkness is also evident.

The bottom portion of Figure 63 reveals the variation of radon concentrations with altitude and time.

The radon began increasing at 1430, or just before maximum temperatures and maximum wind speeds occurred. In general, radon concentrations in the atmosphere decreased with height. However, at the time of night when wind speeds decreased with height, above one meter, rather curious variations of radon with elevation also appear. It is interesting to note that at 0230, when radon concentration reached a maximum at the surface, the total in the air column extending from the surface to 16 meters was less than it had been at 0100. In general the total radon in the column increased throughout the night, and its maximum occurred at 0530 on the 29th.

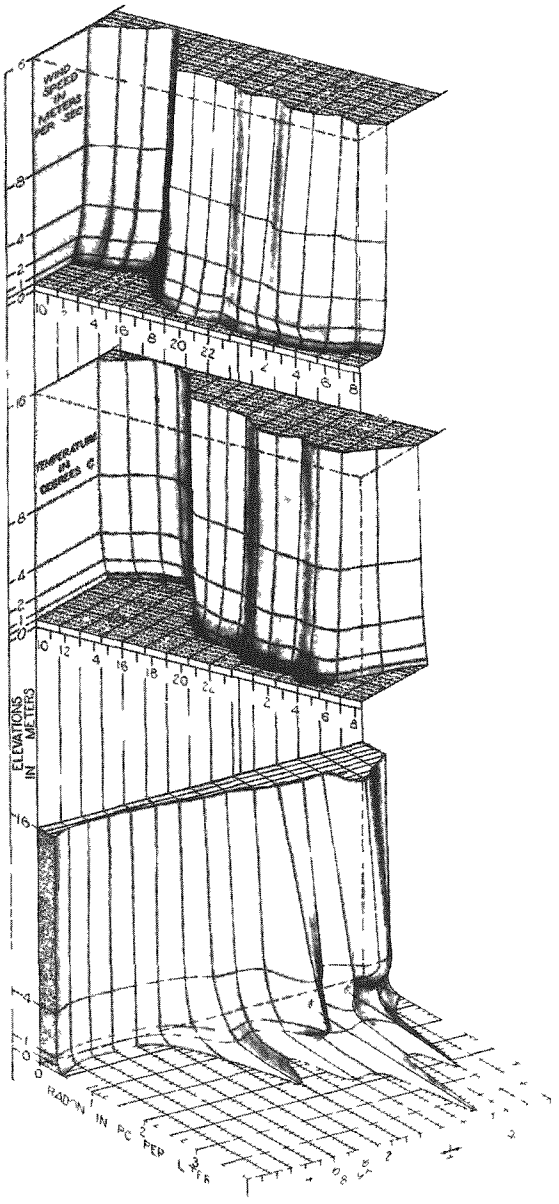

Figure 63

Wind speed temperature and radon data for a typical July day (July 28-29, 1960).

5. Integrated Values of Radon, Kinetic Energy, and Stability

As indicated earlier, numerous associated meteorological data were obtained simultaneously with the radon measurements. However, this study, which is one of several currently in progress based on these data, deals only with the radon measurements and the wind- and temperature-data obtained on the small tower during five 24-hr periods. Presented below are computations of the total amount of radon contained in vertical columns,

one square centimeter in cross section. The heights of the columns are: surface to 50 cm - the layer with the highest concentration of radon; surface to 1600 cm - the layer measured by the small tower; and surface to 4000 cm - the layer extending to the uppermost radon-intake tube. In addition to the total radon content, the total kinetic energy and stability of the 50- to 1600-cm layer were calculated.

(a) Methods of calculation. The total radon content in a given column was calculated by the formula

$$\text{Total radon} = \sum_{i=1}^{n-1} \left(\frac{R_i + R_{i+1}}{2} \right) (Z_{i+1} - Z_i) \qquad (1)$$

where R_i is the radon concentration in picocuries/cm^3 and Z_i is the height in centimeters, both at the i level, and n is the number of levels used in the integration. This technique assumed a linear variation of radon concentration from level to level, but of course not necessarily throughout the entire column.

In calculating the total kinetic energy in the column, it was assumed that the variation of wind speed, u, was logarithmic in each layer. Thus, the wind speed may be expressed as

$$u - u_i = \frac{u_{i+1} - u_i}{\ln Z_{i+1} - \ln Z_i} (\ln Z - \ln Z_i) \quad . \qquad (2)$$

Since the measuring levels were arranged logarithmically, i.e., $Z_{i+1} = 2Z_1$, the equation simplified to

$$u - u_i = \frac{u_{i+1} - u_1}{\ln 2} (\ln Z - \ln Z_i) \quad . \qquad (3)$$

The kinetic energy in a given layer per square centimeter is $\frac{1}{2} \bar{\rho} \int_{Z_i}^{Z_{i+1}} u^2 dZ$, where $\bar{\rho}$ is the mean density. Making use of Eq. (3)

$$\text{Kinetic energy} = \frac{1}{2} \bar{\rho} \int_{Z_i}^{Z_{i+1}} \left[\left(\frac{u_{i+1} - u_i}{\ln 2} \right) \ln Z + \left(u_i - \frac{u_{i+1} - u_i}{\ln 2} \ln Z_i \right) \right]^2 dZ \quad . \qquad (4)$$

After integration and algebraic manipulation

$$\text{Kinetic energy} = 2 \bar{\rho} Z_i [0.1\, u_{i+1}^2 + 0.08\, u_i u_{i+1} + 0.07\, u_i^2] \quad . \qquad (5)$$

The total kinetic energy for the column was obtained by adding the kinetic energy to successive layers.

$$\text{Total kinetic energy in column} = 2\bar{\rho} \sum_{i=1}^{n-1} Z_i \left[0.1\, u_{i+1}^2 + 0.08\, u_i u_{i+1} + 0.07\, u_i^2\right] \tag{6}$$

The stability of the layer from 50 to 1600 cm was obtained by calculating the temperature difference between the top and bottom of this layer.

(b) Results and Discussion. The total radon contents for the three selected air column heights are plotted in Figures 64a and b through 68a and b. To bring out pertinent features concerning the behavior of radon the data were plotted on both linear and semilogarithmic charts. The total kinetic energy from the 50 to the 1600 cm heights was plotted on the semilogarithmic charts, and the stability was plotted on the linear graphs.

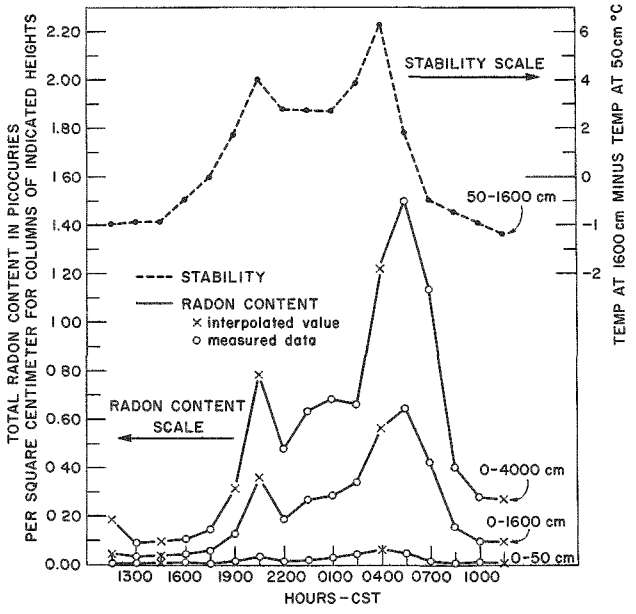

Figure 64a

Time variation of total radon content per square cm and stability.
8-9 June 1960 - Series #1

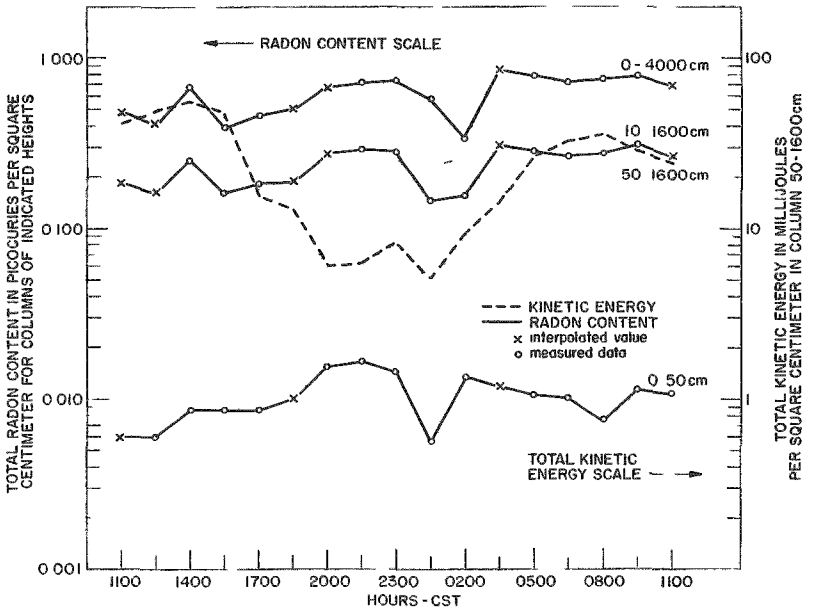

Figure 64b

Time variation of total radon content per square cm and kinetic energy. 8-9 June 1960 - Series #1

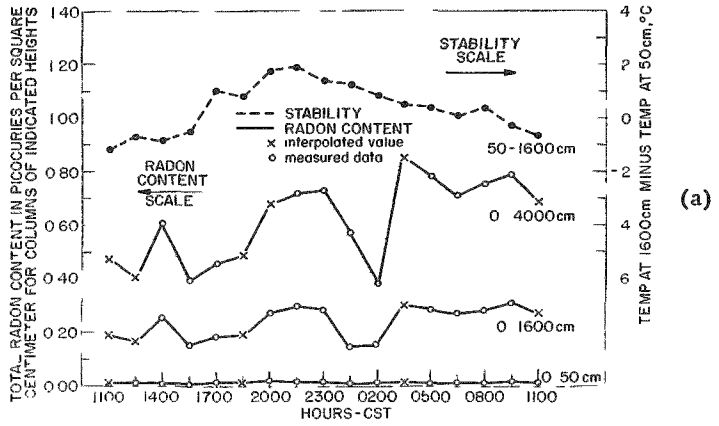

(a)

(b)

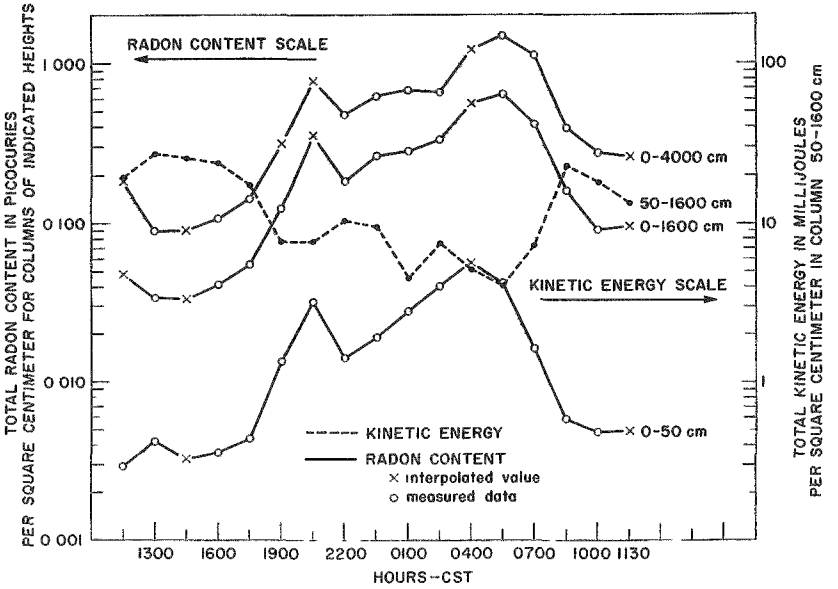

Figure 65a-b

Time variation of total radon content per square cm, stability and kinetic energy. 15-16 June 1960 - Series #2

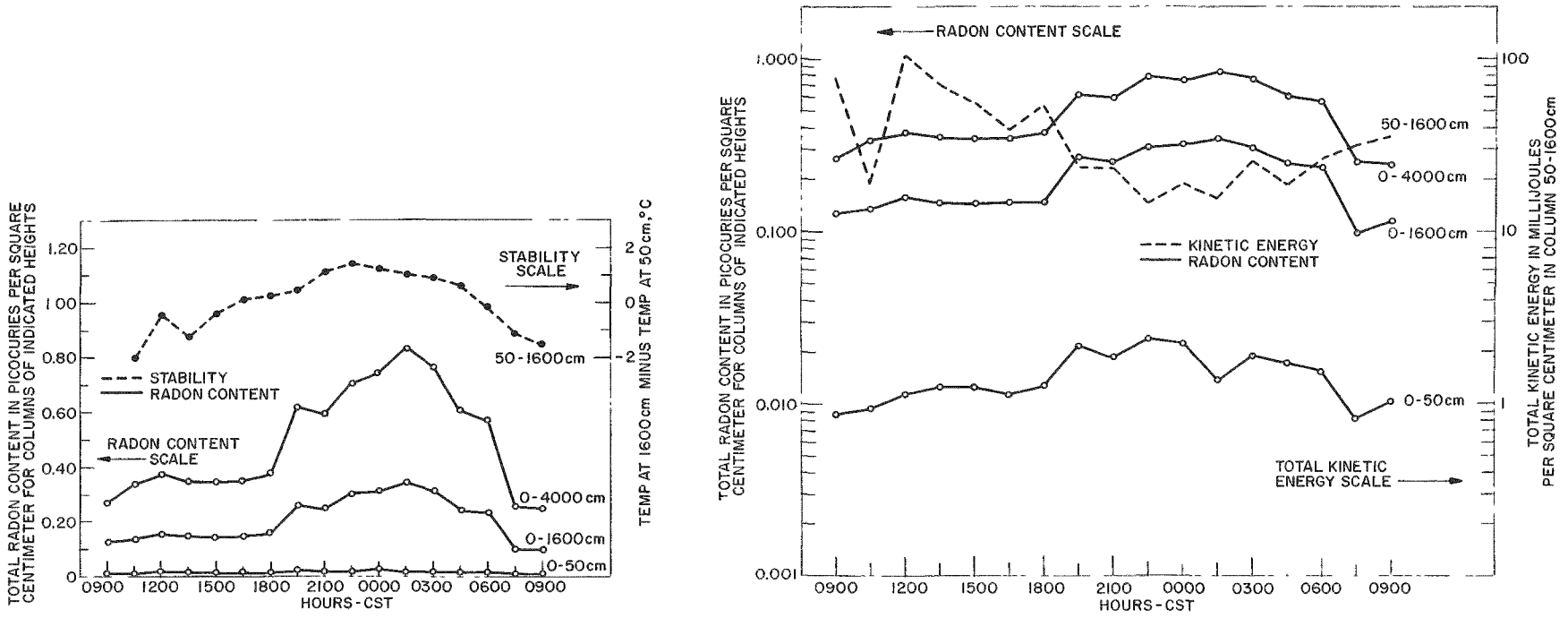

Figure 66

Time variation of total radon content per square cm, stability and kinetic energy.
23-24 June 1960 - Series #3

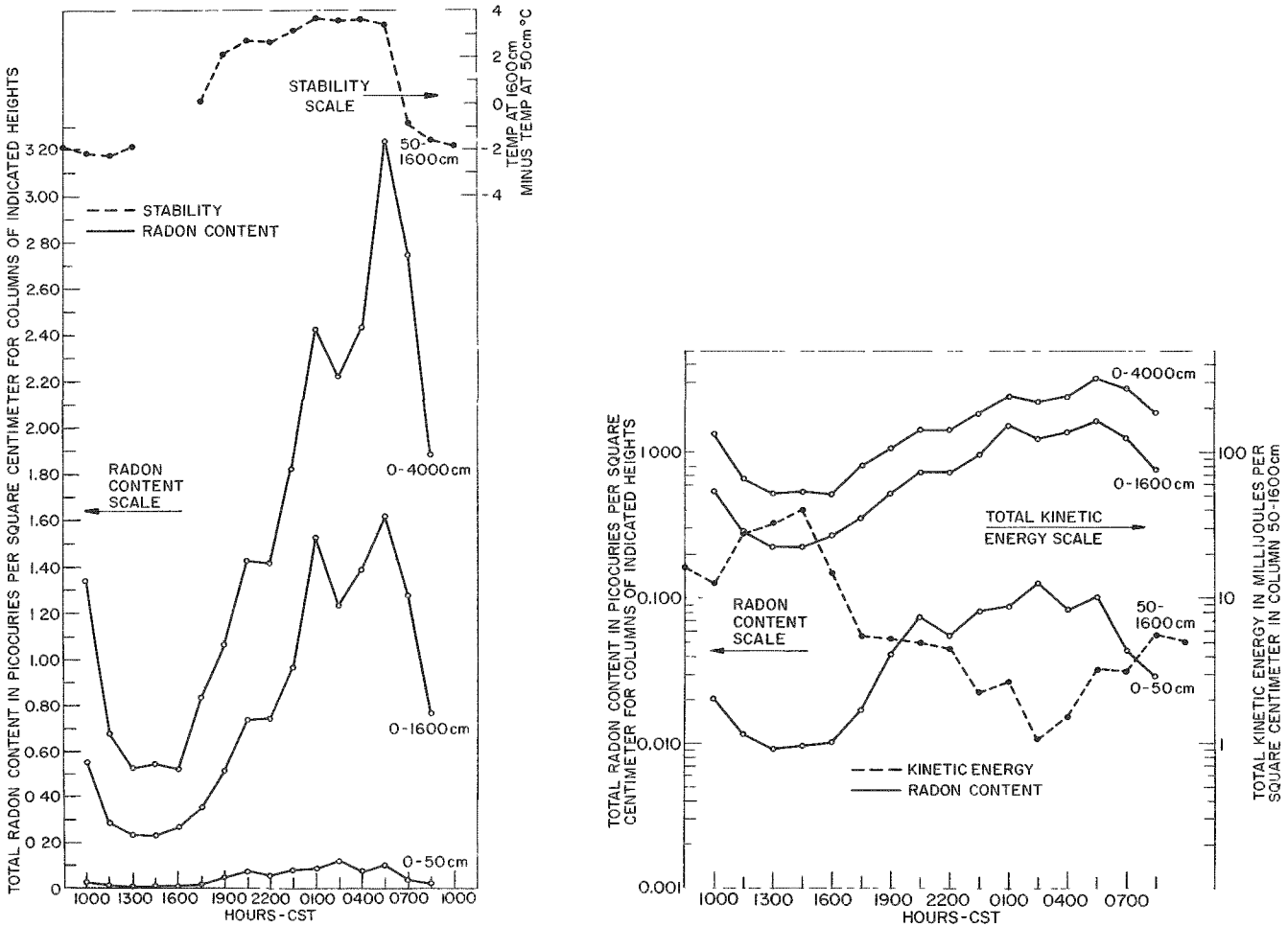

Figure 67

Time variation of total radon content per square cm, stability and kinetic energy. 28-29 July 1960 - Series #8

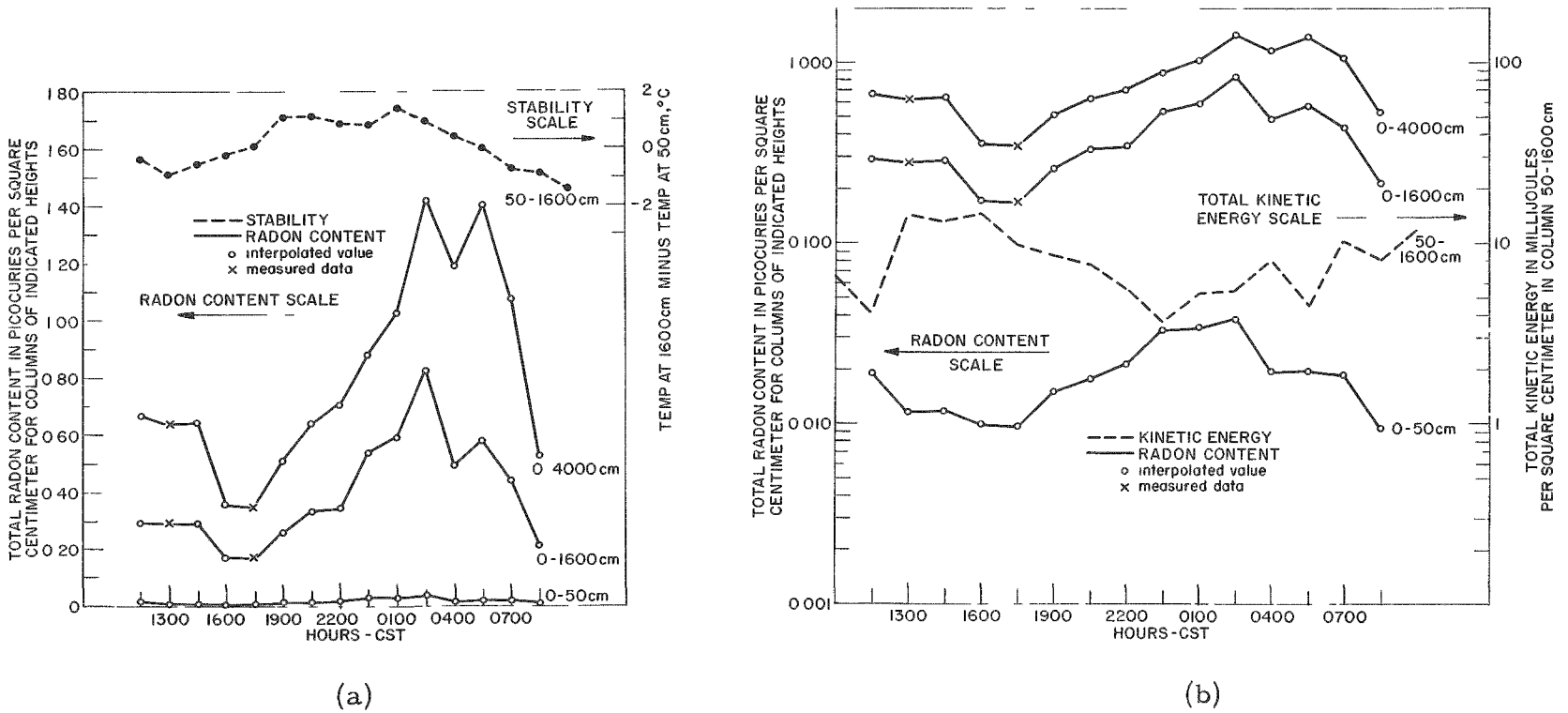

Figure 68

Time variation of total radon content per square cm, stability and kinetic energy.
4-5 Aug. 1960 - Series #9

Examination of these figures shows strikingly the diurnal variation of the radon content in the lower layer of the atmosphere, with the minimum occurring in the afternoon and maximum shortly before sunrise. Although each series differed from the others in detail the gross features of the first, eighth and ninth, Figures 64a and b, 67a and b, and 68a and b were similar in that high radon contents were observed during the hours of darkness. During these periods, the kinetic energy of the column was rather low and the stability was high. The second and third series, Figures 65a and b and 66a and b also resembled each other since the amplitude of the diurnal variation in radon content was low.

The effect of stability appears strikingly in the first series, Figure 64a and b where the stability maxima and minima correspond closely with the maxima and minima in radon content. Of particular interest are the data shown in the eighth series, Figure 67a and b. In this series, the stability is the greatest and the kinetic energy the lowest. As expected, the radon content is highest. In all of the charts, the radon begins to accumulate rapidly once an inversion sets in. Once the inversion is destroyed by solar heating, the radon content decreases sharply.

A surprising feature evident in the eighth and ninth series is that the gross rates (neglecting minor perturbution) of radon accumulation are nearly equal.

The pattern of kinetic energy appears to correlate highly with radon content. Figures 64b-68b indicate that the gross features of the kinetic energy curves are similar but inverted with respect to the radon curves. It is evident that although the kinetic energy and the stability of the column appear to correlate highly with the radon content, the relation among the variables is extremely complex.

Comparison of the data plotted on the semilogarithmic and linear charts shows that the amplitude of the lowermost layer, surface to 50 cm, is greater on the semilogarithmic plots than on the linear plots. The difference occurs because the semilogarithmic chart is a ratio chart and brings out the percentage variation, while the linear chart brings out the incremental changes. It is, therefore, evident that the percent variation of radon content is greater in the lowermost layer than in the total air column extending from either the surface to 1600 cm or the surface to 4000 cm; however, the variation in actual radon content of the higher columns is larger.

The authors are grateful to Hugh G. Daubek, Frank C. Kulhanek, Gunther A. Zerbe and Peter E. Wasko for their help in carrying out the observations and to Lee M. Cherven, Rita M. McDonough and Susan C. Tideman for assisting in the calculations and the preparation of figures.

References

1. H. Moses, A. F. Stehney, and H. F. Lucas, Jr. The effect of meteorological variables upon the vertical and temporal distributions of atmospheric radon. J. Geophys. Res. 65, 1223-1238 (1960).

2. H. Moses and J. H. Willet. Five-year climatological summary, July 1949 - June 1954. Argonne National Laboratory Report ANL-5592 (1954).

3. H. F. Lucas, Jr. Improved low-level alpha scintillation counter for radon. Rev. Sci. Instr. 28, 680-683 (1957).

PUBLICATIONS

Berlman, I. B., and A. Weinreb. On the Fluorescence Spectrum and Decay Time of Naphthalene. Molecular Phys. 5, 313 (1962).

Berlman, I. B. Ultraviolet and Lifetime Studies of Mechanisms in the Scintillation Process. In Luminescence of Organic and Inorganic Scintillators, ed. Kallman and Spruch. John Wiley & Sons, Inc., New York, 1962. p. 62.

Anderson, W. R., and I. B. Berlman. Effect of Irradiation on Liquid Scintillators. Nucleonics 20(7), 62-67 (July 1962).

Berlman, I. B. A study of the α/β Ratio in a Liquid Organic Scintillation Solution. Second International Congress of Radiation Research, Harrogate, England, August 5-11, 1962. Abstracts of Papers, p. 124.

Berlman, I. B., and T. A. Walter. Fluorescence Quenching of a Scintillation Solution by Oxygen. J. Chem. Phys. 37, 1888-1889 (1962).

Chhabra, Amrik S. Sr^{90}-Y^{90} Beta Ray (and Bremsstrahlung) Depth Dose Measurements in Lucite. Radiology 79, 1001-1007 (1962).

Failla, P. Some Effects of Radiation on Rotifers Irradiated at Different Ages. Radiation Res. 16, 573 (1962). (Abstract).

Failla, P. In Vivo and In Vitro Recovery of Irradiated Gametes of Arbacia punctulata. Radiation Res. 17, 767-773 (1962).

Failla, P. Recovery from Radiation-Induced Delay of Cleavage in Gametes of Arbacia punctulata. Science 138, 1341-1342 (1962).

Frenzen, P. On the Origin of Certain Symmetrical Patterns of Atmospheric Convection. Tellus 14(2), 173-176 (1962).

Holtzman, R. B. Desirability of Expressing Concentrations of Mineral-Seeking Constituents of Bone as a Function of Ash Weight. Health Phys. 8, 315-319 (June 1962).

Holtzman, R. B. RaD(Pb^{210}) in the Human Skeleton: Estimates of the Exponent of the Retention Function, the Skeletal Content, and the Dose Rate in High Radium People. Radiology 80, 122-123 (January 1963). (Abstract).

Kastner, J., F. R. Shonka, and J. E. Rose. Construction and Performance of a Muscle-Equivalent Environmental Radiation Meter of Extreme Sensitivity. Radiology 80, 122 (January 1963). (Abstract).

Lucas, H. F., Jr., D. E. Wallace, A. F. Stehney and F. H. Ilcewicz. Correlation of the Ra^{228} and Ra^{226} Content of Man with That of the Food and Water of His Environment. Second International Congress of Radiation Research, Harrogate, England, August 5-11, 1962. Abstracts of Papers, p. 102.

Marinelli, L. D., and H. F. Lucas, Jr. The Translocation of Thorium Daughters to the Skeleton of Thorotrast Patients. Tenth International Congress of Radiology, Montreal Canada, Aug. 26-Sept. 1, 1962. Book of Abstracts, p. 279.

Marinelli, L. D., and H. F. Lucas, Jr. Translocation of Thorium Daughters to Bone. In Some Aspects of Internal Irradiation, ed. T. F. Dougherty, W. S. S. Jee, C. W. Mays and B. J. Stover. Pergamon Press, London, 1962. pp. 499-515.

Marshall, J. H. Radioactive Hotspots, Bone Growth, and Bone Cancer: Self-Burial of Calcium-Like Hotspots. In Radioisotopes and Bone. ed. F. C. McLean, P. Lacroix and Ann Budy. F. A. Davis Co., Philadelphia, 1962. pp. 35-50.

Wald, N., C. E. Miller, W. H. Borges and J. Kim. Preliminary Observations of Blood Cell Chromosome Patterns in Radium Dial-Painters. Radiation Res. 16, 592 (1962). (Abstract).

Finkel, A. J., and C. E. Miller. Analysis of Radium Retention After Continuous Ingestion. Radiation Res. 16, 592 (1962). (Abstract).

Finkel, A. J., and C. E. Miller. Patterns of Radium Retention in Mice as Related to Man. Second International Congress of Radiation Research, Harrogate, England, August 5-11, 1962. Abstracts of Papers, p. 213.

Hasterlik, R. J., C. E. Miller and A. J. Finkel. Carcinoma of the Mastoid and Paranasal Sinuses in Radium-Bearing Patients. Proc. 8th International Cancer Conf., Moscow, Russia, July 22-28, 1962. Abstracts of Papers, p. 238.

Wald, N., C. E. Miller, W. M. Borges and J. Kim. A Cytogenic Study of Some Radium Dial-Painters and Their Progeny. Second International Congress of Radiation Research, Harrogate, England, August 5-11, 1962. Abstracts of Papers, p. 61.

Hasterlik, R. J., A. J. Finkel and C. E. Miller. The Late Effects of Radium Deposited in Humans. Second International Congress of Radiation Research, Harrogate, England, August 5-11, 1962. Abstracts of Papers, p. 52.

Moses, H., H. F. Lucas, Jr., and G. A. Zerbe. The Effect of Meteorological Variables upon Radon Concentration Three Feet Above the Ground. J. Air Pollution Control Assoc. 13, 12-19 (January 1963).

Platzman, R. L. Dissociative Attachment of Subexcitation Electrons in Liquid Water, and the Origin of Radiolytic "Molecular" Hydrogen. Second International Congress of Radiation Research, Harrogate, England, August 5-11, 1962. Abstracts of Papers, p. 128.

Platzman, R. L. Superexcited States of Molecules. Radiation Res. 17, 419-425 (1962).

Platzman, R. L. Superexcited States of Molecules, and the Primary Action of Ionizing Radiation. The Vortex 23(8), 372-389 (October 1962).

Jesse, W. P., and R. L. Platzman. An Isotope Effect in the Probability of Ionizing a Molecule by Energy Transfer from a Metabolic Nobel-gas Atom Nature 195, 790 (August 25, 1962).

Rowland, R. E. High Resolution Autoradiographic and Microradiographic Studies of Bone and Teeth from Human Radium Cases. Tenth International Congress of Radiology, Montreal, Canada, Aug. 26-Sept. 1, 1962. Book of Abstracts, pp. 281-282.

Rowland, R. E. Skeletal Retention of the Alkaline Earth Radioisotopes and Bone Dosimetry. In Some Aspects of Internal Irradiation. Pergamon Press, London, 1962. pp. 455-469.

Rowland, R. E., R. D. Ray, Jack Stevens and Irving Lyon. Uptake of Calcium-45 and Carbon-14-Labelled Proline by Dead and Living Bone. In Radioisotopes and Bone, ed. F. C. McLean, P. Lacroix and Ann Budy. F. A. Davis Co., Philadelphia, 1962. pp. 69-83.

PAPERS ACCEPTED FOR PUBLICATION

Berlman, I. B. Nanosecond Fluorescence Decay Time Measurements. Bull. Am. Phys. Soc. (Abstract).

Bowe, J. C. Residual-Gas Concentrations in Evacuated Chambers. (Note) Rev. Sci. Instr.

Carson, J. E. Analysis of Soil- and Air-Temperature Data by Fourier Techniques. J. Geophys. Res.

Carson, J. E., and H. Moses. The Annual and Diurnal Heat-Exchange Cycles in Upper Layers of Soil. J. Appl. Meteorol.

Holtzman, R. Solubility Value of $RaSO_4$ in Water. (Letter) Health Phys.

Holtzman, R. B. The Natural Contents of RaD(Pb^{210}) and RaF(Pb^{210}) in the Human Body. Symposium on Radioactivity in Man, Northwestern University, Evanston, Ill., Sept. 5-7, 1962.

Holtzman, R. B. Measurement of the Natural Contents of RaD(Pb^{210}) and RaF(Pb^{210}) in Human Bone. Estimates of Whole-Body Burdens. Health Phys.

Emrich, G., and H. F. Lucas, Jr. Geologic Occurrence of Natural Radium-226 in Ground Water in Illinois. Hydrogeology Section of 1962 Meeting of Geological Society of America, Houston, Texas. (Abstract).

Marinelli, L. D. Dosimetrie. Chapter III-1, Handbook of Medical Radiology, Vol. 15, No. 11. Springer-Verlag.

Marinelli, L. D., C. E. Miller, H. A. May and J. E. Rose. Low-Level Gamma-Ray Spectrometry: Experimental Requirements and Biomedical Applications. Advances in Biological and Medical Physics, Vol. VIII. Academic Press.

Marinelli, L. D., H. F. Lucas, Jr., and C. E. Miller. Elimination and Retention of Ra^{226} in Humans: Long Follow-Up of a Single Inhalation Case. Radiology. (Abstract).

Remenchik, A. P., J. Talso and C. E. Miller. Correlation of Total Body Potassium and Tissue Potassium Measurements. Symposium on Radioactivity in Man, Northwestern University, Evanston, Ill., Sept. 5-7, 1962.

Wenger, P., and C. E. Miller. Research on Radium and Radiostrontium Accumulation and Toxicity in the Human Body. II. The Geneva Whole Body Counter. Helv. Chim. Acta.

Rowland, Robert E. Radium in Human Teeth: A Quantitative Autoradiographic Study. Arch. Oral Biol.

Rowland, R. E. Local Distribution and Retention of Radium in Man. IAEA Scientific Meeting on the Diagnosis and Treatment of Radioactive Poisoning, Vienna, October 15-19, 1962.

Steingraber, O. J., and I. B. Berlman. Versatile Technique for Measuring Fluorescence Decay Times in the Nanosecond Region. Rev. Sci. Instr.

PAPERS SUBMITTED FOR PUBLICATION

Berlman, I. B., R. Grismore and B. G. Oltman. α/β Ratios and Relative Radiation Sensitivity of Organic Scintillation Solutions. Trans. Faraday Soc.

Frenzen, Paul. A Laboratory Investigation of the Lagrangian Autocorrelation Function in Stratified Fluids. Submitted in partial fultillment of requirements for Ph.D., Univ. Chicago, 1962.